# Investigation of bioactive natural compounds for cardiovascular diseases and *daqu* fermentation, and the exploration of *Beauveria bassiana* as a biocontrol agent for the mountain pine beetle epidemic

by

Kleinberg Xiandrell Fernandez

A thesis submitted in partial fulfillment of the requirements for the degree of

Doctor of Philosophy

Department of Chemistry
University of Alberta

# Abstract

Peptide-based compounds are crucial components of current research and development efforts, namely in the field of pharmaceutical therapeutics. Peptides possess complex secondary structures, resulting in a wide array of functions (e.g., signalling, or cellular structural capabilities). Advances in the introduction of non-canonical amino acid building blocks have allowed for the synthesis of diverse analogues of naturally-derived peptides through solid phase peptide synthesis (SPPS). In this thesis, several modifications (e.g., *N*-methylation, homologue-substitution, etc.) were used to develop non-canonical amino acids to form highly-stable and biologically active apelin analogues.

Apelin is a 77-amino acid long prepropeptide, which is cleaved into the resulting active isoforms: apelin-55, apelin-36, apelin-17, and (pyr-1)-apelin-13. Apelin peptides are part of the cardioprotective hormone system (i.e., apelinergic system), alongside the G-protein coupled apelin (APJ) receptor. The apelinergic system is an influential regulator of various metabolic functions, including nitric oxide production and cardiovascular output. In addition, apelin peptides have also shown promise as biomarkers for cancer diseases and as regulatory components for age-associated sarcopenia. In this study, we probed the extension of apelin peptides at the *N*-terminus through the addition of head group-protected PEG chains, to determine the optimal modifications for stability against KLKB1 proteolysis. In addition, homologue substitution at the critical RPRL binding site was performed to further analyze the peptide-receptor interactions at this vital site. Furthermore, alanine scans and methylation efforts were performed on the four *N*-terminal residues for apelin-17 peptides to determine the importance of these amino acid substitutions and conformational restrictions on receptor binding and activation. In addition, ongoing work on retro-enantio peptides is being undertaken to determine the significance of the apelin peptide backbone. Lastly, work is

being performed to explore the potential of apelin peptides as oral-based therapeutics through the synthesis of polysaccharide-based hydrogels. Through synthetic interventions, we can optimize naturally-derived and cardio-physiologically-essential apelin peptides to surmount their metabolic liability and clearance and harness such analogues as potent therapeutic drug targets for cardiovascular health.

Work on the determination of the effects of microbial composition on *daqu* fermentation will also be explored. *Daqu* is a saccharification starter in the fermentation process for the production of *baijiu*, an extremely popular Chinese liquor. In this study, a comprehensive qualitative analysis of the production of several lipopeptide congeners, produced by *Bacillus* spp. was performed on several fermentation conditions (i.e., LB broth, and simple and complex *daqu*). It is important to determine the contribution of these diverse lipopeptides on the resulting bacterial community assembly, to assess the quality of the *baijiu* end product.

In a tangential direction, work was directed towards the investigation of *Beauveria bassiana* as a biocontrol agent for the management of the mountain pine beetle (MPB), or *Dendroctonus ponderosae*, population. First, this fungal strain was tested *in vitro* and *in planta* conditions to determine their conidial stability and efficacy. A fermentation approach was also developed to produce multi-hundred-gram scale of conidial biomass. Furthermore, *in natura* field infection experiments were performed to determine the effects of *B. bassiana* on the MPB reproductive success. Lastly, analyses of the genomic and transcriptomic features of *B. bassiana* were performed to identify sources of virulence and secondary metabolite biosynthesis. Through cultivation and formulation, these fungal strains can withstand the conditions inhabited by the mountain pine beetle, to exert their biocontrol potential on these forest pests.

# Preface

Chapter 2 has been published as two articles: (1) Fischer, C.; Lamer, T.; Fernandez, K.; Gheblawi, M.; Wang, W.; Pascoe, C.; Lambkin, G.; Iturrioz, X.; Llorens-Cortes, C.; Oudit, G. Y.; Vederas, J. C. Optimizing PEG-Extended Apelin Analogues as Cardioprotective Drug Leads: Importance of the KFRR Motif and Aromatic Head Group for Improved Physiological Activity. *Journal of Medicinal Chemistry* 2020, *63* (20), 12073–12082., and (2) Fernandez, K. X.; Fischer, C.; Vu, J.; Gheblawi, M.; Wang, W.; Gottschalk, S.; Iturrioz, X.; Llorens-Cortés, C.; Oudit, G. Y.; Vederas, J. C. Metabolically Stable Apelin-Analogues, Incorporating Cyclohexylalanine and Homoarginine, as Potent Apelin Receptor Activators. *RSC Medicinal Chemistry* 2021, *12* (8), 1402–1413. This chapter involved the collaboration between several members in our research lab as well as our collaborators in other research groups. For section 2.2 Optimization of PEG-Extended Apelin Peptides, I was responsible for designing and synthesizing several analogues, evaluating these analogues through *in vitro* tests, as well as designing new methodologies with Dr. Conrad Fischer for determination of plasma protein binding $\log D_{7.4}$. For section 2.3 Determining the Importance of hArg/Cha Modifications in the RPRL Region, I was responsible for designing and synthesizing all the target analogues, as well as carrying out all the *in vitro* bioassays. For both sections, all the binding affinity assays were performed by Dr. Xavier Iturrioz in Dr. Catherine Llorens-Cortés' lab from the CEA Paris-Saclay, and all *in vivo* mice assays were performed by Jenny Vu, Mahmoud Gheblawi, and Dr. Wang Wang in Dr. Gavin Oudit's lab from the University of Alberta. For section 2.4.1 Determining the Importance of the KFRR Motif, I worked with Dr. Conrad Fischer and Dr. Cameron Pascoe to synthesize all alanine scans and the *N*- and $\alpha$-methyl analogues. All *in vitro* and *in vivo* experiments were performed by the respective people stated above. For section 2.4.2 Pharmacokinetics and Development of Oral Apelin Delivery System, I

synthesized the apelin analogue required for the *in vivo* canine degradation assays performed by Dr. Pavel Zhabyeyev in Dr. Gavin Oudit's lab. I also conducted the *in vitro* enzymatic assays to determine the metabolic stability of target analogues. In addition, I developed and synthesized polysaccharide-based hydrogels for the investigation of oral drug delivery of apelin peptides. Lastly, for section 2.4.3 Determining the Importance of the Apelin Peptide Backbone, I was responsible for the design and synthesis of the retro-enantio peptides, as well as carrying out the purification, characterization, and testing for the *in vitro* stability assays.

Chapter 3 has been published as Li, Z.; Fernandez, K. X., Vederas, J. C., Gänzle, M. G. Composition and activity of antifungal lipopeptides produced by *Bacillus* spp. in *daqu* fermentation, *Food Microbiology*, 2022, *111*:104211. In this chapter, we were collaborators with Dr. Zhen Li in Dr. Michael Gänzle's lab at the University of Alberta, and my main contributions were to the identification and quantification of antifungal lipopeptides in LB broth, simple media, and complex media. I was also involved in designing extraction and purification methodologies of these antifungal lipopeptides, as well as preparing the manuscript.

Chapter 4 has been published as two articles: (1) Fernandez, K. X., Pokorny, S., Ishangulyeva, G., Ullah, A., Peng, L., Nadeau, M., Todorova, S. I., Carroll, A., Erbilgin, N., Vederas, J. C. Greenhouse and field evaluation of *Beauveria bassiana* dry formulation for the population management of Mountain Pine Beetle, *Dendroctonus ponderosae*. *Applied Microbiology and Biotechnology*, 2023, *107*:3341-3352. and (2) Li, J. X., Fernandez, K. X., Ritland, C., Jancsik, S., Engelhardt, D. B., Coombe, L., Warren, R. L., van Belkum, M. J., Carroll, A. L., Vederas, J. C. Genomic virulence features of *Beauveria bassiana* as a biocontrol agent for the mountain pine beetle population. *BMC Genomics*, 2023, *24*:390. For section 3.2 *Beauveria bassiana* Shows Effective Lethalness to *Dendroctonus ponderosae* Populations in Greenhouse and

Field Experiments, this project was collaborative with research groups from several departments and institutions. For my contributions, I was tasked with managing the project and designing and performing all experimental methodologies. For the large-scale production of conidial biomass and *in planta* greenhouse assays, I worked with Guncha Ishangulyeva and Aziz Ullah from Dr. Nadir Erbilgin's lab at the University of Alberta, and Dr. Albert Rosana from our research group. For the *in natura* field infection assays, I collaborated with Dr. Stanley Pokorny and Lucas Peng in Dr. Allan Carroll's lab at the University of British Columbia. For section 3.3 Genomic and Transcriptomic Virulence of *Beauveria bassiana*, my main contributions were the preparations of the DNA and RNA mycelial samples, determination of oosporein production levels, and analyses of the genomic and transcriptomic results. I collaborated with several members from the research groups of Dr. Inanc Birol and Dr. Joerg Bohlmann at the University of British Columbia.

## Dedication

I dedicate this thesis to my moms, Joy Fernandez and Rowenalyn Dahilig, and to my sister, Arlette Fernandez. Thank you so much for all your sacrifices, unwavering love, support, inspiration, and guidance throughout this journey. Words cannot describe my deepest gratitude and appreciation to you. Thank you for always reminding me to believe in myself, to be determined, to always persevere, and to not be scared to take the road less taken. I love you all, always and forever, ayayaten kayo. Love wins, love always wins.

Two roads diverged in a yellow wood,
And sorry I could not travel both
And be one traveler, long I stood
And looked down one as far as I could
To where it bent in the undergrowth;

Then took the other, as just as fair,
And having perhaps the better claim,
Because it was grassy and wanted wear;
Though as for that the passing there
Had worn them really about the same,

And both that morning equally lay
In leaves no step had trodden black.
Oh, I kept the first for another day!
Yet knowing how way leads on to way,
I doubted if I should ever come back.

I shall be telling this with a sigh
Somewhere ages and ages hence:
Two roads diverged in a wood, and I—
I took the one less traveled by,
And that has made all the difference.

"The Road Not Taken" by Robert Frost

# Acknowledgements

"Science is made up of mistakes, but they are mistakes which it is useful to make because they lead little by little to the truth… See obstacles as opportunities. See obstacles as inspirations."

- Anthony Doerr

This scientific journey would not have been possible without the continuous contributions of many individuals. First and foremost, I would like to send my deepest thank you to my supervisor and mentor, Dr. John C. Vederas for taking a chance and believing in me many years ago. Thank you for your knowledge and numerous outlooks on life, your enthusiasm for science, art and teaching, and your willingness for a supportive and open learning environment. Furthermore, I am forever grateful for the mentorship from you and Dr. Hayley Wan to allow me to grow as a scientist, a mentor, and as a person.

I would also like to send my deepest gratitude to the number of support staff in the department who have worked tirelessly with me throughout my research. My heartfelt thank you and appreciation for Jing Zheng, Béla Reiz, Dr. Angie Morales-Izquierdo, and Dr. Randy Whittal from the Mass Spectrometry Facility; Mark Miskolzie and Dr. Ryan McKay from the NMR Facilities; Dr. Wayne Moffat and Jennifer Jones from the Analytical and Instrumentation Laboratory; Gareth Lambkin from Biological Services; and Andrew Yeung, Ryan Lewis, and Mike Barteski from the Chemistry Stores. My work would not have been possible without you.

I would also like to thank my friends from the Vederas lab for your support and comradery throughout these six years. To Dr. Conrad Fischer, thank you for the mentorship, friendship, and positive outlook on life. To Dr. Jonathan Beadle, for all the laughs and adventures together. To Dr. Wayne Vuong, for always challenging me and for all the bubble tea runs. To Dr. Daniel

Engelhardt, for sharing our common interest in sports, cooking, plants, and “mugs”. To Dr. Cameron Pascoe, for our “tea times” and bonding time with Scout and Steele. To Dr. Marco van Belkum, for his vast knowledge in molecular biology and microbiology, as well as for sharing all the Dumpert videos. To Dr. Bethan Donnelly for the endless optimism and enthusiasm, and for our shared love of performative arts. For Yu-Ting Hsiao, thank you for all the memories of volleyball, dogs, and shuài gē. To Karizza Catenza, Samantha Gottschalk, Kurtis Willoughby, and Ashlyn Waters, my mentees, thank you for entrusting me to mentor you throughout your scientific journey. Furthermore, I would like to thank Dr. Bethan Donnelly and Karizza Catenza for their help in editing this thesis.

Lastly, I would be remiss to forget the support from friends and family outside of the lab. To my Special Olympics Edmonton family, thank you for brightening my days and reminding me to keep a positive outlook on life. To my Working for Inclusivity in Chemistry (WIC) friends, thank you for advocating for equity, diversity and inclusion in the university – keep fighting the good fight. To Cindy Vuong, Fatima Mohamed, and Cathy Agyeman, thank you for helping me endure undergrad with all the laughs. To my family in Edmonton, Cheryl Vicera, Jose Vicera, and Columbina Fernandez, thank you for your continuous love, support, and encouragement. At last, the titas and titos to my future anaks, Mischelle Remigio, Nicole Rodriguez, Klaudine Villaflor, Andrea Simeon, Therese Rodriguez, and Quentin Champdoizeau, thank you for always keeping me on my toes, making life enjoyable, and for all your tiwala para sa akin – mahal kayo. Finally, the financial support from Alberta Graduate Excellence, Canadian Institutes of Health Research, Natural Sciences and Engineering Research Council of Canada, and Alberta Innovates, is gratefully acknowledged.

# Table of Contents

# List of Tables

# List of Figures

# List of Schemes

# Abbreviations

**$[\alpha]_D^{26}$** specific rotation at 26 ℃

**ACE2** angiotensin converting enzyme 2

**Aib** aminoisobutyric acid

**Ala** alanine

**Arg** arginine

**Asn** asparagine

**Asp** aspartic acid

**Boc** *tert*-butoxycarbonyl

**$Boc_2O$** di-*tert*-butyl dicarbonate

**BP** blood pressure

**BrF** bromophenylalanine

**BSF** blue stain fungi

**Cbz** carboxybenzoyl

**CFU** colony forming unit

**CFU/g** colony forming unit per gram

**CFU/$cm^2$** colony forming unit per $cm^2$

**Cha** cyclohexylalanine

**CMC** carboxymethylchitosan

**CMCD** carboxymethylcyclodextrin

**CMCD-*g*-CMC** carboxymethylcyclodextrin-*grafted*-carboxymethylchitosan

**DBP** diastolic blood pressure

**DCM** dichloromethane

**DIPEA** diisopropeylethylamine

**DMF** dimethylformamide

**$EC_{50}$** half maximal effective concentration

**EDC** 1-ethyl-3-[3-dimethylaminopropyl]carbodiimide hydrochloride

**Fmoc** fluorenylmethyloxycarbonyl

**FRET** fluorescence resonance energy transfer

**FTIR** fourier transform infrared

**FUA** Food microbiology culture collection at the University of Alberta.

**Gln** glutamine

**Glu** glutamic acid

**Gly** glycine

**GRAS** generally recognized as safe

**hArg** homoarginine

**HATU** 1-[*N*-[dimethylamino)-1*H*-1,2,3-triazolo-[4,5-b]pyridine-1-ylmethylene]-*N*-methylmethananium hexafluorophosphate *N*-oxide

**His** histidine

**HMBC** heteronuclear multiple bond correlation

**HOBt** hydroxybenzotriazole

**HPLC** high-performance liquid chromatography

**HSQC** heteronuclear single quantum coherence

**$IC_{50}$** half maximal inhibitory concentration

**IH** MPB-infested bolt with high dose BioTitan WP formulation (MPB exit experiment)

**IL** MPB-infested bolt with low dose BioTitan WP (MPB exit experiment)

**Ile** isoleucine

***J*** coupling constants

**KLKB1** human plasma kallikrein

**LCMS** liquid chromatography mass spectrometry

**Leu** Leucine

**Lys** lysine

**MABP** mean arterial blood pressure

**MEA** malt extract agar

**Met** methionine

**MFS** Major Facilitator Superfamily

**MIC** minimum inhibitory concentration.

**MIRI** myocardial ischemia reperfusion injury

**mMRS** modified MRS broth

**MPB** mountain pine beetle

**NEP** neprilysin

**NH** non-infested food bolt with high dose BioTitan WP (MPB entry experiment)

**NHS** *N*-hydroxysuccinimide

**NL** non-infested food bolt with low dose BioTitan WP (MPB entry experiment)

**Nle** norleucine

**NMR** nuclear magnetic resonance

**Oic** octahydroindole-2-carboxylic acid

**PALM** palmitoyl

**Pbf** 2,2,4,6,7-pentamethyldihydrobenzofuran-5-sulfonyl

***p*BPa** *para*-benzoylphenylalanine

**PEG** polyethylene glycol

**pGlu** pyroglutamic acid

**Phe** phenylalanine

**Pmc** 2,2,5,7,8-pentamethylchroman-6-sulfonyl group

**Pro** proline

**PyBOP** benzotriazol-1-yloxytripyrrolidinophosphonium hexafluorophosphate

**SBP** systolic blood pressure

**Ser** serine

**S.E.M.** Standard error of means

**SPPS** solid phase peptide synthesis

**TFA** trifluoroacetic acid

**THF** tetrahydrofuran

**TLC** thin layer chromatography

**Trp** tryptophan

**Tyr** tyrosine

**UAMH** University of Alberta Microfungus Herbarium (Canada)

**Val** valine

# Chapter 1 Introduction

## 1.1 Background

### 1.1.1 Peptides Background

Chemical biology, a sub-discipline of organic chemistry with application to biological systems, aims to investigate, understand, and rationally influence biological processes and systems using chemical tools. This thesis will look at the development of biological- and chemical-based tools for improving therapeutics for cardiovascular protection, investigating and understanding of peptide-protein structures, understanding the role of peptides in fermentation, and lastly, investigating microbial organisms for ecosystem protection. This thesis will greatly focus on modified amino acids and peptides but will also touch on polyketide synthase (PKS), terpene synthase (TS) and nonribosomal peptide synthase (NRPS) products.

Peptides constitute an extremely important class of biomolecules, usually consisting of several amino acid subunits connected as a repeating backbone of — $NH_x$ — CHR — C(O) —, with (*S*)-stereochemistry (except for L-cysteine which has an (*R*)-stereochemistry by the Cahn-Ingold-Prelog rules).[1–3] In nature, peptides are responsible for many physiological roles, including antibiotics,[4] enzymatic cellular machineries,[5] medicines,[6–8] signalling molecules,[9] and structural elements,[10]. Peptides commonly are made of 20 canonical amino acids, with varying electronic and steric properties due to the different sidechains or R-groups (**Fig. 1**). Amino acids, and their complex secondary structures as peptides and proteins, are ubiquitous and greatly diverse in their function in biological systems; highlighting the potential to manipulate these structures to probe biological and biochemical processes. In addition to the 20 canonical amino acids, the use of

modified unnatural or non-canonical amino acids provides further opportunities to expand the characteristics and functions of peptides and proteins in nature.

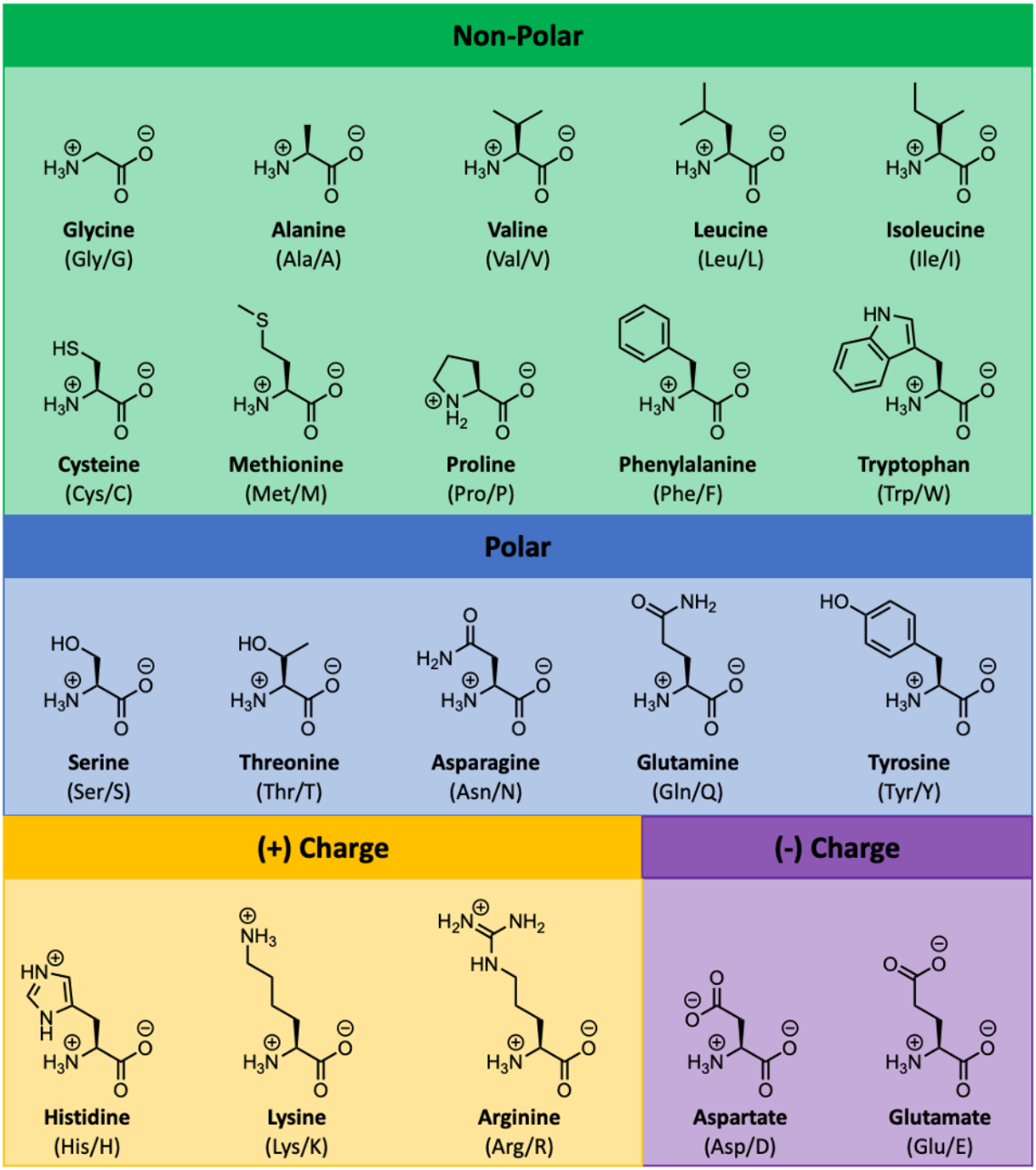


**Fig. 1** Chemical structures of 20 canonical/natural amino acids.

### 1.1.2 Peptide-Based Therapeutics

Since the discovery of insulin,[11] peptide-based drugs have been clinically used for the treatment of several illnesses and diseases[1,3]. Many of these peptides are isolated from natural sources (e.g., bovine stomach tissue), but with the introduction of protein sequencing and peptide synthesis, drugs like oxytocin and vasopressin can be made synthetically.[1] These advances in peptide-based therapeutics have resulted in increased interest in pharmaceutical research and development and have now become one of the fastest-growing classes of therapeutics in clinical trials.[12] In 2017, 155 peptide-based drugs were active in clinical development, of which half were in phase 2; 68 more peptide-based drugs were approved for therapeutic use.[1,7] Briefly after, over 1000 ongoing peptide-based clinical trials were performed in 2019.[13] Peptides have complex and well-defined three-dimensional structures, and they are greatly specific to their respective targets, making them attractive drug targets.[7,14] Contrary to many small molecule-based therapeutics, peptides have less off-target binding, therefore reducing off-target toxicity and the resulting side effects.[1] In addition, peptide-based drugs can be administered in conjunction with other treatments, leading to increased potency.[12] Despite these advantages, peptides also possess many drawbacks not seen with small molecule therapeutics. For example, peptide-based drugs tend to exhibit poor pharmacokinetics due to the body's many responses in clearing them from the body.[12] Peptides have low plasma half-lives due to the rapid degradation by endogenous proteases *via* proteolytic degradation.[7,12] In addition, peptides have low metabolic stability and oral bioavailability due to their relatively large sizes.[12] Although peptide therapeutics can be administered intravenously, intramuscularly, and subcutaneously, unwanted pain and low patient compliance have pushed for further development of these therapeutics for oral administration.[15,16]

### 1.1.3 Peptide Synthesis Solid-Phase Peptide Synthesis Overview and Advances

The term peptide was first coined by Emil Fischer and Ernest Fourneau in 1901 when they performed the first peptide synthesis.[15] Peptides and proteins are made up of amino acid building blocks, which can be biologically and chemically synthesized in an iterative process. In 1932, the first reversible $N^{\alpha}$-protecting group, carboxybenzoyl (Cbz), compatible with peptide synthesis, was invented. The synthesis of two peptide hormones, oxytocin and vasopressin, was performed by Vincent du Vigneaud; this work was recognized with the Nobel Prize in Chemistry in 1955.[17]

Shortly thereafter, Bruce Merrifield introduced solid phase peptide synthesis (SPPS) techniques, which further piqued the interest of many researchers in the field of peptide synthesis, garnering him the Nobel Prize in Chemistry in 1984.[18] These techniques use the same chemistry as previous solution-phase methods, except now, the growing peptide is covalently linked to an insoluble, commonly polystyrene-based, solid support (or resin). The peptide is linked from the *C*-terminus, and peptide elongation occurs sequentially, the opposite of naturally synthesized peptides. Anchoring the growing peptide chain to solid support allows for the removal of excess reagents from the previous step, allowing for further coupling of subsequent amino acids. Initially, SPPS used *N,N*'-dicyclohexylcarbodiimide (DCC) as the coupling reagent, and Cbz or Boc (*tert*-butoxycarbonyl) as the *N*-terminal protecting group.[18] Furthermore, SPSS relied on "relative acidolysis" where the Boc or Cbz group were labile in strong acid (e.g., trifluoroacetic acid (TFA)), and release of the peptide from the solid support used hydrogen fluoride (HF).[18,19] However, an alternative protecting group, 9-fluorenylmethoxycarbonyl (Fmoc), was introduced, which required only a moderate base for the removal.[20] The Fmoc group allows for selective deprotection in the presence of acid-labile protecting groups, resulting in great control over peptide synthesis (**Scheme 1**).[20,21]

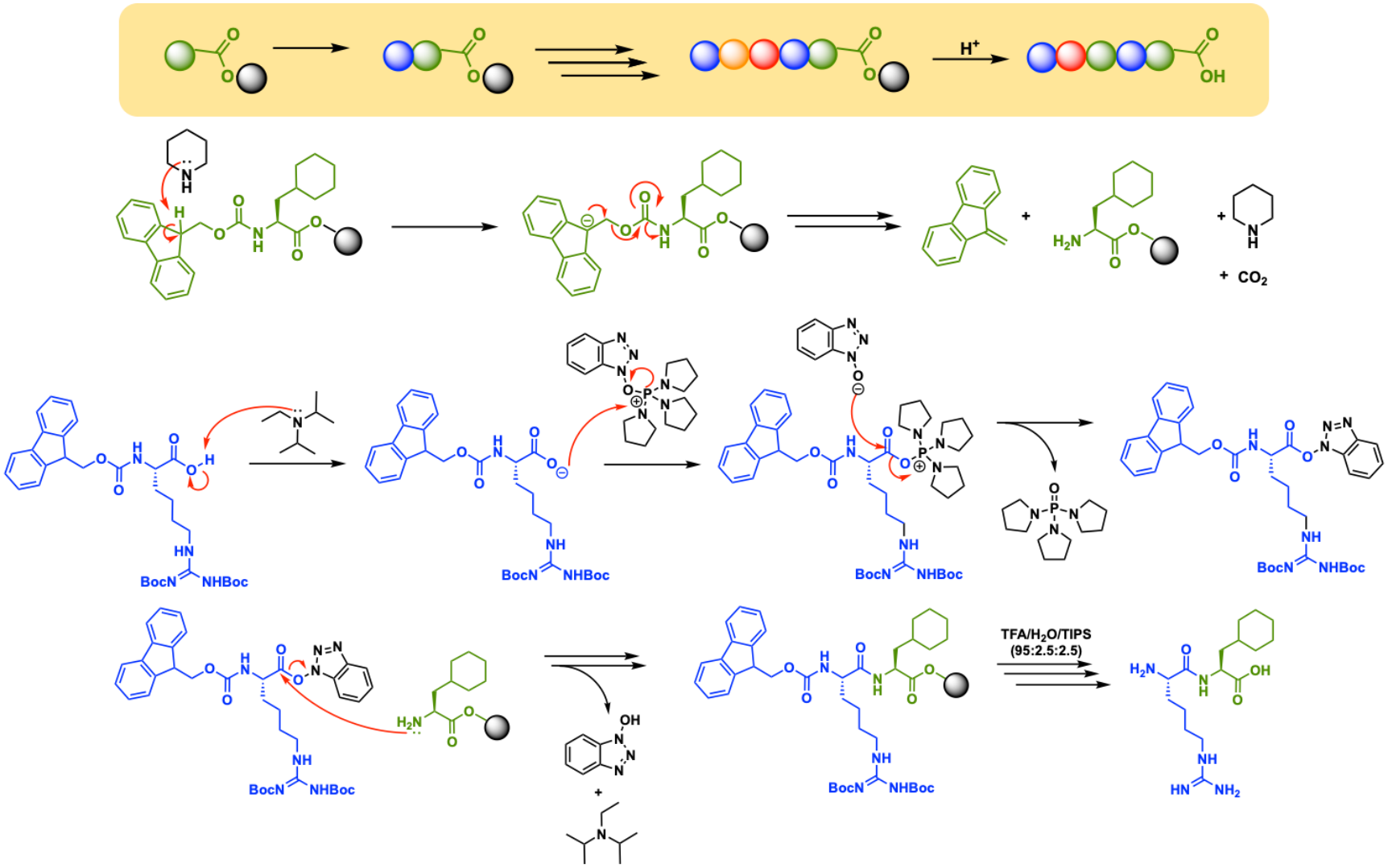


**Scheme 1** Schematic overview of solid phase peptide synthesis (SPPS).

With the rapid development in the field of SPPS, the development of more effective coupling reagents is needed. Peptide activity is highly dependent on the overall stereochemistry; however, many earlier coupling reagents tend to epimerize the $\alpha$-carbon, potentially resulting in an inactive peptide. $N^{\alpha}$-carbamate protecting groups slow epimerization but do not eliminate it entirely. New and more active coupling reagents (e.g., hydroxybenzotriazole/HOBt) were developed which activate the amino acid and allow for a rapid attack of the incoming nucleophile, therefore lowering the likelihood of racemization.[22,23] Peptide synthesis continues to evolve with new methodologies, with one being the development of automated peptide synthesizers which have allowed for the synthesis of long peptides (> 60 amino acids).[3,24–26]

### 1.1.4 Peptide Stability

Despite the many advantages of peptides being used as therapeutics, many limitations exist, especially when it comes to their susceptibility to proteolytic degradation. These enzymes cleave their respective peptide substrate to clear them from the bloodstream, resulting in the loss of therapeutic activity of the peptide. Many chemical modifications have been developed to mitigate this stability problem, including minor changes like the substitution with *D*-amino acids or amino acid isosteres,[27,28] methylation on the $\alpha$-carbon or -nitrogen,[28,29] and the incorporation of $\beta$- or aza-amino acids [30–32]. Furthermore, larger modifications can be implemented to increase stability and activity by enforcing rigidity in the secondary structures of these peptides.[3,33,34] These modifications (e.g., lactam formation between Lys to Glu or Asp) stabilize the secondary structure through covalent linkages, allowing these peptides to escape the binding pocket of degradative proteases.[3] These modifications provide a foundation for the rational design of peptides for the next generation of therapeutics.

# Chapter 2 Development of Apelin Peptides as Therapeutics for Cardiovascular Diseases

## 2.1 Project Background

### 2.1.1 Cardiovascular Diseases and Apelinergic System

Cardiovascular diseases (CVDs) are one of the leading causes of death in the world, accounting for approximately 31%, or 18 million, deaths per year worldwide.[35,36] In many countries around the world, CVDs continue to be a major burden on healthcare systems.[37] Coronary heart disease, which leads to heart failure, can result in myocardial infarction (MI), which is commonly referred to as a heart attack.[38] MI is often treated with percutaneous coronary intervention (PCI) to restore blood flow to the affected heart tissue; however, this process can lead to the production of reactive oxygen species and necrosis, eventually resulting in myocardial ischemia reperfusion injury (MIRI).[39] At present, there are no effective single-drug pharmaceuticals on the market for the treatment of MIRI, presenting a major challenge to physicians administering PCI.[39,40]

The human body is equipped with the apelinergic system, an endogenous cardioprotective hormone system which consists of the G-protein coupled apelin (APJ) receptor and the natural substrates, apelin and elabela.[41–44] Apelin has been physiologically shown as an influential regulator of several metabolic functions, including fluid homeostasis,[45] cardiovascular output,[46–49] and carbohydrate and fat metabolism.[50] In addition, apelin has been shown to be expressed at higher levels in various types of cancers, such as colon, gastroesophageal, glioblastoma, prostate, and oral squamous cell carcinoma.[51] In cancer diseases, apelin peptides induce cell proliferation

and migration in tumour neo-angiogenesis, as well as being a biomarker in cancerous tissues due to the elevated expression.[52] Recently, researchers have also found that the apelinergic system is involved in age-associated sarcopenia, or degradation of muscle tissue, where apelin levels are negatively correlated with age in rodent and human models.[53]

Apelin, the product of the human APLN gene, was first identified in bovine stomach extracts (apelin-36) as a ligand for the human orphan receptor APJR.[54] This X-linked gene, when transcribed, expresses a 77-amino acid long prepropeptide (**Fig. 2**).[55–57] The *N*- and *C*-termini have distinctive roles; the 22 *N*-terminal residues convey the secretory signal, and the 55 *C*-terminal residues are involved in receptor binding signalling.[58] The *N*-terminal amino acids are cleaved and the resulting apelin-55 is subsequently processed into bioactive peptides of various lengths forming apelin-36, apelin-17, and apelin-13.[54,59,60] This cleavage is catalyzed by proprotein convertase subtilisin kexin (PCSK), which recognizes the di-basic amino acid motifs. Furthermore, the *N*-terminal region of apelin-13 can be post-translationally modified to generate pyr-1-apelin-13, which is a more stable analogue than its counterpart;[61,62] this analogue is the major isoform in plasma[62] and the human heart[63]. The physiologically active isoforms of apelin all contain 12 conserved *C*-terminal amino acids, which contain some regions vital for its interactions with the APJ receptor. The "RPRL" region is the recognition motif required for receptor binding,[64,65] while the *C*-terminal Phe residue is essential for peptide internalization.

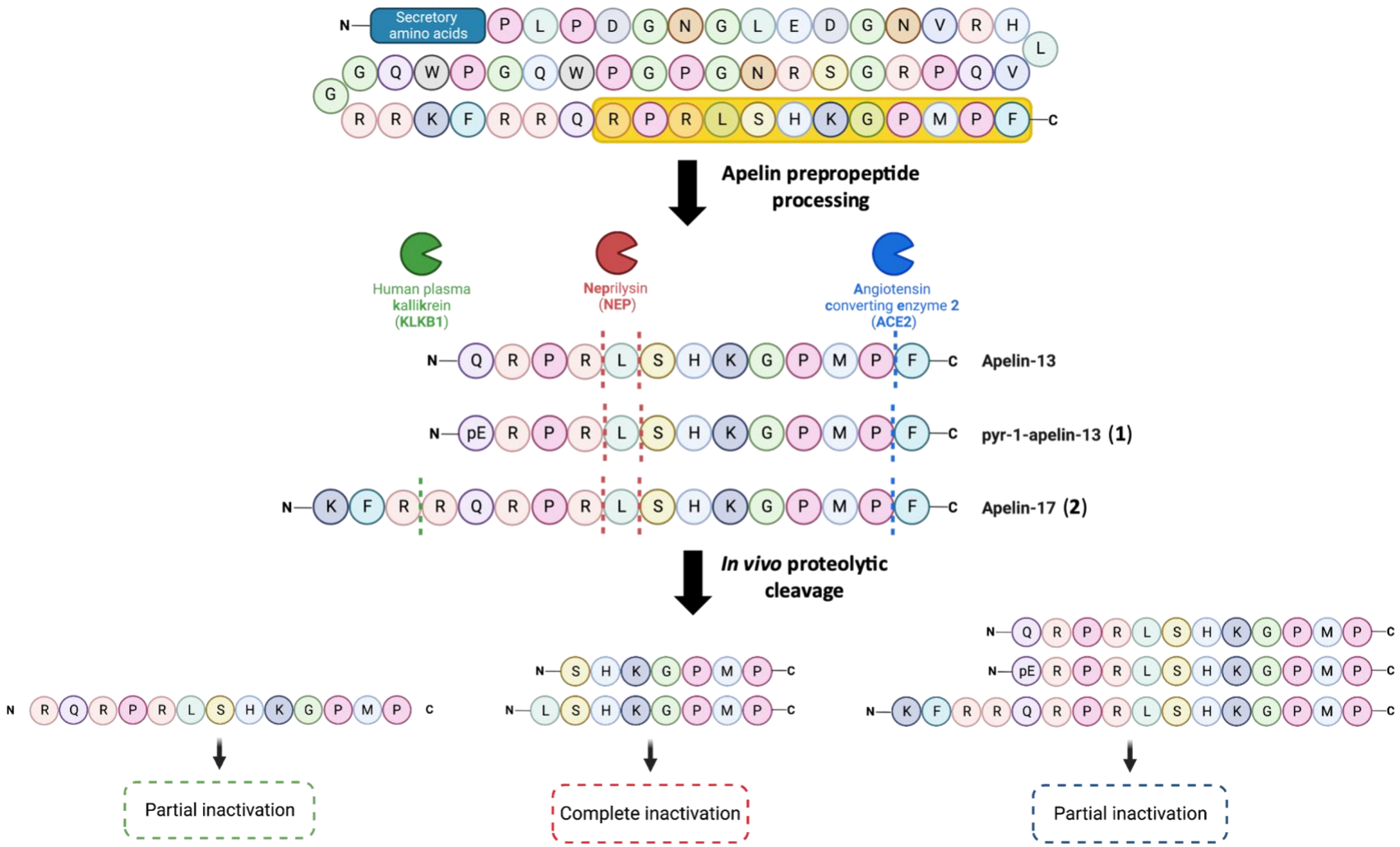


**Fig. 2** Apelin biochemistry pathway. The apelin (APLN) gene encodes a 77-amino acid prepropeptide, which is processed and cleaved into smaller active isoforms (apelin-13, pyr-1-apelin-13, and apelin-17). These isoforms are rapidly degraded by proteases (i.e., ACE2, NEP, and KLKB1) leading to the loss and/or reduction of cardiovascular protection. Secretory amino acids represent the 22 *N*-terminal

residues. The yellow box represents the 12 conserved *C*-terminal residues. Dotted lines represent the site of cleavage. pE = pyroglutamic acid. Created with BioRender.com.

### 2.1.2 Apelin Peptides and Proteolytic Enzymes and Resistant Analogues

Although apelin peptides play critical protective roles in the cardiovascular system, these peptides are quite limited in their biological half-life (<5 min); due to the rapid metabolism by several endogenous proteases, namely ACE2, NEP, and KLKB1 (**Fig. 2**).[47,66] First, ACE2, or angiotensin converting enzyme 2, catalyzes the hydrolysis of the *C*-terminal phenylalanine residue, generating partially inactive peptides apelin-12, pyr-1-apelin-12, and apelin-16.[67] Neprilysin, or NEP, cleaves at two sites within the critical "RPRL" region, to form fully inactive apelin fragments[57]; highlighting NEP as an endogenous negative regulator of apelin peptides. The third protease, KLKB1, the human plasma kallikrein, cleaves the three *N*-terminal residues of apelin-17, within the KFRR motif, to form apelin-14, a partially inactive peptide.[68] A decreased degradation of apelin peptides is desired as more stable analogues can illicit their protective effects longer (e.g., positive inotropy[69,70] and vasodilation/reduced afterload[46,47,66,71]) in instances of heart failure.

Various strategies have been tested on apelin-related peptides to enhance proteolytic stability, including the insertion of non-canonical amino acids[72], D-amino acids[72,73], and *N*- and *C*-methylation[57]. Our lab and many others have worked on apelin analogues which have shown improved plasma half-life *in vivo* (**Fig. 3**). Briefly, the incorporation of non-canonical amino acids at the first three *C*-terminal residues (i.e., the substitution of Met-Pro-Phe for Nle-Aib-BrF) or *C*-terminal lactamization resulted in complete resistance to ACE2, with retained cardiovascular activity and improved pharmacokinetics.[67,74,75] These analogues were referred to as the "A2" generation (**Fig. 4**). *N*- and $\alpha$-methylation at the leucine residue within the RPRL motif led to a significant increase in biological stability against NEP as well as a higher plasma half-life.[57] These analogues are referred to as the "NMe" generation (**Fig. 4**). Lastly, an extension of the *N*-terminus

*via* acylation using fatty acids,[68,76,77] PEGylation,[68,78,79] or the addition of a fluorocarbon chain[73] resulted in further improvement in stability, as well as cardiac inotropy, receptor binding affinity, and hypotensive effects. In combination, these modifications resulted in the target apelin-17 analogue, annotated as Fmoc-PEG$_6$-NMe17A2, exhibiting a plasma half-life of over 27 h *in vivo*, as well as improved physiological effects compared to the native apelin-17 peptide (**Fig. 4**).[68] This chapter will cover the work that was done on optimizing the biological stability of apelin peptides against KLKB1, the investigation of substrate-receptor interactions between the RPRL and KFRR motifs, and the peptide backbone with the apelin receptor, and lastly, the future work on establishing metabolic stability of apelin peptides *via* oral distribution.

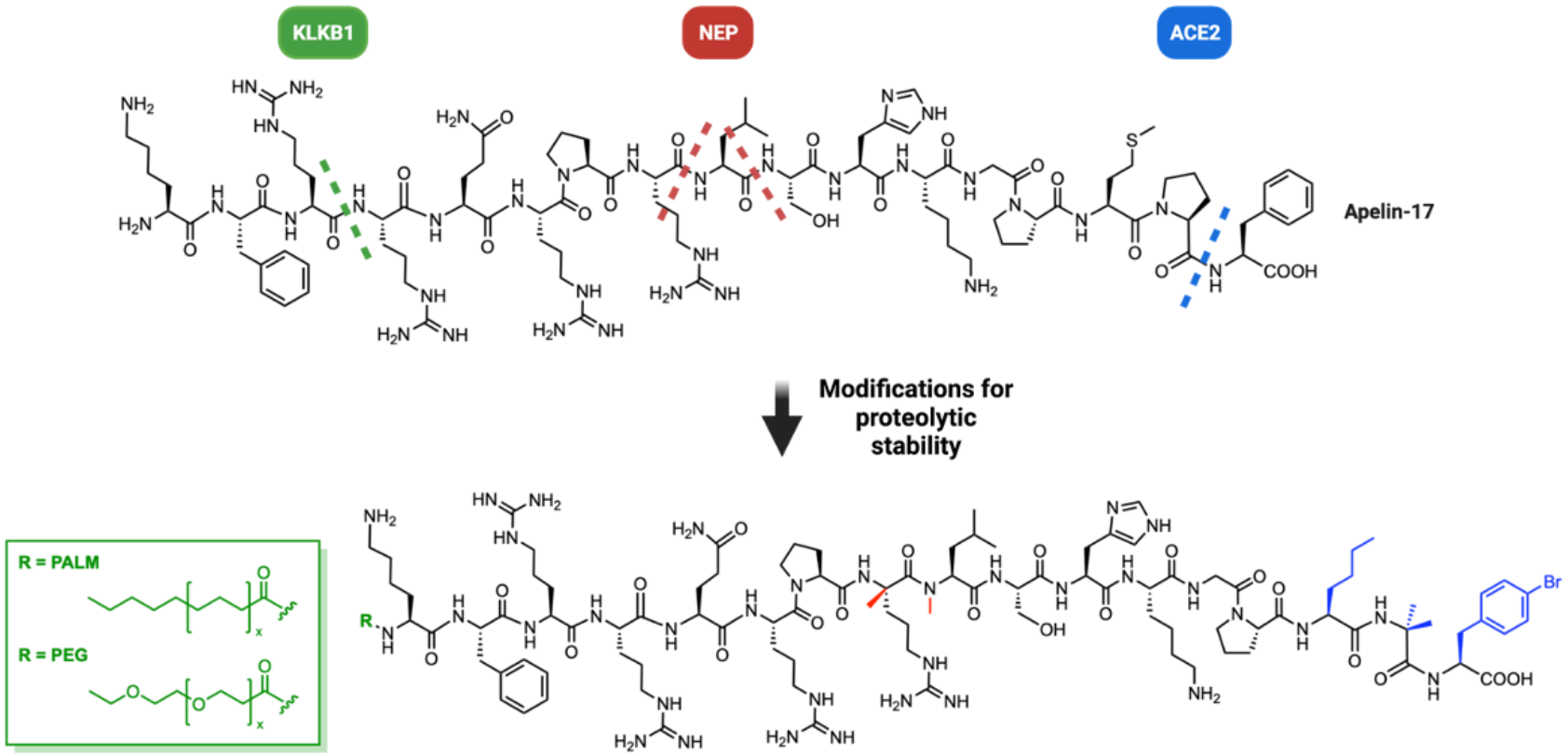


**Fig. 3** Chemical modifications on apelin-17 for improved proteolytic stability. Modifications are highlighted in different colours: for angiotensin converting enzyme 2 (ACE2: Nle-AIb-BrF substitution for Met-Pro-Phe) depicted in blue; for neprilysin (NEP): $\alpha$- and N-methylation) in red, and human plasma kallikrein (KLKB1: extension with PALM and PEG chain) in green.

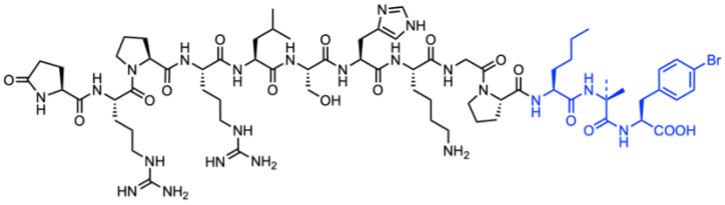

Apelin-13A2 (**3**)

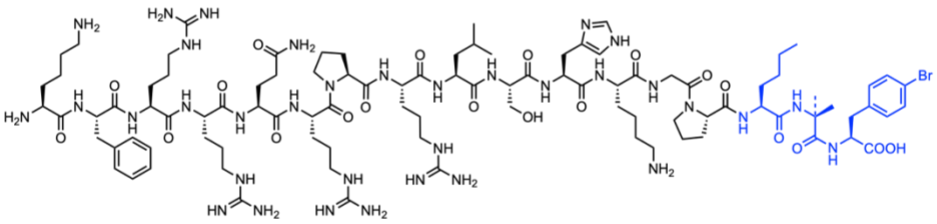

Apelin-17A2 (**4**)

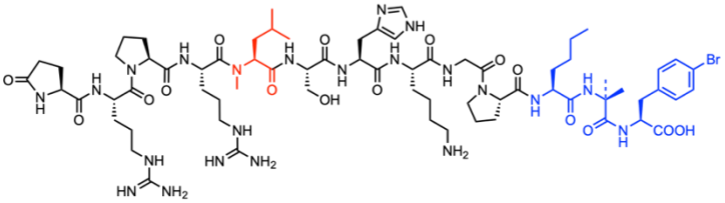

NMe13A2 (**5**)

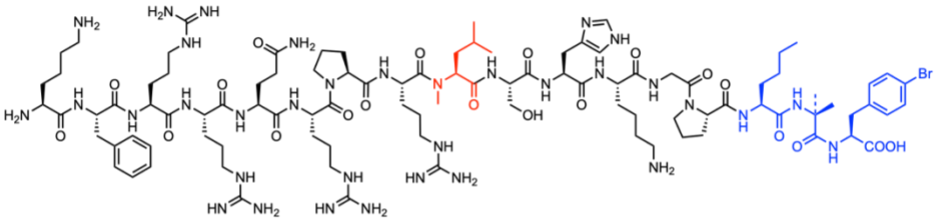

NMe17A2 (**6**)

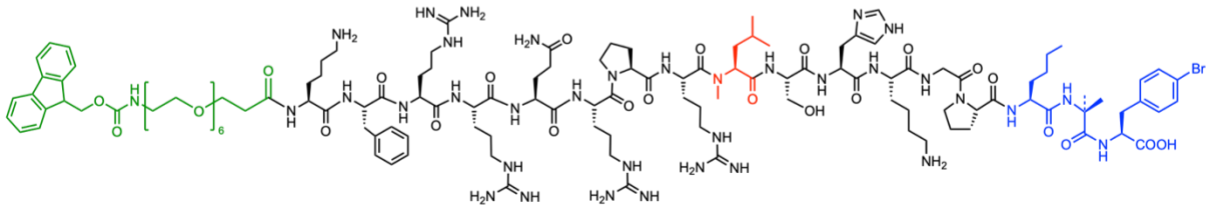

Fmoc-PEG$_6$NMe17A2 (**7**)

**Fig. 4** Structures of the apelin analogues (**3-7**) from three generations of modifications. Chemical modifications are depicted by the different colours: blue for ACE2 resistance, red for NEP resistance, and green for KLKB1 resistance.

## 2.2 Optimization of PEG-Extended Apelin Peptides

### 2.2.1 Background and Aims of Study

In addition to proteolytic cleavage by ACE2 and NEP, apelin peptides also contain a cleavage site for the human plasma kallikrein, KLKB1, at the *N*-terminal.[68] Our lab has previously published on *N*-terminally extended apelin-17 analogues with modifications to address the three proteases, resulting in the development of the Fmoc-PEG$_6$-NMe17A2 analogue.[57,67,68,80] We initially suggested *N*-terminal extension *via* PALMitoylation (with a fatty acid) or PEGylation (with a polyethylene glycol chain) as potential stabilization approaches to increase the size of the peptide enough to escape the active site pocket volume of 2500 g/mol.[68] We hypothesized that this extension would not affect the conformational integrity of the *N*-terminus; the respective PEGylation substantially improved the proteolytic stability and cardio-physiological effects (**7**, **Fig. 4**). In our initial study, we used an Fmoc-protected PEG$_6$-tether attached to the $\alpha$-amino group of the *N*-terminal lysine. This analogue led to a remarkable 27 h plasma half-life in human plasma *in vivo* and excellent blood-pressure-lowering effects, however, the potential carcinogenicity or cytotoxicity of the fluorenyl system led us to investigate suitable replacements for the Fmoc protecting group.

In this study, additional apelin peptides were synthesized by myself, Dr. Conrad Fischer, and Tess Lamer, based on the Fmoc-PEG$_6$-NMe17A2 analogue to address two questions: (1) what are the ideal length and optimal biocompatible head groups for the *N*-terminal tether (**8**-**16**, **Fig. 5**), and (2) is it possible to improve the blood-pressure-lowering effects and physiological durability of apelin-13 peptides by attaching a long PEG-tether (**17**-**18**, **Fig. 5**)[79] The effects of these analogues, with varying PEG chain lengths and head group modifications, on stability,

receptor binding, and cardiovascular activity are reported. In addition, the physiological activity of the optimized apelin-17 analogues towards the prevention of MIRI was tested by Dr. Gavin Oudit's research group *via* a Langendorff ischemia-reperfusion assay to determine its potential as a lead therapeutic for drug-based MIRI treatment.[81]

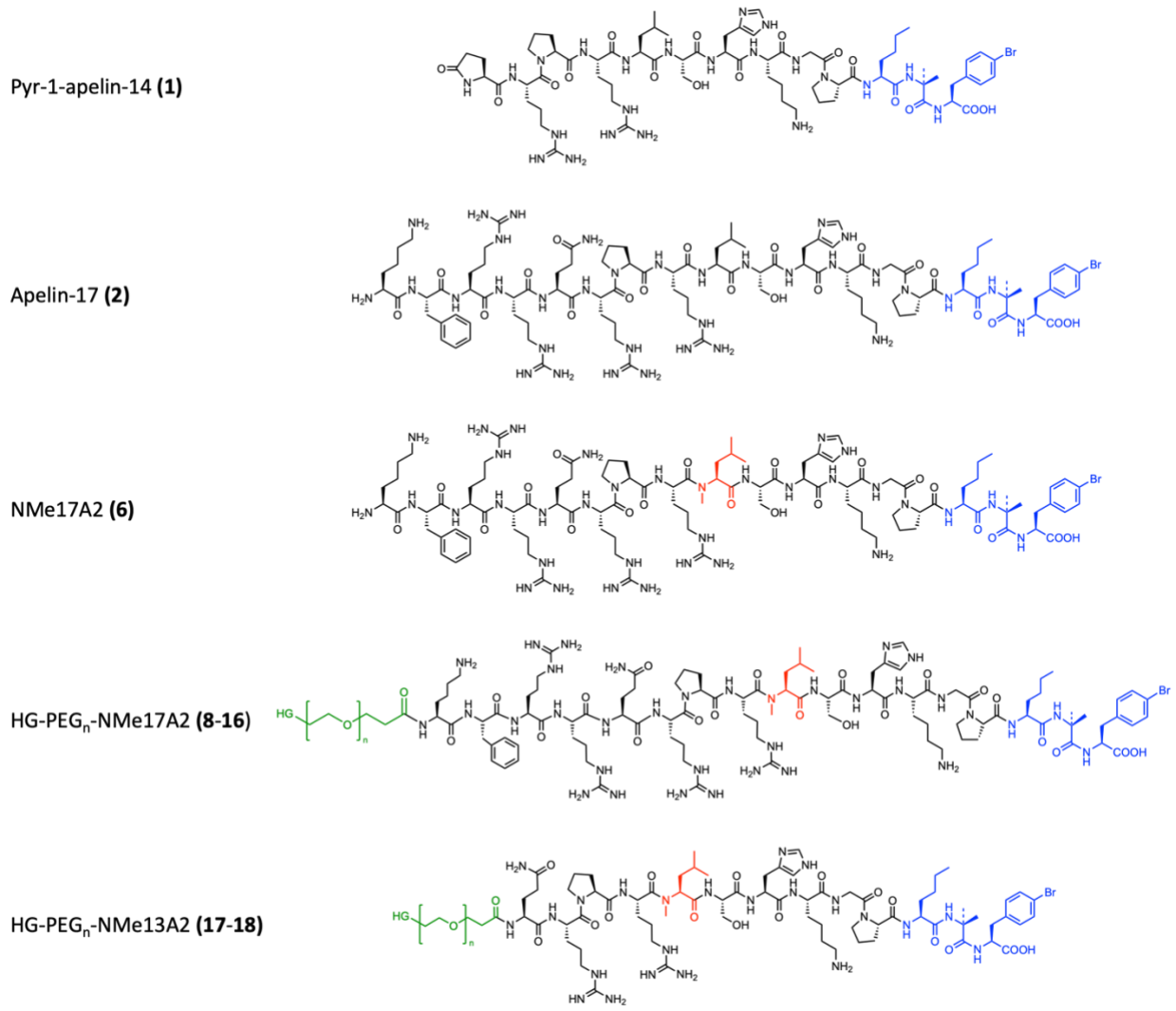


**Fig. 5** Isostere-substituted and *N*-terminally PEG-extended apelin analogues (**1**, **2**, **6**, **8-18**) used in this study. Chemical modifications are depicted by the different colours: blue for ACE2 resistance, red for NEP resistance, and green for KLKB1 resistance. HG = head group.

### 2.2.2 Results and Discussion

#### 2.2.2.1 Tether and Head Group Optimization

A series of apelin-17 analogues containing either an Fmoc, methoxy, or free amine headgroups, as well as PEG chains including 3, 4, 6, or 10 monomer units (**8-16**, **Fig. 6**) were synthesized. Furthermore, three apelin-17 analogues incorporating the same $PEG_6$-chain, with either a carboxybenzyl (Cbz, **13**), a *para*-benzoylphenylalanine residue with a free *N*-terminus (pBpa, **14**), or a phenylalanine residue with a free *N*-terminus (Phe, **15**) *N*-terminal head group. These more biocompatible head groups represent less toxic and better pharmacophoric targets. These analogues (**13**-**15**) were made to test whether aromaticity in the head group was sufficient for increased physiological activity and whether a free *N*-terminal amine impedes this activity.

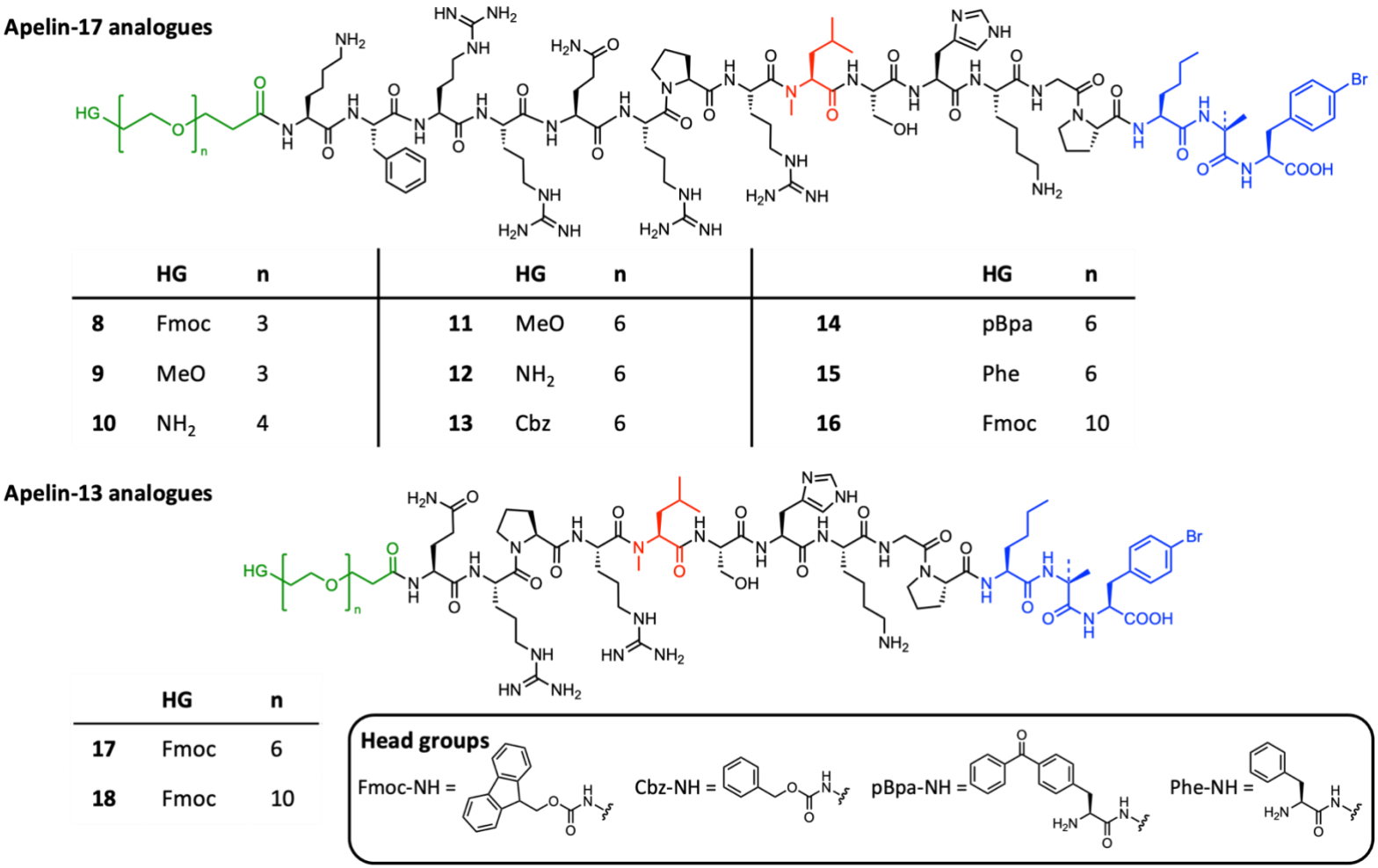


| | HG | n | | HG | n | | HG | n |
|---|---|---|---|---|---|---|---|---|
| **8** | Fmoc | 3 | **11** | MeO | 6 | **14** | pBpa | 6 |
| **9** | MeO | 3 | **12** | $NH_2$ | 6 | **15** | Phe | 6 |
| **10** | $NH_2$ | 4 | **13** | Cbz | 6 | **16** | Fmoc | 10 |

| | HG | n |
|---|---|---|
| **17** | Fmoc | 6 |
| **18** | Fmoc | 10 |

**Fig. 6** PEG-extended apelin-17 (**8-16**) and apelin-13 (**17-18**) analogues. Chemical structures of the head groups (HG) are displayed in the box; n = number of units.

Regarding plasma stability, a trend is seen where increasing the length of the PEG-chain supports improved plasma stability, where the $PEG_6$-analogues, except **11**, were the most stable (Table 1). This increase in stability is observed in both human and murine plasma, although more pronounced in the human plasma assays, and we propose that this is likely caused by an increased self-aggregation. Considering the remarkable 27 h half-life of the Fmoc-$PEG_6$ (**7**) and the 18 h half-life of Cbz-$PEG_6$ (**13**) analogues in human plasma, compared to the free *N*-terminal head groups, shows that the *N*-terminal aromaticity may additionally boost proteolytic resistance likely through secondary effects (e.g., membrane interactions). In addition, the higher plasma protein binding detected for analogues **7** and **13**, in comparison to the non-PEGylated analogue **6**, may contribute to higher plasma stability (**Table 2**).[82] Comparing the head group modifications, an increase of stability for carbamates **7** and **13**, compare to amides **14** and **15**, were prevalent, supporting the superior metabolic stability of carbamates as amide bond surrogates.[83] Furthermore, the relatively lower plasma half-life of the Phe-$PEG_6$ analogue **15** may be due to the aminopeptidase cleavage of the phenylalanine residue; the resulting cleavage compound **12** also shows a lesser extent of plasma protein binding (**Table 2**).[84]

**Table 1** Proteolytic stability, calcium mobilization, receptor binding, and blood-pressure data of *N*-terminally-modified apelin analogues. Calcium mobilization efficacy relative to **2** (= 100%). The average difference in mean arterial blood pressure is reported for before and after compound administration. Experiments were performed in duplicates of three replicates. Errors are S.E.M.

| | **Apelin analogue** | **$t_{1/2}$ human plasma (h)** | **$t_{1/2}$ murine plasma (h)** | ***p*$EC_{50}$** | **$Ca^{2+}$ mobilization efficacy (%)** | ***p*$IC_{50}$ binding affinity (nM)** | **$\Delta_{MABP}$ (mmHg)** |
|---|---|---|---|---|---|---|---|
| **1** | pyr-Apelin-13 (native) | 0.1 ± 0.03 | | 8.62 ± 0.15 | 93 | 9.52 ± 0.09 | -15 ± 5 |
| **2** | Apelin-17 (native) | 0.02 ± 0.01 | 0.03 ± 0.02 | 8.72 ± 0.18 | 100 | 10.30 ± 0.08 | -17 ± 4 |
| **6** | NMe17A2 | 1.2 ± 0.1 | 0.9 ± 0.2 | 8.31 ± 0.08 | 104 | 9.22 ± 0.07 | -36 ± 4 |
| **7** | Fmoc-$PEG_6$-NMe17A2 | 27 ± 0.4 | 2.8 ± 0.7 | 8.60 ± 0.20 | 108 | 9.26 ± 0.10 | -47 ± 5 |
| **8** | Fmoc-$PEG_3$-NMe17A2 | 2.0 ± 0.5 | | 7.77 ± 0.17 | 111 | 8.60 ± 0.15 | -32 ± 9 |
| **9** | MeO-$PEG_3$-NMe17A2 | 2.8 ± 0.6 | | 7.27 ± 0.14 | 106 | 8.48 ± 0.07 | -32 ± 3 |
| **10** | $NH_2$-$PEG_4$-NMe17A2 | 2.0 ± 0.3 | | 8.11 ± 0.14 | 99 | 8.20 ± 0.12 | -24 ± 9 |
| **11** | MeO-$PEG_6$-NMe17A2 | 0.7 ± 0.1 | | 8.09 ± 0.17 | 95 | 8.77 ± 0.09 | -30 ± 10 |
| **12** | $NH_2$-$PEG_6$-NMe17A2 | 3.0 ± 0.2 | | 8.54 ± 0.13 | 96 | 8.77 ± 0.17 | -35 ± 7 |
| **13** | Cbz-$PEG_6$-NMe17A2 | 18.2 ± 0.3 | 2.9 ± 0.8 | 8.21 ± 0.12 | 120 | 8.72 ± 0.06 | -43 ± 6 |
| **14** | pBpa-$PEG_6$-NMe17A2 | 8.2 ± 0.8 | | 7.05 ± 0.09 | 122 | 8.89 ± 0.14 | -43 ± 5 |
| **15** | Phe-$PEG_6$-NMe17A2 | 6.4 ± 0.8 | | 7.59 ± 0.15 | 103 | 8.77 ± 0.05 | -24 ± 7 |
| **16** | Fmoc-$PEG_{10}$-NMe17A2 | 17.2 ± 0.6 | | 8.31 ± 0.15 | 105 | 8.62 ± 0.13 | -28 ± 8 |
| **17** | Fmoc-$PEG_6$-NMe13A2 | 6.9 ± 0.3 | | 7.31 ± 0.11 | 103 | 8.52 ± 0.18 | -9 ± 1 |
| **18** | Fmoc-$PEG_{10}$-NMe13A2 | 8.6 ± 0.3 | | < 6.70 | 116 | 8.72 ± 0.12 | +1 ± 6 |

**Table 2.** Plasma protein binding and $logD_{7.4}$ of select apelin analogues. Experiments were performed on duplicates of three replicates. Errors are S.E.M.

| | Apelin analogue | Human plasma protein binding (%) | Murine plasma protein binding (%) | $logD_{7.4}$ |
|---|---|---|---|---|
| **2** | Apelin-17 (native) | 57 ± 10 | 51 ± 15 | -2.57 ± 0.15 |
| **6** | NMe17A2 | 52 ± 11 | 55 ± 13 | -2.01 ± 0.11 |
| **7** | Fmoc-$PEG_6$-NMe17A2 | 94 ± 6 | 89 ± 7 | -1.45 ± 0.20 |
| **12** | $NH_2$-$PEG_6$-NMe17A2 | 79 ± 10 | 69 ± 14 | -1.82 ± 0.16 |
| **13** | Cbz-$PEG_6$-NMe17A2 | 85 ± 5 | 83 ± 4 | -1.54 ± 0.19 |

Calcium release can be used as an indicator for G-protein activation, and lower effective concentrations can be seen in all $PEG_6$ analogues compared to the shorter extended isoforms (**Fig. 7**). This improved receptor activation may partially result from the higher affinity binding to the APJ receptor compared to the shorter PEG isoforms (Table 1). Furthermore, the excellent plasma stability and APJ receptor activation of the $PEG_6$ analogues **7** and **13** correlated with a strong hypotensive effect with an average mean arterial blood pressure drop of ~ 47 and ~ 43 mmHg, respectively (Table 1, Fig. 8). In fact, this time-stable MABP drop was superior to the native apelin-17 peptide **2** and the NMe17A2 analogue **6**.

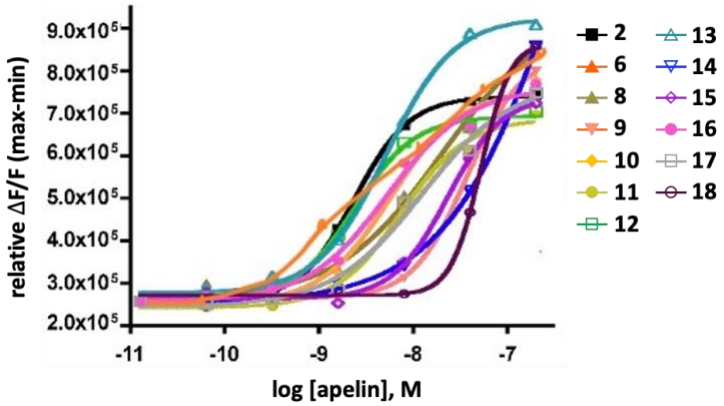


**Fig. 7** Concentration-response curves of $Ca^{2+}$-mobilization triggered by PEG-substituted apelin analogues (**6**, **8-18**) in comparison to native compound **2**. Experiments were performed in three replicates. Values represent means ± S.E.M.

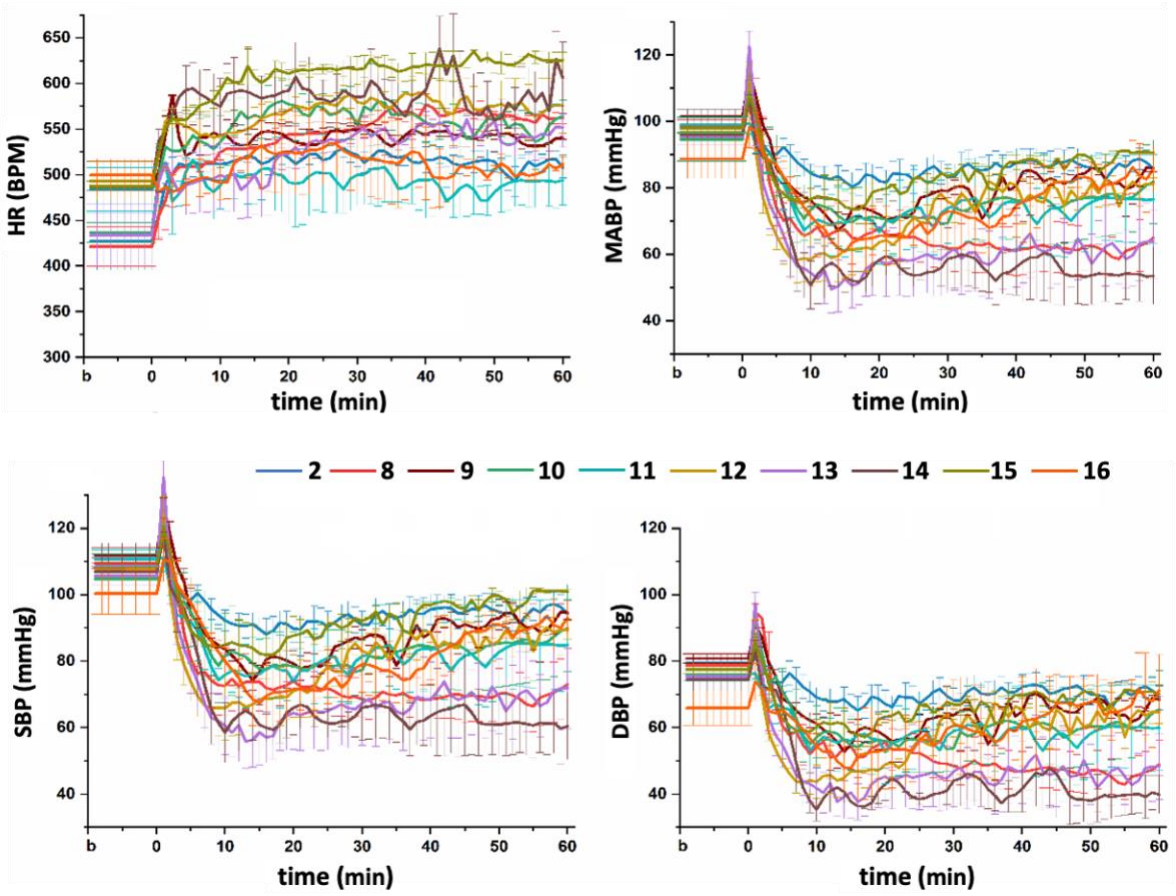


**Fig. 8** Changes in heart rate (HR), mean arterial blood pressure (MABP), and systolic (SBP) and diastolic (DBP) blood pressure after IV injection of apelin analogues (**2**, **8-16**). One-way ANOVA

statistical analysis indicated no significant changes in MABP ($p > 0.05$). The experiments were done in triplicates. Values represent means ± S.E.M.

#### 2.2.2.2 PEG-Extended Apelin-13 Analogues

NMe13A2, compound **5**, surprisingly showed low hypotropic effects in mice, contrary to the longer NMe17A2 analogue, compound **6**, which had better physiological activity (Fig. 4).[57] Therefore, the extension of the apelin-13 compound with either an Fmoc-$PEG_6$ (**17**)or Fmoc-$PEG_{10}$ (**18**) chain was performed to evaluate if PEGylation could restore physiological activity (**Fig. 5**). If successful, this surrogate approach would make peptide synthesis more facile (13-mers vs. 17-mers) and eliminate additional cleavage sites found in the longer isoforms. A $PEG_{10}$ chain was chosen to achieve approximately the same molecular weight as the Fmoc-$PEG_6$-NMe17A2 (**7**) analogue. Both analogues **17** and **18** showed moderate stability ($t_{1/2}$ = ~ 6.9 and 8.6 h) in human plasma, which is significantly higher than that for the native pyr-1-apelin-13 (**1**), but still significantly lower than the size-related NMe17A2 analogues **7** and **16**. Both analogues triggered calcium release at higher concentrations compared to **1** and **7** (Table 1, Fig. 7). However, both analogues **17** and **18** had negligible physiological activity in the blood-pressure assays ($p > 0.05$; Table 1, Fig. 9). This suggests that the simple addition of the molecular length of the inactive NMe13A2 backbone can extend proteolytic stability but does not restore full biological activity. These results may indicate that the four *N*-terminal residues (KFRR) in the 17-mer analogues are required for apelin peptides to exert the targeted physiological effects.

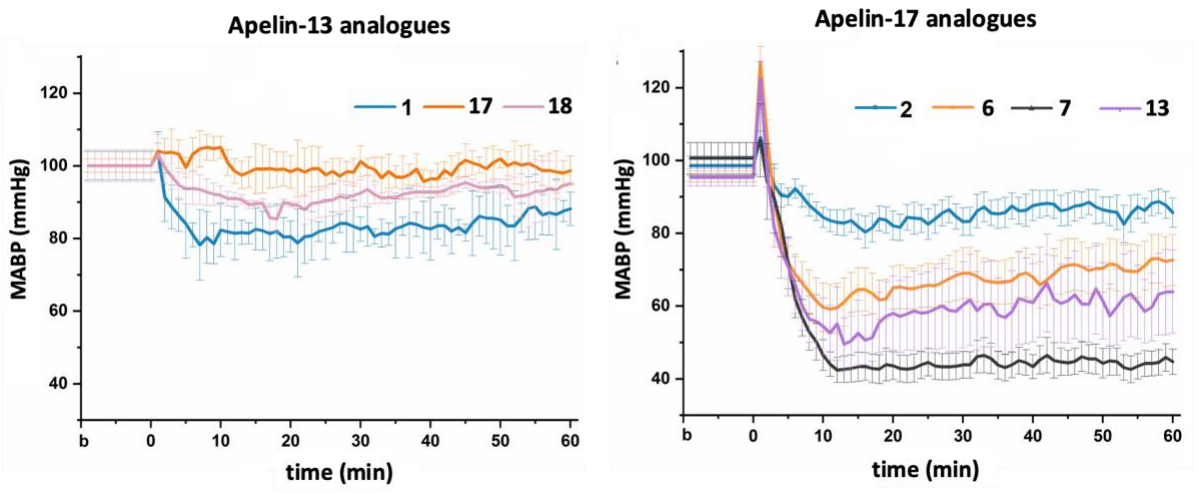


**Fig. 9** Mean arterial blood pressure (MABP) data of PEG-extended apelin-13 (**17-18**) and -17 analogues (**6-7**, **13**). Experiments were performed in three replicates. Values represent mean ± S.E.M.

### 2.2.2.3 Physiological and Cardioprotective Potential Experiments

The two most potent analogues, with regards to plasma stability and hypotensive activity, Fmoc-PEG$_6$-NMe17A2 (**7**) and Cbz-PEG$_6$-NMe17A2 (**13**), were then assessed by Dr. Oudit's lab for their ability to prevent myocardial ischemia reperfusion injury (MIRI) using the Langendorff protocol.[81] Stable isolated mice hearts were subjected to ischemic conditions for 30 mins and then were reperfused with either saline (vehicle), native apelin-17 (**2**), NMe17A2 (**6**), and the vasoactive analogues **7** and **13**; 1 $\mu$M concentrations were used as per the postconditioning protocol (**Fig. 10**). The heart was measured *ex vivo* to establish the following parameters to indicate heart performance and function: left ventricle developed pressure (LVDP), the rate-pressure product (RPP), the minimum derivative of change in diastolic blood pressure over time (min dP/dt), and the maximum derivative of change in systolic blood pressure over time (max dP/dt). Compounds **2** (LVDP = 30 ± mmHg; RPP = 1019 ± 215) and **6** (LVDP = 25 ± 7 mmHg; RPP = 778 ± 132) showed relatively minor effects. Surprisingly, both analogues **7** (LVDP = 90 ± 2

mmHg; RPP = 2051 ± 204) and **13** (LVDP = 119 ± 6 mmHg; RPP = 2604 ± 214) showed a pronounced magnitude and prolongation in effect, therefore demonstrating an improved ability to rescue the heart from MIRI. These results indicate the potential of vasoactive analogues **7** and **13** for an overall rapid and enduring heart recovery with minimal heart damage post-MIRI.

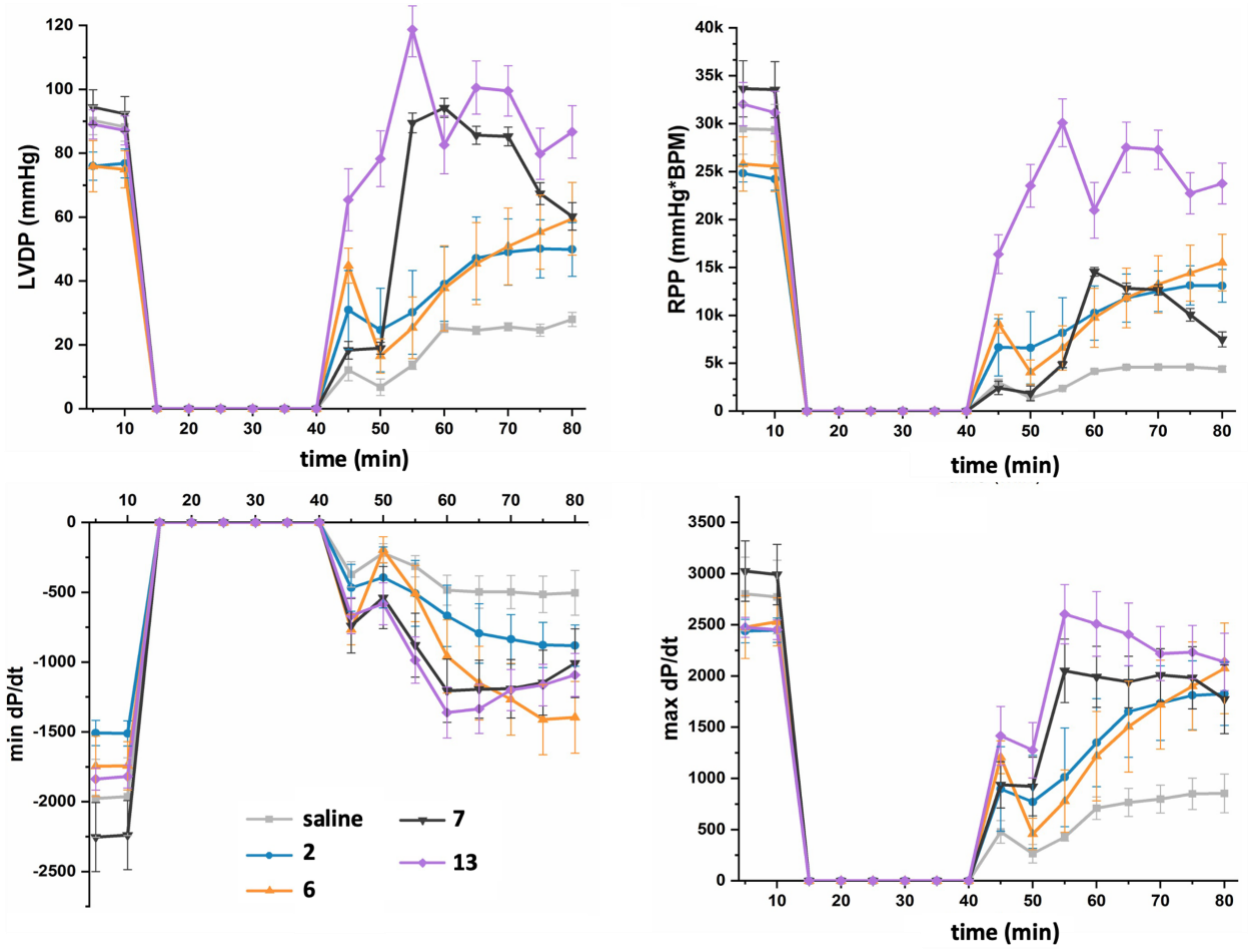


**Fig. 10** Langendorff isolated heart experiments of select apelin analogues. Results were reported following reperfusion of saline (negative control), native apelin-17 (**2**, positive control), NMe17A2 analogue **6**, and PEG-extended analogues **7** and **13**, after a 30 min period of ischemia. Parameters assessed include the left ventricular developed pressure (LVDP), the rate pressure product (RPP, mmHg × BPM), the minimum derivative of change in diastolic pressure over time (min dP/dt), and the maximum derivative of change in systolic pressure over time (max dP/dt). The experiments were performed in five replicates. Values represent mean ± S.E.M.

### 2.2.3 Conclusion and Future Studies

The development of therapeutics that are selective for target sites is vital to sustainably address and treat cardiovascular diseases. Except for surgical procedures, effective single drug-based treatments have not been significantly established for MIRI. In this project, we presented optimized *N*-terminally PEG-extended apelin-17 analogues with long plasma half-lives and time-stable cardioprotective benefits. We found that the addition of six ethylene glycol units ($PEG_6$), with an *N*-terminal Fmoc (**7**) or Cbz (**13**) group has been found optimal for plasma stability, hypotensive effects, and promising potential for MIRI rescue. These analogues can be used as lead structures for further MIRI-related drug design and cardioprotective potential.

Our results also show that the *N*-terminal KFRR sequence may be crucial for functionality, as the shorter PEG-extended apelin-13 isoforms do not show cardio-physiological effects, as shown in the blood pressure assays performed by Dr. Oudit's group. Further studies could be employed to investigate the structural importance of the four *N*-terminal residues in receptor binding and activity through isostere substitutions and alanine scans. In addition, our group is undertaking work to study the beneficial balance of the pharmacokinetics (PK) and pharmacodynamics (PD) properties of headgroup-PEGylated apelin-17 analogues for wider applications in various cardiovascular disease systems.[44,52,85–88]

## 2.3 Determining the Importance of hArg/Cha Modifications in the RPRL Region

### 2.3.1 Background and Aims of Study

A recently published X-ray crystal structure of an inactive modified APJ receptor, in complex with an inactive apelin derivative (AMG3054), suggests substrate-receptor binding

interactions at a minimum of two sites.[89] Two approaches, amino acid isostere substitution and macrolactamization between Glu8 and Lys5, were used in combination to structurally rigidify the peptidic analogue AMG3054 to allow for a better fit into the modified APJ receptor. Among these modifications, L- cyclohexylalanine (L-Cha) and L-homoarginine (L-hArg) were introduced at positions 9 and 10 from the C-terminus within the "RPRL" receptor binding site. Despite an apparent good fit, the impact of AMG3054 on the agonistic vs. antagonistic interactions with the native APJ receptor was not disclosed.

This chapter will look at the work performed to examine the metabolic stabilization and receptor activation of these homologue-substituted apelin peptides by dissecting the individual and combined binding contributions of these substitutions. Since these substitutions are situated within the RPRL binding motif, even minute spatial changes in this region may likely affect the overall receptor binding and conformation change, which could define the extent of downstream G-protein signalling. Starting from the first generation "A2" analogues **3** and **4**, already shown to possess higher proteolytic resistance compared to the native isoforms,[67] nine new derivatives (**3**-**5**, **8**-**13**), incorporating methylation and/or L-Cha/L-hArg at positions 9 and 10, respectively, were synthesized (**Fig. 11**). The metabolic stability of these analogues was determined through the isolated enzyme and human and mice plasma assays. In addition, the analogues were further characterized for their receptor activation through their capacity for calcium mobilization by Dr. Catherine Llorens-Cortès' research group. Lastly, *in vivo* blood pressure assays in mice were performed by Dr. Oudit's research lab to determine cardioprotective effects.

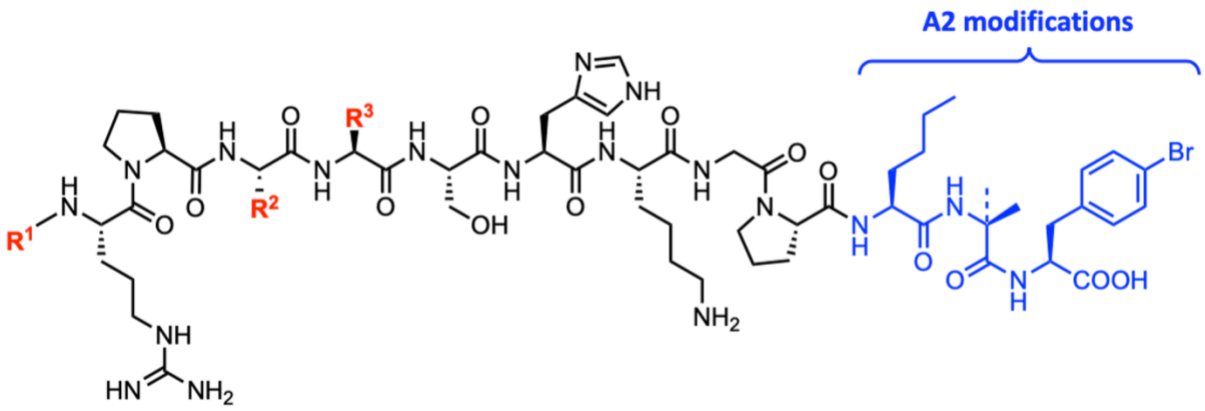


| | R¹ | R² | R³ | | R¹ | R² | R³ |
|---|---|---|---|---|---|---|---|
| **3** | pGlu | Arg | Leu (13A2) | **4** | KFRRQ | Arg | Leu (17A2) |
| **5** | pGlu | Arg | *N*MeLeu (NMe13A2) | **6** | KFRRQ | Arg | *N*MeLeu (NMe17A2) |
| **19** | pGlu | hArg | Leu | **22** | KFRRQ | hArg | Leu |
| **20** | pGlu | Arg | Cha | **23** | KFRRQ | Arg | Cha |
| **21** | pGlu | hArg | Cha | **24** | KFRRQ | hArg | Cha |
| | | | | **25** | KFRRQ | Arg | *N*MeCha |
| | | | | **26** | KFRRQ | hArg | *N*MeCha |
| | | | | **27** | KFRRQ | hArg | *N*MeLeu |

**Fig. 11** Apelin derivatives synthesized in this study. ACE2-resistant analogues (**3**, **4**), NEP-stabilized analogues (**5**, **6**), and newly synthesized derivatives (**19**-**27**) based on the A2 analogue generation. pGlu = L-pyroglutamic acid; hArg = L-homoarginine; Cha = L-cyclohexylalanine; *N*MeLeu = *N*-methylated L-leucine; *N*MeCha = *N*-methylated L-cyclohexylalanine.

### 2.3.2 Solid-phase peptide synthesis and dipeptide synthesis

Starting from the ACE2-resistant analogue series (compounds **3** and **4**),[67] we attempted to achieve improved metabolic stabilization through relatively conservative homologue substitution (i.e., L-hArg and/or L-Cha substitution). This approach has the advantage of affordable and commercially available amino acids, which can be readily incorporated via solid phase peptide synthesis (SPPS) in good yield. Additionally, it has been reported that the use of L-hArg and L-Cha in other studies may have intrinsic advantages for cardiovascular activity. L-Cha has been shown to increase regulatory function in body fluid and blood pressure homeostasis, as well as exhibit

vasodilatory activities when substituted for phenylalanine in an atrial natriuretic peptide.[54,90,91] L-hArg has been shown as an independent protective biomarker,[92,93] where lower L-hArg plasma levels were correlated with reduced nitric oxide bioavailability[94] and renal failure[95]. Furthermore, L-hArg can be metabolically formed through the replacement of ornithine for lysine in liver enzyme-catalyzed reactions in urea cycles[96,97] or *via* L-arginine:glycine amidinotransferase (AGAT) catalysis[98], further contributing to its role as a biomarker.

Apelin analogues **19-21** (apelin-13) and **22-27** (apelin-17) were synthesized on 2-chlorotritylchloride-resin using Fmoc-chemistry. The incorporation of the appropriate Arg/Leu to hArg/Cha modifications was completed after the formation of the octapeptide. Since the peptides also intend to address stability toward NEP cleavage, *N*-methylation of residue 9 (i.e., Leu or Cha) was performed to compare the metabolic and physiological features of *N*MeA2 generation analogues **5** and **6** (**Scheme 2**).[57]

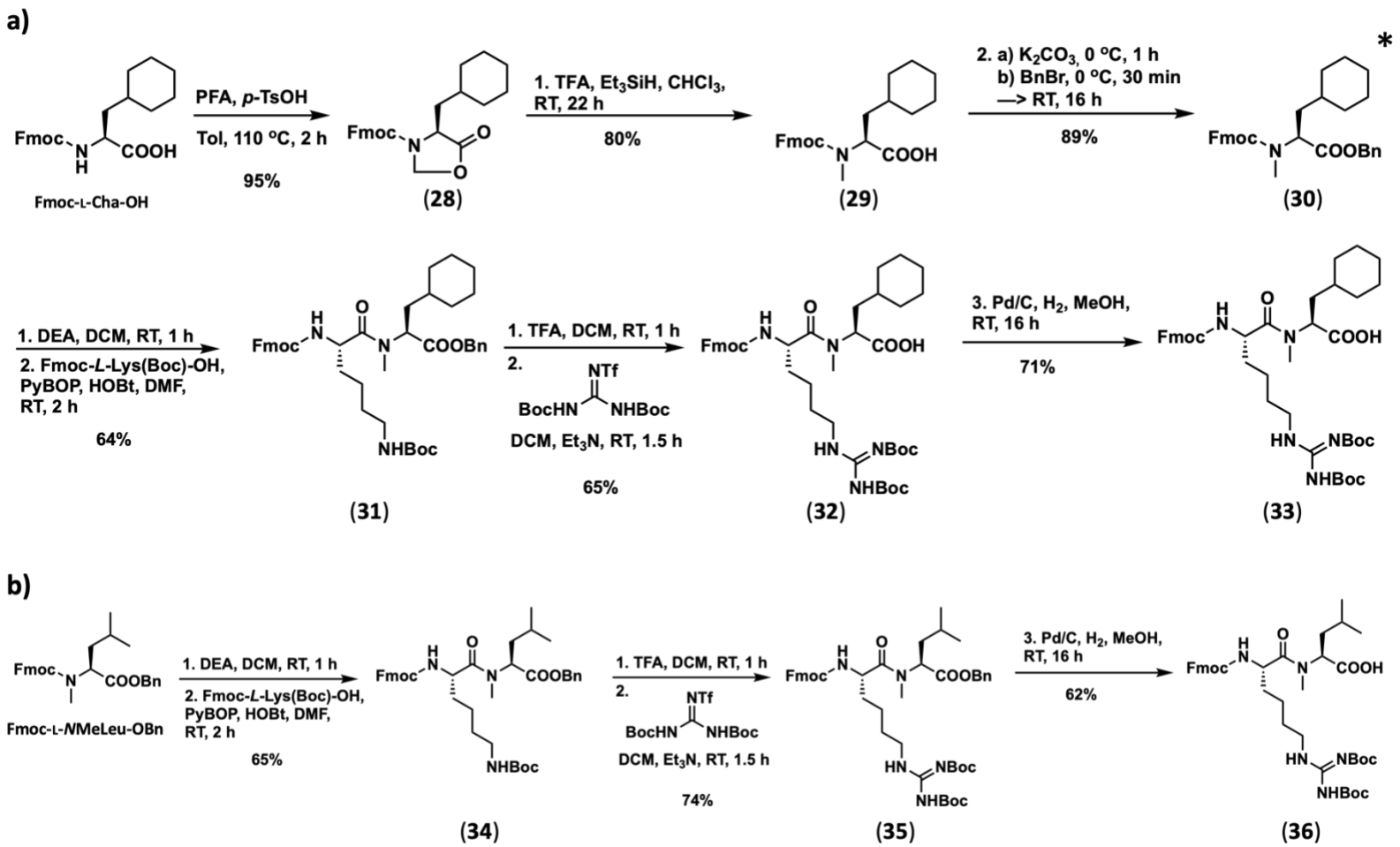


**Scheme 2** Synthetic scheme for *N*-methylation of L-Leu or L-Cha at position 9. * = Direct coupling of **30** (Fmoc-*N*MeCha-OBn) to Ser9 of growing peptide chain or formation of dipeptide **33**. PFA = paraformaldehyde; *p*-TsOH = *para*-toluenesulfonic acid; TFA = trifluoroacetic acid; $Et_3SiH$ = triethylsilane.

### 2.3.3 *In vitro* Enzymatic and Plasma Stability

First, the *in vitro* recombinant human neprilysin (*rh*NEP) stability of the newly developed analogues was compared to the native peptides, the ACE2-resistant first-generation analogues (**3**, **4**), and the NEP-stabilized pendants (**5**, **6**) (Table 3, Fig. 12). The apelin peptides were incubated with *rh*NEP and the extent of degradation was analyzed. The A2 analogues **3** and **4** showed comparable NEP degradation rates to the native apelin isoforms, as previously reported.[57] When examining the effects of the homologue substitutions, all new analogues (**19**-**24**) showed improved proteolytic stability compared to the A2 analogues, even showing comparable resistance to the *N*MeA2 analogues **5** and **6**. Overall, the apelin-17 analogues (**22-24**) showed higher stability compared to the shorter 13-mer analogues (**19-21**). Furthermore, substitutions with both L-Cha and L-hArg, for residues 9 and 10, respectively, showed highly comparable stability as the *N*MeA2 analogues **5** and **6**.

**Table 3** Metabolic features of reference (**3**-**6**) and homologue-substituted (**19**-**27**) apelin analogues. Experiments were done in duplicates of three replicates. Errors represent the S.E.M.

| | Analogue | $t_{1/2}$ human NEP (h) | $t_{1/2}$ human plasma (h) | $t_{1/2}$ mice plasma (h) |
|---|---|---|---|---|
| **1** | pyr-1-apelin-13 | | 0.1 ± 0.03 | |
| **3** | Apelin13A2 | 10.31 ± 0.01 | 0.81 ± 0.20 | |
| **5** | NMeLeu13A2 | 40.27 ± 0.01 | 3.54 ± 0.12 | |
| **19** | hArg13A2 | 19.01 ± 0.01 | 1.31 ± 0.42 | |
| **20** | Cha13A2 | 22.07 ± 0.01 | 1.77 ± 0.34 | |
| **21** | hArgCha13A2 | 21.91 ± 0.02 | 2.58 ± 0.19 | |
| **2** | Apelin-17 | | 0.02 ± 0.01 | 0.03 ± 0.02 |
| **4** | Apelin17A2 | 10.95 ± 0.03 | 0.90 ± 0.17 | |
| **6** | NMeLeu17A2 | >48 | 8.29 ± 0.21 | 0.99 ± 0.11 |
| **22** | hArg17A2 | 40.59 ± 0.01 | 3.06 ± 0.04 | |
| **23** | Cha17A2 | 47.03 ± 0.01 | 4.34 ± 0.03 | |
| **24** | hArgCha17A2 | 46.39 ± 0.01 | 6.28 ± 0.02 | 0.52 ± 0.12 |
| **25** | NMeCha17A2 | | 2.90 ± 0.03 | 0.44 ± 0.07 |
| **26** | hArgNMeCha17A2 | | 3.41 ± 0.05 | 0.36 ± 0.25 |
| **27** | hArgNMeLeu17A2 | | 5.63 ± 0.08 | 0.38 ± 0.21 |

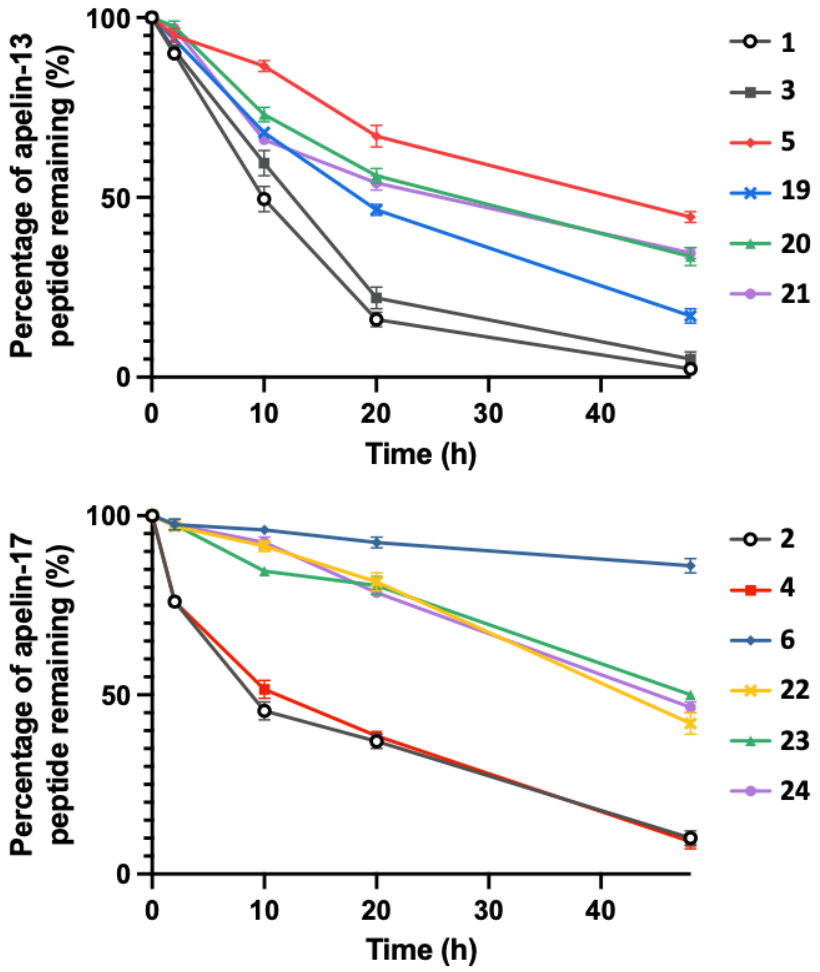


**Fig. 12** *In vitro rh*NEP degradation trends for apelin-13 and apelin-17 analogues. Analogues include native apelin (**1**, **2**), ACE-resistant (**3**, **4**), NEP-resistant (**5**, **6**), and newly synthesized hArg/Cha (**19**-**27**). Experiments were performed in duplicates of three replicates. Errors represent S.E.M.

Next, the *in vitro* human plasma stability of the analogues was examined (Table 3, Fig. 13). All apelin-13 (**19**-**21**) and apelin-17 (**22**-**27**) analogues displayed enhanced stability compared to analogues **3** and **4**, and these effects were more pronounced for the longer apelin-17 isoforms. These results suggest that NEP proteolysis appears to be more significant in the degradation of apelin-13 analogues compared to the 17-mer counterparts. However, compared to the inherently NEP-stabilized analogues **5** and **6**, all newly synthesized analogues (**19**-**27**) still showed lower

levels of plasma stability. This stability difference may suggest that the modifications of the peptide sidechains, regardless of the bulkiness (i.e., Leu vs. Cha), have a lower ability in stabilizing the peptide against proteases, compared to modifications on the peptide backbone alone (e.g., methylation). The most stable apelin-17 analogue **24** (hArgCha17A2) still displayed a 25% lower plasma half-life compared to analogue **6**.

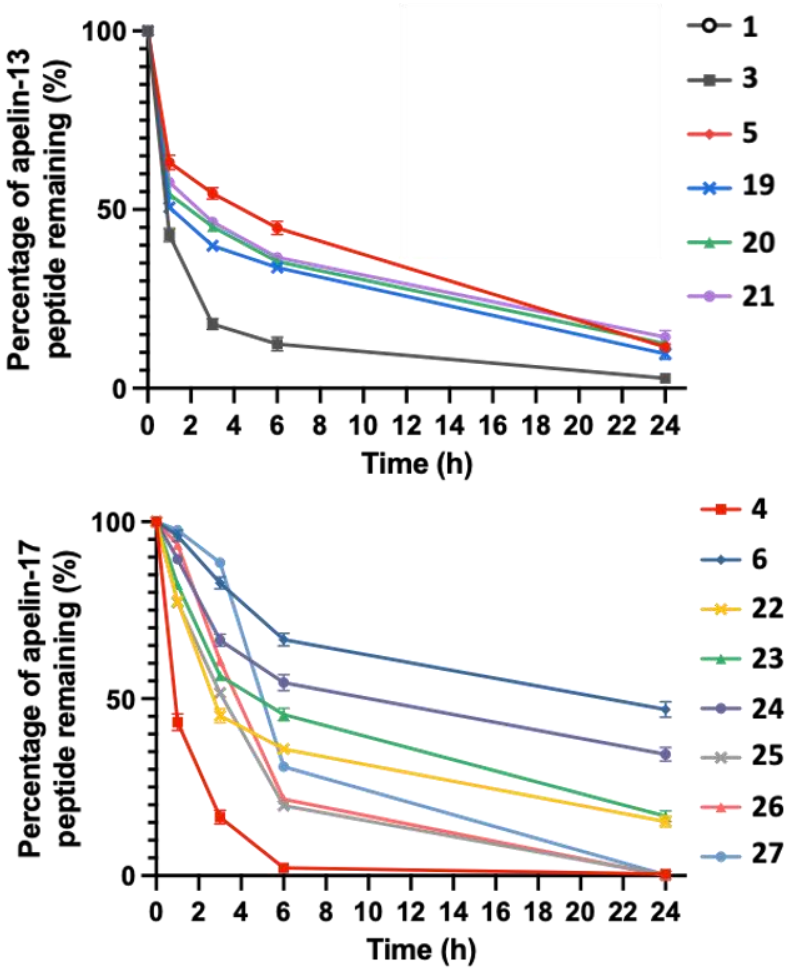


**Fig. 13** *In vitro* human plasma degradation trends for apelin-13 and apelin-17 analogues. Analogues include native apelin (**1**, **2**), ACE-resistant (**3**, **4**), NEP-resistant (**5**, **6**), and newly synthesized hArg/Cha (**19-27**). Experiments were performed in duplicates of three replicates. Errors represent S.E.M.

Lastly, the *in vitro* murine plasma stability of four target analogues (**24-27**) was tested and compared to the ACE2-resistant (**4**) and NEP-stabilized (**6**) analogues (**Table 3**, **Fig. 14**). In general, the proteolytic stability of peptides is significantly lower in rodents compared to humans, and this is due to the higher metabolic rate and renal clearance in rodents.[99] Compared to analogue **6** (~ 60 min), all apelin-17 analogues (**24-27**) showed slightly lower rates of proteolytic stability in murine plasma (≤40 min); analogue **24** (hArgCha17A2) displayed the highest stability of the apelin-17 isoforms. Nevertheless, compared to analogue **4**, all new analogues showed enhanced *in vitro* plasma stability, which encouraged the further exploration of the physiological activities of each analogue *in vivo* mice models.

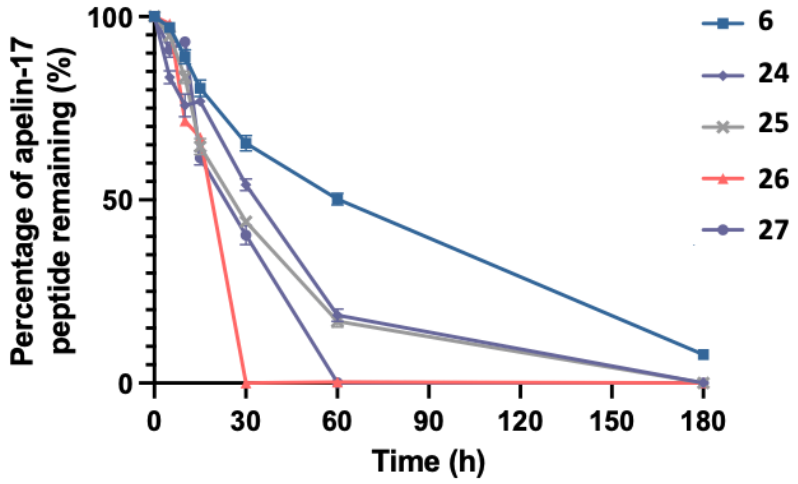


**Fig. 14** *In vitro* murine plasma degradation trends for apelin-13 and apelin-17 analogues. Analogues include native apelin (**1**, **2**), ACE-resistant (**3**, **4**), NEP-resistant (**5**, **6**), and newly synthesized hArg/Cha (**19-27**). Experiments were performed in duplicates of three replicates. Errors represent S.E.M.

### 2.3.4 APJR Receptor Radioligand Binding Experiments

Next, the newly synthesized analogues 19-27 were compared to determine their ability to compete with [$^{125}$I]-labelled pyr-1-apelin-13 binding on membrane preparations of CHO (Chinese hamster ovary) cells stably expressing the EGFP (enhanced green fluorescent protein)-labelled wild-type rat apelin receptor (**Fig. 15**, **Table 4**). These experiments were performed by Dr. Llorens-Cortès' lab. All apelin-13 analogues (**19-21**) showed improved competitive binding in comparison to the radiolabeled ligand; lower *p*Ki values compared to the ACE2-resistant analogue **3** (*p*Ki = 8.70 ± 0.06 nM). In addition, the apelin-17 analogues (**22-27**) showed comparable *p*Ki values at the nanomolar range compared to the ACE2-resistant (**4**; *p*Ki = 9.72 ± 0.01 nM) and NEP-stabilized (**6**; *p*Ki = 9.35 ± 0.09 nM) isoforms (**Fig. 15**). In conclusion, these data show that all the newly synthesized analogues were orthosteric ligands, as they were able to interact with the APJ receptor at the same binding site as the natural ligand.

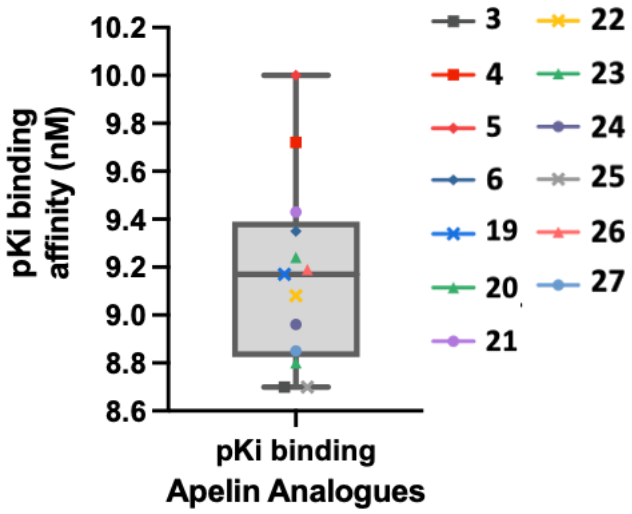


**Fig. 15** Box-and-whisker plot depicting the distribution of APJ receptor radioligand binding. Analogues include native apelin (**1**, **2**), ACE-resistant (**3**, **4**), NEP-resistant (**5**, **6**), and newly synthesized hArg/Cha (**19-27**). Experiments were performed in three replicates. Values represent means ± S.E.M.

**Table 4** Receptor binding and physiological response data of reference and homologue-substituted apelin analogues. [a]Hypotensive effects maintained for the duration of the experiment. Experiments were performed in three replicates. Errors represent S.E.M.

| | Analogue | *p*Ki binding affinity /nM | $pEC_{50}$ $Ca^{2+}$ - mobilization (nM) | Plasma protein binding efficacy (%) | ΔMABP (mmHg) | Duration of hypotensive effect (min) |
|---|---|---|---|---|---|---|
| **3** | Apelin13A2 | 8.70 ± 0.06 | 8.37 ± 0.14 | | 23.88 ± 7.60 | 60[a] |
| **5** | NMeLeu13A2 | 10.00 ± 0.17 | 8.17 ± 0.12 | | 9.52 ± 5.60 | 26 |
| **19** | hArg13A2 | 9.17 ± 0.07 | 8.66 ± 0.17 | | 26.44 ± 12.60 | 60[a] |
| **20** | Cha13A2 | 9.24 ± 0.10 | 8.62 ± 0.13 | | 0.23 ± 5.30 | 15 |
| **21** | hArgCha13A2 | 9.43 ± 0.01 | 8.43 ± 0.12 | | 15.33 ± 7.70 | 57 |
| **4** | Apelin17A2 | 9.72 ± 0.01 | 8.37 ± 0.14 | 52 ± 11 | 10.24 ± 2.60 | 33 |
| **6** | NMeLeu17A2 | 9.35 ± 0.09 | 8.56 ± 0.18 | 55 ± 10 | 31.98 ± 5.90 | 60[a] |
| **22** | hArg17A2 | 9.08 ± 0.13 | 8.17 ± 0.12 | | 40.45 ± 13.30 | 60[a] |
| **23** | Cha17A2 | 8.80 ± 0.13 | 8.42 ± 0.10 | | 19.72 ± 6.00 | 60[a] |
| **24** | hArgCha17A2 | 8.96 ± 0.15 | 8.36 ± 0.11 | 65 ± 9 | 44.90 ± 12.80 | 60[a] |
| **25** | NMeCha17A2 | 8.70 ± 0.11 | 7.79 ± 0.42 | 68 ± 8 | 28.83 ± 8.00 | 60[a] |
| **26** | hArgNMeCha17A2 | 9.19 ± 0.08 | 7.14 ± 0.20 | 69 ± 8 | 47.57 ± 4.60 | 60[a] |
| **27** | hArgNMeLeu17A2 | 8.85 ± 0.11 | 6.56 ± 0.17 | | 34.69 ± 4.90 | 60[a] |

### 2.3.5 APJR Receptor Activation and Plasma Protein Binding

To study the extent to which the newly derived analogues trigger downstream APJ receptor activation, fluorescence-coupled calcium release assays were performed (**Table 4**, **Fig. 16**). All analogues (**19**-**27**) displayed comparable *p*$EC_{50}$ values as the reference apelin compounds (**3**-**6**), suggesting a similarly strong APJ receptor activation potential; these results support the obtained receptor binding affinity values (**Table 4**). Furthermore, the binding curves all indicate a positive sigmoidal functionality indicating that the analogues are agonistic ligands to the APJ receptor (Fig. 16).

In addition, target analogues **24**-**26**, generally displayed a slightly higher plasma protein binding (65 ± 9%, 68 ± 8%, and 69 ± 8%, respectively) compared to the native apelin-17 (**2**)[79] and analogues **4** (52 ± 11) and **6** (55 ± 10) (**Table 4**). Considering the improved plasma half-lives ($t_{1/2}$) of the apelin-17 analogues (**22**-**27**) compared to ACE2-resistant analogue **4**, it appears that subtle homologue substitution (i.e., Arg10 to hArg10, or Leu9 to Cha/*N*MeCha/*N*MeLeu9) may increase the lipophilicity of apelin peptides proteolytic stability through plasma protein binding.[100]

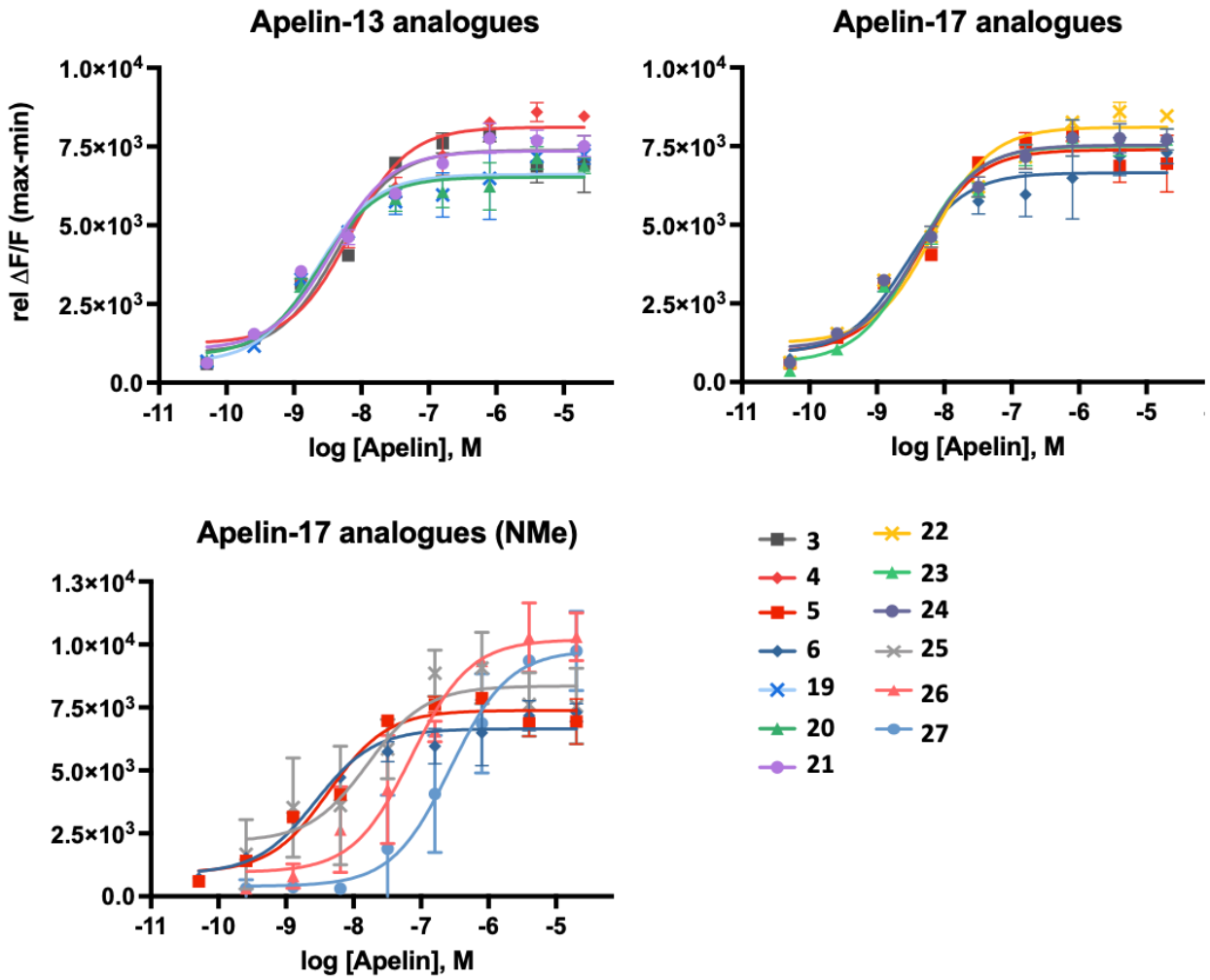


**Fig. 16** Concentration-response (fluorescence) curves of reference and newly synthesized apelin analogues. Analogues include native apelin (**1**, **2**), ACE-resistant (**3**, **4**), NEP-resistant (**5**, **6**), and newly synthesized hArg/Cha (**19-27**). Experiments were performed in three replicates. Errors represent S.E.M.

### 2.3.6 *In Vivo* Physiological Tests

Lastly, the analogues were evaluated, by Dr. Oudit's group, for their cardioprotective abilities using *in vivo* mice models. Several parameters were measured including heart rate (HR), mean arterial blood pressure (BP), and systolic (SBP) and diastolic (DBP) blood pressure. The shorter apelin-13 analogues (**19-21**) displayed only marginal cardiovascular effects (**Fig. 17**).

However, all apelin-17 analogues (**22-27**) showed more pronounced cardio-physiological activity (**Fig. 18**, **Fig. 19**). In fact, analogues **24** and **26** showed a rapid and stable recovery in heart rate as well as prolonged blood-pressure lowering effects, rivalling the most potent compound (**6**) from our previous studies. These cardioprotective results suggest that in addition to the enhanced binding to the APJ receptor, substitutions with L-hArg and/or L-Cha are cardio-physiologically well tolerated and beneficial for the host, as well as providing a foundation for further development of cardiovascular-active apelin analogues.

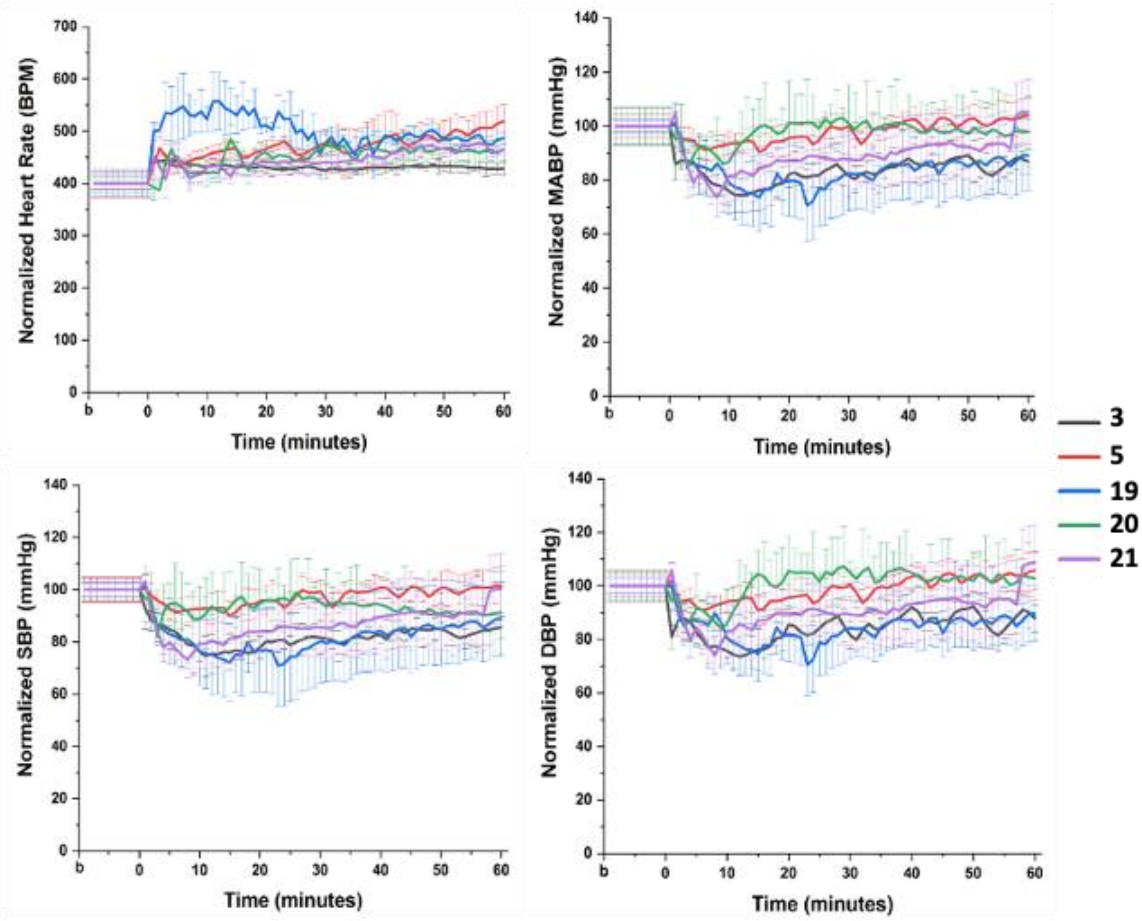


**Fig. 17** *In vivo* heart rate (HR), mean arterial blood pressure (MABP), systolic blood pressure (SBP), and diastolic blood pressure (DBP) analyses for analogues **3**, **5**, and **19-21**. Experiments were performed in three replicates. Values represent mean ± S.E.M.

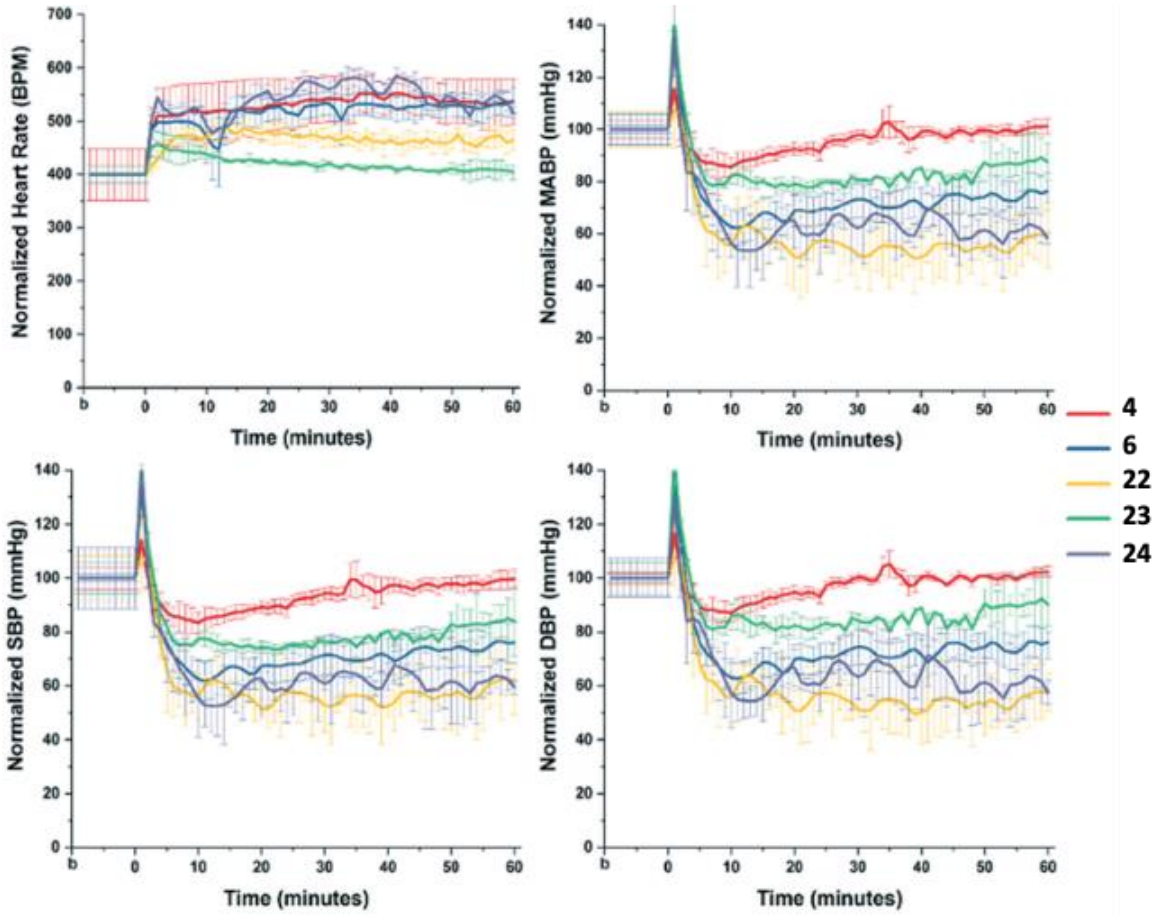


**Fig. 18** *In vivo* heart rate (HR), mean arterial blood pressure (MABP), systolic blood pressure (SBP), and diastolic blood pressure (DBP) analyses for analogues **4**, **6**, and **22**-**24**. Experiments were performed in three replicates. Values represent mean ± S.E.M.

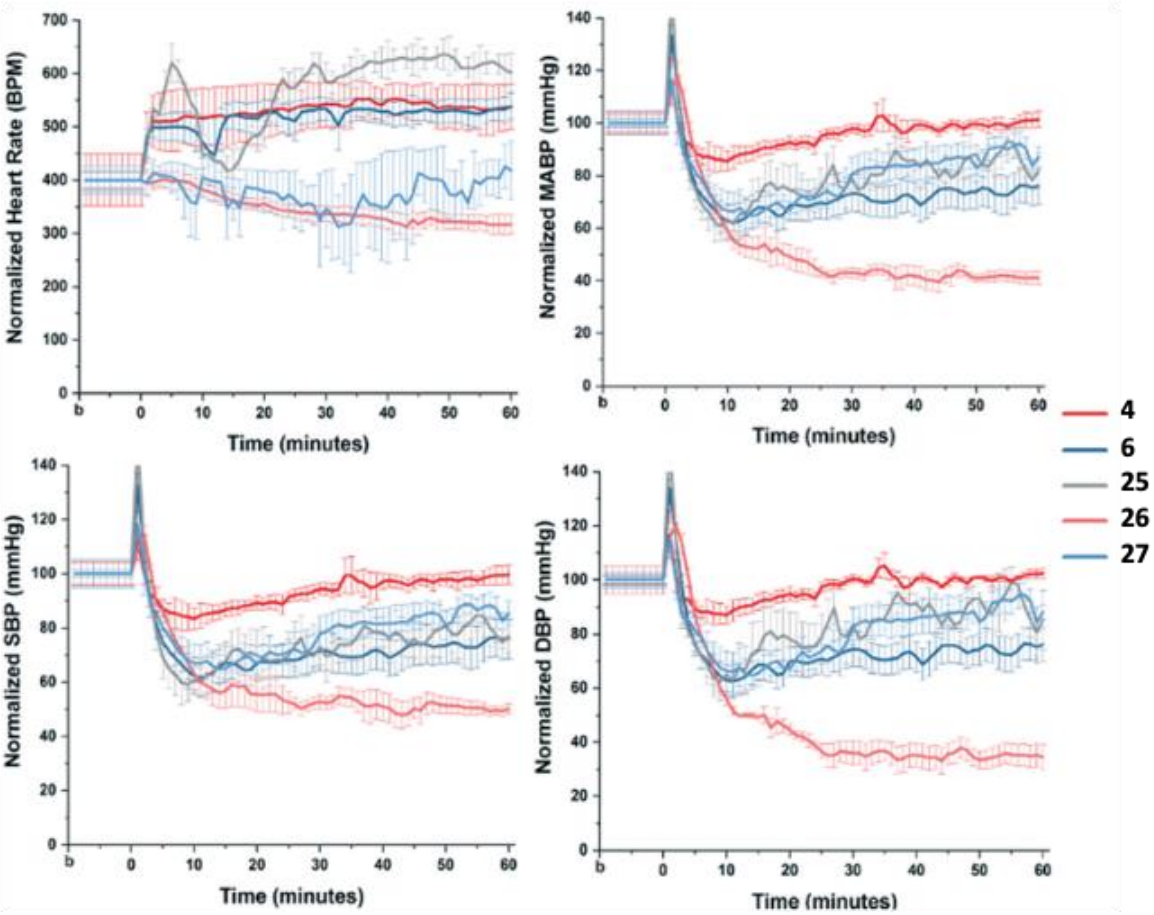


**Fig. 19** *In vivo* heart rate (HR), mean arterial blood pressure (MABP), systolic blood pressure (SBP), and diastolic blood pressure (DBP) analyses for analogues **4**, **6**, and **25**-**27**. Experiments were performed in three replicates. Values represent mean ± S.E.M.

### 2.3.7 Conclusion and Future Directions

In this study, apelin analogues were modified at the NEP cleavage site (Leu10-Arg9), through methylation and substitution with L-hArg and/or L-Cha, to investigate their influence on metabolic stability and cardiovascular activity. A new and facile synthetic route was developed, resulting in the synthesis of *N*-methylated dipeptides using non-canonical amino acids. These unnatural dipeptides were then introduced in the natural peptide sequence and still showed biological activity. *In vitro* isolated enzyme, human plasma, and mice plasma stability assays were performed, and all newly synthesized analogues showed elevated metabolic stability. *In vivo* blood

pressure experiments were also performed, and the results indicate stable and prolonged blood pressure-lowering effects for all 17-mer analogues, especially analogues **24** and **26**. In addition, the synthesized apelin derivatives displayed comparable or even improved APJ receptor binding and activation, compared to the reference compounds (**3**-**6**). Lastly, these results indicate that relatively conservative homologue-substitution in positions 9 and 10, from the C-terminus, contributes to a moderate metabolic peptide stabilization, yielding cardiovascular-active apelin analogues as promising therapeutic targets for cardiovascular diseases.

Further studies could be performed by combining both modifications, highlighted in the reference paper for this work (i.e., macrolactamization and homologue substitution), to determine their effects on the active native apelin receptor.[89] In addition, molecular docking studies could be performed to determine the potential binding contributions of these modifications on the native APJ receptor.

## 2.4 Additional and Future Apelin Investigations

### 2.4.1 Determining the Importance of the KFRR Motif

#### 2.4.1.1 Background and Aims of Study

Several studies have been performed at investigating crucial structure-activity relationships (SARs) of the shorter pyr-1-apelin-13 peptide through alanine-[101,102] and D-amino acid[72] scans. These scans can predict the influence of certain amino acid residues on plasma stability, receptor binding, and downstream signalling, which have been supported by a published X-ray crystal structure of a truncated version of the APJ receptor.[89] However, these vital SAR studies are missing

for the four *N*-terminal residues (i.e., KFRR motif) of apelin-17. In this study, in order to characterize the functional impact of these four amino acids, we generated two sets of alanine scans including the native apelin-17 (**37**-**40**) and our first-generation "A2" analogue series (**41**-**44**) (**Table 5**). From these alanine scan analogues, our lab, in collaboration with Dr. Llorens-Cortès' and Dr. Oudit's labs, performed *in vitro* APJ receptor binding and activation, as well as *in vivo* cardio-physiological experiments, to determine potential deficiencies as a result of these amino acid substitutions.

**Table 5** Binding, activation, and blood-pressure data of KFRR-modified apelin analogues. Tests compounds include native apelin-17 (**2**), *N*MeLeu17A2 (**6**), alanine-substituted (**37**-**44**), and methylated KFRR (**45**-**46**) analogues. Plasma protein binding efficacy relative to compound **2** (=100%). *C*-terminal Nle-Aib-BrF modification for ACE2-resistance highlighted in blue. Experiments were performed in three replicates. Values represent ± S.E.M.

| | **Modification** | **$t_{1/2}$ human plasma (h)** | ***p*$IC_{50}$ binding affinity (nM)** | ***p*$EC_{50}$ $Ca^{2+}$ - mobilization (nM)** | **Plasma protein binding efficacy (%)** | **ΔMABP (mmHg)** |
|---|---|---|---|---|---|---|
| **2** | Apelin-17 | 0.02 ± 0.01 | 10.30 ± 0.08 | 8.72 ± 0.18 | 100 | −18 ± 6 |
| **6** | *N*MeLeu17A2 | 8.29 ± 0.21 | 9.35 ± 0.09 | 8.56 ± 0.18 | 104 | −31.98 ± 5.90 |
| **37** | **A**FRRQRPRLSHKGPMPF | | 9.70 ± 0.02 | | | |
| **38** | K**A**RRQRPRLSHKGPMPF | | 9.53 ± 0.11 | | | |
| **39** | KF**A**RQRPRLSHKGPMPF | | 9.66 ± 0.10 | | | |
| **40** | KFR**A**QRPRLSHKGPMPF | | 9.52 ± 0.09 | | | |
| **41** | **A**FRRQRPRLSHKGPNleAibBrF | | 9.00 ± 0.11 | 8.27 ± 0.14 | 92 | −14 ± 7 |
| **42** | K**A**RRQRPRLSHKGPNleAibBrF | | 9.00 ± 0.23 | 8.21 ± 0.14 | 90 | −3 ± 5 |
| **43** | KF**A**RQRPRLSHKGPNleAibBrF | | 8.85 ± 0.15 | 7.40 ± 0.12 | 112 | +1 ± 5 |
| **44** | KFR**A**QRPRLSHKGPNleAibBrF | | 8.66 ± 0.02 | 7.13 ± 0.09 | 114 | −9 ± 7 |
| **45** | *N*MeArg14-*N*Me17A2 | 5.20 ± 0.20 | 8.82 ± 0.08 | 8.46 ± 0.18 | | −14 ± 4 |
| **46** | $\alpha$MeArg14-*N*Me17A2 | 7.10 ± 0.50 | 9.00 ± 0.18 | 8.62 ± 0.21 | | −18 ± 4 |

#### 2.4.1.2 Results and Discussion

Analogues **37**-**40** and **41**-**44** were synthesized manually by solid phase peptide synthesis, based either on the native apelin-17 (**2**) or the ACE2-resistant apelin-17 analogue (**4**), respectively. The peptide analogues were synthesized through sequential amino acid coupling up to the Gln13 residue. An alanine residue was then substituted for one of the four *N*-terminal amino acids (i.e., Lys17, Phe16, Arg15, or Arg14); referred to as the "KFRR head motif". Although all analogues still showed low nanomolar binding affinity to the APJ receptor, certain trends were noticeable. Generally, the analogues displayed lower $pIC_{50}$ values, with at least 5 times lower affinity than the native apelin-17 (**2**) and apelin-17A2 (**4**) analogues (**Table 5**, **Fig. 20**). Interestingly, the binding affinity decreases even more when either Arg15 or Arg14 is substituted with alanine. This trend is reflected in 39 times (Arg15, compound **43**) or 21 times (Arg 14, compound **44**) lower binding potency to trigger downstream $Ca^{2+}$ release (**Fig. 20**). Despite the slightly increased efficacy of some alanine-substituted analogues (**43** and **44**), all analogues still showed an overall significantly lower potency, indicating a loss of signal transduction due to the substitution of alanine residues within the KFRR motif.

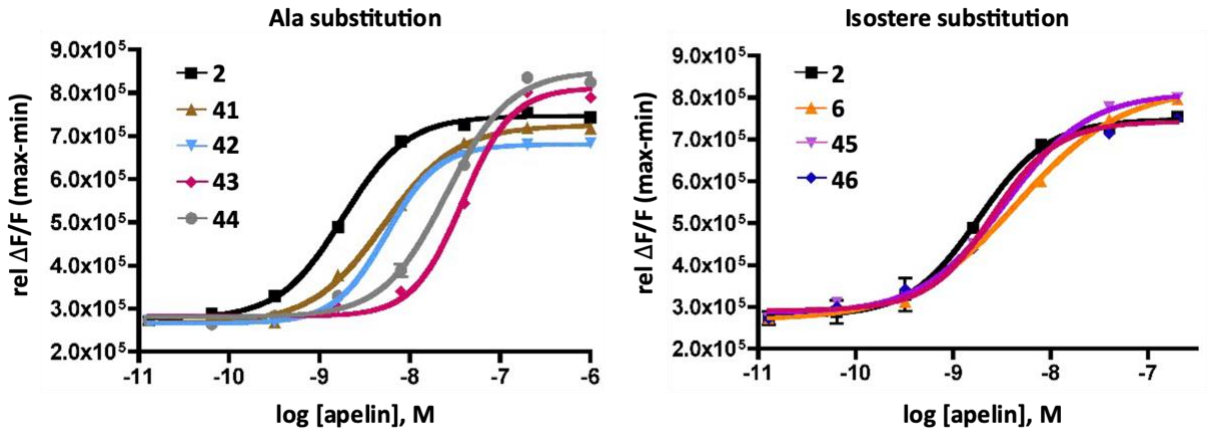


**Fig. 20** Concentration-response (fluorescence) curves of alanine- and isostere-substituted apelin analogues. Isoforms include native apelin-17 (**2**), ACE-resistant (**4**), Ala-substituted (**41-44**) and isostere substituted (**45-46**). Experiments were performed in three replicates. Values represent mean ± S.E.M.

From the *in vivo* blood pressure data, alanine substitution in the KFRR head region dramatically influences the physiological activity of the synthesized alanine-scan analogues (**Fig. 21**). In particular, the substitution of alanine for the Arg15 (**43**) and Arg 14 (**44**) residues resulted in much less physiologically-active analogues. These alanine scan results suggest that the KFRR head motif may play an important role in the regulation of cardiovascular physiology. These alanine-scan analogues behave similarly to the parent pyr-1-apelin-13 (**1**)[67] and apelin-17 (**2**) peptides, showing only a modest and short-term decrease in mean arterial blood pressure.

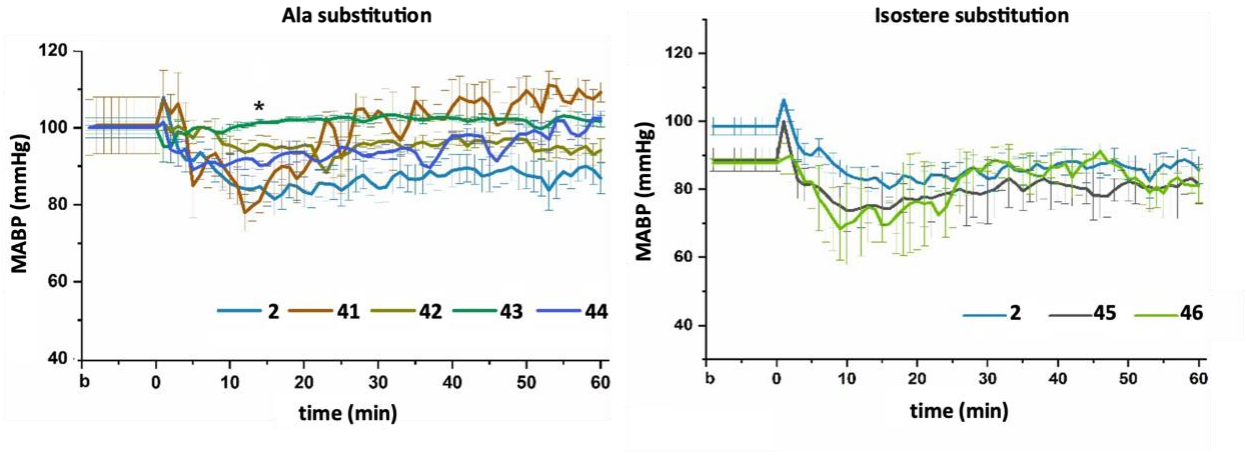


**Fig. 21** *In vivo* mean arterial blood pressure (MABP) analyses for analogues **2**, and **41-46**. Experiments were performed in three replicates. Values represent mean ± S.E.M.

The results suggest that this cationic KFRR head motif may likely be involved in vital membrane interactions through the formation of salt bridges with the APJ receptor (i.e., Arg14 and/or Arg 15 bridged with Asp92 and/or Asp94) and/or the possible recruitment of other GPCR proteins[103] which regulate the renin-angiotensin system (**Fig. 22**).

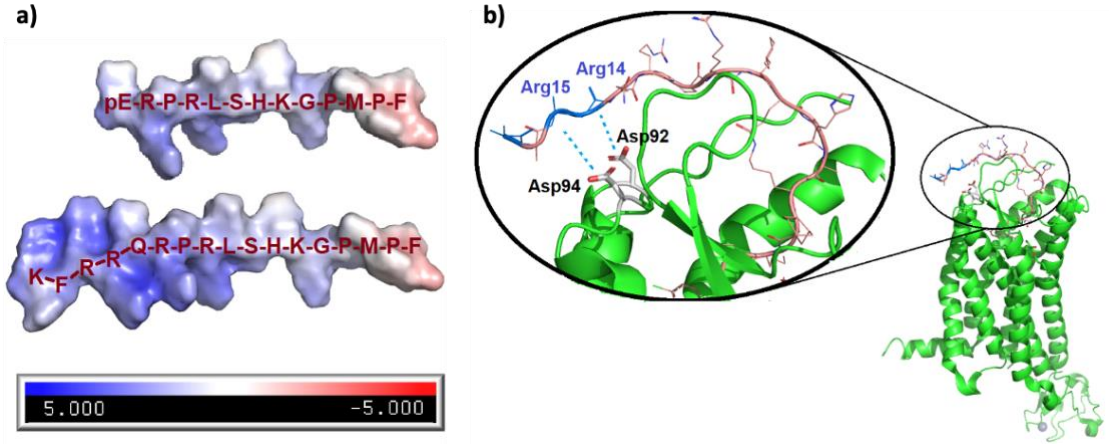


**Fig. 22** Predicted apelin peptide-APJ receptor binding interactions at the KFRR motif. A) Electrostatic potential surface of pyr-1-apelin-13 (**1**) and apelin-17 (**2**). B) Suggested ligand-receptor interactions in the X-ray crystal structure of the APJ receptor with a sidechain modified

apelin-17 analogue (PDB code 5VBL). The side chains of the *N*-terminal KFRR motif are not well resolved. Potential salt bridges are indicated by blue dotted lines.

To further investigate the importance of the KFRR motif in receptor interactions, myself, Dr. Conrad Fischer and Dr. Cameron Pascoe, introduced *N*-methylation (**45**) and $\alpha$-methylation (**46**) at the Arg14 residue (**Fig. 23**, **Scheme 3**). The synthesis of these modified amino acids was previously done by Dr. Shaun McKinnie in our lab and showed that incorporating the *N*MeLeu residue as a dipeptide with Arg10 into the growing peptide chain was the best approach. This approach overcame the following disadvantages of direct coupling of the *N*Me-Leu benzyl ester *p*-toluenesulfonate salt with a Pmc/Pbf-protected Fmoc-Arg-OH residue: the incompatibility of Pbf or Pmc with benzyl ester hydrogenolysis, and the propensity of arginine to react intramolecularly to form lactams when they are C-terminally activated,[104,105] particularly when being coupled to a sterically hindered amino acid. These disadvantages can be mitigated by coupling the *N*- or $\alpha$- methylated Arg14 residue to a protected ornithine, which can be subsequently reacted with *N*,*N*'-di-Boc-*N*"-guanidine triflate to afford the arginine moiety followed by hydrogenation of the benzyl ester for coupling to the peptide chain.

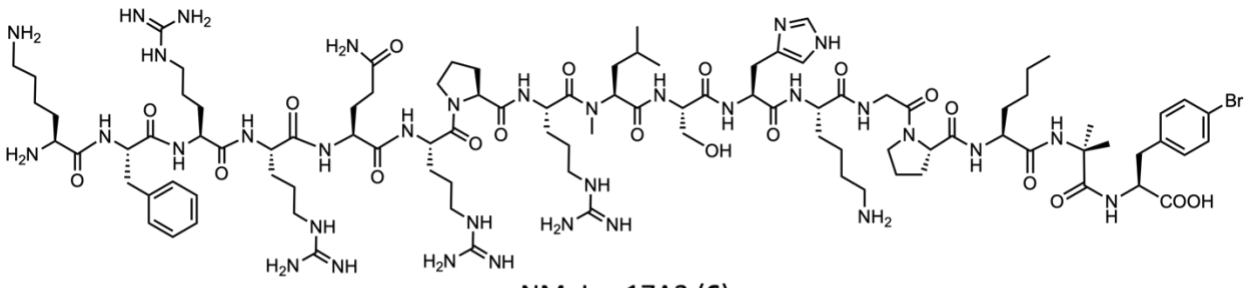

NMeLeu17A2 (**6**)

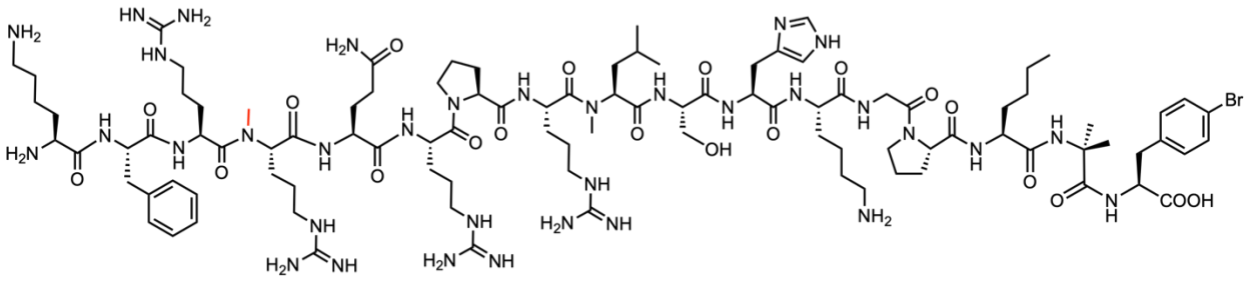

*N*MeArg14-NMe17A2 (**45**)

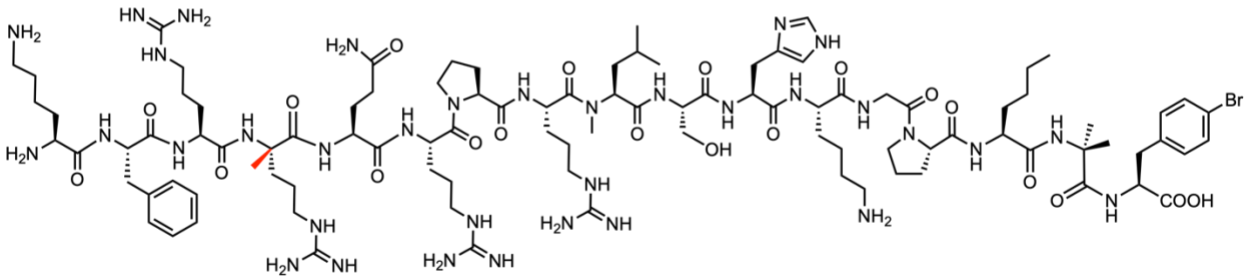

*α*MeArg14-NMe17A2 (**46**)

**Fig. 23** Structures of methylated-Arg14 analogues (**45**-**46**) within the KFRR head motif of *N*MeLeu17A2 (**6**).

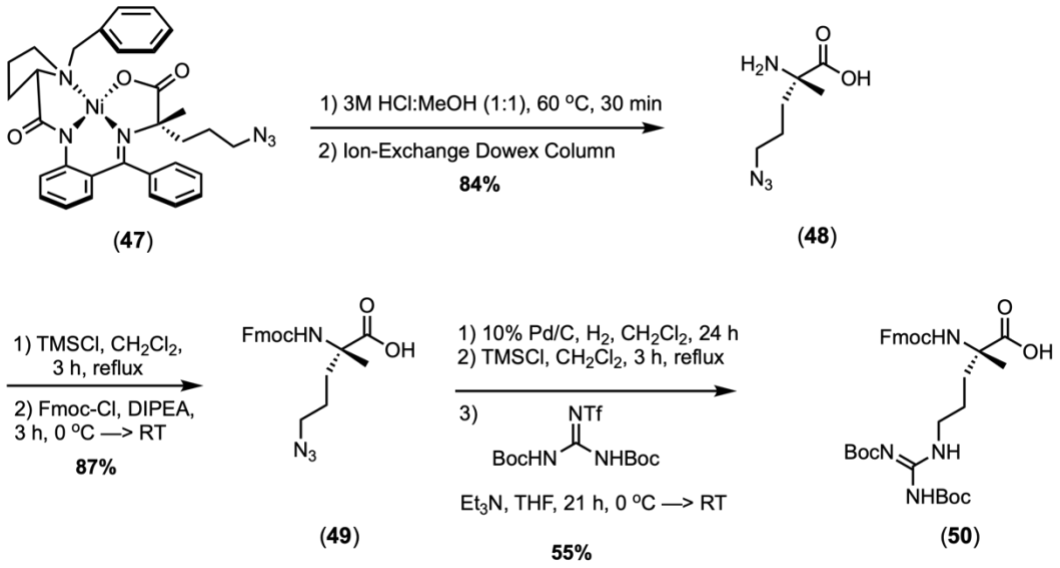


**Scheme 3** Synthetic scheme for the formation of $\alpha$-methylated Arg14 residue (**50**).

Both analogues significantly increased the plasma stability compared to the parent apelin-17 (**2**; about 300× increase) and the *N*MeLeu-17A2 analogue (**6**; about 5× increase) (**Table 5**).In addition, both analogues exhibited low nanomolar affinities towards the APJ receptor, as well as comparable abilities to trigger calcium release as a result of downstream G-protein activation as the reference peptides **2** and **6** (**Fig. 20**). However, it was surprising that neither of the methylated analogues displayed hypotensive effects, suggesting that they may be unpromising modifications for further physiologically active analogues (**Fig. 21**). It appears that the steric bulk in addition to the loss of H-bonding and the conformational restriction imposed by the additional methyl groups at Arg14 compromises the integrity of the *N*-terminus of apelin-17. These results support the findings from the alanine scans, as the stiffening of the KFRR motif, through the introduction of an *N*-methyl or $\alpha$-methyl group (**45**, **46**), correlated with a loss of function. Although the physiological activity of these analogues may pale in comparison to the reference compounds, these results provide a better understanding of the importance of the KFRR motif for APJ receptor downstream interactions. Recent reports suggest that peptide-based agonists can have differential

biases toward $\beta$-arrestin recruitment or to G-protein-coupled receptor activation.[106] As the major indicator we used in our studies was blood pressure lowering associated with $\beta$-arrestin, the compounds should also be further investigated through Langendorff isolated perfused heart assays.

### 2.4.2 Pharmacokinetics and Development of Oral Apelin Delivery System

#### 2.4.2.1 Background and Aims of Study

After thoroughly investigating the importance of vital motifs in the apelin sequence (i.e., KFRR, RPRL, and *C*-terminal Phe) on peptide stability and activity, we looked to explore alternative routes of administration for apelin peptides. To date, apelin peptides, like insulin, are administered to the body *via* subcutaneous injections.[16,107] Although this administration route allows for apelin to exert its beneficial cardiovascular effects, the development of an effective delivery system for oral apelin is desired to overcome obstacles (e.g., patient compliance) for future human trials. The oral delivery of apelin has several limitations, including sensitivity to enzymatic degradation and hydrolysis in the digestive system, rapid clearance from the site of deposition, and poor epithelial membrane absorption in the small intestine. The use of encapsulation approaches with polymers stands as a promising strategy, where many natural polymers (e.g., chitosan, casein, alginate, pectin, and cyclodextrin) have shown promising results in other similar applications.[16,108–111] In these preliminary studies, we aim to examine target apelin peptides (compounds **6**, **7**, and **13**) for their pharmacokinetics features, as well as investigate the potential of an oral polymeric-based particle system using chitosan and cyclodextrin.

### 2.4.2.2 Results and Discussion

From our previous studies, we decided to further test apelin analogues **6** (*N*MeLeu17A2), **7** (Fmoc-PEG$_6$-NMe17A2), and **13** (Cbz-PEG$_6$-NMe17A2) due to their high plasma stability, enhanced APJ receptor binding and activation, and their excellent cardioprotective ability. With one of our industry collaborators, PEARKO Therapeutics, compound **13** was tested in dog models to determine the time course for the distribution of the peptide drug. The dogs were injected with **13** intravenously, and the blood was sampled at several time points. The results show that the half-life ($t_{1/2}$) for Dog 1 was approximately 7.4 min and about 4.6 min for both Dogs 2 and 3. These values are dramatically less than expected, compared with the plasma degradation assays performed in humans (Table 1), however, as was the case with the mice plasma degradation assays, this prompt decline may be due to rapid renal clearance[99,112]; further studies will be performed to address this decline in detectable analogue levels.

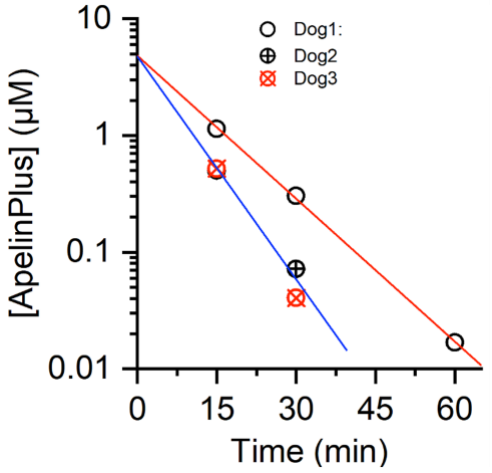


**Fig. 24.** *In vivo* degradation of compound **13** (Cbz-PEG$_6$-NMe17A2) in canine blood ($n$ = 3).

Drug metabolism, specifically regarding the metabolic enzymes present in the digestive system, is an important pharmacokinetic factor that we are studying for future oral drug

development.[113] The metabolic system consists of several key enzymes, namely elastase[114], carboxypeptidase A[115], trypsin[116], and chymotrypsin[117], which exhibit the ability to cleave apelin peptides at various proteolytic sites (**Fig. 25**).

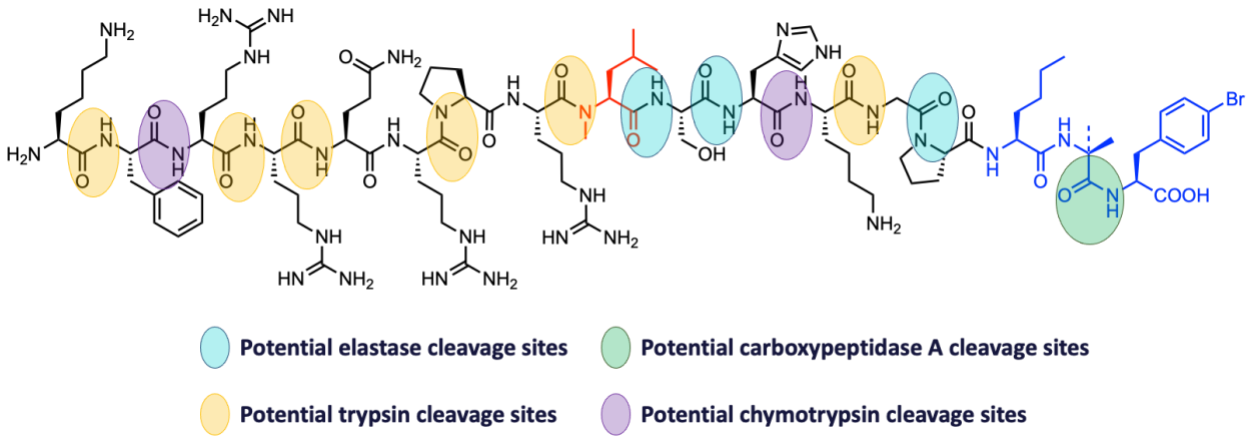


**Fig. 25** Potential cleavage sites of four metabolic enzymes (elastase, carboxypeptidase A, trypsin, and chymotrypsin) presented on compound **6**.

In this work, only compounds **6** (*N*MeLeu17A2) and **7** (Fmoc-PEG$_6$-NMe17A2) have been tested in the *in vitro* metabolic enzyme assays (**Fig. 26**). From these results, both analogues showed relatively good stability in the presence of elastase and carboxypeptidase A after the 24 h incubation period. However, rapid cleavage of both analogues was seen in the presence of trypsin and chymotrypsin. These results are not extremely surprising, as trypsin and chymotrypsin account for 8 of the 12 potential cleavage sites within the peptide. Cleavage by carboxypeptidase A may be hindered by the substitution of the halogenated aromatic residue (i.e., BrF at position 1).[118] Furthermore, cleavage by elastase may be reduced by the increased steric bulk through the introduction of an *N*MeLeu9 residue or through a hindered cleavage site by a rigid Pro4 residue.

Future studies will need to be performed to investigate the stability of apelin peptides in the presence of gastric juices and intestinal contents.

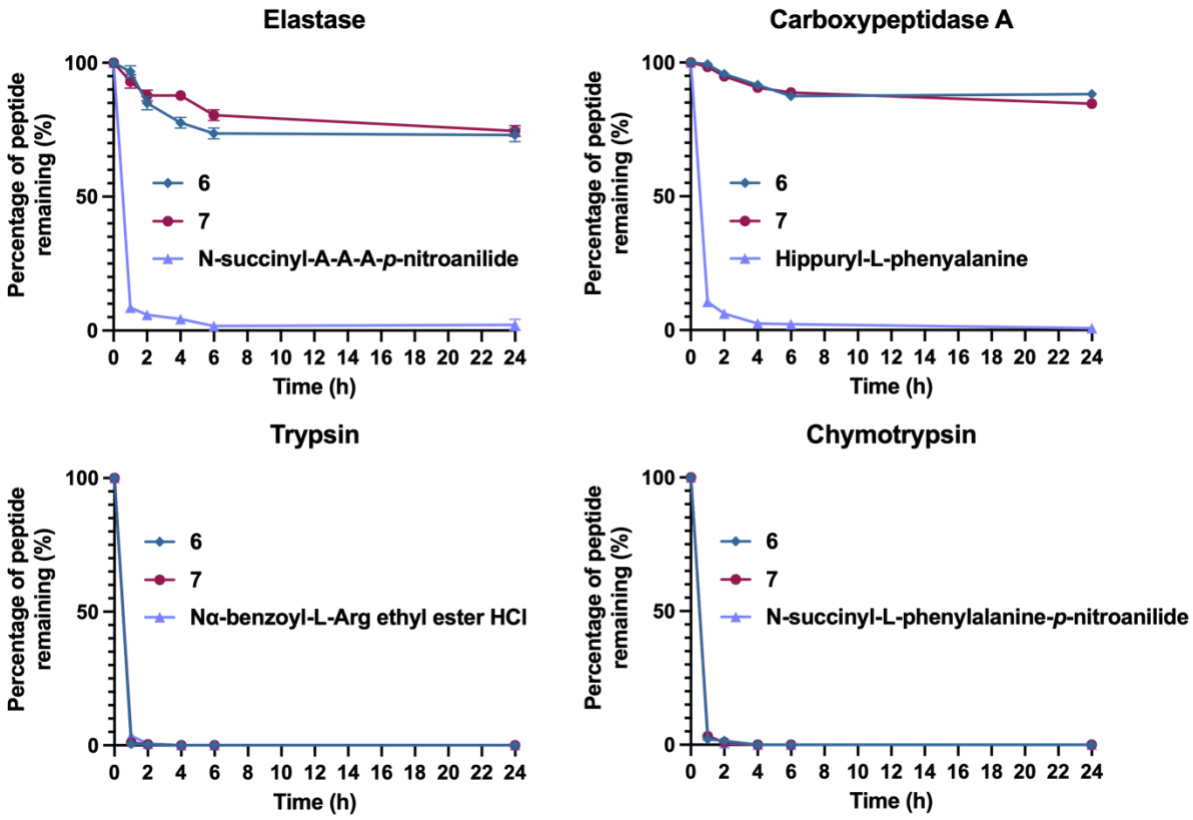


**Fig. 26** *In vitro* metabolic enzyme degradation trends for target apelin-17 analogues. Analogues include NEP-resistant (**6**), and Fmoc-protected (**7**) isoforms. Experiments were performed in duplicates of three replicates. Errors represent S.E.M.

Lastly, preliminary studies using natural saccharides for the formation of oral hydrogels were studied, using chitosan and $\beta$-cyclodextrin.[16,119] Chitosan is a cationic and non-toxic polysaccharide consisting of randomly distributed *N*-acetylglucosamine and glucosamine units and is made by treating the chitin shells of crustaceans with an alkaline substance (e.g., NaOH). Chitosan has been shown to be easily converted into gels, which can be used to orally transport

drugs. Cyclodextrins are a family of cyclic oligosaccharides made of glucose units in a macrocyclic ring; $\beta$-cyclodextrin consists of 7 glucose units.[16] These cyclic oligosaccharides have previously been used as "shuttles" which encompass the drug in their lipophilic central cavity to escape metabolic degradation and allow for direct release in the intestine.[110,111] The synthesis of the CMCD-*g*-CMC compound **53**, from the crosslinking of CMC (**51**) and CMCD (**52**), was performed and characterized with FTIR and X-ray diffraction (**Scheme 4**). However, the amount (%) of crosslinked product was relatively low (<40%) compared to previous papers, therefore, further synthetic endeavours must be taken to reach the approximate 80% threshold to have enough cavities available for apelin peptides to occupy. Once the desired CMCD-*g*-CMC hydrogel is formed, the swelling behaviour and apelin loading content, as well as quantifying the amount of apelin released will be determined. In addition, cytotoxicity assays of the hydrogels in HEK or Caco-2 cells must be performed. Furthermore, transepithelial transport of the apelin-loaded hydrogel may be quantified using lab-grown epithelial cells, prior to tests on *in vivo* mice models. The combination of these pharmacokinetic studies and the formation of a chitosan-cyclodextrin-based hydrogel may allow for insight into the formation of an effective oral drug delivery system for apelin peptides to manage cardiovascular diseases.

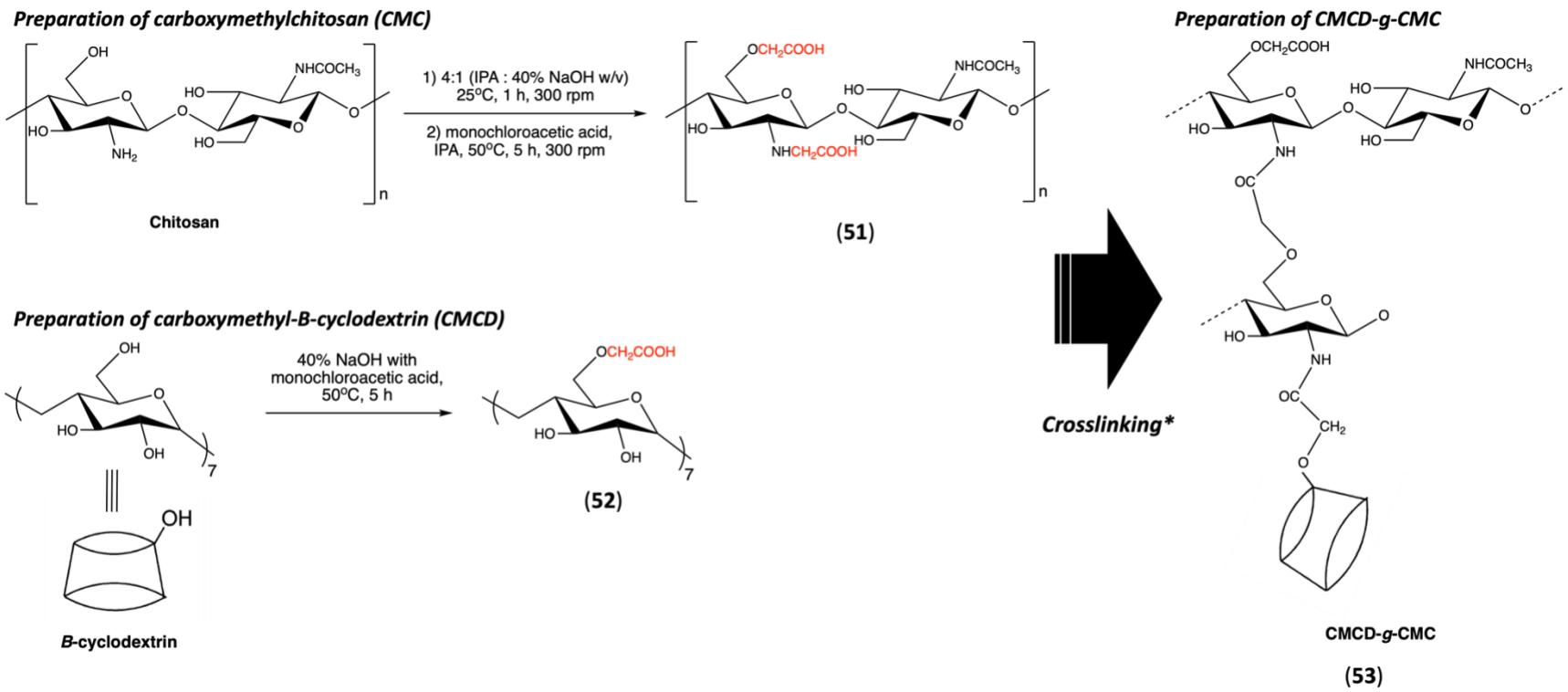


**Scheme 4** Synthetic scheme for the production of a chitosan-cyclodextrin-based hydrogel. *Crosslinking conditions: EDC, NHS, $H_2O$, 25 °C, 24h. Abbreviations: MCA = monochloroacetic acid; EDC = 1-ethyl-3-[3-dimethylaminopropyl]carbodiimide hydrochloride; NHS = *N*-hydroxysuccinimide; CMC = carboxymethylchitosan; CD = cyclodextrin; CMCD = carboxymethyl-$\beta$-cyclodextrin; CMCD-*g*-CMC = carboxymethyl-$\beta$-cyclodextrin-*grafted*-carboxymethylchitosan.

### 2.4.3 Determining the Importance of the Apelin Peptide Backbone

#### 2.4.3.1 Background and Aims of Study

As therapeutics, peptides possess fascinating properties, including high specificity and binding affinity, low risk of peptide-drug interactions, and generally low toxicity.[120] In addition, due to their sequence- and structure-dependence, peptides can be designed as therapeutics for many diseases. However, natural peptides are highly sensitive to most proteases, resulting in degradation and excretion, resulting in poor bioavailability and distribution, as well as rapid renal clearance – limiting therapeutic potential.[7,121,122]

Most amino acids, except glycine, possess chiral centers and exist predominantly as L-enantiomers in nature.[7] D-Amino acid-containing peptides often are a result of post-translational modifications and are also found in nature (e.g., some bacteria and frog species).[123,124] Compared to their L-counterparts, D-peptides display an innate resistance to enzymatic degradation, overcoming their limited therapeutic potential.[125,126] However, the introduction of isomerism often leads to the reduction or even suppression of biological activity.[124]

A facile, elegant, and often successful solution to overcoming this diminished biological activity is to incorporate D-amino acids ('enantio') as stable surrogates of L-amino acids[127], but, presented in the reverse ('retro') order compared to the parent molecule[125] (**Fig. 27**). These modifications result in a new analogue composed of all D-amino acids introduced in the sequence in reverse direction – known as retro-all-D or retro-enantio (RE) peptides.[128,129] The importance of this peptide subclass is that when viewed in a fully-extended conformation, the side-chains can be superimposed with those of the parent L-peptide, but with inverted amide bonds, and *N*- and *C*-termini.[130] Therefore, in cases where biological activity is mostly associated with the amino acid

side chains, without a significant contribution from the backbone chemical groups, an RE analogue has the potential to achieve the same activity and function as the L-parent peptide, but with superior stability towards proteolytic degradation.[131–133]

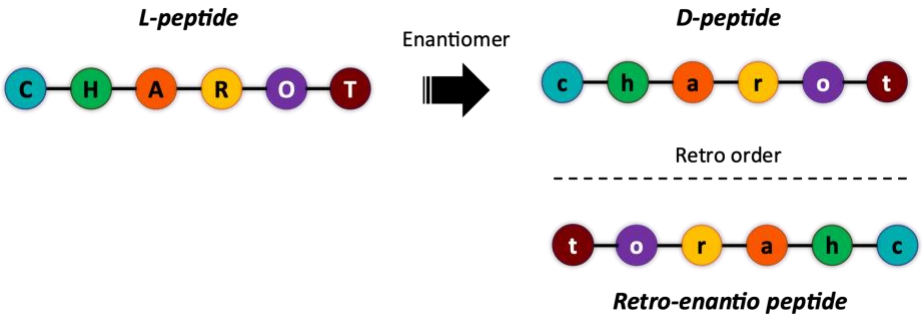


**Fig. 27** Schematic diagram of retro-enantio peptides. L-amino acids are represented as capital one-letter codes: C = cysteine; H = histidine; A = alanine; R = arginine; O = ornithine; T = threonine. D-amino acids are represented as lowercase one-letter codes.

### 2.4.3.2 Results and Discussion

In this study, four preliminary analogues (**54-57**), based on the parent peptide (**1-4**), were synthesized incorporating D-amino acids in retro sequence (**Fig. 28**, **Fig. 29**) using solid-phase peptide synthesis. Based on our previous studies, the interactions between the APJ receptor and apelin peptide (i.e., *C*-terminal Phe receptor internalization, RPRL binding motif, and KFRR membrane-interaction head motif) should ideally be left undisturbed by these D-amino substitutions. Furthermore, the introduction of D-amino acids in the apelin sequence should enhance proteolytic stability (**Fig. 30**), resulting in improved bioavailability. As seen from the results from the human and mice plasma assays, all new retro-enantio analogues (**54-57**) exhibited excellent stability against the inherent proteolytic enzymes, compared to compound **6**, which had a $t_{1/2}$ of approximately 8 min in human plasma and was entirely degraded after 1 h in mice plasma.

Studies are currently ongoing to determine receptor binding through the displacement of a radiolabelled-apelin, as well as cardiovascular output through cardiac pressure-volume (PV) loop analyses. Once these studies have been completed, further investigation will be performed to determine receptor activation through calcium mobilization as well as analyze the potential effects of these retro-enantio peptides on receptor interactions *via* molecular docking experiments.

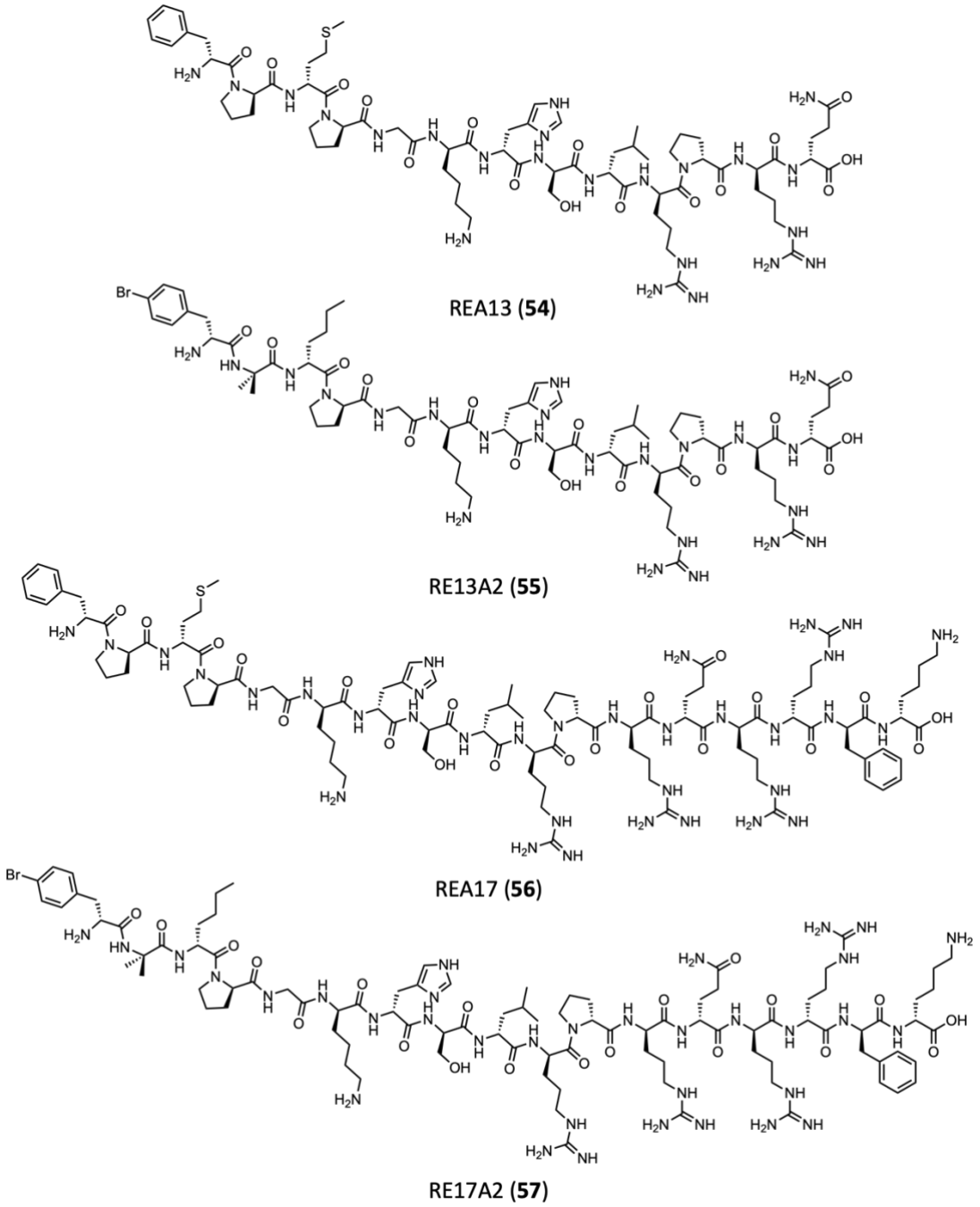


**Fig. 28** Structure of synthesized retro-enantio apelin analogues (**54-57**).

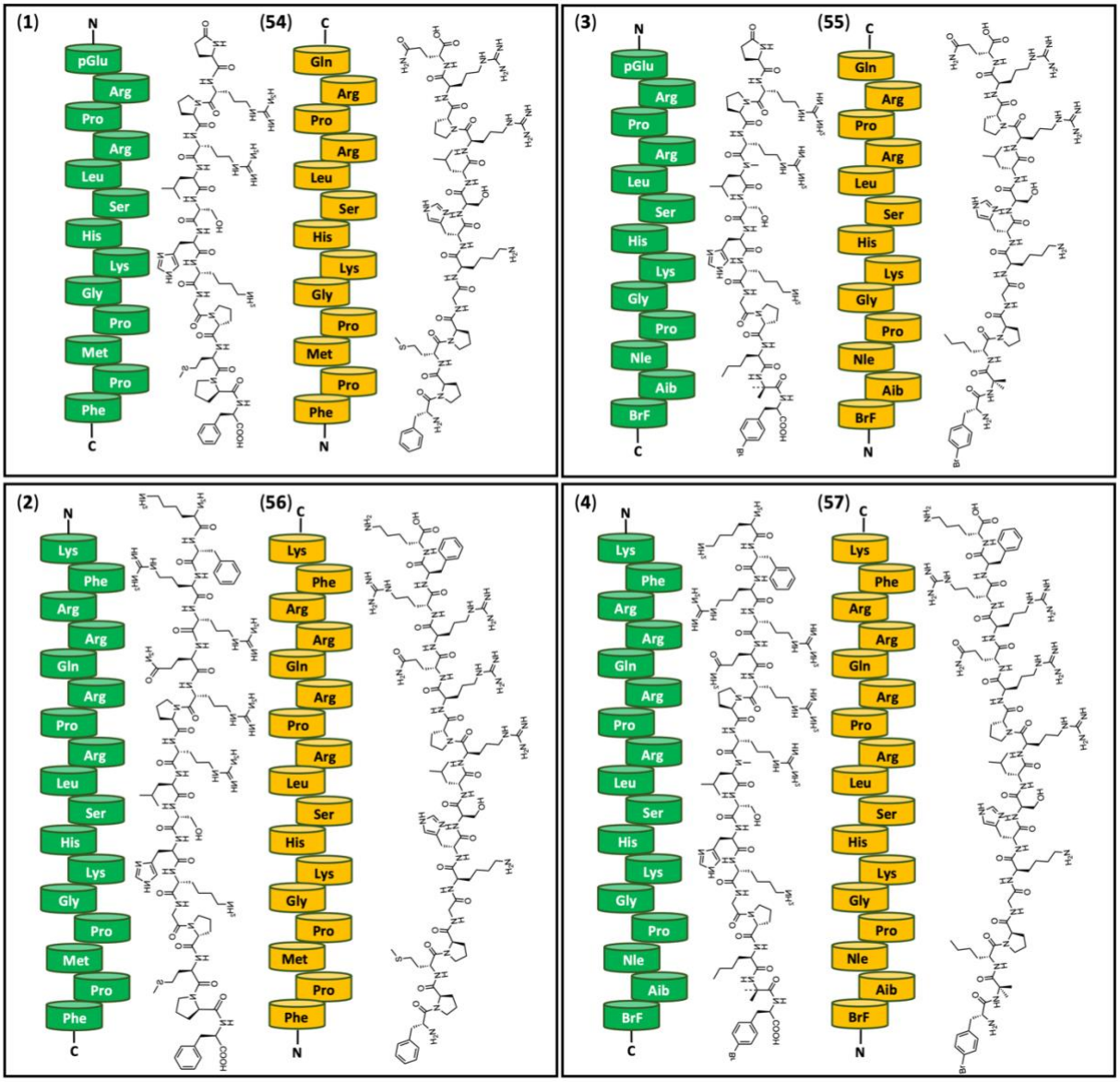


**Fig. 29** Schematic overview of the investigated retro-enantio peptides (**54-57**, yellow) and their mother L-peptides (**1-4**, green).

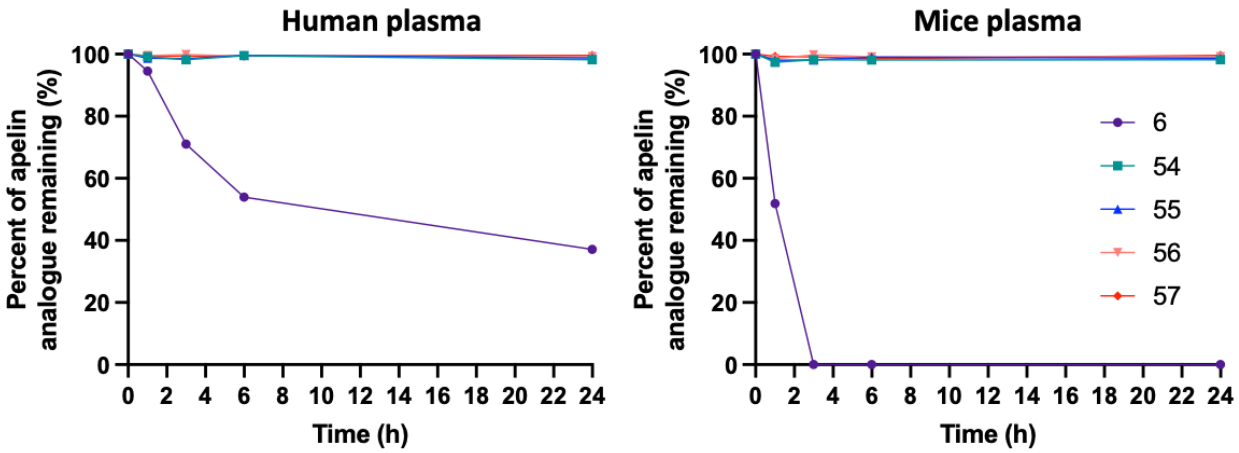


**Fig. 30** *In vitro* human plasma degradation trends for target retro-enantio analogues. Analogues include NEP-resistant (**6**), and RE (**54-57**) isoforms. Experiments were performed in duplicates of three replicates. Errors represent S.E.M.

# Chapter 3 Composition and Activity of Antifungal Lipopeptides Produced by *Bacillus* Spp. During *Daqu* Fermentation

## 3.1 *Daqu* Fermentation and *Bacillus* Spp. Background

*Baijiu*, distilled Chinese liquor, is one of the most popular alcoholic beverages in China,[134] and is usually prepared with wheat, rice, barley, sorghum, or corn.[134,135] *Baijiu* differs from Japanese sake, which uses back-slopped *koji* (cooked rice or soya bean) with domesticated strains of *Aspergillus oryzae* as the main fermentation organisms.[136] In addition, *baijiu* differs from the alcoholic cereal fermentations in Europe and Africa where malt is used as a source of enzymes; but for *baijiu*, hydrolytic enzymes are provided by microbial saccharification cultures including *daqu*, which is produced by spontaneous fermentation of cereals.[137–139] The fermentation process of Chinese liquor consists of two stages: (1) the production of the saccharification starter *daqu*, and (2) the mash fermentation for ethanol production.[140,141] *Daqu* is divided into three categories: low-, medium-, and high-temperature *daqu*, which result in either a light, soy sauce, or strong *baijiu* flavour, respectively.[142] The medium-temperature *daqu* is the most widely used starter in the production of traditional Chinese *baijiu*.[143]

The microorganisms in *daqu* consist of various bacteria, yeasts, and mycelial fungi.[144] Bacterial species include *Bacillus* species, such as *Lactobacillaceae* and *Enterobacteriaceae*. *Bacillus* species are found to be the dominant organism throughout the fermentation process.[144–146] *Saccharomyces* spp. are the most frequently isolated yeasts,[145] and the fungal strains consist of *Mucor* spp., *Penicillium* spp., and the dominant strain, *Aspergillus* spp.[145,147].

*Daqu* is produced using unsterilized raw materials exposed to an open environment, without a starter culture or inoculum, where the fermentation organisms are obtained from the raw

material or the environment. *Bacillus* spp. are invariably present in cereal grains[148] because they form stable associations with plants in the rhizosphere or as endophytes.[149,150] *Daqu* blocks provide a large surface area to support the growth of aerobic bacilli, and the low moisture content limits the growth of *Enterobacteriaceae* and lactic acid bacteria.[134] These ecological parameters, and the ability of *Bacillus* endospores to remain active at high-temperature conditions and low relative humidity, allow *Bacillus* spp. to dominate throughout the production.[146,151]

During *daqu* production, hydrolytic enzymes (e.g., amylolytic enzymes) are produced by bacteria and fungi, where *Bacillus* spp. are the major producers of extracellular amylolytic enzymes.[152,153] *Bacillus* amylases are the major components for starch liquefication and saccharification in the subsequent mash fermentation.[154] In addition, proteolytic enzymes, produced by bacilli and fungi, produce amino acid precursors for the synthesis of volatile flavour compounds during mash fermentation.[153] *Bacillus* spp. also produces a variety of lipopeptides that exhibit antimicrobial activity,[155,156] which are produced by polyketide synthases (PKS) and non-ribosomal peptide-synthetases (NRPS).[157] The lipopeptides produced by *Bacillus* spp. in this study are grouped into several families (e.g., fengycins, iturins, and surfactins).[155] These lipopeptides inhibit or kill fungi either by affecting spore germination, inhibiting mycelial growth, or causing the hyphae or spores to swell or lyse.[158] The genes responsible for the production of these antifungal lipopeptides, *bioA*, *bymB*, *fenD*, *ituC*, *srfAA*, *srfAB*, *yngG*, and *yndJ*, were identified in the bacilli genome isolated from *daqu*.[159] *Bacillus* lipopeptides were also identified in *daqu* and *baijiu*, where surfactin accumulated to a concentration of 7 mg/kg in the *daqu* stage of *baijiu* fermentation, where the concentration of the non-volatile peptide in the distilled end-product was $< 1$ $\mu$g/L. [152,160]

### 3.2 Aims of Study

In this study, initiated and done in collaboration with Dr. Michael Gänzle's research group, we looked to provide a comprehensive qualitative analysis of several antifungal lipopeptide congeners of fengycin, iturin A, and surfactin, from LB broth, and simple and complex *daqu* models. In addition, we looked to determine the *in situ* antifungal activity in simple and complex *daqu* models, since previous studies discovered only one or two peptides in *jiuqu*/*baijiu* samples and did not verify their biological activity.[160,161] In addition, current studies on the contribution of the diverse microbes in *daqu* to enzymatic and microbial compositions is based on uncontrolled, spontaneous fermentations,[140,143,147] but we looked to perform targeted analysis of *daqu* models to determine the role of the *Bacillus* species, and the correlated production of antifungal lipopeptides, on community assembly in *daqu*.

### 3.3 Results and Discussions

#### 3.3.1 Antimicrobial Lipopeptides in LB Cultures

antiSMASH was performed by Dr. Gänzle's lab to predict the production of antimicrobial peptides in the genomes of three *Bacillus* species, *B. amyloliquefaciens* Fad We, *B. amyloliquefaciens* Fad 82, and *B. velezensis* FUA2155. The predicted peptides (i.e., bacillaene, bacillibactin, bacilysin, butirosin A/B, fengycin, iturin, and surfactin) and percent sequence identity of these peptides were identical in the two strains of *B. amyloliquefaciens* (**Fig. 31**). *B. velezensis* FUA2155 was predicted to also produce three additional antimicrobial peptides; two surfactin, a difficidin, and a macrolactin H gene clusters. Difficidin has been shown to exhibit both antibacterial and antifungal activity,[162] and macrolactin H has shown antibacterial activity against

*Staphylococcus aureus* (MIC = 10 mg/L).[163] BLASTn was used to verify the predictions by antiSMASH. Based on the presence of the gene clusters for antimicrobial lipopeptides and literature data on their antifungal activity, the peptides fengycin, iturin, and surfactin were selected for subsequent experiments.

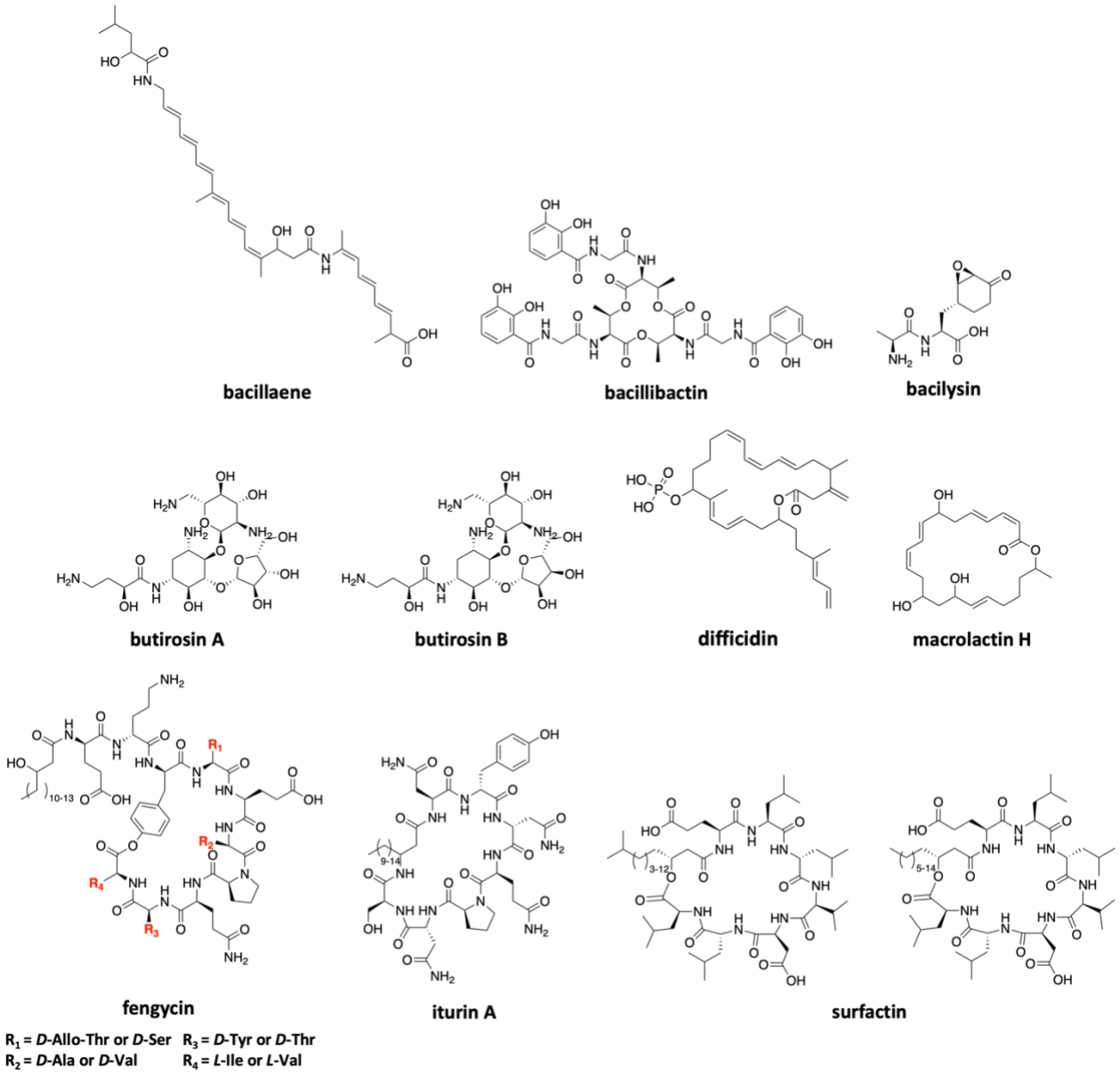


**Fig. 31** Chemical structures of predicted products from the genomes of three *Bacillus* strains, *B. amyloliquefaciens* Fad We, *B. amyloliquefaciens* Fad 82, *B. velezensis* FUA2155, using

antiSMASH. Fengycin peptides (A-D, S) differentiated by $R_1$-$R_4$: A = D-Allo-Thr, D-Ala, D-Tyr, L-Ile; B = D-Allo-Thr, D-Val, D-Tyr, L-Ile; C = D-Allo-Thr, D-Ala, D-Thr, L-Ile; D = D-Allo-Thr, D-Val, D-Tyr, L-Val; and S = D-Ser, D-Val, D-Tyr, L-Val.

To determine whether the presence of these gene clusters is correlated with the production of the corresponding lipopeptide, a mixture of lipopeptides were extracted from LB culture supernatants of *B. amyloliquefaciens* Fad We, *B. amyloliquefaciens* Fad 82, and *B. velezensis* FUA2155. The signal intensities of fengycin, iturin A, and surfactin were qualitatively analyzed with high performance liquid chromatography coupled with mass spectrometry (HPLC-MS), and the signal intensities were $\log_{10}$ transformed and shown in a gradient (Fig. 32). Of the three families of lipopeptides assessed, fengycins were not detected in any of the LB cultures. Iturins were produced by all three strains, but the log[signal intensities] in the methanol extracts, from the LB cultures of *B. amyloliquefaciens* Fad We and *B. amyloliquefaciens* Fad 82, were present at approximately 100 times lower than that in the *B. velezensis* FUA2155 extracts. However, surfactins were detected in all three strains of *Bacillus* with high signal intensity. The signal intensity of most surfactin congeners from the LB cultures of *B. amyloliquefaciens* Fad 82 were several orders of magnitude lower than that of the other two strains.

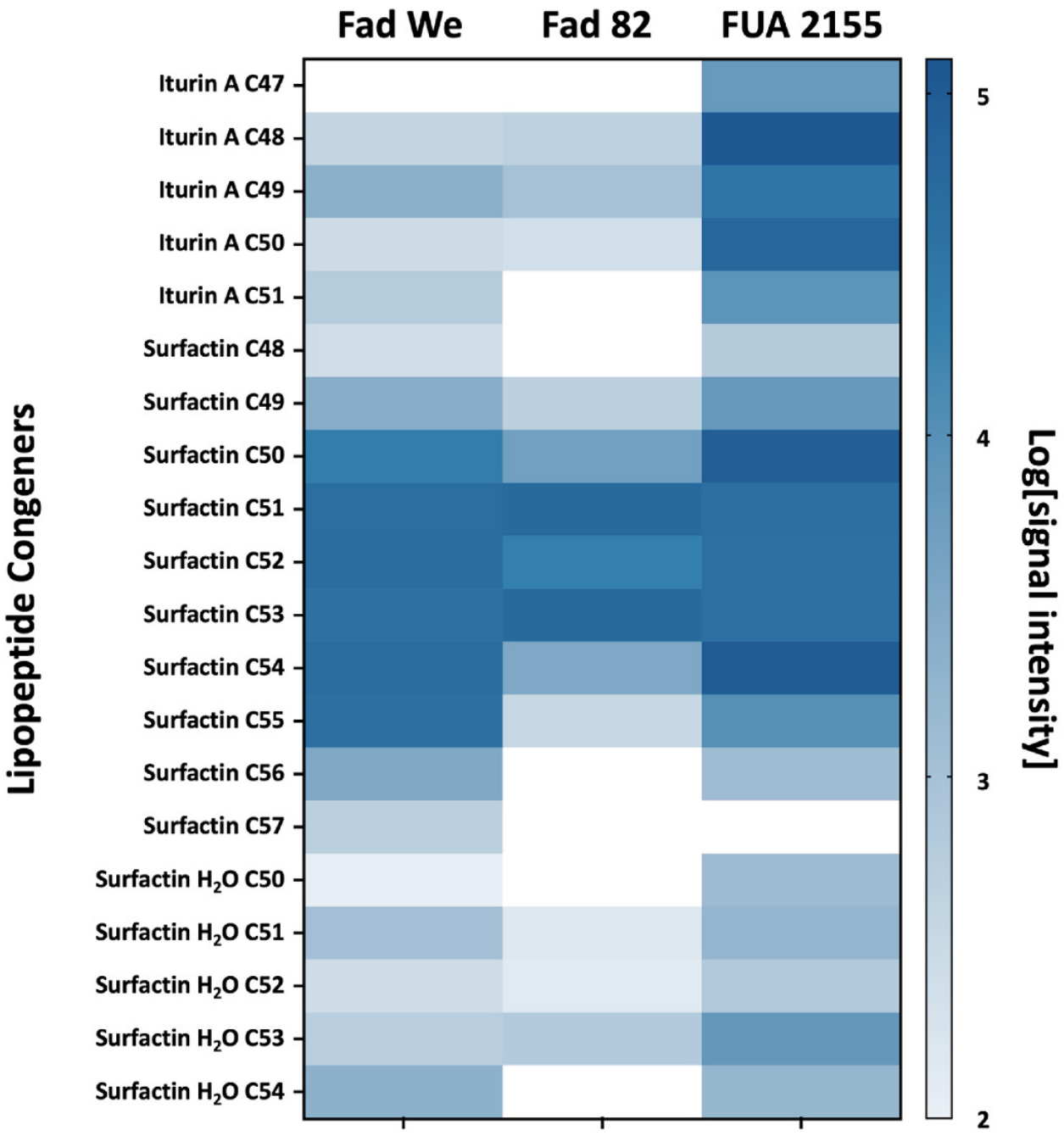


**Fig. 32.** Heat map of detected lipopeptide congeners from *Bacillus amyloliquefaciens* Fad We, *B. amyloliquefaciens* Fad 82, and *B. velezensis* in LB broth samples. Each LB sample was analyzed *via* high performance liquid chromatograph coupled with mass spectrometry (HPLC-MS) and the log[signal intensities] are represented in a gradient. CX (X = number of total carbons in the molecule). The heatmap is representative of experiments performed in three biological replicates.

Lastly, using commercial fengycin, iturin A and surfactin, critical dilution assays were performed to determine the minimum inhibitory concentration (MIC) (**Fig. 33**). Five filamentous fungi and three yeasts were used as indicator strains. Iturin A inhibited 7 of the 8 indicator strains, exhibiting a MIC range of 10 to 50 mg/L; only *Saccharomycopsis fibuligera* FUA4036 was relatively resistant. The MIC values of fengycin and surfactin against most indicator strains ranged from 300 to 500 mg/L; with the higher value being the highest concentration tested. Fengycin showed inhibition of *Mucor racemosus* FUA5009 and *Saccharomyces cerevisiae* FUA4002 at a concentration of approximately 200 mg/L.

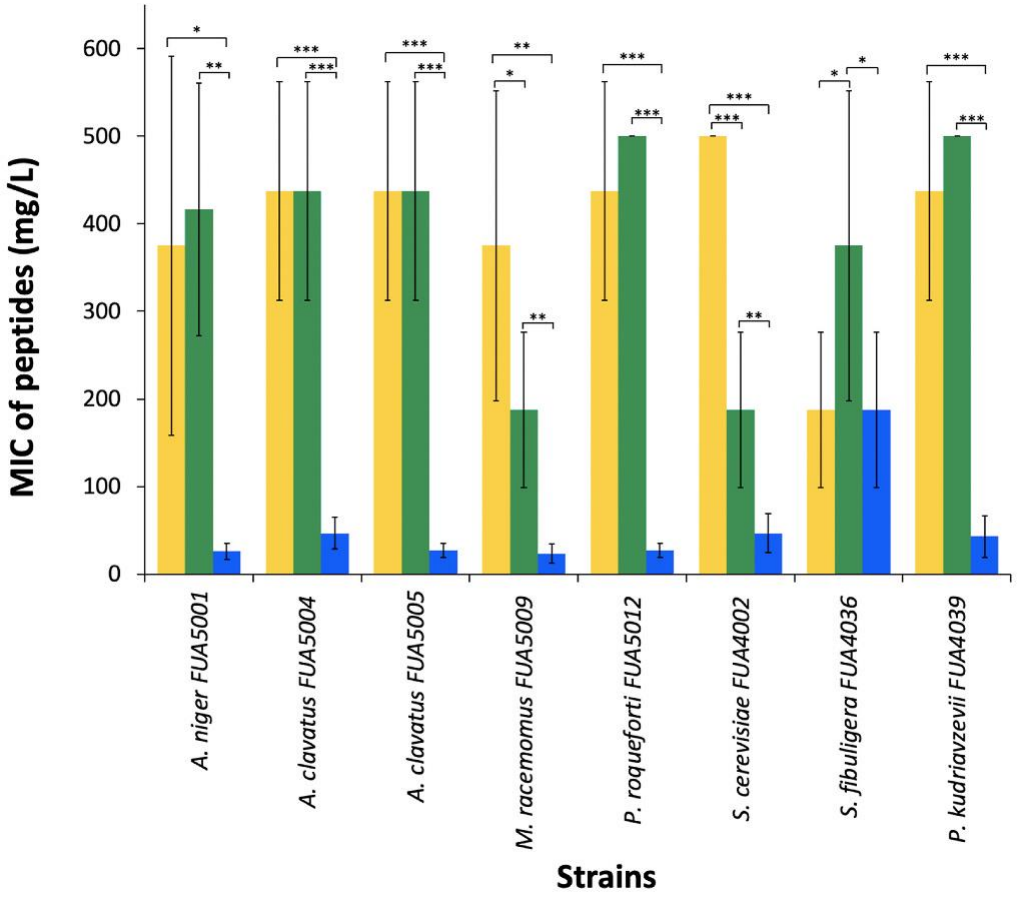


**Fig. 33** Minimum inhibitory concentration (MIC) of three lipopeptides against filamentous fungi and yeasts. Surfactin (yellow bar), fengycin (green bar) and iturin A (blue bar). MIC values are

presented as means ± standard deviation of four independent experiments. Significant differences (labelled with asterisks, *) were determined using a *t*-test: *, $P < 0.05$, **$P < 0.01$, ***, and $P < 0.001$.

### 3.3.2 Antimicrobial Lipopeptides in Simplified *Daqu* Model

The three strains of *Bacillus* used in this study were isolated from *daqu* (*B. velezensis* FUA2155)[164] and ropy bread (*B. amyloliquefaciens* Fad We and *B. amyloliquefaciens* Fad 82)[165]. These strains are beneficial technological traits in *daqu* as they encode several amylases which can hydrolyze starch during the storage of bread.[148] In order to determine their suitability as cultures for *daqu* fermentation, the strains were evaluated in a simplified *daqu* model, where each treatment was inoculated with one strain of the *Bacillus*; un-inoculated wheat flour was used as a control. From these fermentations, a similar trend in the pH changes was seen between the three *Bacillus* species and the control treatment (**Fig. 34**).

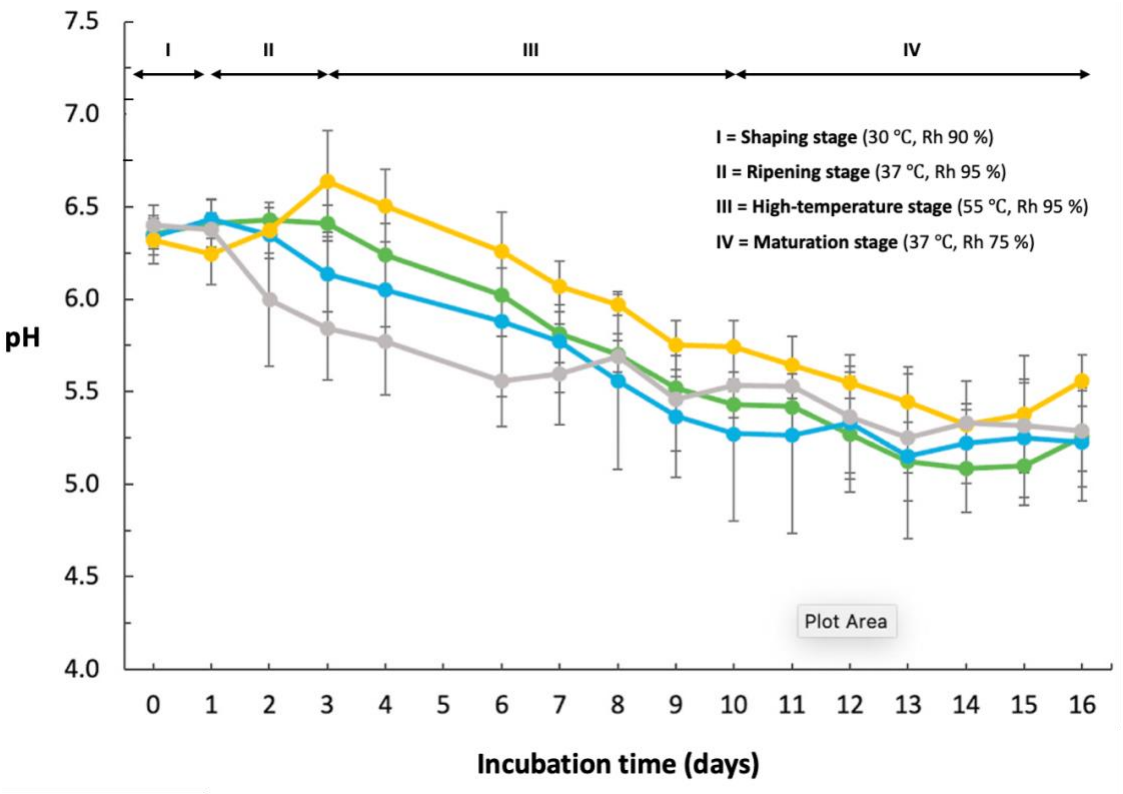


**Fig. 34** pH changes throughout the fermentation of the simplified *daqu* model. The different stages of the fermentation process are indicated; Rh = relative humidity. Different line colours indicate the *Bacillus* strains used to inoculate the *daqu* models: *B. amyloliquefaciens* Fad We (green); *B. amyloliquefaciens* Fad 82 (blue); *B. velezensis* FUA2155 (yellow); and control (grey, without the addition of a *Bacillus* strain). Results represent the means ± standard deviation for five biological replicates.

For all treatments, a pH decrease was seen from 6.5 to approximately 5.5, with a slight overall higher pH for samples inoculated with *B. velezensis* FUA2155, especially during the ripening stage. The total viable cell counts were also determined during the simplified *daqu* fermentation (**Fig. 35**). *B. amyloliquefaciens* Fad We and *B. velezensis* FUA2155 showed consistent and high cell counts of approximately 8 log(CFU/mL) throughout the fermentation stages. However, the cell counts of samples inoculated with *B. amyloliquefaciens* Fad 82 significantly dropped after the ripening stage; a similar trend was observed in the control treatment.

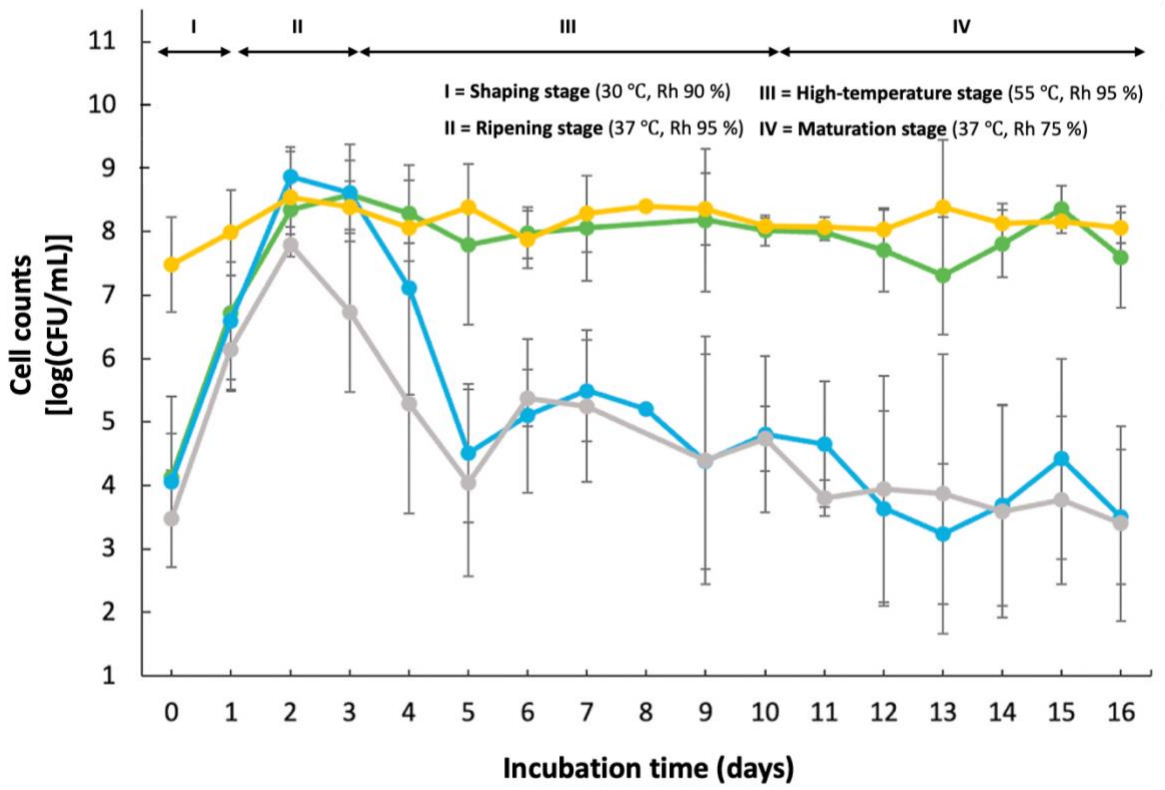


**Fig. 35** Viable cell counts during the incubation of the simplified *daqu* model. The different stages of the fermentation process are indicated; Rh = relative humidity. Different line colours indicate the *Bacillus* strains used to inoculate the *daqu* models: *B. amyloliquefaciens* Fad We (green); *B. amyloliquefaciens* Fad 82 (blue); *B. velezensis* FUA2155 (yellow); and control (grey, without the addition of a *Bacillus* strain). Results represent the means ± standard deviation for five biological replicates.

To determine the longevity or viability of the *Bacillus* inocula, an initial assessment was done to observe the colony morphology on LB agar plates. In the uninoculated control samples, less than 10% of the total colonies matched the characteristic colony morphologies for the *Bacillus* strains used. However, in the samples inoculated with *B. amyloliquefaciens* Fad 82, approximately 70% of the total colonies resembled the morphology of the *Bacillus* strain. Furthermore, samples inoculated with *B. amyloliquefaciens* Fad We or *B. velezensis* FUA2155 resulted in more than 90%

of the total colonies displaying the same morphology as the inoculum. From the quantification of gene expression, cell counts, and observation of the colony morphologies, these results suggest that *B. amyloliquefaciens* Fad We and *B. velezensis* FUA2155 were the dominant fermentation microbes in the simplified *daqu* models. In addition to the bacterial growth, the growth of mycelial fungi was also observed on the *daqu* sample surfaces (**Fig. 36**). In the uninoculated control samples, substantial mould growth was observed at day 2, and by day 3, most of the surface was covered with mycelia. The mould growth on samples inoculated with *B. amyloliquefaciens* Fad 82 was comparable to the control. Samples inoculated with *B. amyloliquefaciens* Fad We did not show visible mould growth and formation of conidia until day 4. *Daqu* samples inoculated with *B. velezensis* FUA2155 showed no visible mould growth throughout the fermentation period. On day 4, all *daqu* samples were transferred to 55 °C, which would inhibit further growth of moulds.

| Inoculated strain | Incubation time | | | | |
|---|---|---|---|---|---|
| | Day 0 | Day 1 | Day 2 | Day 3 | Day 4 |
| Control | — | — | + + + | + + + + | + + + + |
| *B. amyloliquefaciens* Fad We | — | — | + | + | + + |
| *B. amyloliquefaciens* Fad 82 | — | — | + + + + | + + | + + + |
| *B. velezensis* FUA2155 | — | — | — | — | — |

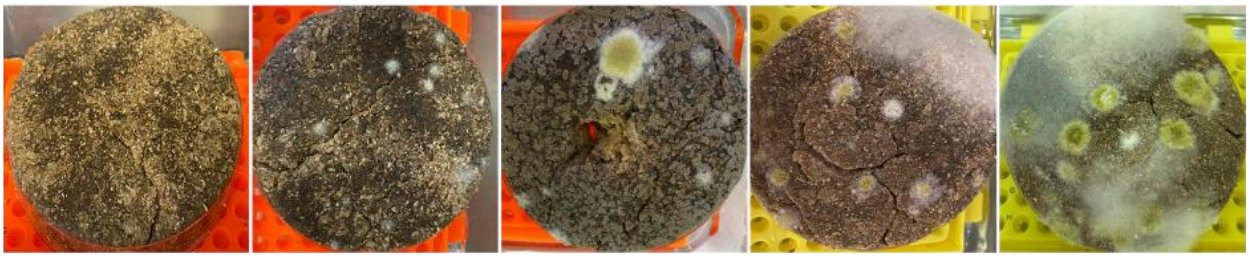

| - | + | ++ | +++ | ++++ |
|---|---|---|---|---|

**Fig. 36** Degree of mould growth during the first 4 days of the simplified *daqu* model. Fungal growth was indicated as follows: —, no visible mycelial growth; +, small spots of mycelial growth; + +, spots of mycelial growth and conidia, + + +, 25-50 % of surface covered by mycelia; and + + + +, >50 % of surface covered by mycelia.

To determine whether antifungal lipopeptides are expressed during bacilli growth in the simplified *daqu* model, quantification of the mRNA, encoding for *fenA*, *ituA*, and *srfAA*, was performed using RT-qPCR (**Fig. 37**). All three genes were expressed by all three *Bacillus* strains, where overexpression of *fenA* and *srfAA* was observed at day 1 and/or day 2 of fermentation. On day 3, *srfAA* was downregulated in all three strains. *FenA I* and *ituA* were also down-regulated on day three of incubation with *B. amyloliquefaciens* Fad 82. With these results, the expression of *fenA*, *ituA*, and *srfAA* indicates that the corresponding lipopeptides may be present in the simplified *daqu* preparation.

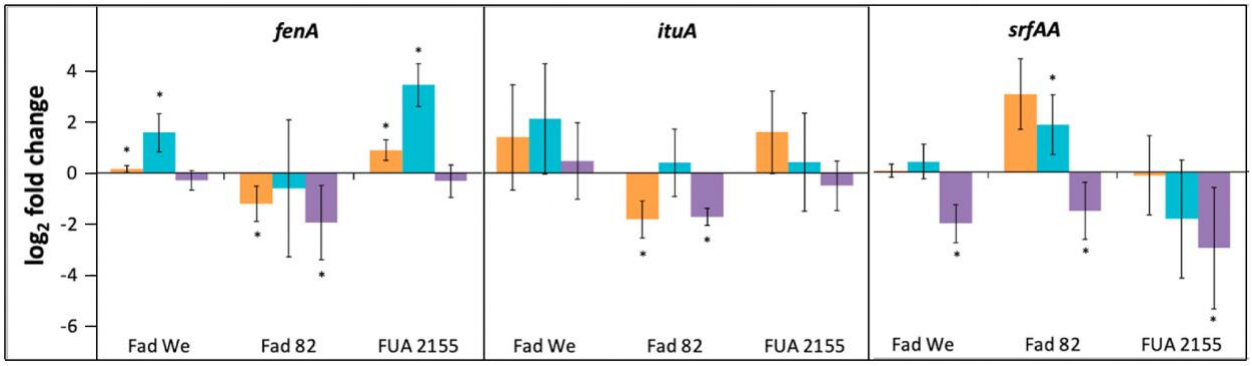


**Fig. 37** Gene expression levels of *fenA, ituA*, and *srfAA* in the simplified *daqu* model inoculated with *B. amyloliquefaciens* Fad We, *B. amyloliquefaciens* Fad 82 and *B. velezensis* FUA2155. Days are depicted as coloured bars: 1st (orange bar), 2nd (blue bar), and 3rd day (purple bar). Relative gene expression was quantified with RT-qPCR using *gyrB* as the housekeeping gene and the exponential cultures in LB broth as reference conditions. Significant differences (*, $P < 0.05$) were determined between the *daqu* model and LB broth conditions with *t*-tests. Data represent the means ± standard deviation from three independent experiments.

### 3.3.3 Antimicrobial Lipopeptides in Complex *Daqu* Model

To provide evidence of the production of antifungal lipopeptides in *Bacillus*-inoculated *daqu* samples, extracts were analyzed for their antifungal activity and the presence of fengycin, iturin A, and surfactin (**Table 6**). A complex *daqu* model was prepared for this investigation, which consists of inoculating *daqu* samples with one of the *Bacillus* strains and the following fermentation organisms: Aspergillus *niger* FUA5001, *Mucor racemosus* FUA5009, *Penicillium roqueforti* FUA5012, *Saccharomyces cerevisiae* FUA4002, *Saccharomycopsis fibuligera* FUA4036, *Pichia kudriavzevii* FUA4039, *Kosakonia cowani*i FUA10121 and *Weissella cibaria* FUA3456. Control samples included inoculation with all 8 fermentation organisms, in the absence of the *Bacillus* strains; *Aspergillus niger* FUA5001 was used as the indicator strain. Methanol extracts from the control samples did not inhibit mould growth, indicating that the *Bacillus* strains may be the sole or main contributors to antifungal activity. After 1 d of incubation, the inhibitory

activity of the *daqu* extracts was highly variable. Extracts from *daqu* samples inoculated with *B. amyloliquefaciens* Fad We, *B. amyloliquefaciens* Fad 82, and *B. velezensis* FUA2155 showed strong and consistent antifungal activity from days 1 to 6; however, the inhibitory activity of the two *B. amyloliquefaciens* strains was weaker compared to the *daqu* with *B. velezensis* FUA2155.

**Table 6** Antifungal activity of peptides extracted from the complex *daqu* model. *daqu* samples were inoculated with eight fermentation organisms with or without (control) one of the *Bacillus* strains in this study. 0 = no inhibition; 0-0.9 = slight inhibition; 1-1.9 = moderate inhibition; 2-2.9 = strong inhibition; ≥ 3 = significant inhibition. Data represent the means ± standard deviation of three independent experiments, performed in three replicates.

| **Inoculated strain** | **Incubation time** | | | | | |
|---|---|---|---|---|---|---|
| | Day 1 | Day 3 | Day 6 | Day 10 | Day 13 | Day 16 |
| Control | 0 | 0 | 0 | 0 | 0 | 0 |
| *B. amyloliquefaciens* Fad We | $3 \pm 4$ | $1 \pm 1$ | $1 \pm 0.5$ | $1 \pm 0.5$ | $0 \pm 0$ | $0.3 \pm 0.5$ |
| *B. amyloliquefaciens* Fad 82 | $0.3 \pm 0.5$ | $2 \pm 1.7$ | $1 \pm 0.8$ | $1 \pm 0$ | $1 \pm 0$ | $2 \pm 2$ |
| *B. velezensis* FUA2155 | $3 \pm 4$ | $3 \pm 1$ | $2 \pm 1$ | $1 \pm 0$ | $1 \pm 0.5$ | $1 \pm 2$ |

To confirm the antifungal activity of the *Bacillus* strains, an analysis of the microbiota was performed to quantify the *Bacillus* strains, total bacteria, and fungi (**Fig. 38**). In the ripening stage (days 1 to 3), an increase of the three parameters (*Bacillus*, total bacteria, and fungi) was found in each sample. *B. velezensis* FUA2155 showed the highest log(copies/g) of *Bacillus* and total bacteria gene copies with the lowest log(copies/g) of fungal gene copies throughout the fermentation period. The log(copies/g) of total bacteria of the samples inoculated with *B. amyloliquefaciens* Fad We and *B. amyloliquefaciens* Fad 82, during the high-temperature stage

(days 3 to 10), ranged from 11 to 12 but decreased on the 13th day; the log(copies/g) of fungi remained stabled after day 3. Overall, the gene copies of *Bacillus*, total bacteria, and fungi, differed among the complex *daqu* samples inoculated with the three *Bacillus* strains, however, inoculation with *B. velezensis* FUA2155 showed competitive growth against fungal organisms.

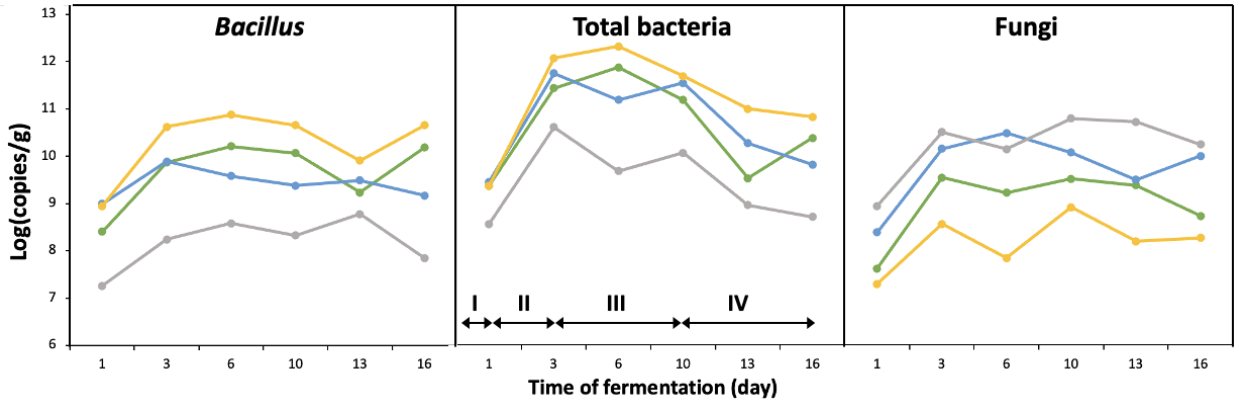


**Fig. 38** Microbiota analysis of the complex *daqu* samples. Different line colours indicate the *Bacillus* strains used to inoculate the *daqu*: *B. amyloliquefaciens* Fad We (green); *B. amyloliquefaciens* Fad 82 (blue); *B. velezensis* FUA2155 (yellow); and control (grey, without the addition of a *Bacillus* strain). I = shaping stage (30 ℃, Rh 90 %); II = ripening stage (37 ℃, Rh 95 %); III = high-temperature stage (55 ℃, Rh 95 %); and IV = shaping stage (37 ℃, Rh 75 %).

### 3.3.4 Analysis of antifungal lipopeptides in extracts from the complex *daqu* model by LCMS-MS

To further assess the production of the lipopeptides from the three *Bacillus* strains in *daqu*, methanol extracts from the complex *daqu* model were analyzed for the presence of three target antifungal lipopeptides (Fig. 39). The signal intensities (area under the curve) of the lipopeptides extracted from several incubation time points were detected by reverse phase-high performance liquid chromatography-mass spectrometry (RP-HPLC-MS). The signal intensities of fengycin, iturin A, and surfactin were $\log_{10}$ transformed, log[signal intensity]. The signal intensity of the

three lipopeptide families was variable among the different *daqu* samples. Similar to the results from the LB culture extracts, fengycin was not detected in any of the samples. Some surfactin congeners were detected among all the samples, including the control group; low levels of the lipopeptides can be expected since the grains used as the substrate for *daqu* fermentation already contained *Bacillus*. Signal intensities for surfactins C52-C55 in the *B. amyloliquefaciens* Fad We samples were relatively high from days 1 to 10 (**Fig. 39**). Surfactin C50-C55 showed the highest intensities in the *B. velezensis* FUA2155 samples from days 3 to 10. The signal intensities for the surfactin congeners were not as high for the *B. amyloliquefaciens* Fad 82 samples, where the signal intensities decreased below the limit of detection after day 10. Finally, the log[signal intensity] of the iturin congeners demonstrated a substantial difference between the complex *daqu* samples. For the *B. velezensis* FUA2155 samples, iturin C47-C51 was found at relatively high intensities throughout the incubation period. The trend was similar for the *B. amyloliquefaciens* Fad We samples but at a lower signal intensity and absence of detection of the iturin A C47 congener. Lastly, the signal strengths of iturin congeners were low or below the limit of detection for the *B. amyloliquefaciens* Fad 82 and control samples.

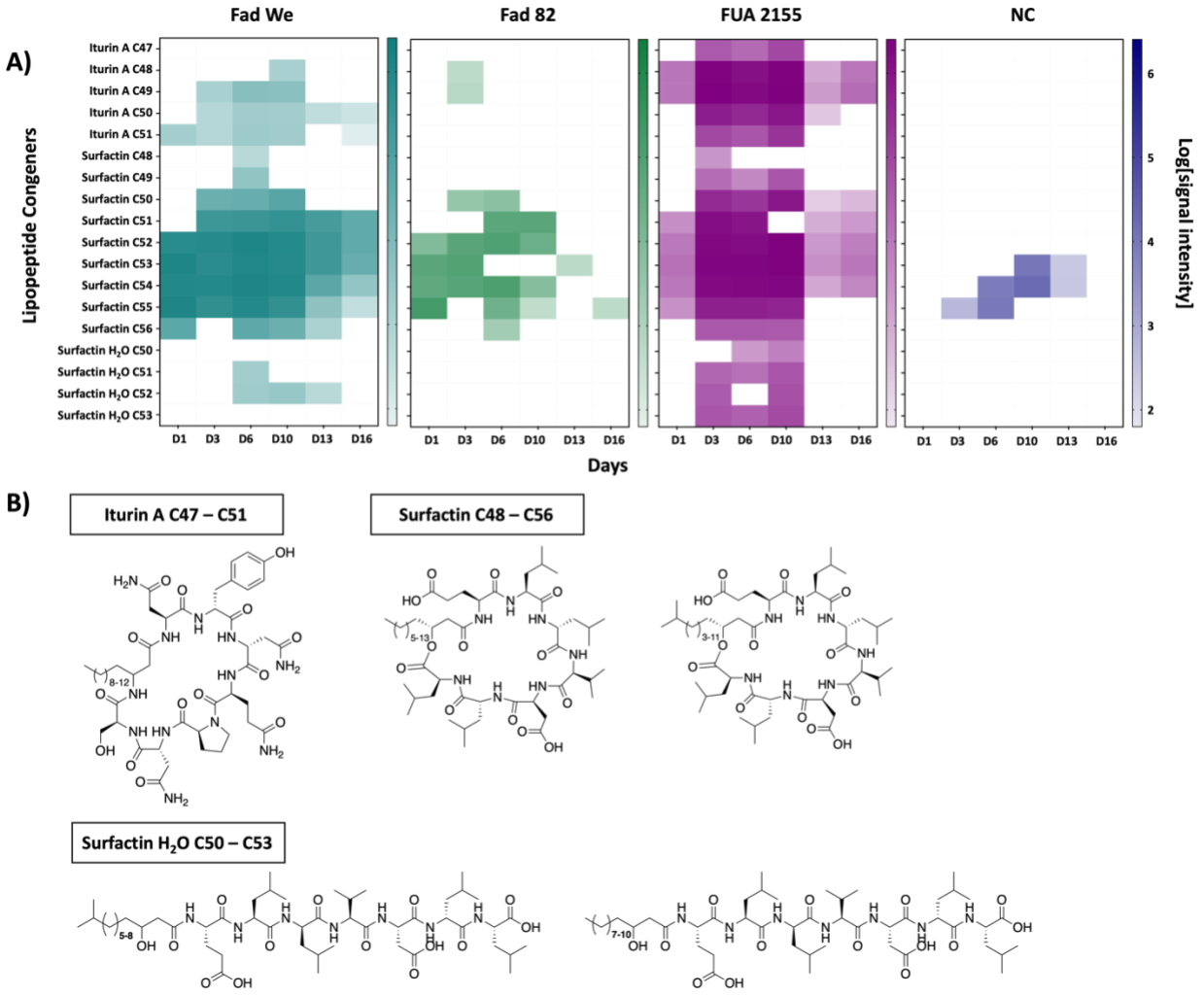


**Fig. 39** Signal intensities of lipopeptides extracted from the complex *daqu* model at different time points of incubation. (A) Heat map of lipopeptide congeners produced by *B. amyloliquefaciens* Fad We (teal), *B. amyloliquefaciens* Fad 82 (green), and *B. velezensis* FUA2155 (magenta) in the complex *daqu* model inoculated with an additional eight bacterial and fungal strains. The control samples (blue) represent inoculation with the eight bacterial and fungal strains, in the absence of the *Bacillus* strains. Samples were analyzed *via* reverse phase- high performance liquid chromatography-mass spectrometry (RP-HPLC-MS), and the log[signal intensities] are shown as a gradient. (B) Base structures of the present antifungal lipopeptide congeners; varying alkyl chain lengths are denoted by the bolded numbers. CX (X = number of total carbons in the molecule). The heatmap is representative of three biological replicates, performed in two replicates.

### 3.4 Conclusions and Future Directions

The production of antifungal lipopeptides has been previously described for multiple *Bacillus* strains isolated from solid-state fermented products.[159,166,167] These lipopeptides have unique chemical structures and biological activities (e.g., broad-spectrum antimicrobial activity).[155] For example, fengycin and iturin interact with lipid layers to alter the permeability of cell membranes,[168,169] or surfactins, which are powerful biosurfactants with emulsifying properties able to tightly anchor into lipid layers and can thus interfere with the integrity of the biological membrane.[170] The substrate used for bacilli growth strongly impacts the overall amount of lipopeptides produced, as well as the relative abundance of the different lipopeptides,[171] therefore, studies in laboratory media are not reliable to predict the production of lipopeptides in food fermentations. In this study, we were able to demonstrate the presence and production of three families of antifungal lipopeptides, fengycin, iturin, and surfactin in LB media, and simple and complex *daqu* fermentation.

To date, the formation of these lipopeptides and their different congeners, in food fermentations, have not been described. Based on the MIC assays performed of fengycin, iturin A, and surfactin against several strains of fungi and yeasts, iturin A showed the highest antifungal activity against 7 of the 8 indicator strains, resulting in an MIC range of 10 to 50 mg/L, which supports earlier studies.[172,173] Considering the MIC assays and mass spectrometry analysis of the simple and *daqu* samples, iturin A, produced by *B. velezensis* FUA2155, is likely the main contributor to the higher antifungal effect of this strain compared to the two *B. amyloliquefaciens* strains.[174,175] In conclusion, the presence of *Bacillus* species in *daqu* fermentation affects both the production of amylolytic and proteolytic enzymes and the community assembly through the production of antimicrobial lipopeptides. The bacterial production of both hydrolytic enzymes and

lipopeptides are dependent on the growth medium, therefore, further studies are necessary to understand the interaction between the *Bacillus* species and fungi, and its impact on product quality. Moreover, the role of the length of the acyl side chain on antifungal activity is not completely understood since these studies are limited by the presence of multiple isoforms or multiple lipopeptides in even purified fractions. Therefore, more specific purification techniques could be developed to further separate these congeners and determine their antifungal properties.[176–178]

# Chapter 4 Investigation on the Biocontrol Potential of *Beauveria bassiana* Against the Mountain Pine Beetle, *Dendroctonus ponderosae*, Epidemic

## 4.1 MPB epidemic and *B. bassiana* background

The mountain pine beetle (MPB), *Dendroctonus ponderosae* (Hopkins; *Coleoptera: Curculionidae*), is an irruptive bark beetle that has infested millions of hectares of pine (*Pinus*) forests in western Canada.[179] In addition, in the Western continental United States, over 10 million hectares of pine forests have been affected by MPB, resulting in approximately 50% of the total area affected by all bark beetle species in this region.[180] Periodic outbreaks of mountain pine beetles can cause mortality of trees over large areas, where the most recent outbreak, beginning in the late 1990s, was exacerbated due to the warming environment. This change in climate increased MPB populations and their spread, as well as increased the abundance of susceptible host trees.[181] At present, over 50% of mature lodgepole pine trees (*Pinus contorta* Dougl. ex. Loud.) have been lost in British Columbia, resulting in an estimated loss of $57 billion CAD in GDP (gross domestic product) and $90 billion CAD in welfare.[179] MPB is now considered an invasive species in northern Alberta, as these beetles have not historically occupied the boreal and subboreal pine forests east of the Rocky Mountains (Fig. 40).[182–185] Eastward expansion into Alberta has facilitated infestations within populations of lodgepole pine (*P. contorta*), jack pine (*P. banksiana*), and their hybrid (*P. contorta* × *P. banksiana*); hosts with limited defensive capacity due to inadequate coevolutionary interactions with MPB.[185–188] MPB poses a highly alarming

threat to the continent, as jack pine is the predominant species which extends across the Canadian boreal forest and the Atlantic Coast of Canada.[182,188–191]

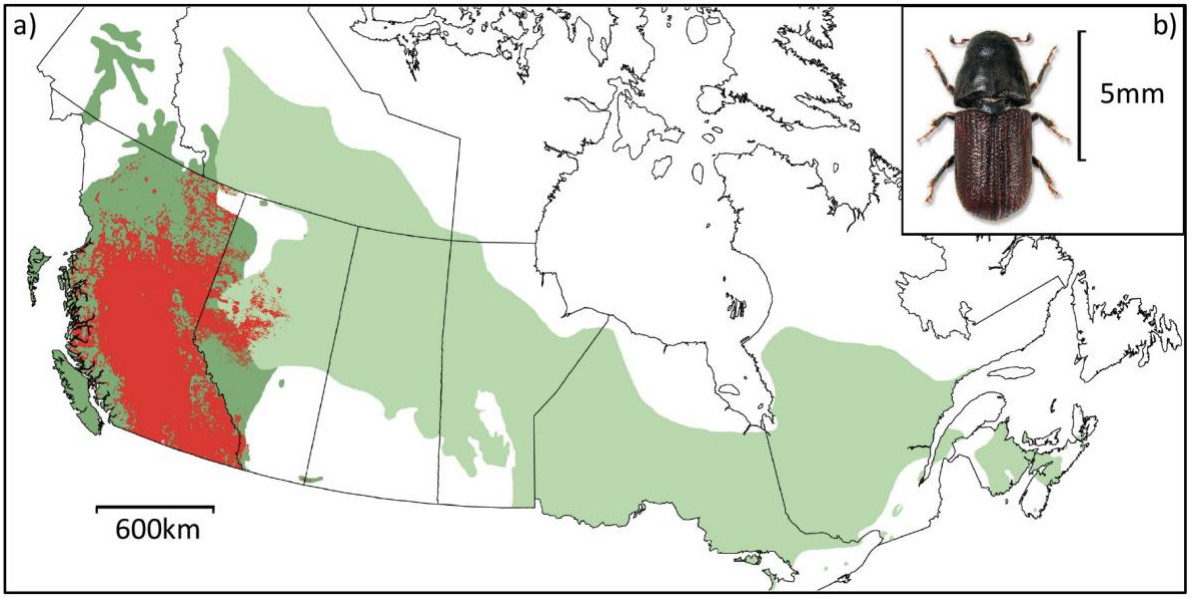


**Fig. 40** Geographical distribution of the *Dendroctonus ponderosae* epidemic in Canada. (A) Outbreak (red) in relation to *Pinus contorta* (dark green) and *P. banksiana* (light green) populations. (B) Mountain pine beetle adult. Photo provided by K. Bolte.

Efforts to mitigate the spread of MPB have been restricted by the lack of effective control methods, where the conventional approach comprises of the detection and physical removal of infested trees, through salvage harvesting and processing, or felling and burning.[192] However, these approaches are labour-intensive, costly, and logistically difficult, especially for remote infestations.[192] In the use of burning or fire as a direct control of MPB infestations, previous attempts have shown that high fire intensity was required for appreciable mortality; however, controlling high-intensity fires was difficult. The cryptic nature of MPBs also limits the development of alternative approaches to manage their populations. With the exception of the beetle flight periods from the parental trees, MPBs spend their entire life under the tree bark, where

they feed and develop – making the application of conventional exogenous pesticides impractical.[193] Furthermore, the mutualistic ophiostomatoid blue stain fungi, vectored by attacking MPBs during colonization, reduces the efficacy of systemic insecticides due to the blockage of the tree's vascular system.[194,195] From the limited registered pesticides used for the management of Canadian forests,[196] only chemical-based pesticides (e.g. carbaryl)[197] have been used for the management of trees colonized by MPB populations. However, these chemicals are often hazardous to both the ecosystem in general, and to off-target eukaryotic hosts, including humans.[198,199] The biological and physiochemical transformation, and the environmental persistence of these synthetic pesticides may affect the entire ecosystem negatively.[198,200,201] Therefore, exploration of an environmentally-friendly and biological-based mitigation approach, directly targeting MPBs, is critical for the management of their population; one approach being the use of entomopathogenic fungi (EPF).[199,202] Although the biocontrol potential of these fungal species had not been widely investigated, recent studies have shown that they demonstrate high host specificity while showing low detrimental effects on non-arthropod organisms (e.g., domesticated avian species).[203]

Studies of the mysterious silkworm disease in Italy lead to the discovery of the white muscardine fungus, *Beauveria bassiana*.[204] This organism is an entomopathogenic fungus that has previously been demonstrated to efficiently kill many species of insect pests, including the pine shoot beetle (*Tomicus piniperda* L.),[205] the European spruce bark beetle (*Ips typographus* L.),[206] the spruce beetle (*Dendroctonus rufipennis*),[207] and the red palm weevil (*Rhynchophorus ferrugineus*)[208]. Although certain *B. bassiana* strains have been shown to be lethal to MPB[209,210] and other bark beetle species in the laboratory[207,211], field tests in North America have often failed to demonstrate the desirable mycosis propagation and control of MPB populations. These field

observations may be associated with the harmful effects of ultraviolet (UV) light damage, lack of drought tolerance, and inefficient conidial density and viability of the *B. bassiana* strains.[207,212,213] Because of the extensive effort involved in these laboratory and field tests, most studies focus on only a few strains.

Recently, ninety-three *B. bassiana* isolates from various culture collections worldwide were evaluated and selected for their different phenotypes and virulence toward *D. ponderosae.*[210] A criterion was established (i.e., colony morphology, growth rate, conidial capacity, mycelial density, and pigmentation) to assess the pathogenicity and virulence potential of these *B. bassiana* strains against MPB in the laboratory. The strains were also categorized into three phenotypic classes based on the production of the pigment, oosporein. Oosporein is an extensively-studied red-coloured dibenzoquinone virulence factor, associated with insecticidal activity, which may also show potential UV resistance.[214–217] Class I strains grew felty, reddish colonies which produce high oosporein levels and display the highest levels of virulence against MPB.[210] Class II strains grew thin, cream-coloured powdery colonies with no pigment and had the lowest virulence against MPB; requiring a higher conidial titer to achieve the same pathogenicity. Lastly, the class III strains grew felty, yellowish colonies, with intermediate levels. Furthermore, several strains of *B. bassiana* have been approved as safe biological insecticides for agricultural purposes,[207,210,211,218,219] due to their limited effects on beneficial pollinating insects (e.g., honeybees, *Apis melligera*). In this thesis, we will look at the work we performed to evaluate the biocontrol potential of target *B. bassiana* strains to manage the MPB population, *in planta* and *in natura* conditions; in collaboration with Dr. Nadir Erbilgen's and Dr. Allan Carroll's research groups. In addition, the genome and transcriptome of several strains were assessed to determine

potential virulence factors; in collaboration with Dr. Inanc Birol's and Dr. Joerg Bohlmann's research groups.

## 4.2 *Beauveria bassiana* Shows Effective Lethalness to *Dendroctonus ponderosae* Populations in Greenhouse and Field Experiments

### 4.2.1 Aims of Study

In this study, we selected several target *Beauveria bassiana* isolates, representative of the various phenotypic morphotypes we previously established,[210] and evaluated their efficacy as a potential biocontrol agent for *Dendroctonus ponderosae* populations in greenhouse and field studies. We looked to develop and evaluate these isolates for their conidial stability under cold storage, *in planta* (i.e., greenhouse) and *in natura* (i.e., acreage and forest stand) conditions. To access the large *B. bassiana* conidial biomass, required for our infection assays in the field, we also looked to develop a large-scale biphasic liquid-solid fermentation approach using commercial fungal broth and parboiled rice substrate.[220] In addition, we formulated *in planta* bioassays to assess the virulence of *B. bassiana* powder formulations against MPB under greenhouse conditions. Lastly, we devised *in natura* experiments, under forest field conditions, to determine the effects of *B. bassiana* on the reproductive success of MPB.

### 4.2.2 Results and Discussion

#### 4.2.2.1 Conidial Stability of *B. bassiana* Powder Formulation Under Variable Conditions, and Comparative Conidial Yield of Biphasic Liquid-Solid Conidial Fermentation

The stability of entomopathogenic fungi-based powder formulations is dependent on various abiotic factors, including the type of formulation carrier and water activity.[221–224] An integral aspect that must be considered during mycoinsecticide development is the maintenance of the conidial state as a function of time, especially during storage. In this study, we used a proprietary kaolin clay-soluble starch-xantham gum-calcium carbonate powder formulation to determine the time-course conidial viability of representative *B. bassiana* conidial formulations under several abiotic factors (i.e., long-term cold storage, and *in planta* greenhouse and *in natura* acreage/field conditions). Using serial dilution, coupled with spread-plating techniques, the viable conidial population of select *B. bassiana* strains (i.e., UAMH 299, UAMH 1076, ANT-0, UAMH 4510, and 110.25) was monitored routinely. Across the eight-week cold storage at 4 °C, the conidial titer was consistent for the BioTitan WP powder formulation, containing the *B. bassiana* strain ANT-03, maintaining a culturable conidial yield of approximately 1.0 x $10^{10}$ CFU/g (Fig. 41). In addition, a year-old batch of BioTitan WP maintained the same conidial titre, supporting the commercial claim of a minimum concentration of 1.0 × $10^{10}$ CFU/g of *B. bassiana* ANT-03 for 18 months. Although starting at a much lower titer (1.0 × $10^{7}$ CFU/g) than the BioTitan WP formulation, our in-house powder formulations, containing either *B. bassiana* strain UAMH 299, UAMH 4510, and 110.25, also supported conidial formulation stability after eight weeks of storage at 4 °C. However, the powder formulations containing UAMH 4510 and 110.25 decreased in

conidial titer (< $1.0 \times 10^6$ CFU/g) to the extent that they were excluded from further *in planta* and *in natura* insect bioassays.

With the cold storage conidial stability results, we looked at developing a fermentation approach that we could use to produce enough conidia, relative to the starting titer of the BioTitan WP formulation, for our field trials. We developed a biphasic liquid-solid state fermentation approach, using a combination of Czapex Dox Yeast Extract Broth (CDBYE) medium and parboiled rice substrate. This fermentation approach resulted in a significant increase in conidial yield for both UAMH 299 by 10-fold, and UAMH 1076 by 100-fold (Fig. 41). This increase in conidial yield is likely a result of the enhanced aeration and increased surface area of the individual rice grains, which increases the mycelial yield during fermentation.[225] In addition, the higher vertical mycelial biomass may play a role in increasing the surface area for the aerial development of conidiophores, thereby enhancing the conidial yield.[225,226]

The *in planta* conidial viability of the powder formulations of ANT-03 and UAMH 299 were also tested on lodgepole pine bolts, which were incubated under greenhouse conditions at 25 °C for 8-12 weeks (Fig. 41). When applied to the bolts, the high titer (HIGH: $1.0 \times 10^9$ CFU/cm$^2$) of ANT-03, in the BioTitan WP formulation, resulted in significant stability over 12 weeks. However, the low titer (LOW: $1.0 \times 10^7$ CFU/cm$^2$) decreased a 100-fold by the eighth week. The conidial viability of both titers of the UAMH 299 formulation (HIGH: $1.0 \times 10^8$ CFU/cm$^2$, LOW: $1.0 \times 10^6$ CFU/cm$^2$) decreased by a 100-fold by the eight-week, resulting in a conidial concentration below the culturable limit of detection ($1.0 \times 10^6$ CFU/cm$^2$). These results prompted us to substitute UAMH 299 with another phenotypically similar strain within the red morphotype, UAMH 1076, due to its increased conidia l fermentation yield (10-fold vs. 100-fold, respectively).

Lastly, *in natura* conidial viability experiments were performed prior to the in-field infection assays (Fig. 41). We observed an average 10-fold reduction in conidial viability per week for all treatments throughout the three-week time course, suggesting that the abiotic factors had similar effects, regardless of the *B. bassiana* strains. The high titer of BioTitan WP, with the ANT-03 strain, declined from $1.0 \times 10^9$ CFU/cm$^2$ to $1.0 \times 10^7$ CFU/cm$^2$, while all the other treatments, BioTitan WP LOW ($1.0 \times 10^7$ CFU/cm$^2$), UAMH 1076 HIGH ($1.0 \times 10^8$ CFU/cm$^2$), and UAMH 1076 LOW ($1.0 \times 10^6$ CFU/cm$^2$), all declined under the effective lethal dose ($1.0 \times 10^6$ CFU/cm$^2$). We suspect that the viability may be affected by fluctuations in abiotic factors (i.e., temperature, humidity, and UV index), potentially limiting the stability and survival of the conidial formulation.[207,224] These results suggest that the powder formulations are sufficiently stable for 1 to 2 weeks in the field, to provide a viable conidial concentration that will cause MPB death.[210,223] At a regional scale, the MPB flight period typically occurs over a 2-3 month period in the summer, the majority of beetles, in localized infestations, will emerge and disperse within a 2 week period.[193] A recent degree-day model was developed which accounted for almost 90% of the timing variation in MPB emergence.[227] This model can be used to predict the emergence of beetles in local infestations and time the application of *B. bassiana* formulations to maximize MPB contact and mortality.

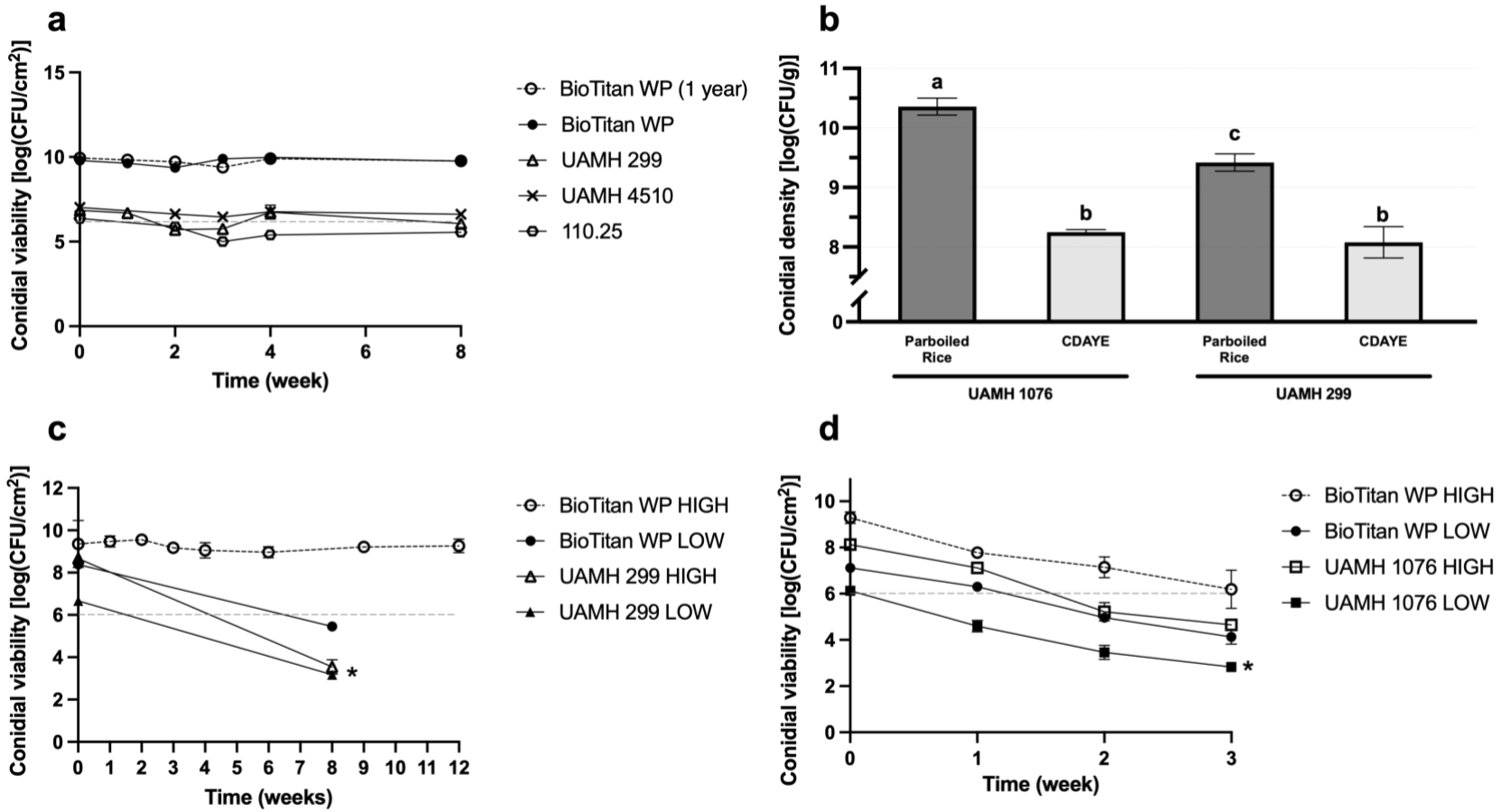


**Fig. 41** Conidial viability of *Beauveria bassiana* formulations under cold storage, *in planta* and *in natura* conditions, and biphasic liquid-solid fermentation conidial yield. (A) *In vitro* conidial stability of *B. bassiana* conidial powder formulations (BioTitan WP (1 year), BioTitan WP, UAMH 299, UAMH 4510, and 110.25) incubated at 4 °C for 8 weeks. (B) Conidial density [log(CFU/g)] of *B. bassiana* strains UAMH 1076 and 299, grown on CDAYE media or parboiled rice substrate. Vertical bars represent the mean conidial yield ± standard deviation. The letters represent the post hoc Tukey's HSD pairwise comparison among the four treatments, where different letters indicate a significant difference ($\alpha = 0.05$). (C) *In planta* conidial viability of *B. bassiana* powder formulations (BioTitan WP

and UAMH 299) applied on lodgepole pine bolts incubated at 25 ℃ for 12 weeks. (D) *In natura* conidial viability of *B. bassiana* powder formulations (BioTitan WP and UAMH 1076) applied on lodgepole pine bolts under pseudo-*in natura* conditions for three weeks. Starting conidial titers (CFU/cm$^2$): BioTitan WP HIGH – $1.0 \times 10^9$, BioTitan WP Low – $1.0 \times 10^7$, UAMH 1076 HIGH – $1.0 \times 10^8$, UAMH 1076 LOW – $1.0 \times 10^6$, UAMH 299 HIGH – $1.0 \times 10^8$, and UAMH 299 LOW – $1.0 \times 10^6$. The dotted grey line indicates the effective lethal dose ($1.0 \times 10^6$ CFU/cm$^2$). Conidial concentrations below the culturable limit of detection are indicated by an asterisk (*).

#### 4.2.2.2 Evaluation of Virulence of *B. bassiana* Powder Formulations Against *D. ponderosae* Under *In Planta* Greenhouse Conditions

Due to their long-term greenhouse stability and high *in vitro* MPB virulence,[210] we then tested two powder formulations containing either *B. bassiana* ANT-03 or UAMH 299, to establish the *in planta* efficacy (Fig. 42). Naturally MPB-infested trees were felled near Whitecourt, AB, Canada, in September 2020, and were sub-sectioned into 0.4 m bolts. Both ends of the bolts were sealed with melted wax to reduce desiccation and then incubated at 4 °C for 2 months to simulate winter. The bolts were then placed in an emergence bin at 25 °C for the *in planta* experiments. The emerging beetles from the bolts were collected and used to infest healthy bolts to provide An $F_1$ MPB generation.

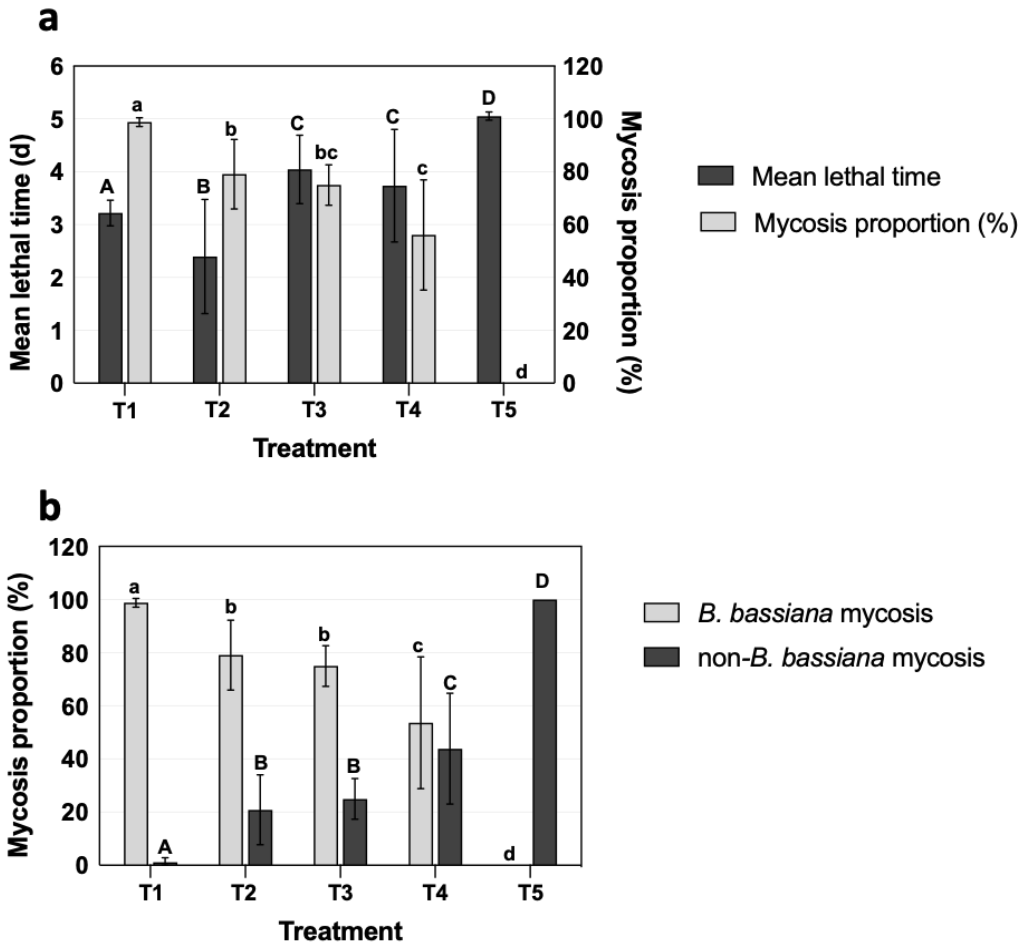


**Fig. 42** Mean lethal times and mycosis proportions of *Beauveria bassiana* ANT-03 (BioTitan WP) and UAMH 299 powder formulation-treated *Pinus contorta* bolts, under *in planta* greenhouse conditions. (A) Mean lethal time (days, dark grey bars) and corresponding *B. bassiana*-associated mycosed mountain pine beetle collected in the glass trap containers (%, light grey bars*),* of conidial powder formulation treatments. (B) Mycosis proportion of *B. bassiana* (%, light grey bar) and non-*B. bassiana* (%, dark grey bar) -associated mycosis from emerged mountain pine beetles. The BioTitan WP formulation, containing *B. bassiana* ANT-03, was applied on the bark at two titers: $1.0 \times 10^9$ CFU/cm$^2$ (T1) or $1.0 \times 10^7$ CFU/cm$^2$ (T2). In-house powder formulations containing *B. bassiana* UAMH 299 were applied on the bark at either $1.0 \times 10^8$ CFU/cm$^2$ (T3) or $1.0 \times 10^6$ CFU/cm$^2$ (T4). The control group (T5) was not treated with any formulations. Error bars represent the standard deviation of three biological replicates. The letters represent the post hoc Tukey's HSD pairwise comparisons, where different letters indicate a significant difference ($\alpha = 0.05$). The

capital letters represent the differences between the dark grey bars, and the lowercase letters represent the differences between the light grey bars.

Five bolt treatments (T), with three replicates, were sprayed with two titers (CFU/g = colony forming units per gram) of the conidial powder formulations: T1, ANT-03 at $1.0 \times 10^9$ CFU/g; T2, ANT-03 at $1.0 \times 10^7$ CFU/g; T3, UAMH 299 at $1.0 \times 10^8$ CFU/g; T4, UAMH 299 at $1.0 \times 10^6$ CFU/g; T5, carrier powder negative control. The *B. bassiana* powder formulation was manually sprayed on the bark surface under a sterile BioSafety Cabinet (model MB4-2A-49) using a powder duster application pump (Amazon, Toronto, Canada). The bolts were stored in sealed rearing bins fitted with a messed glass trap for the collection of emerging MPBs. The bins were incubated at the BioTron Facility, University of Alberta, under greenhouse conditions: 25 °C, 26-30% relative humidity, and continuous illumination (30 $\mu$mol photons $m^{-2}$ $s^{-1}$).

Daily collection and counting of the emerged live and dead MPBs, that reached the glass collection jars through phototropism,[228] were performed for fifty-five consecutive days, with over 600 beetle emergence events. All collected live MPBs from each respective rearing bin were transferred to a Petri dish lined with a moist Kimwipe and incubated at 25 °C until they were dead (i.e., lethal time). Once the MPBs were dead, the carcasses were transferred to individual cells in a 96-well titer plate, lined with a moist Kimwipe to maintain a relative humidity of 70%, and incubated at 25 °C for 14 days to determine *B. bassiana*-associated mycosis. In addition, we debarked all pine bolts and assessed *B. bassiana*-associated mycosis of the non-emerged MPBs.

Each well was assessed for *B. bassiana*-associated mycosis using three parameters. First, each well was assessed for the characteristic white and granular conidiation. Second, each mycosed MPB was viewed under a dissecting microscope to analyze for the distinct staphylococcal-like arrangement of *B. bassiana* conidial clusters at the end of the conidiophores.[229] Lastly, a swab of

the mycelial biomass was obtained using a nichrome wire and stained with lactophenol blue and viewed to assess the *B. bassiana* mycelial morphology using an inverted phase contrast microscope. In addition, an inoculating needle was used to touch-point *B. bassiana*-infected MPB to support the classical Koch's postulate of infection[230]. CDAYE plates, with 150 $\mu$g/mL chloramphenicol, were spot-inoculated with the conidial samples. Non-*B. bassiana*-mycosed MPBs were evaluated using the same procedure.

The mean lethal times exhibited a conidial concentration-dependent effect for the BioTitan WP (ANT-03) treatments (Fig. 42). Both the high (T1, $1.0 \times 10^9$ CFU/cm$^2$) and low (T2, $1.0 \times 10^7$ CFU/cm$^2$) titer treatments showed the shortest killing time at about 3 days. However, the lower dose treatment (T2) showed greater variations. The high and low conidial treatments exhibited 98% and 80% *B. bassiana*-specific mycosis rates, respectively. The mycosis data supported the classical Koch's postulate of microbial infection because the desired *B. bassiana* ANT-03 strain was re-isolated from the mycosed MPB (Fig. 43). Lastly, the conidial concentrations used in these *in planta* experiments resulted in comparable mean lethal times as the *in vitro* results on the direct conidial application on MPB exoskeleton.[209,210,231]

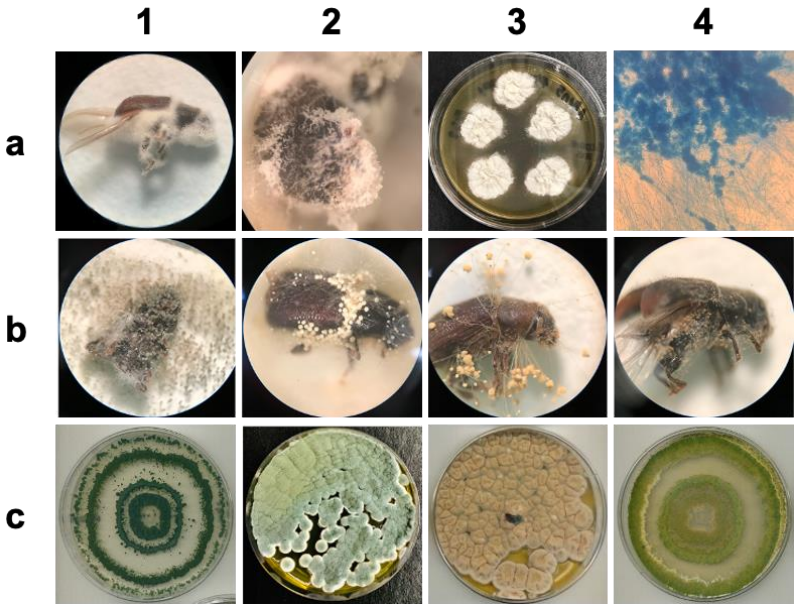


**Fig. 43** Mountain pine beetle mycosis after application on *Pinus contorta* bolts with *B. bassiana* ANT-03 (BioTitan WP) powder formulation. (A) (1) Stereomicroscope image of *B. bassiana*-mycosed mountain pine beetle, (2) *B. bassiana* conidiophore clusters on the insect exoskeleton, (3) *B. bassiana*-isolated from mycosed MPB and grown on CDAYE agar, and (4) a lactophenol-blue stained *B. bassiana* mycelium and conidiophores. (B) Four visually and morphologically distinctive fungal conidiophores from non-*B. bassiana* mycosed MPB. (C) Re-isolated axenic fungi from non-*B. bassiana* mycosed MPB, grown on CDAYE media.

However, treatment with the *B. bassiana* UAMH 299 powder formulation resulted in an extended mean lethal time of about one day (Fig. 42). This extended mean lethal time was seen regardless of the conidial concentration (T3, $1.0 \times 10^8$ CFU/cm$^2$; T4, $1.0 \times 10^6$ CFU/cm$^2$), although the lower dose treatments also showed greater variation. The conidial treatments resulted in approximately 76% (T3) and 55% (T4) of the MPB population showing *B. bassiana*-associated mycosis. As expected, no *B. bassiana*-associated mycosis was detected in the control treatments (T5) (Fig. 42), however, several autochthonous fungal species were observed on the MPB exoskeleton (Fig. 43). The success of the *in planta* greenhouse experiments was affected by the variations in MPB emerging from the naturally-infested and laboratory-infested lodgepole pine

bolts (Table 7). Three of the eleven naturally-infested bolts did not produce an F1 generation, but the laboratory-infested bolts showed a consistent population of MPB emergence (100%) compared to the naturally-infested bolts (73%). After the 55 day greenhouse incubation, the residual *B. bassiana* powder titer was determined, and the titer was shown to be strain-dependent and conidial concentration-dependent (Fig. 41, Table 7). T1, the high-dose BioTitan WP treatment, showed a consistently high viable and culturable residual conidia. However, T2, the low-dose BioTitan WP treatment, resulted in lower and ineffective conidial titer, after the 55 day greenhouse incubation (Fig. 41). Both the high (T3) and low (T4) dose UAMH 299 treatments resulted in undetectable and ineffective *B. bassiana* titer, which may have resulted from being outcompeted by the autochthonous fungal species on the bark surface (Fig. 41, Table 7). With these results, the current application should be sufficient in providing an effective dose of *B. bassiana* to elicit MPB death, if the application coincided with the emergence of the MPB population.[221–223] In order for maximum conidial contact, we propose a single application of the *B. bassiana* powder formulation during the estimated date of the massive MPB emergence event.[227] A bi-weekly application may be considered as an alternative if the culturable titer shows a weekly one-log reduction under *in natura* conditions.

**Table 7** Status summary of debarked *Pinus contorta* bolts treated with *Beauveria bassiana* powder formulations incubated for 55 days under greenhouse conditions. BioTitan WP – T1, T2; UAMH 299 – T3, T4; Control – T5. R = replicate. MPB = mountain pine beetle. 3 = High, 2 = Average, 1 = Minimal, and 0 = Absent. T = treatment; R = Replicate.

| Code | MPB infection source | *B. bassiana* conidial titer (CFU/cm$^2$) | MPB presence | | | Fungal status of *P. contorta* outer bark | | Fungal status of bolt and gallery | MPB parental gallery and pupal chamber development |
|---|---|---|---|---|---|---|---|---|---|
| | | | Bins | Glass trap | Debarked bolt | *B. bassiana* | Axenic fungi | | |
| **T1 R1** | Natural | 1.0 x $10^9$ | Not detected | Not detected | Not detected | 3 | 1 | Bark excellent, sapwood good, non-mouldy | Parental galleries interrupted |
| **T1 R2** | Natural | 1.0 x $10^9$ | Present | Present | Present | 3 | 1 | White mouldy galleries | Successful development |
| **T1 R3** | Laboratory | 1.0 x $10^9$ | Present | Present | Present | 3 | 2 | White and green mouldy galleries | Successful development |
| **T2 R1** | Natural | 1.0 x $10^7$ | Present | Present | Present | 2 | 2 | Mouldy, variable moisture | Successful development |
| **T2 R2** | Laboratory | 1.0 x $10^7$ | Present | Present | Present | 2 | 2 | White mouldy galleries | Successful development |
| **T2 R3** | Laboratory | 1.0 x $10^7$ | Present | Present | Present | 2 | 2 | White and green mouldy galleries | Successful development |
| **T3 R1** | Laboratory | 1.0 x $10^8$ | Present | Present | Present | 0 | 3 | Mouldy & decaying bolt; white mouldy galleries | Successful development |

| | | | | | | | | | |
|---|---|---|---|---|---|---|---|---|---|
| **T3 R2** | Natural | $1.0 \times 10^8$ | Not detected | Not detected | Not detected | 0 | 1 | Bark excellent, sapwood good, non-mouldy | Parental galleries interrupted |
| **T3 R3** | Natural | $1.0 \times 10^8$ | Present | Present | Present | 0 | 3 | Mouldy & decaying bolt; white mouldy galleries | Successful development |
| **T3 R4** | Natural | $1.0 \times 10^8$ | Present | Present | Present | 0 | 3 | Mouldy and dried bolt | Successful development |
| **T4 R1** | Laboratory | $1.0 \times 10^6$ | Present | Present | Present | 0 | 3 | Mouldy & decaying bolt; white mouldy galleries | Successful development |
| **T4 R2** | Natural | $1.0 \times 10^6$ | Present | Present | Present | 0 | 3 | Mouldy and dried bolt | Successful development |
| **T4 R3** | Natural | $1.0 \times 10^6$ | Present | Present | Present | 0 | 3 | Mouldy, variable moisture | Successful development |
| **T4 R4** | Natural | $1.0 \times 10^6$ | Not detected | Not detected | Not detected | 0 | 3 | Mouldy and dried bolt | No galleries detected |
| **T5 R1** | Natural | ___ | Present | Present | Present | 0 | 2 | Mouldy and dried bolt | Successful development |
| **T5 R2** | Laboratory | ___ | Present | Present | Present | 0 | 3 | Mouldy & decaying bolt; white mouldy galleries | Successful development |
| **T5 R3** | Natural | ___ | Present | Present | Present | 0 | 3 | Mouldy & decaying bolt; white mouldy galleries | Successful development |

#### 4.2.2.3 Field Evaluations of BioTitan WP (*B. bassiana* ANT-03) Powder Formulation Against *D. ponderosae* Under *In Planta* and *In Natura* Conditions

Following the conidial viability and greenhouse infection assays, we assessed the efficacy of the BioTitan WP powder formulations, containing *B. bassiana* strain ANT-03, in reducing the reproductive success of MPB. Using two infection modes, an exit and entry approach, we evaluated the parental and larval characteristics of field populations of MPBs. The two infection modes are categorized into four treatments: IL — MPB-infested bolt with low dose BioTitan WP (MPB exit experiment); NL — non-infested food bolt with low dose BioTitan WP (MPB entry experiment); IH — MPB-infested bolt with high dose BioTitan WP (MPB exit experiment); and NH — non-infested food bolt with high dose BioTitan WP (MPB entry experiment).

The mean parental gallery length and mean larvae per parental gallery were significantly lower in all the treated enclosures compared to the control enclosures (Fig. 44). Treatment with BioTitan WP, regardless of concentration, resulted in a significant decrease in parental gallery length and termination of the larval gallery network, compared to the untreated control (C) treatments (45 ± 15 cm long parental galleries, 48 ± 10 MPB larvae per gallery). A high dose ($1.0 \times 10^9$ CFU/cm$^2$) treatment of BioTitan WP (IH, NH) resulted in a significant reduction in parental gallery length ($F(4,13) = 9.885$, $P < 0.001$). The parental galleries measured were less than 5 ± 1 cm in length and were associated with zero reproduction (i.e., absence of MPB larvae) (Fig. 44). The recovered parental MPBs from these reduced galleries were covered in *B. bassiana* mycelia. The low-dosage ($1.0 \times 10^7$ CFU/cm$^2$) treatments of BioTitan WP also resulted in shorter mean parental gallery length for the MPB entry (NL; 10 ± 4 cm) and MPB exit (IL; 20 ± 10 cm) experiments. The reduced capacity for female MPBs to create parental and larval galleries was

associated with a significant reduction in the mean number of larvae per female ($F(4,13) = 8.772$, $P = 0.0011$) in a concentration-dependent manner (Fig. 44). In addition, the larval yield dropped to approximately 30% (IL) AND 15% (NL) for the low-dose BioTitan WP treatments; the mean larval yield was reduced to virtually zero with the high dose treatments (IH, NH).

The data suggests that by utilizing a low dose of BioTitan WP formulation, the ability to reduce reproductive success seems to be more effective when MPBs encounter *B. bassiana* while tunnelling into healthy *P. contorta* bolts (entry experiment), suggesting that the MPBs emerging from treated trees may shed some conidia during flight (exit experiment). However, a successful reproductive reduction can be attained using a higher titer of BioTitan WP, regardless of the infection mode. We proposed that the developed infection modes can be implemented to treat every infested tree over an infested area, fulfilling an essential requirement for successful and significant direct control of MPB populations.[192]

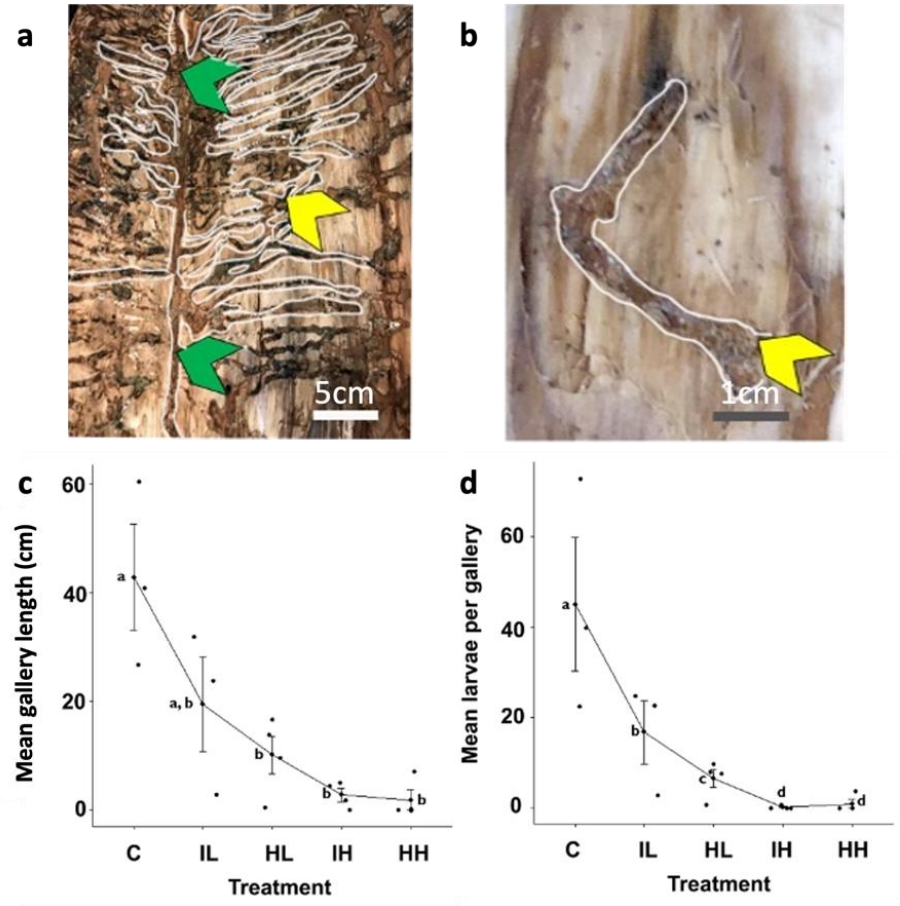


**Fig. 44** Mountain pine beetle (MPB), *Dendroctonus ponderosae*, reproductive success in MPB-infested *Pinus contorta* bolts with or without BioTitan WP (*Beauveria bassiana* ANT-03) powder formulation treatment. (A) Untreated control *P. contorta* bolts with successful MPB colonization shown by the extensive network of MPB vertical parental galleries (green arrow) and horizontal larval galleries (yellow arrow). (B) MPB-infested *P. contorta* bolts, treated with a high dose of BioTitan WP powder formulation (IH), baited with non-infested *P. contorta* food bolts; shortened parental gallery length (yellow arrow). (C) Mean parental gallery lengths of *P. contorta* bolts and (D) corresponding mean larvae per gallery observed in 75 cm debarked logs. *P. contorta* treatment codes: C – control, untreated; IL – MPB-infested bolt with low dose BioTitan WP (MPB exit experiment); NL –non-infested food bolt with low dose BioTitan WP (MPB entry experiment); IH – MPB-infested bolt with high dose BioTitan WP (MPB exit experiment); NH – non-infested food bolt with high dose BioTitan WP (MPB entry experiment). Connected dots are the treatment mean, and the vertical bars represent the mean ± standard deviation. Letters indicate a significant difference at $\alpha = 0.05$.

### 4.2.3 Conclusions and Future Directions

This study provides an intensive investigation of the efficacy of several phenotypically diverse strains of *B. bassiana* in managing MPB populations. The development of an entomopathogenic fungi-based biocontrol agent may provide an alternative approach to the currently limited mitigation efforts (i.e., removal and destruction of infested trees).[192] Five candidate *B. bassiana* strains were identified and assessed for their conidial viability under various conditions (i.e., cold storage, *in planta* greenhouse and *in natura* acreage). In addition, we developed a liquid-solid fermentation approach to access large-scale *B. bassiana* conidial biomass. Lastly, we developed infection modes, using *B. bassiana* conidial formulations, to spray on lodgepole pine trees to effectively reduce MPB reproductive success under forest field conditions.

For future studies, we propose a variety of ways to suppress MPB populations using the developed *B. bassiana* formulation. For instance, during the peak flight period of MPBs, aerial application of the formulation can be employed to maximize the infection of dispersing individual beetles, which can further contaminate uninfected male and female beetles, already under the bark, during host colonization.[196] In addition, bark beetle traps can be used as "assisted autodissemination" of *B. bassiana* spores to infect field populations of bark beetles. This requires modification of the current bark beetle traps, to allow beetles to enter and exit the traps, where the beetles can carry the fungal spores as they exit the traps. We hypothesize that these proposed applications would be more successful in the established range of MPB, because beetle densities are more closely monitored (i.e., location of majority of the infested trees has been determine) and more vulnerable to local extinction[133, 232].

## 4.3 Genomic and Transcriptomic Virulence of *Beauveria bassiana*

### 4.3.1 Aims of Study

Due to the numerous strains of *B. bassiana* and their phenotypes,[233] identification of the genomic or molecular markers to determine the potential efficacy of the fungus as a biocontrol agent for MPB,[209,210] are highly desirable. In our previous study, we characterized 93 strains based on colony morphology, pigmentation, growth rate, conidial rate, infection rate, and MPB virulence in the laboratory.[210] The strains were categorized into three phenotypic groups based on the red pigment, oosporein (**Fig. 45**). Oosporein is an extensively studied red dibenzoquinone compound, which has been previously reported to have limited insecticidal activity,[234,235] but can synergistically improve insect mortality when combined with *B. bassiana* conidia.[234] Oosporein has been shown to contribute to immune system evasion by *B. bassiana*, as well as suppressing the insect host immune system, resulting in infection.[217] The Group I *B. bassiana* all produce this red pigment, albeit at variable intensities, but they produce the highest levels of oosporein and displayed the highest levels of virulence against MPB. The Group II strains develop thin, cream-coloured colonies, no detectable oosporein production, and had the lowest virulence against MPB, requiring a higher conidial titer to be effective. Lastly, the Group III strains develop felty, yellowish colonies with intermediate virulence levels.

In this study, eight potential *B. bassiana* isolates, across the three phenotypic groups, were used for genome sequencing and transcriptome analysis. These analyses assessed the genome and transcriptome signatures to identify those associated with UV resistance, virulence, and secondary metabolite biosynthesis. The presence and absence of secondary metabolite biosynthetic gene clusters (BGC) were assessed to identify those associated with MPB virulence. Types of BGCs

were determined, including terpenoids synthases, non-ribosomal peptide synthetases (NRPS), and polyketide synthases (PKS). Of special interest was the oosporein BGC, a PKS cluster identified in all the sequenced *B. bassiana* strains, and differentially expressed in some. Large-scale differences between the eight strains were identified through the assessment of phylogenetic relationships, gene content, and differential expression.

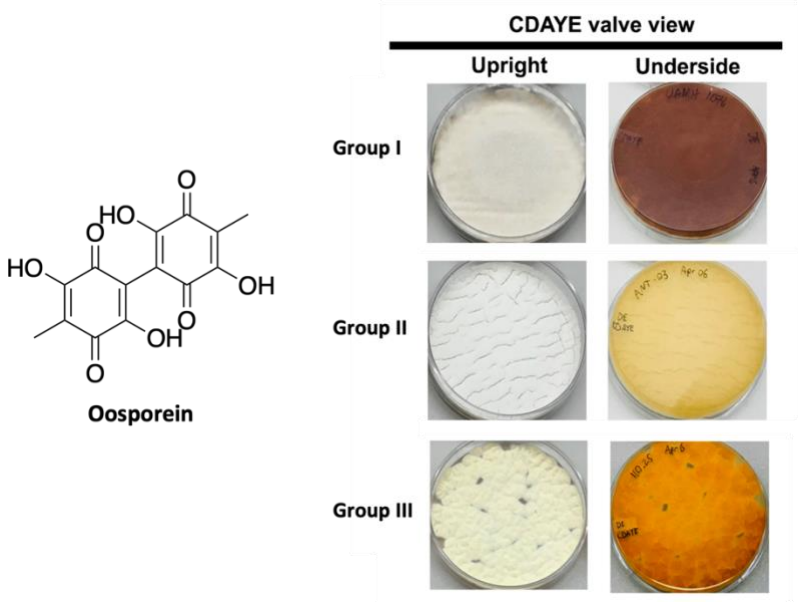


**Fig. 45** Oosporein structure and the phenotypic differences of the three *Beauveria bassiana* groups plated on CDAYE media.

### 4.3.2 Results and Discussion

#### 4.3.2.1 *In Vitro* Competition Assays Between *Beauveria bassiana* and *Grosmannia clavigera*

The blue stained fungi (BSF), are a group of phenotypically and phylogenetically heterogeneous fungal species that have established symbiotic associations with several bark beetle systems.[236,237] In the MPB system, there are three known associated BSF species; *Grosmannia clavigera*, *Ophiostoma montium*, and *Leptographium longiclavatum*.[238–241] Our studies focused on

*G. clavigera* as it is the most prevalent BSF in the teneral adult stage of MPBs[237,242], and is the most invasive BSF in *P. contorta.*[243] Two types of interaction responses were determined between the eight strains of *B. bassiana* and two strains of *G. clavigera* (**Fig. 46**): (1) positive mycelial contact but non-inhibition of *G. clavigera* strains EL033 and EL035 by the red-pigmented and non-pigmented strains UAMH 298, UAMH 298-UVR, UAMH 4510, and ANT-03 (**Fig. 46**), and (2) inhibition of *G. clavigera* strains EL033 and EL035 by the red-pigmented and yellow-pigmented strains UAMH 299, UAMH 299-UVR, UAMH 1076, and 110.25 (**Fig. 46**).

The first interaction responses showed no zones of inhibition (ZOI) and contact at the mycelial front, shown by the *B. bassiana* ANT-03 mycelial growing on top of the *G. clavigera* (**Fig. 46**). Contact of the two mycelial fronts suggests the absence of any radially-diffusible antagonist molecules, and that the available space occupied by either species is related to its media-dependent growth rate alone. Interestingly, under a media with a high C/N ratio (e.g., PDA), the interaction assays for the non-inhibitory *B. bassiana* strains delayed the melanization of the mycelial front of the *G. clavigera* strains.

The second interaction resulted in the formation of a clear zone of inhibition, noted by the stop of mycelial expansion of both the *B. bassiana* and *G. clavigera* strains (**Fig. 46**). On high C/N media (i.e., PDA, MEA, 0.25xSDA), crescent-shaped ZOIs were seen, supporting potential radially diffusible compound(s) produced by *B. bassiana* to prevent the further mycelial expansion and colonization of *G. clavigera*. Interestingly, faster growth rates of *G. clavigera* than *B. bassiana* on high C/N media correlated with slower melanization of *G. clavigera* (**Fig. 46**). However, competition assays on low C/N media (i.e., CDAYE) showed comparable growth rates between *B. bassiana* and *G. clavigera*, colonizing equal areas on the agar surface. In addition, the low C/N media did not induce *G. clavigera* melanization until the zone of inhibition was formed at interface

of the mycelial fronts. Although the ZOI was observed consistently across the red-pigmented *B. bassiana* strains (i.e., UAMH 299, UAMH 299-UVR, UAMH 1076), the yellow-pigmented strain, 110.25, also showed significant ZOI. Attributing the inhibitory activity solely to oosporein is not fully supported in these results because of the presence of the ZOI in the tenellin-producing 110.25 strain.[244] Furthermore, ZOIs were present across media conditions (i.e., high C/N ratios) that do not support oosporein or tenellin production.

The mycelial growth of *G. clavigera* depended on the C/N ratio of the assay media (fig 5c-e). High C/N media (i.e., PDA) allowed for the fastest mycelial expansion of *G. clavigera*, until a ZOI developed on day 4. The clear inhibitory region significantly decreased the mycelial expansion rate, up to 10 d. However, in the absence of inhibition, the *G. clavigera* mycelial expansion showed exponential growth and plateaued only when reaching the contact point with the *B. bassiana* strain (**Fig. 46**). Growth on a low C/N media (i.e., CDAYE) showed similar response curves for all treatments (**Fig. 46**). Regardless, in both high and low C/N media, the end of the logarithmic growth rate coincided with the development of the zones of inhibition. This suggests that the *B. bassiana* strain-specific inhibitory potential, against *G. clavigera*, is independent of the available nutritional content. However, it has yet to be established if these inhibitions will be relevant under *in vivo* and *in planta* competition experiments.

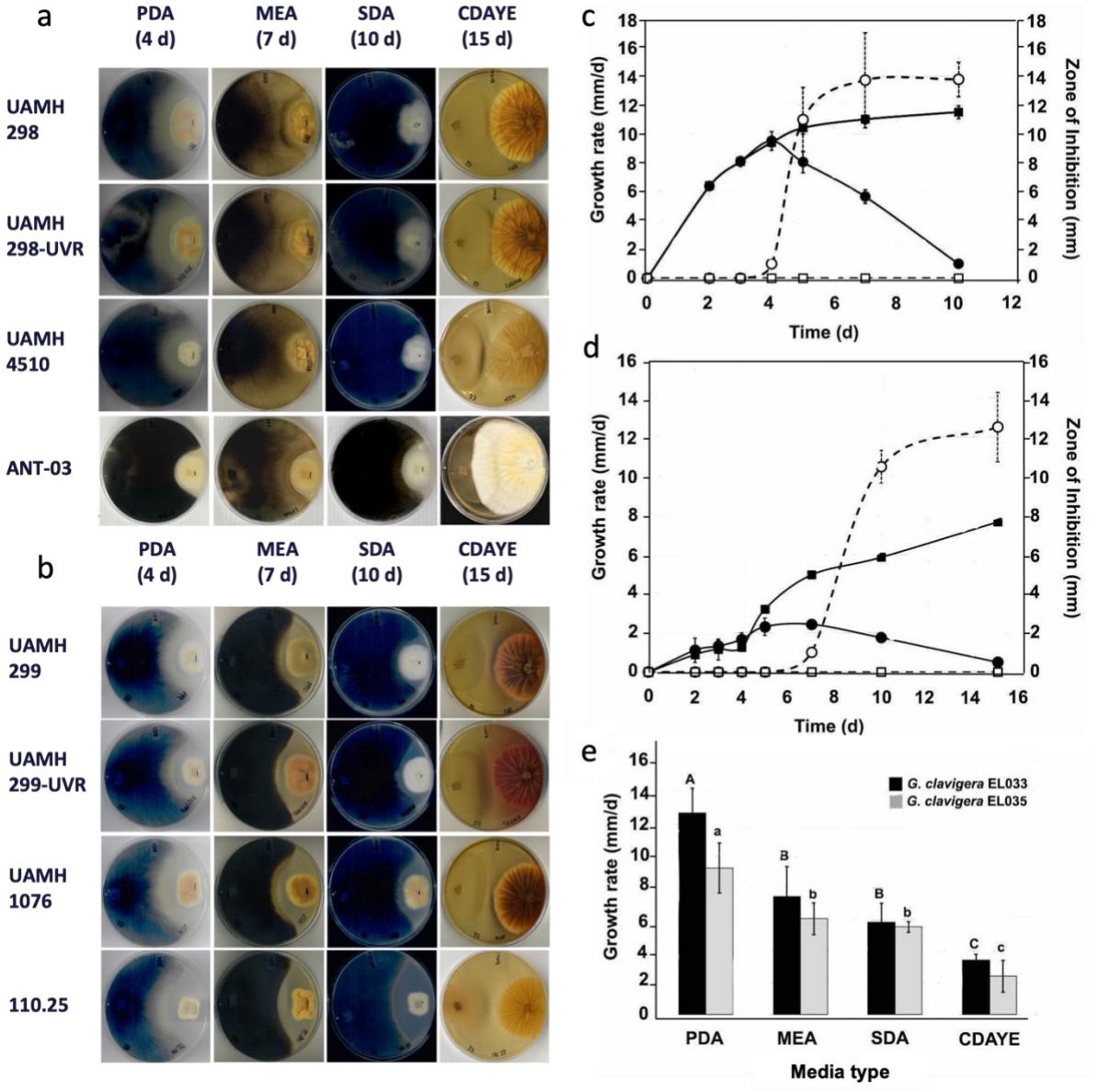


**Fig. 46** *In* vitro interactions between *Beauveria bassiana* and the MPB-associated symbiotic blue stain fungus, *Grosmannia clavigera*. (A) Non-inhibitory or (B) inhibitory mycelial expansion of *G. clavigera* strains EL033 and EL035, under high (PDA, MEA, 0.25xSDA) or low (CDAYE) C/N ratio media. (C) PDA or (D) CDAYE) media-grown *G. clavigera* strain EL033, and the corresponding growth rate and zone of inhibition, in the presence of non-inhibitory (black square) and inhibitory (black circle) *B. bassiana* groups. Zones of inhibition are indicated by the presence of non-inhibitory (white square) and inhibitory (white circle) *B. bassiana* groups. (E) The growth rate of *G. clavigera* strains EL033 and EL035 on media with different C/N ratios. Vertical bars represent the mean growth rate (mm/d) of three biological experiments, and the error bars represent

the standard deviation. The letters represent the post hoc Tukey's HSD difference ($\alpha$ = 0.05). Capital letters depict the differences between the black bars, and lowercase letters depict the differences between the grey bars.

#### 4.3.2.2 Functional Genomics of *Beauveria bassiana* Biosynthetic Gene Clusters

The genome of the eight *B. bassiana* strains were assembled in relation to the reference *B. bassiana* strain ARSEF 2860, *Beauveria pseudobassiana*, and *Cordyceps militaris* (outgroup), to estimate a phylogenetic tree (**Fig. 47**). The eight *B. bassiana* isolates fell into two distinct clusters with high bootstrap support. The Group I strains: UAMH 298, UAMH 298-UVR, UAMH 299, UAMH 299-UVR, and UAMH 1076 were clustered together, while the other strains from Group II (ANT-03 and UAMH 4510) and Group III (110.25) formed a separate cluster with ARSEF 2860. The two phylogenetic clusters were designated as the red and non-red groups, respectively, and the strains within these groups were designated as the red and non-red strains, with respect to oosporein production. *B. bassiana* ARSEF 2860 has been shown in previous studies to produce oosporein,[235] but our findings suggest an increased capacity for oosporein synthesis by the red strains as well as differential content of oosporein BGC genes. Interestingly, the red strains formed a clade with *B. pseudobassiana* rather than the reference *B. bassiana* strain, ARSEF 2860. The *B. pseudobassiana* species was first described using a multilocus phylogeny of 68 *Beauveria* strains based on the partial gene sequences of Rpb1, Rpb2, Tef 1-a, and the nuclear intergenic region Bloc.[245] As the name suggests, *B. pseudobassiana* is phenotypically similar to *B. bassiana*, albeit with smaller conidia, and has been shown to exhibit entomopathogenic properties.[246,247] Whole genome annotations would be required to confirm the phylogenetic placement of the five red strains and *B. pseudobassiana*, but our current results show that the two isolate groups have

undergone different evolutionary histories, demonstrating different virulence and oosporein production levels.

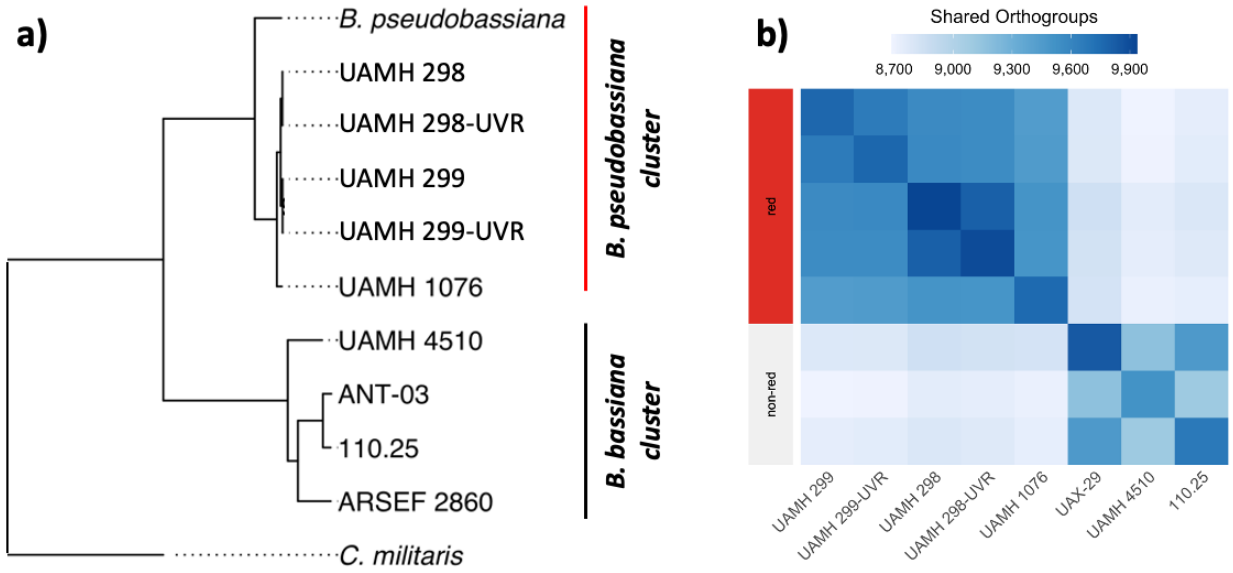


**Fig. 47** Comparative genomics analysis of *Beauveria bassiana* isolates. (A) Best-scoring maximum-likelihood phylogenetic tree based on 3,939 complete, single-copy Benchmarking Universal Single-Copy Ortholog (BUSCO) proteins. The phylogenetic inference includes the eight *B. bassiana* strain, the reference *B. bassiana* strain ARSEF 2860, *Beauveria pseudobassiana* strain KACC 47484, and *Cordyceps militaris* strain CM01 as the outgroup. All non-labelled nodes have bootstrap support values of 100. (B) Orthogroups shared between pairs of isolates. Red and non-red groups are indicated on the y-axis.

The predicted gene counts of the eight genomes, between 10,117 and 10,754 predicted genes, were shown to be comparable to the 10,366 genes encoded in ARSEF 2860,[248] and the genome annotations were highly complete. Orthogroups (OGs), analogous to an ortholog, are a set of two or more genes descended from a single ancestral gene; however, orthogroups allow for the comparison of several species of strains rather than a pair.[249] A total of 11,120 orthogroups were inferred between the *B. bassiana* isolates (**Fig. 47**). There was a considerable amount of gene

content variation between the isolates; the red and non-red strains shared more orthogroups with strains from the same group.

antiSMASH analysis showed that the secondary bioactive metabolic profiles of the eight *B. bassiana* genomes correlated with an arsenal of known and unknown biomolecules. More clusters were predicted in the red strains than in the non-red strains, which could reflect an increased capacity of secondary metabolism and virulence. The three major biosynthetic gene cluster types among all strains include non-ribosomal peptide synthetase (NRPS), type I polyketide synthase (PKS) and terpene synthase (**Table 8**, **Fig. 48**). The oosporein BGC, a polyketide gene cluster, was detected across all sequenced *B. bassiana* genomes, however, oosporein production was detected only in the group I strain (UAMH 298-UVR, UAMH 299, UAMH-299-UVR, and UAMH 1076) (Table 9). The main biosynthetic genes responsible for oosporein production (OpS1-OpS7) were detected in all strains with 90.50 to 97.75% identity to ARSEF 2860. However, the putative cell surface protein (OpS9) was absent in all eight strains, and the putative heat-labile enterotoxin IIB, A chain (OpS10), was absent in UAMH 298, UAMH 298-UVR, UAMH 1076, and UAMH 4510.

**Table 8** Bioinformatic predictions of common, group- and strain-specific gene clusters from the draft genome sequences of eight *Beauveria bassiana* strains. Predictions were performed with the phylogenetically-close reference strain, *B. bassiana* ARSEF 2860, using antiSMASH's KnownClusterBlast algorithm.

| Strains | Accession | Chemical Name | Cluster Type |
|---|---|---|---|
| **Common Clusters** | | | |
| **All** | BGC0001249 | dimethylcoprogen | NRPS |
| **All** | BGC0001720 | oosporein | PKS |
| **All** | BGC0001248 | clavaric acid | triterpene |
| **All** | BGC0001839 | squalestatin S1 | PKS |
| **All** | BGC0000313 | beauvericin | NRPS |
| **Pigment Group-Specific** | | | |
| **Red** | BGC0000030 | bikaverin | PKS |
| **Non-red** | BGC0000312 | bassianolide | NRPS |
| **Strain-Specific** | | | |
| **UAMH 299** | BGC0001811 | trichodiene-11-one | terpene |
| **UAMH 1076** | BGC0001966 | BII-rafflesfungin | NRPS |
| **UAMH 1076** | BGC0001882 | chrysoxanthone A/B/C | PKS |
| **UAMH 1076** | BGC0001278 | nivalenol/deoxynivalenol/3-acetyldeoxynivalenol/15-acetyldeoxynivalenol/neosolaniol/calonectrin/apotrichodiol/isotrichotriol/15-decalonectrin/T-2 toxin/3-acetyl T-2 toxin/trichodiene | sesquiterpene |
| **UAMH 1076** | BGC0001775 | sespendole | indole;terpene |

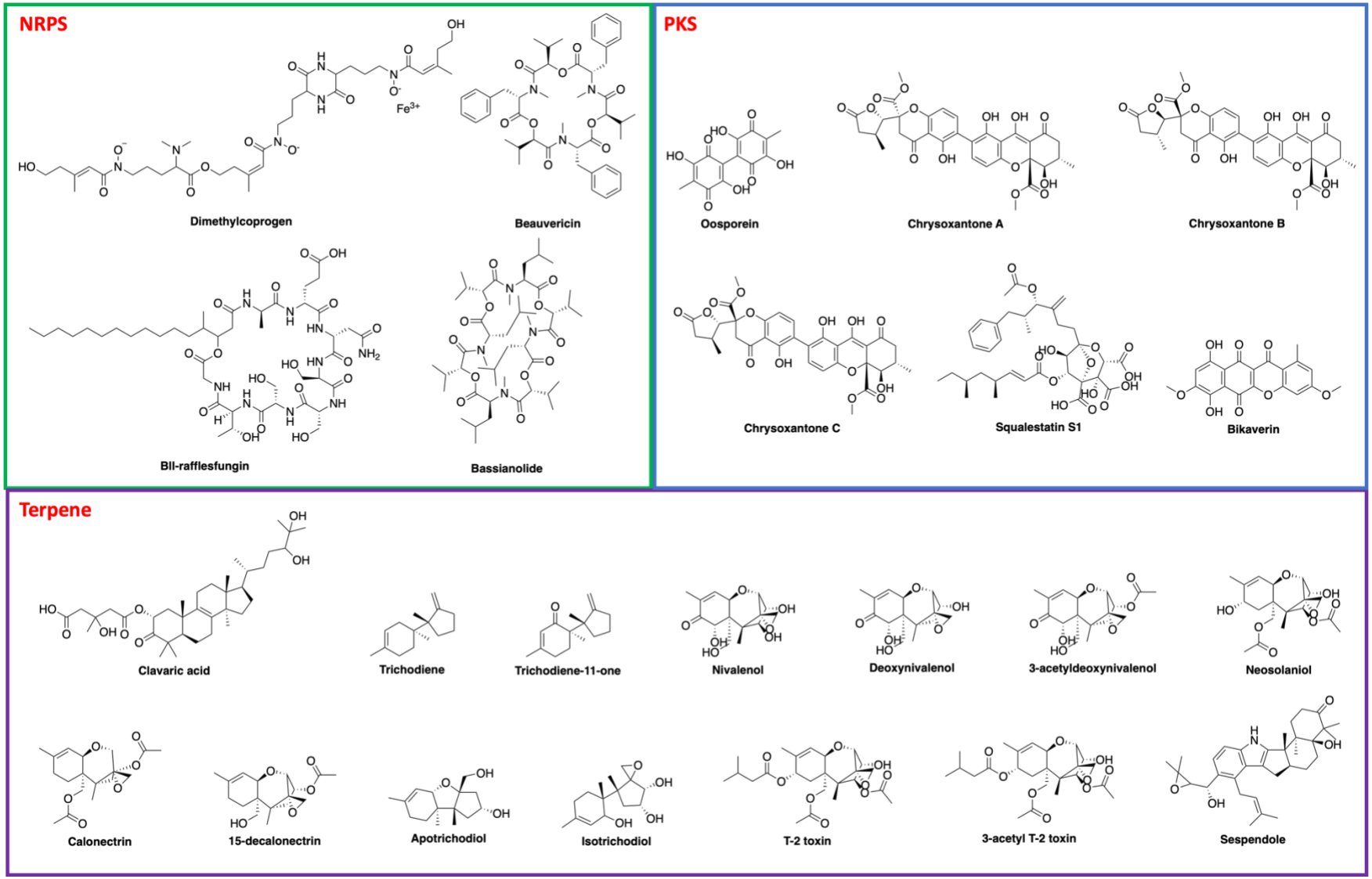


**Fig. 48** Chemical structures of common, group- and strain-specific gene clusters predicted by antiSMASH.

**Table 9** Presence (+) and absence (—) of oosporein in purified *B. bassiana* mycelial supernatant extracts, detected on LCMS.

| **Strain/Day of detection** | UAMH 298 | UAMH 298-UVR | UAMH 299 | UAMH 299-UVR | UAMH 1076 | ANT-03 | UAMH 4510 | 110.25 |
|---|---|---|---|---|---|---|---|---|
| Day 5 | — | + | + | + | + | — | — | — |
| Day 10 | — | — | + | — | + | — | — | — |
| Day 15 | — | — | + | — | + | — | — | — |

Additionally, several previously characterized gene clusters were found in all eight strains (**Table 8**, **Fig. 48**). The gene clusters responsible for the production of beauvericin, an NRPS product, was nearly complete, where all genes, except the predicted pseudogene glycolate oxidase (orf4), were identified in all strains. The clusters for dimethylcoprogen (NRPS product) and clavaric acid (triterpene product), both containing only one gene, were found in all strains. Finally, the squalestatin SI PKS cluster was identified in all strains, but only two of the five genes were detected in each strain. The gene clusters for a similar red-pigmented PKS product from *Fusarium* species, bikaverin,[250] were detected in all red strains, but absent in the non-red strains. Bikaverin exhibits antibiotic and antifungal activity and could function similarly to oosporein by outcompeting other organisms in the host microbiome during infection.[251] Additionally, the NRPS gene cluster for bassianolide, a virulence factor, was unique to the non-red strains, and this may contribute to the insecticidal activity in these strains. The bikaverin and bassianolide gene clusters may potentially contribute also to the phenotypic separation of the Group I strains from the Group II and III *B. bassiana* strains. The trichodiene-11-one terpene cluster was uniquely identified in the UAMH 299 isolate, and UAMH 1076 contained four unique clusters including nivalenol

(sesquiterpene) and sespendole (indole-terpene). Further characterization of these biosynthetic gene clusters and their products is necessary to determine their role in *B. bassiana* virulence.

#### 4.3.2.3 Functional Genomics of Oosporein Biosynthetic Gene Clusters

Given the phenotypic diversity of *B. bassiana* strains, it was originally hypothesized that the Group I strains contained oosporein BGCs, while the strains from Groups II and III did not. The core biosynthetic genes in the oosporein cluster (*OpS1*-*OpS7*) were identified in all eight strains by antiSMASH, indicating that the high levels of oosporein production in the Group I red strains are a result of regulatory factors or differential expression (**Fig. 49**). The conserved seven-gene *OpS* operon includes: *OpS1* (catalytic polyketide synthase), *OpS2* (putative MFS multidrug resistance transporter, *OpS3* (GAL4-like Zn2Cys6 transcription factor), *OpS4* (FAD- binding domain-containing hydroxylase), *OpS5* (a laccase-multicopper oxidase, *OpS6* (a glutathione-S-transferase, and *OpS7* (cupin 2 superfamily protein). The transcriptome data supported the previously stated hypothesis, where oosporein genes *OpS1*-*OpS7* were upregulated, except for *OpS3*, which raised additional questions about the regulation of this gene cluster. Many *OpS* genes displayed $\log_2$ fold change (LFC) values greater than 5, including *OpS1*, the core PKS enzyme responsible for the synthesis of the precursor orsellinic acid.[235] *OpS11*, a putative evolved D-lactonohydrolase,[215] was also upregulated. *OpS3* is a GAL4-like Zn2-Cys6 fungal transcription factor (TF) and is required for the expression of the main biosynthetic genes (*OpS1*-*OpS7*), including *OpS3* itself.[235]

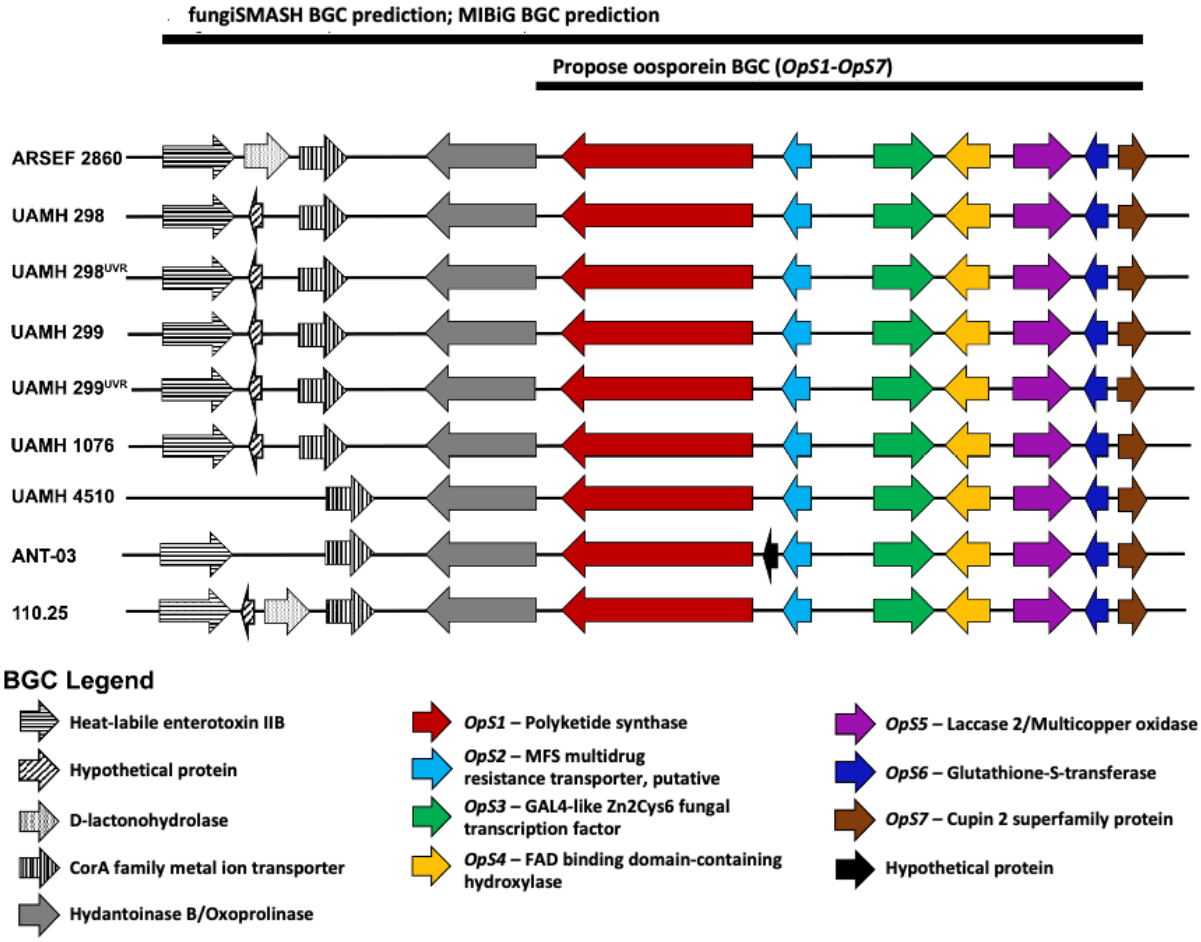


**Fig. 49** Organization of the oosporein biosynthetic gene cluster of the eight *Beauveria bassiana* sequenced draft genomes. The reference strain, *B. bassiana* ARSEF 2860, was used to determine the core genes, *OpS1-OpS7*, using the MiBiG database. The putative upstream genes were predicted using the fungiSMASH database.

Regulation of the oosporein BGC is not well understood, but some regulatory factors were identified with the transcriptomic analysis. Bbmsn, a zinc finger TF and stress response protein, negatively regulates oosporein in a pH-dependent manner.[252] This regulatory factor was upregulated in the red strains, which are contradictory to their phenotype and the differential expression results. Unfortunately, the genetic mechanisms underlying the regulation of oosporein expression by Bbmsn2 have not been elucidated. Differential co-expression analysis identified

several potential transcription factors involved in regulating *OpS1* and *OpS3* expression. Many identified were Zn2-Cys6 type TFs, the same type of TF as *OpS3*, and may play a role in regulating oosporein gene cluster expression and oosporein production, upstream of *OpS3*. In addition, VeA, the Velvet protein-encoding gene, is of interest, as it is responsible for conidiation, secondary metabolism, and stress response in *B. bassiana;* therefore, potentially plays a role in the virulence of the red strains.[253] Differential co-expression results showed a negative regulatory relationship between VeA and *OpS3*, which contradicts the findings of this protein's function. Although these results are inconclusive, it is possible that there is an intermediate positive regulator of *OpS3*, whose expression is regulated by VeA, or vice versa. Given the fact that a complete oosporein BGC is present in the strains of the non-red groups, induction of oosporein expression may occur when infecting a host. These conditions are difficult to replicate under laboratory growth conditions, so the mechanism by which oosporein may be upregulated in the non-red group will need further investigation.

### 4.3.3 Conclusions and Future Directions

In conclusion, the outcome of this study provides an intensive investigation on the efficacy of various phenotypically diverse *Beauveria bassiana* strains in managing MPB populations. From an economic standpoint, the development of an entomopathogenic fungi-based biocontrol agent may provide a more economically-viable and environmentally-conscious approach to the currently limited mitigation efforts. The combination of conidial stability and viability of the powder formulation, and the effective treatment concentration, coupled with critical beetle emergence, resulted in a successful reduction of MPB reproduction under dynamic forest conditions. In addition, we provided a biphasic fermentation approach for the large-scale production of conidial

biomass. Further studies could implement the use of aerial application of the powder formulation during the peak flight period of MPBs, ultimately maximizing the infection of dispersing individuals. In addition, modified bark beetle traps can be used as "assisted autodissemination" of fungal spores, where MPBs can pick up *B. bassiana* spores as they exit these traps.

In addition, this work has characterized the genomic and transcriptomic features of eight *B. bassiana* strains, and how these features contribute to increased virulence and oosporein production. Oosporein biosynthetic cluster genes were upregulated in the red group, and differential co-expression analysis was performed to infer regulatory factors for the oosporein BGC. In addition, several secondary bioactive metabolites were identified and inferred for *B. bassiana* virulence. This broad-scale analysis reveals major genetic features and patterns which contribute to the phenotypic diversity of these strains, and further *in vivo* studies will be needed to further validate these results. Furthermore, *in vitro* competition bioassays were performed between *B. bassiana* strains and two strains of *G. clavigera*, an MPB-symbiotic blue stain fungus, and the results show potential competition with several Group I and Group III strains. These results can provide a foundation for future exometabolomics work to isolate and elucidate the potential bioactive molecules expressed by *B. bassiana* in the presence of different *G. clavigera* species.

# Chapter 5 Experimental Procedures

## 5.1 General procedures

### 5.1.1 General Information. Reagents, Solvents, and Purification.

Commercially available biological and chemical reagents and solvents were purchased from Alfa Aesar Ltd., Caledon, Chem-Impex International Inc., Fisher Scientific Ltd., Harvard Apparatus, R&D Systems, Sigma-Aldrich Canada, Tocris Bioscience, or VWR International. All reagents and solvents were of American Chemical Society (ACS) grade and used without further purification unless otherwise stated. All anhydrous reactions were performed under a positive pressure of argon using flame-dried glassware. Distillation of solvents for anhydrous reactions were performed: dichloromethane (DCM) and dichloroethane were distilled over calcium hydride, diethyl ether and tetrahydrofuran were distilled over sodium with benzophenone as an indicator, and methanol was distilled over magnesium. HPLC-grade acetonitrile (ACN), dimethylformamide (DMF), hexanes, 2-propanol (IPA), and methanol (MeOH) were used without further purification. Commercially available ACS-grade solvents (> 99% purity) were used for column chromatography. A Milli-Q reagent water filtration system (Millipore Co., Milford, MA) was used for deionized water). All reactions and fractions (from column chromatography) were monitored by glass-back thin layer chromatography (TLC) plates with a UV fluorescent indicator (normal $SiO_2$, Merck 60 F254). TLC plate visualization was performed by fluorescence quenching or staining with ninhydrin (ninhydrin/acetic acid/*n*-butanol, 0.6 g/6 mL/200 mL), phosphomolybdic acid in ethanol (10 g in 100 mL), or potassium permanganate ($KMnO_4$, $K_2CO_3$/NaOH, $H_2O$; 1.5 g/10 g/0.12 g/200 mL). Flash column chromatography was performed using Merck type 60, 230-400 mesh silica gel. Analytical and semipreparative scale high performance liquid chromatography

was performed on a Gilson chromatograph (fitted with a model 322 pump heads, a model 171 diode array detector, a FC 203B fraction collector, and a Rheodyne 7725i injector fitted with a 1000 $\mu$L sample loop) or an Agilent chromatograph (fitted with a model 1260 Infinity II binary pump heads, a model 1260 Infinity II variable wavelength detector, a model 1260 Infinity II analytical (semi-preparative)-scale fraction collector, and a Rheodyne 7725i injector fitted with a 500 $\mu$L sample loop). HPLC solvents were filtered through a Millipore filtration system under vacuum prior to use. Peptides were purified to a > 95% purity, as assessed by analytical re-injection.

Optical rotation values (in $10^{-1}$ deg cm$^2$ g$^{-1}$) were measured on a PerkinElmer 241 polarimeter with a microcell (10 cm, 1 mL) at ambient temperature. All reported optical rotations were referenced against air and measured at the sodium D line ($\lambda$ = 589.3 nm). Mass spectra (MS) were recorded on Kratos AEIMS-50, Bruker 9.4 T Apex-QE FTICR (high resolution, HRMS), or Perspective Biosystems Voyager Elite MALDI-TOF-MS, using 4-hydroxy-$\alpha$-cyanocinnamic acid as the matrix. MS/MS was performed on a Bruker Ultraflextreme MALDI-TOF-TOF. LCMS was performed on an Agilent Technologies 6130 LCMS instrument. Infrared (IR) spectra were recorded on a Nicolet Magna 750 or a 20SX FT-IR spectrometer; a cast film refers to the evaporation of the chemical solution on a NaCl plate. Nuclear magnetic resonance (NMR) spectra were recorded using an Inova 400, DD2 MR 400, Unity 500, Unity Agilent/Varian Inova 600, or a VNMRS 700 spectrometer, at 27 °C. For $^1$H (400, 500, 600, or 700 MHz) spectra, $\delta$ values were referenced to $CDCl_3$ (7.26 ppm), $D_2O$ (4.79 ppm), or $CD_3OD$ (3.30 ppm). For $^{13}$C (100, 125, 150, or 175 MHz) spectra, $\delta$ values were referenced to $CDCl_3$ (77.0 ppm) or $CD_3OD$ (49.0 ppm). Reported splitting patterns are abbreviated as: s = singlet, d = doublet, t = triplet, q = quartet, sept

= septet, m = multiplet, app. s = apparent singlet, dd = doublet of doublets, and dt = doublet of triplets.

### 5.1.2 General Solid-Phase Peptide Synthesis Procedures.

#### 5.1.2.1 General 2-Chlorotrityl Chloride Resin Loading Procedure.

Resin beads were washed with DCM (3 × 5 mL) then DMF (3 × 5 mL) in a solid phase peptide synthesis (SPPS) vessel; resin bubbled under argon for 1 min in between washing steps. The resin was resuspended in DMF (5 mL) and swelled for 10 min under argon. To achieve the desired resin loading (mmol/g), 1 equiv of the first Fmoc-protected amino acid was pre-mixed in 10 mL of a 1:1 solution of DCM/DMF with 5 equiv of DIPEA. The amino acid solution was then added to the resin and bubbled for 2.5 h under argon, with continuous replenishment of DCM. MeOH was added to the vessel (0.8 mL/g), to end-cap any remaining chlorotrityl groups, and bubbled for 15 min under argon. The resin was then washed with DMF (3 × 5 mL), DCM (3 × 5 mL), and MeOH (3 × 5 mL), with 1 min bubbling in between each washing step, and then dried under argon until further use.

#### 5.2.2.2 General Manual SPPS Elongation Procedure

The resin was suspended in DMF (5 mL) and bubbled for 15 min under argon to swell in an SPPS vessel. Fmoc-deprotection was performed by bubbling 20% piperidine in DMF (3 x 5 mL) for 5 min each, with a 1 min resin wash with DMF (3 × 5 mL) after each deprotection. The extent of Fmoc-deprotection was monitored by TLC by observing the presence of the dibenzofulvene-piperidine adduct as a bright, dark purple spot under UV. The coupling protocol

consisted of pre-activation of the subsequent amino acid (1.1 equiv compared to resin loading) with a solution of PyBOP (1.0 equiv), HOBt (1.1 equiv), DIPEA (4.0 equiv) in DMF (5 mL), and stirred for 10 min. The activated amino acid solution was added to the resin and bubbled under argon for 2 h. After coupling, the resin was washed with DMF (3 × 10 mL), and the coupling process was assessed by cleaving a small sample of resin with a solution of 95:2.5:2.5 TFA/TIPS/$H_2O$ for 1-2 h and analyzing the crude mass by MALDI-TOF. To end-cap any unreacted amines, a solution of 20% acetic anhydride in DMF (5 mL) was added to the resin and bubbled for 10 min under argon. The resin was washed thoroughly with DMF (3 × 5 mL), subjected to either Fmoc-deprotection for further peptide elongation or rinsed with DCM (3 × 5 ml) and dried for storage or cleavage from the resin.

#### 5.2.2.3 General *N*-terminal PEGylation Procedure.

Fmoc-deprotected peptide on resin (1 equiv to loading) was combined with an *N*-terminally protected PEG chain (5 equiv), HOBt (5 equiv), and DIC (5 equiv) in dry DMF (5 mL) and shaken for 24 h, at room temperature. The solution was filtered to collect the resin beads, and the peptide was then cleaved from the resin according to the procedure below.

#### 5.2.2.4 General Resin Cleavage Procedure

Resin-bound apelin peptides (0.05 mmol) were suspended in a solution of 95:2.5:2.5 TFA/TIPS/$H_2O$ with shaking under argon for 2-3 h. The cleaved resin was filtered through a ball of glass wool and rinsed thoroughly with TFA. The crude solution was concentrated *in vacuo*. Cold diethyl ether (2 × 5 mL) was added to triturate the crude peptide, and the solvent was decanted into a 15 mL falcon tube and centrifuged briefly to pellet any residual peptide. The

triturated crude residue and diethyl ether pellet were pooled together and dissolved in 0.1% aqueous trifluoroacetic acid (TFA).

### 5.1.3 General HPLC Method

Apelin peptides were purified with either a $C_{18}$ or a diphenyl RP-HPLC column, with an eluent system consisting of 0.1% aqueous TFA (solvent A) and 0.1% TFA in acetonitrile (solvent B). The analytical and semi-preparative purification methods are as follows: 0-3 min (10% B), 3-18 min (ramp 10-45% B), 18-25 min (ramp 45-100% B), 25-26.15 min (100% B), 26.15-27.25 min (ramp 100-10% B), and 27.25-36 min (10% B).

### 5.1.4 $Ca^{2+}$ Mobilization Assay

Chem-5 cells (Millipore, USA), expressing the APJ receptor, were incubated in 100 $\mu$L of media (HBSS, 20 mM HEPES, pH 7.4) in 96-well plates (approximately 20,000 cells/well) at 37 °C and 5% $CO_2$ for 24 h. The media was exchanged for a new buffer system (HBSS, 20 mM HEPES, 2.5 M probenecid, pH 7.4) and a fluorescence dye was added (Calcium 6-GF, Molecular Devices, USA). The cells were incubated at 37 °C and 5% $CO_2$ for 2 h. Apelin analogues were diluted in HBSS buffer at pH 7.4 and an aliquot was added to the cells according to a serial dilution of known concentration. Change in fluorescence after the addition of the apelin peptides was monitored with a Spectramax i3x plate-reader (Molecular Devices, USA); values were analyzed using Prism 5.01 (GraphPad, USA). Experiments were performed in three replicates.

### 5.1.5 Plasma protein binding

Adapting from a published protocol, plasma protein binding studies were performed using a custom-built 96-well equilibrium dialysis apparatus (25 kDa MWCO membrane).[254] 1 mM DMSO stock solutions for each peptide (final concentration of 100 $\mu$M) were diluted in EDTA and MLN-4760 stabilized pooled 55% human or mouse plasma. 150 $\mu$L of the peptide-plasma solution was added to the retentate side of the dialysis vial and 150 $\mu$L of PBS buffer (pH 7.4) was added to the dialysate side. The 96-well plate was incubated at 37 °C and shaken at 120 rpm for 3 h; 3 h was determined to be sufficient to reach equilibrium. After the incubation period, 25 $\mu$L of retentate was mixed with 25 $\mu$L of PBS buffer, and 25 $\mu$L of dialysate was mixed with 25 $\mu$L of pooled plasma and incubated on ice for 10 min. Samples were quenched with 20 $\mu$L of 10% aqueous TFA, and 5 $\mu$L of 1mM Dans-YVG was added as the standard. These samples were purified using a pre-equilibrated $C_{18}$ spin column as previously described prior to LCMS quantification of the area under the curve (AUC) ratios.

### 5.1.6 Log $D_{7.4}$ Determination

Adapting from a published protocol from OECD40, log $D_{7.4}$ values were measured using a shake flask procedure using *n*-octanol (>99%, Sigma-Aldrich, St. Louis, USA) and phosphate-buffered saline (PBS) at pH 7.4 and at room temperature.[255] A 10 $\mu$m stock solution of each peptide were prepared in either 1 mL of PBS-saturated *n*-octanol or 1 mL *n*-octanol-saturated PBS buffer. 100 $\mu$L of the solution was submitted for LCMS (10 $\mu$L onto a $C_{18}$ column) for reference quantification before shaking. 300 $\mu$L of each solution was added to an Eppendorf tube and vortexed for 10 min. The phases were allowed to settle for 10 min and were then centrifuged at

10,200 × *g* for 10 min. 100 $\mu$L of each phase was submitted for LCMS quantification (10 $\mu$L onto a C8 column).

### 5.1.7 Experimental Animals and Protocol

All experiments were performed by Dr. Oudit's lab, with experimental discussions and advice from our lab. Wildtype male mice at 12 weeks of age (C57BL/6, 24-30 g in weight) were purchased from Jackson Laboratories (Bar Harbor, ME, USA). Mice were provided water and standard chow ad libitum and housed in a 12 h light:dark cycle facility. The experiments were performed as per the University of Alberta institutional animal care and use guidelines, which conform to the Canadian Council on Animal Care and U.S. National Institutes of Health Guide for the Care and Use of Laboratory Animals guidelines.

### 5.1.8 *In Vivo* Mice Blood Pressure Assays

All experiments were performed by Dr. Oudit's lab, with experimental discussions and advice from our lab. Male mice (24-30 g in weight) were anesthetized with 1.5 % isoflurane/oxygen, and the body temperature was maintained and monitored at 36 °C by a heating pad. The aorta was cannulated *via* the right carotid artery using a PV loop catheter (model 1.2F from Scisense Transonic) to continuously record arterial blood pressure and heart rates (LabScribe 2.0, Scisense). Apelin peptide (1.4 $\mu$M/kg body weight) or the same volume of saline was injected *via* the right jugular vein (n = 3). The results are reported as heart rate (HR), mean arterial blood pressure (MABP), systolic blood pressure (SBP), and diastolic blood pressure (DBP). Changes in HR, MABP, SBP, and DBP (i.e., Δ MABP) from the baseline at 15 min post-injection are presented as mean ± SEM. Blood pressure traces were analyzed with LabScribe2 (iWorx Systems Inc.), and

plotted using OriginLab (Northhampton, MA), and analyzed with SPSS (IBM Corporation, Chicago, IL). One-way ANOVA tests were performed, and Tukey post-hoc analyses were conducted to determine statistical significance for the MABP values at 15 min post-injection with the apelin peptides; $P < 0.05$ was considered significant.

### 5.1.9 Langendorff Isolated Heart Assays

All experiments were performed by Dr. Oudit's lab, with experimental discussions and advice from our lab. Langendorff isolated heart assays were performed to measure cardiac function and heart perfusion post ischemia-reperfusion injury. Male mice (24-30 g in weight) were heparinized and anesthetized with 1.5-2 % isoflurane inhalation. The heart was excised from the mouse and mounted on a Langendorff set-up, and then subsequently perfused with modified Krebs−Henseleit solution (116 mM NaCl, 3.2 mM KCl, 2.0 mM $CaCl_2$, 1.2 mM $MgSO_4$, 25 mM $NaHCO_3$, 1.2 mM $KH_2PO_4$, 11 mM glucose, 0.5 mM EDTA, and 2 mM pyruvate). The heart was kept at 37 ℃ and continuously oxygenated with 95 % $O_2$ and 5 % $CO_2$, which maintained the perfusion buffer at pH 7.4. After stabilization and 10 min of baseline recording, global ischemia was induced for 30 min followed by 40 min of reperfusion. Apelin peptides were given at the start of reperfusion for 10 min at a concentration of 1 $\mu$M (n=5). Left ventricular functions were obtained continuously by the PowerLab system (ADInstruments, Australia). Data were reported as the mean value of every 5 min. Left ventricular functions were reported as the LVDP, HR, max dP/dt, min dP/dt, and RPP. Ischemia reperfusion traces were analyzed using LabChart (ADInstruments, Australia) and presented as mean ± SEM. The resulting graphs were plotted with OriginLab, and statistical analysis was conducted with SPSS. One-way ANOVA followed by

Tukey post-hoc analysis was conducted for LVDP, RPP, and max and min dP/dt values at 15 min post-reperfusion; $P < 0.05$ was considered statistically significant.

### 5.1.10 Radioligand Receptor Binding Assay

All experiments were performed by Dr. Llorens-Cortès' lab, with experimental discussions and advice from our lab. Membrane preparations from Chinese hamster ovary (CHO) cells, stably expressing the wild-type rat apelin receptor-EGFP were previously described.[256,257] Crude membrane preparations (1 $\mu$g total mass of membranes/assay) were incubated at 20 °C for 3 h with 0.2 nM [$^{125}$I]-pyr-1-apelin-13 (monoiodinated on Lys9 with the Bolton-Hunter reagent, PerkinElmer, Wellesley, MA, USA) in binding buffer (50 mM HEPES, 5 mM $MgCl_2$, pH 7.5, bovine serum albumin (BSA) 1 %) with or without the different apelin compounds at various concentrations. The reaction was quenched with 4 mL of cold binding buffer, and the product was filtered on Whatman GF/C filters and washed with 5 mL of cold binding buffer. Radioactivity was counted using a Wizard 1470 Wallac $\gamma$ counter (PerkinElmer, Turku, Finland). Binding experiment data were analyzed with GraphPad Prism 6.

## 5.2. Procedures for the Optimization of PEG-extended Apelin Peptides

### 5.2.1 Synthesis of Analogues 7-18

#### 5.2.1.1 Synthesis of $PEG_6$-NMe17A2 (7).

Fmoc-Phe(4-Br)-OH was loaded onto 2-chlorotrityl chloride resin using the general resin loading procedure at 0.8 mmol/g loading scale. Resin-bound Fmoc-Phe(4-Br)-OH was then subjected to manual SPPS (general method) introducing L-amino acids in the following order: Fmoc-Aib-OH, Fmoc-Nle-OH, Fmoc-Pro-OH, Fmoc-Gly-OH, Fmoc-Lys(Boc)-OH, Fmoc-His(Trt)-OH, and Fmoc-Ser(tBu)-OH. The Arg*N*MeLeu dipeptide was attached manually as described previously.[57] The peptide was then extended with automated SPPS with additional amino acids in the following order: Fmoc-Pro-OH, Fmoc-Arg(Pmc)-OH, Fmoc-Gln(Trt)-OH, Fmoc-Arg(Pmc)-OH, Fmoc-Arg(Pmc)-OH, Fmoc-Phe-OH, and Fmoc-Lys(Boc)-OH. Resin-bound peptide was then coupled to Fmoc-$PEG_6$-$CH_2CH_2COOH$ was coupled according to the general *N*-terminal PEGylation procedure and subsequently cleaved from the resin. The peptide was purified with a Vydac Diphenyl RP-HPLC column (300 Å, 5 $\mu$m, 250 mm × 4.6 mm). The desired peptide was eluted at 17.1 min and isolated as a white solid after lyophilization (6.5 mg, 8%). Monoisotopic mass calculated for $C_{127}H_{199}BrN_{35}O_{29}$ 690.1142, found (FTICR-ESI-MS) 690.1151 $[M + 4H]^{4+}$.

#### 5.2.1.2 Synthesis of $FmocPEG_3$ -NMeLeu17A2 (8)

Fmoc-Phe(4-Br)-OH was loaded onto 2-chlorotrityl chloride resin using the general resin loading procedure at 0.8 mmol/g loading scale. Resin-bound Fmoc-Phe(4-Br)-OH was then

subjected to manual SPPS (general method) introducing L-amino acids in the following order: Fmoc-Aib-OH, Fmoc-Nle-OH, Fmoc-Pro-OH, Fmoc-Gly-OH, Fmoc-Lys(Boc)-OH, Fmoc-His(Trt)-OH, and Fmoc-Ser(t-Bu)-OH, with end-capping after each step. The Arg*N*MeLeu dipeptide was attached manually as described previously but extended for 4 h.[57] Manual SPPS then proceeded with amino acids in the following order: Fmoc-Pro-OH, Fmoc-Arg(Pmc)-OH, Fmoc-Gln(Trt)-OH, Fmoc-Arg(Pmc)-OH, Fmoc-Arg(Pmc)-OH, Fmoc-Phe-OH, and Fmoc-Lys(Boc)-OH. After the final *N*-terminal deprotection, Fmoc-$(PEG)_3$-$CH_2CH_2COOH$ was coupled according to the general *N*-terminal PEGylation procedure. The peptide was then cleaved from the resin and purified using the HPLC general method and a Vydac Diphenyl RP-HPLC column (300 Å, 5 $\mu$m, 250 mm × 4.6 mm). The desired peptide was isolated as a white solid after lyophilization (0.075 mmol, 15 mg, 7.6%). Monoisotopic mass calculated for $C_{121}H_{186}BrN_{35}O_{26}$ 2624.3492, found (FTICR-ESI-MS) 2624.3361 $[M+H]^+$.

#### 5.2.1.3 Synthesis of MeOPEG$_3$-NMeLeu17A2 (9)

Fmoc-Phe(4-Br)-OH was loaded onto 2-chlorotrityl chloride resin using the general resin loading procedure at 0.8 mmol/g loading scale. Resin-bound Fmoc-Phe(4-Br)-OH was then subjected to manual SPPS (general method) introducing L-amino acids in the following order: Fmoc-Aib-OH, Fmoc-Nle-OH, Fmoc-Pro-OH, Fmoc-Gly-OH, Fmoc-Lys(Boc)-OH, Fmoc-His(Trt)-OH, and Fmoc-Ser(t-Bu)-OH, with end-capping after each step. The Arg*N*MeLeu dipeptide was attached manually as described previously but extended for 4 h.[57] Manual SPPS then proceeded with amino acids in the following order: Fmoc-Pro-OH, Fmoc-Arg(Pmc)-OH, Fmoc-Gln(Trt)-OH, Fmoc-Arg(Pmc)-OH, Fmoc-Arg(Pmc)-OH, Fmoc-Phe-OH, and Fmoc-Lys(Boc)-OH. After the final *N*-terminal deprotection, MeO-(PEG)3-$CH_2CH_2COOH$ was coupled according

to the general *N*-terminal PEGylation procedure. The peptide was then cleaved from the resin and purified using the HPLC general method and a $C_{18}$ RP-HPLC analytical column (Supelco Ascentis Si, $C_{18}$ 100 Å, 5 $\mu$m, 25 cm × 4.6 mm). The desired peptide was isolated as a white solid after lyophilization (0.075 mmol, 12 mg, 6.6%). Monoisotopic mass calculated for $C_{107}H_{177}BrN_{34}O_{25}$ 2417.2721, found (FTICR-ESI-MS) 2417.2808 $[M+H]^+$.

#### 5.2.1.4 Synthesis of $NH_2PEG_4$-NMeLeu17A2 (10)

Fmoc-Phe(4-Br)-OH was loaded onto 2-chlorotrityl chloride resin using the general resin loading procedure at 0.8 mmol/g loading scale. Resin-bound Fmoc-Phe(4-Br)-OH was then subjected to manual SPPS (general method) introducing L-amino acids in the following order: Fmoc-Aib-OH, Fmoc-Nle-OH, Fmoc-Pro-OH, Fmoc-Gly-OH, Fmoc-Lys(Boc)-OH, Fmoc-His(Trt)-OH, and Fmoc-Ser(t-Bu)-OH, with end-capping after each step. The Arg*N*MeLeu dipeptide was attached manually as described previously but extended for 4 h.[57] Manual SPPS then proceeded with amino acids in the following order: Fmoc-Pro-OH, Fmoc-Arg(Pmc)-OH, Fmoc-Gln(Trt)-OH, Fmoc-Arg(Pmc)-OH, Fmoc-Arg(Pmc)-OH, Fmoc-Phe-OH, and Fmoc-Lys(Boc)-OH. After the final *N*-terminal deprotection, $NH_2$-$(PEG)_4$-$CH_2CH_2COOH$ was coupled according to the general *N*-terminal PEGylation procedure. The peptide was then cleaved from the resin and purified using the HPLC general method and a $C_{18}$ RP-HPLC analytical column (Supelco Ascentis Si, $C_{18}$ 100 Å, 5 $\mu$m, 25 cm × 4.6 mm). The desired peptide was isolated as a white solid after lyophilization (0.075 mmol, 16 mg, 8.7%). Monoisotopic mass calculated for $C_{108}H_{180}BrN_{35}O_{25}$ 2446.3073, found (FTICR-ESI-MS) 2446.2956 $[M+H]^+$.

#### 5.2.1.5 Synthesis of MeOPEG$_6$-NMeLeu17A2 (11)

Fmoc-Phe(4-Br)-OH was loaded onto 2-chlorotrityl chloride resin using the general resin loading procedure at 0.8 mmol/g loading scale. Resin-bound Fmoc-Phe(4-Br)-OH was then subjected to manual SPPS (general method) introducing L-amino acids in the following order: Fmoc-Aib-OH, Fmoc-Nle-OH, Fmoc-Pro-OH, Fmoc-Gly-OH, Fmoc-Lys(Boc)-OH, Fmoc-His(Trt)-OH, and Fmoc-Ser(t-Bu)-OH, with end-capping after each step. The Arg*N*MeLeu dipeptide was attached manually as described previously but extended for 4 h.[57] Manual SPPS then proceeded with amino acids in the following order: Fmoc-Pro-OH, Fmoc-Arg(Pmc)-OH, Fmoc-Gln(Trt)-OH, Fmoc-Arg(Pmc)-OH, Fmoc-Arg(Pmc)-OH, Fmoc-Phe-OH, and Fmoc-Lys(Boc)-OH. After the final *N*-terminal deprotection, MeO-PEG$_6$-$CH_2CH_2$COOH was coupled according to the general *N*-terminal PEGylation procedure. The peptide was then cleaved from the resin and purified using the HPLC general method and a $C_{18}$ RP-HPLC analytical column (Supelco Ascentis Si, $C_{18}$ 100 Å, 5 $\mu$m, 25 cm × 4.6 mm). The desired peptide was isolated as a white solid after lyophilization (0.075 mmol, 9 mg, 4.7%). Monoisotopic mass calculated for $C_{113}H_{189}BrN_{34}O_{28}$ 2539.3594, found (FTICR-ESI-MS) 2549.3484 $[M+H]^+$.

#### 5.2.1.6 Synthesis of $NH_2$PEG$_6$-NMeLeu17A2 (12)

Fmoc-Phe(4-Br)-OH was loaded onto 2-chlorotrityl chloride resin using the general resin loading procedure at 0.8 mmol/g loading scale. Resin-bound Fmoc-Phe(4-Br)-OH was then subjected to manual SPPS (general method) introducing L-amino acids in the following order: Fmoc-Aib-OH, Fmoc-Nle-OH, Fmoc-Pro-OH, Fmoc-Gly-OH, Fmoc-Lys(Boc)-OH, Fmoc-His(Trt)-OH, and Fmoc-Ser(t-Bu)-OH, with end-capping after each step. The Arg*N*MeLeu dipeptide was attached manually as described previously but extended for 4 h.[57] Manual SPPS then

proceeded with amino acids in the following order: Fmoc-Pro-OH, Fmoc-Arg(Pmc)-OH, Fmoc-Gln(Trt)-OH, Fmoc-Arg(Pmc)-OH, Fmoc-Arg(Pmc)-OH, Fmoc-Phe-OH, and Fmoc-Lys(Boc)-OH. After the final *N*-terminal deprotection, Fmoc-$PEG_6$-$CH_2CH_2COOH$ was coupled according to the general *N*-terminal PEGylation procedure. The peptide was then Fmoc-deprotected by bubbling 20% piperidine in DMF (3 × 10 mL for 5 min each). The peptide was then cleaved from the resin and purified using the HPLC general method and a $C_{18}$ RP-HPLC analytical column (Supelco Ascentis Si, $C_{18}$ 100 Å, 5 $\mu$m, 25 cm × 4.6 mm). The desired peptide was isolated as a white solid after lyophilization (0.075 mmol, 10 mg, 5.3%). Monoisotopic mass calculated for $C_{113}H_{188}BrN_{33}O_{28}$ 2534.3485, found (FTICR-ESI-MS) 2534.3462 $[M+H]^+$ .

**5.2.1.7 Synthesis of CbzPEG$_6$-NMeLeu17A2 (13)**

Fmoc-Phe(4-Br)-OH was loaded onto 2-chlorotrityl chloride resin using the general resin loading procedure at 0.8 mmol/g loading scale. Resin-bound Fmoc-Phe(4-Br)-OH was then subjected to manual SPPS (general method) introducing L-amino acids in the following order: Fmoc-Aib-OH, Fmoc-Nle-OH, Fmoc-Pro-OH, Fmoc-Gly-OH, Fmoc-Lys(Boc)-OH, Fmoc-His(Trt)-OH, and Fmoc-Ser(t-Bu)-OH, with end-capping after each step The Arg*N*MeLeu dipeptide was attached manually as described previously but extended for 4 h.[57] This dipeptide was coupled according to the general method but extended for 4 h. Manual SPPS then proceeded with amino acids in the following order: Fmoc-Pro-OH, Fmoc-Arg(Pmc)-OH, Fmoc-Gln(Trt)-OH, Fmoc- Arg(Pmc)-OH, Fmoc-Arg(Pmc)-OH, Fmoc-Phe-OH, and Fmoc-Lys(Boc)-OH. After the final *N*-terminal deprotection, Fmoc-$PEG_6$-$CH_2CH_2COOH$ was coupled according to the general *N*-terminal PEGylation procedure. The peptide was then Fmoc-deprotected by bubbling 20% piperidine in DMF (3 × 10 mL for 5 min each). The peptide *N*-terminus was then protected

by coupling with benzyl chloroformate: Resin-bound Fmoc-deprotected peptide (1 equiv) was suspended in 10 mL of DMF along with benzyl chloroformate (2 equiv) and DIPEA (5 equiv). The reaction mixture was shaken for 24 hours at room temperature, and then filtered, washed with 3 x 10 mL DMF, and set up again for another 24 hours. After filtering and washing this reaction solution, the peptide was then cleaved from the resin and purified using the HPLC general method and a Vydac Diphenyl RP-HPLC column (300 Å, 5 $\mu$m, 250 mm × 4.6 mm). The desired peptide was isolated as a white solid after lyophilization (0.075 mmol, 13 mg, 6.5%). Monoisotopic mass calculated for $C_{120}H_{198}BrN_{35}O_{29}^{3+}$ 668.1064, found (FTICR-ESI-MS) 668.1069 $[M+4H]^{4+}$.

#### 5.2.1.8 Synthesis of pBpaPEG$_6$-NMeLeu17A2 (14)

Fmoc-Phe(4-Br)-OH was loaded onto 2-chlorotrityl chloride resin using the general resin loading procedure at 0.8 mmol/g loading scale. Resin-bound Fmoc-Phe(4-Br)-OH was then subjected to manual SPPS (general method) introducing L-amino acids in the following order: Fmoc-Aib-OH, Fmoc-Nle-OH, Fmoc-Pro-OH, Fmoc-Gly-OH, Fmoc-Lys(Boc)-OH, Fmoc-His(Trt)-OH, and Fmoc-Ser(t-Bu)-OH, with end-capping after each step. The Arg*N*MeLeu dipeptide was attached manually as described previously but extended for 4 h. Manual SPPS then proceeded with amino acids in the following order: Fmoc-Pro-OH, Fmoc-Arg(Pmc)-OH, Fmoc-Gln(Trt)-OH, Fmoc-Arg(Pmc)-OH, Fmoc-Arg(Pmc)-OH, Fmoc-Phe-OH, and Fmoc-Lys(Boc)-OH. After the final *N*-terminal deprotection, Fmoc-PEG$_6$-$CH_2CH_2COOH$ was coupled according to the general *N*-terminal PEGylation procedure. The peptide was then Fmoc-deprotected by bubbling 20% piperidine in DMF (3 × 10 mL for 5 min each). Fmoc-4-benzoyl-L-phenylalanine was then coupled according to the general elongation procedure and finally deprotected to give a free *N*-terminal amine. The peptide was then cleaved from the resin and purified using the HPLC

general method and a Vydac Diphenyl RP-HPLC column (300 Å, 5 $\mu$m, 250 mm × 4.6 mm). The desired peptide was isolated as a white solid after lyophilization (0.075 mmol, 10 mg, 4.8%). Monoisotopic mass calculated for $C_{128}H_{210}BrN_{36}O_{293}^{3+}$ 930.4925, found (FTICR-ESI-MS) 930.4928 $[M + 3H]^{3+}$.

#### 5.2.1.9 Synthesis of PhePEG$_6$-NMeLeu17A2 (15)

Fmoc-Phe(4-Br)-OH was loaded onto 2-chlorotrityl chloride resin using the general resin loading procedure at 0.8 mmol/g loading scale. Resin-bound Fmoc-Phe(4-Br)-OH was then subjected to manual SPPS (general method) introducing L-amino acids in the following order: Fmoc-Aib-OH, Fmoc-Nle-OH, Fmoc-Pro-OH, Fmoc-Gly-OH, Fmoc-Lys(Boc)-OH, Fmoc-His(Trt)-OH, and Fmoc-Ser(t-Bu)-OH, with end-capping after each step. The Arg*N*MeLeu dipeptide was attached manually as described previously but extended for 4 h.[57] Manual SPPS then proceeded with amino acids in the following order: Fmoc-Pro-OH, Fmoc-Arg(Pmc)-OH, Fmoc-Gln(Trt)-OH, Fmoc-Arg(Pmc)-OH, Fmoc-Arg(Pmc)-OH, Fmoc-Phe-OH, and Fmoc-Lys(Boc)-OH. After the final *N*-terminal deprotection, Fmoc-PEG$_6$-$CH_2CH_2COOH$ was coupled according to the general *N*-terminal PEGylation procedure. The peptide was then Fmoc-deprotected by bubbling 20% piperidine in DMF (3 × 10 mL for 5 min each). Fmoc-Phe-OH was then coupled according to the general elongation procedure and finally deprotected to give a free *N*-terminal amine. The peptide was then cleaved from the resin and purified using the HPLC general method and a Vydac Diphenyl RP-HPLC column (300 Å, 5 μum, 250 mm × 4.6 mm). The desired peptide was isolated as a white solid after lyophilization (0.075 mmol, 11 mg, 5.3%). Monoisotopic mass calculated for $C_{121}H_{200}BrN_{36}O_{283}^{3+}$ 895.8171, found (FTICR-ESI-MS) 895.8167 $[M + 3H]^{3+}$.

#### 5.2.1.10 Synthesis of FmocPEG$_{10}$-NMeLeu17A2 (16)

Fmoc-Phe(4-Br)-OH was loaded onto 2-chlorotrityl chloride resin using the general resin loading procedure at 0.8 mmol/g loading scale. Resin-bound Fmoc-Phe(4-Br)-OH was then subjected to manual SPPS (general method) introducing L-amino acids in the following order: Fmoc-Aib-OH, Fmoc-Nle-OH, Fmoc-Pro-OH, Fmoc-Gly-OH, Fmoc-Lys(Boc)-OH, Fmoc-His(Trt)-OH, and Fmoc-Ser(t-Bu)-OH, with end-capping after each step. The Arg*N*MeLeu dipeptide was attached manually as described previously but extended for 4 h.[57] Manual SPPS then proceeded with amino acids in the following order: Fmoc-Pro-OH, Fmoc-Arg(Pmc)-OH, Fmoc-Gln(Trt)-OH, Fmoc-Arg(Pmc)-OH, Fmoc-Arg(Pmc)-OH, Fmoc-Phe-OH, and Fmoc-Lys(Boc)-OH. After the final *N*-terminal deprotection, Fmoc-$(PEG)_{10}$-$CH_2CH_2COOH$ was coupled according to the general *N*-terminal PEGylation procedure. The peptide was then cleaved from the resin and purified using the HPLC general method and a Vydac Diphenyl RP-HPLC column (300 Å, 5 $\mu$m, 250 mm × 4.6 mm). The desired peptide was isolated as a white solid after lyophilization (0.075 mmol, 15 mg, 6.7%). Monoisotopic mass calculated for $C_{135}H_{217}BrN_{35}O_{33}$ 978.5182, found (FTICR-ESI-MS) 978.5190 $[M+3H]^{3+}$.

#### 5.2.1.11 Synthesis of FmocPEG$_6$-NMeLeu13A2 (17)

Fmoc-Phe(4-Br)-OH was loaded onto 2-chlorotrityl chloride resin using the general resin loading procedure at 0.8 mmol/g loading scale. Resin-bound Fmoc-Phe(4-Br)-OH was then subjected to manual SPPS (general method) introducing L-amino acids in the following order: Fmoc-Aib-OH, Fmoc-Nle-OH, Fmoc-Pro-OH, Fmoc-Gly-OH, Fmoc-Lys(Boc)-OH, Fmoc-His(Trt)-OH, and Fmoc-Ser(t-Bu)-OH, with end-capping after each step. The Arg*N*MeLeu dipeptide was attached manually as described previously but extended for 4 h.[57] Manual SPPS then

proceeded with amino acids in the following order: Fmoc-Pro-OH, Fmoc-Arg(Pmc)-OH, and Fmoc-Gln(Trt)-OH. After the final *N*-terminal deprotection, Fmoc-$PEG_6$-$CH_2CH_2COOH$ was coupled according to the general *N*-terminal PEGylation procedure. The peptide was then cleaved from the resin and purified using the HPLC general method and a Vydac Diphenyl RP-HPLC column (300 Å, 5 $\mu$m, 250 mm × 4.6 mm). The desired peptide was isolated as a white solid after lyophilization (0.075 mg, 11 mg, 6.3%). Monoisotopic mass calculated for $C_{100}H_{156}BrN_{24}O_{25}$ 724.0280, found (FTICR-ESI-MS) 724.0282 $[M+3H]^{3+}$.

#### 5.2.1.12 Synthesis of FmocPEG$_{10}$-NMeLeu13A2 (18)

Fmoc-Phe(4-Br)-OH was loaded onto 2-chlorotrityl chloride resin using the general resin loading procedure at 0.8 mmol/g loading scale. Resin-bound Fmoc-Phe(4-Br)-OH was then subjected to manual SPPS (general method) introducing L-amino acids in the following order: Fmoc-Aib-OH, Fmoc-Nle-OH, Fmoc-Pro-OH, Fmoc-Gly-OH, Fmoc-Lys(Boc)-OH, Fmoc-His(Trt)-OH, and Fmoc-Ser(t-Bu)-OH, with end-capping after each step. The Arg*N*MeLeu dipeptide was attached manually as described previously but extended for 4 h.[57] Manual SPPS then proceeded with amino acids in the following order: Fmoc-Pro-OH, Fmoc-Arg(Pmc)-OH, and Fmoc-Gln(Trt)-OH. After the final *N*-terminal deprotection, Fmoc-$PEG_{10}$-$CH_2CH_2COOH$ was coupled according to the general *N*-terminal PEGylation procedure. The peptide was then cleaved from the resin and purified using the HPLC general method and a Vydac Diphenyl RP-HPLC column (300 Å, 5 $\mu$m, 250 mm × 4.6 mm). The desired peptide was isolated as a white solid after lyophilization (0.075 mmol, 13 mg, 7.4%). Monoisotopic mass calculated for $C_{108}H_{171}BrN_{24}O_{29}^{2+}$ 1175.0915, found (FTICR-ESI-MS) 1175.0908 $[M + 2H]^{2+}$.

### 5.2.2 *In Vitro* Human and Mice Plasma Stability Assays

20 $\mu$L of pooled human or mouse plasma was aliquoted into 1.7 mL Eppendorf tubes and incubated at 37 ℃ for 10 min. 5 $\mu$L of apelin analogue (400 $\mu$M) was added and incubated at 37 ℃ at varying time lengths. The reaction solutions were quenched with 20 $\mu$L of 10% aqueous TFA, followed by the addition of 5 $\mu$L of an internal standard peptide dansyl-YVG-OH (1 mM). The quenched mixtures were diluted with another 50 $\mu$L of 0.1% aqueous TFA and centrifuged at 10,200 × *g* for 10 min. The supernatant was loaded onto pre-equilibrated $C_{18}$ or diphenyl spin column (Harvard Apparatus) with 100 $\mu$L of 0.1% aqueous TFA; the columns were pre-wetted with 50 % ACN in 0.1% aqueous TFA (2 × 200 $\mu$L) and 0.1% aqueous TFA (2 × 200 $\mu$L) with centrifugation at 300 × *g* for 2 min between each loading. The quenched samples were loaded onto the column at 300 × *g* and then washed with 0.1% aqueous TFA (2 × 200 $\mu$L); filtrated discarded after each wash. The desired peptides were eluted with 40 % ACN in 0.1% aqueous TFA with centrifugation at 300 × *g*. The eluate was stored at -20 ℃ until loading onto an RP-HPLC instrument using the method previously described. The 0 min incubation internal standard/analogue area ratio was used to compare the internal standard/analogue area ratio for the timed experiments and determine the remaining analogue (%). Experiments were performed in three replicates.

## 5.3 Procedures for the hArg/Cha Modifications in the RPRL Region

### 5.3.1 Synthesis of Analogues 19-27

#### 5.3.1.1 Synthesis of hArg13A2 (19)

Fmoc-Phe(4-Br)-OH was loaded onto 2-chlorotrityl chloride resin using the general resin loading procedure at a 0.8 mmol/g loading scale. Resin-bound Fmoc-Phe(4-Br)-OH was then subjected to manual SPPS (general method) introducing L-amino acids in the following order: Fmoc-Aib-OH, Fmoc-Nle-OH, Fmoc-Pro-OH, Fmoc-Gly-OH, Fmoc-Lys(Boc)-OH, Fmoc-His(Trt)-OH, Fmoc-Ser(tBu)-OH, Fmoc-Leu-OH, Fmoc-hArg(Pbf)OH, Fmoc-Pro-OH, Fmoc-Arg(Pmc)-OH, and Fmoc-pGlu-OH. The resin-bound peptide was subsequently cleaved from the resin. The peptide was purified with a Phenomenex Luna $C_{18}$ RP-HPLC column (100 Å, 5 $\mu$m, 250 mm × 4.6 mm). The desired peptide was eluted at 13.2 min and isolated as a white solid after lyophilization (10 mg, 12%). Monoisotopic mass calculated for $C_{72}H_{115}BrN_{22}O_{16}$ 811.4017, found (FTICR-ESI-MS) 811.4019 $[M+2H]^{2+}$.

#### 5.3.1.2 Synthesis of Cha13A2 (20)

Fmoc-Phe(4-Br)-OH was loaded onto 2-chlorotrityl chloride resin using the general resin loading procedure at a 0.8 mmol/g loading scale. Resin-bound Fmoc-Phe(4-Br)-OH was then subjected to manual SPPS (general method) introducing L-amino acids in the following order: Fmoc-Aib-OH, Fmoc-Nle-OH, Fmoc-Pro-OH, Fmoc-Gly-OH, Fmoc-Lys(Boc)-OH, Fmoc-His(Trt)-OH, Fmoc-Ser(tBu)-OH, Fmoc-Cha-OH, Fmoc-Arg(Pbf)OH, Fmoc-Pro-OH, Fmoc-Arg(Pmc)-OH, and Fmoc-pGlu-OH. The resin-bound peptide was subsequently cleaved from the resin. The peptide was purified with a Phenomenex Luna $C_{18}$ RP-HPLC column (100 Å, 5 μm, 250 mm × 4.6 mm). The desired peptide was eluted at 13.3 min and isolated as a white solid after lyophilization (11 mg, 13%). Monoisotopic mass calculated for $C_{70}H_{113}BrN_{22}O_{16}$ 798.3939, found (FTICR-ESI-MS) 798.3916 $[M+2H]^{2+}$.

#### 5.3.1.3 Synthesis of hArgCha13A2 (21)

Fmoc-Phe(4-Br)-OH was loaded onto 2-chlorotrityl chloride resin using the general resin loading procedure at a 0.8 mmol/g loading scale. Resin-bound Fmoc-Phe(4-Br)-OH was then subjected to manual SPPS (general method) introducing L-amino acids in the following order: Fmoc-Aib-OH, Fmoc-Nle-OH, Fmoc-Pro-OH, Fmoc-Gly-OH, Fmoc-Lys(Boc)-OH, Fmoc-His(Trt)-OH, Fmoc-Ser(tBu)-OH, Fmoc-Cha-OH, Fmoc-hArg(Pbf)OH, Fmoc-Pro-OH, Fmoc-Arg(Pmc)-OH, and Fmoc-pGlu-OH. The resin-bound peptide was subsequently cleaved from the resin. The peptide was purified with a Phenomenex Luna $C_{18}$ RP-HPLC column (100 Å, 5 μm, 250 mm × 4.6 mm). The desired peptide was eluted at 13.1 min and isolated as a white solid after lyophilization (13 mg, 15%). Monoisotopic mass calculated for $C_{73}H_{117}BrN_{22}O_{16}$ 818.4095, found (FTICR-ESI-MS) 818.4074 $[M+2H]^{2+}$.

#### 5.3.1.4 Synthesis of hArg17A2 (22)

Fmoc-Phe(4-Br)-OH was loaded onto 2-chlorotrityl chloride resin using the general resin loading procedure at a 0.8 mmol/g loading scale. Resin-bound Fmoc-Phe(4-Br)-OH was then subjected to manual SPPS (general method) introducing L-amino acids in the following order: Fmoc-Aib-OH, Fmoc-Nle-OH, Fmoc-Pro-OH, Fmoc-Gly-OH, Fmoc-Lys(Boc)-OH, Fmoc-His(Trt)-OH, Fmoc-Ser(tBu)-OH, Fmoc-Leu-OH, Fmoc-hArg(Pbf)OH, Fmoc-Pro-OH, Fmoc-Arg(Pmc)-OH, Fmoc-Gln(Trt)-OH, Fmoc-Arg(Pmc)-OH, Fmoc-Arg(Pmc)-OH, Fmoc-Phe-OH, and Fmoc-Lys(Boc)-OH. The resin-bound peptide was subsequently cleaved from the resin. The peptide was purified with a Phenomenex Luna $C_{18}$ RP-HPLC column (100 Å, 5 μm, 250 mm × 4.6 mm). The desired peptide was eluted at 13.2 min and isolated as a white solid after

lyophilization (12 mg, 14%). Monoisotopic mass calculated for $C_{99}H_{164}BrN_{34}O_{20}$ 742.7343, found (FTICR-ESI-MS) 742.7329 $[M+3H]^{3+}$.

#### 5.3.1.5 Synthesis of Cha17A2 (23)

Fmoc-Phe(4-Br)-OH was loaded onto 2-chlorotrityl chloride resin using the general resin loading procedure at a 0.8 mmol/g loading scale. Resin-bound Fmoc-Phe(4-Br)-OH was then subjected to manual SPPS (general method) introducing L-amino acids in the following order: Fmoc-Aib-OH, Fmoc-Nle-OH, Fmoc-Pro-OH, Fmoc-Gly-OH, Fmoc-Lys(Boc)-OH, Fmoc-His(Trt)-OH, Fmoc-Ser(tBu)-OH, Fmoc-Cha-OH, Fmoc-Arg(Pbf)OH, Fmoc-Pro-OH, Fmoc-Arg(Pmc)-OH, Fmoc-Gln(Trt)-OH, Fmoc-Arg(Pmc)-OH, Fmoc-Arg(Pmc)-OH, Fmoc-Phe-OH, and Fmoc-Lys(Boc)-OH. The resin-bound peptide was subsequently cleaved from the resin. The peptide was purified with a Phenomenex Luna $C_{18}$ RP-HPLC column (100 Å, 5 μm, 250 mm × 4.6 mm). The desired peptide was eluted at 13.1 min and isolated as a white solid after lyophilization (15 mg, 18%). Monoisotopic mass calculated for $C_{97}H_{162}BrN_{34}O_{20}$ 734.0624, found (FTICR-ESI-MS) 734.0605 $[M+3H]^{3+}$.

#### 5.3.1.6 Synthesis of hArgCha17A2 (24)

Fmoc-Phe(4-Br)-OH was loaded onto 2-chlorotrityl chloride resin using the general resin loading procedure at a 0.8 mmol/g loading scale. Resin-bound Fmoc-Phe(4-Br)-OH was then subjected to manual SPPS (general method) introducing L-amino acids in the following order: Fmoc-Aib-OH, Fmoc-Nle-OH, Fmoc-Pro-OH, Fmoc-Gly-OH, Fmoc-Lys(Boc)-OH, Fmoc-His(Trt)-OH, Fmoc-Ser(tBu)-OH, Fmoc-Cha-OH, Fmoc-hArg(Pbf)OH, Fmoc-Pro-OH, Fmoc-Arg(Pmc)-OH, Fmoc-Gln(Trt)-OH, Fmoc-Arg(Pmc)-OH, Fmoc-Arg(Pmc)-OH, Fmoc-Phe-OH,

and Fmoc-Lys(Boc)-OH. The resin-bound peptide was subsequently cleaved from the resin. The peptide was purified with a Phenomenex Luna $C_{18}$ RP-HPLC column (100 Å, 5 μm, 250 mm × 4.6 mm). The desired peptide was eluted at 13.8 min and isolated as a white solid after lyophilization (12 mg, 14%). Monoisotopic mass calculated for $C_{100}H_{166}BrN_{34}O_{20}$ 747.4062, found (FTICR-ESI-MS) 747.4050 $[M+3H]^{3+}$.

#### 5.3.1.7 Synthesis of *N*MeCha17A2 (25)

Fmoc-Phe(4-Br)-OH was loaded onto 2-chlorotrityl chloride resin using the general resin loading procedure at a 0.8 mmol/g loading scale. Resin-bound Fmoc-Phe(4-Br)-OH was then subjected to manual SPPS (general method) introducing L-amino acids in the following order: Fmoc-Aib-OH, Fmoc-Nle-OH, Fmoc-Pro-OH, Fmoc-Gly-OH, Fmoc-Lys(Boc)-OH, Fmoc-His(Trt)-OH, and Fmoc-Ser(tBu)-OH. The synthesized Fmoc-*N*MeCha-OH (**29**) was attached manually as described previously.[57] The peptide was then extended with manual SPPS with additional amino acids in the following order: Fmoc-Arg(Pbf)OH, Fmoc-Pro-OH, Fmoc-Arg(Pmc)-OH, Fmoc-Gln(Trt)-OH, Fmoc-Arg(Pmc)-OH, Fmoc-Arg(Pmc)-OH, Fmoc-Phe-OH, and Fmoc-Lys(Boc)-OH. The resin-bound peptide was subsequently cleaved from the resin. The peptide was purified with a Phenomenex Luna $C_{18}$ RP-HPLC column (100 Å, 5 μm, 250 mm × 4.6 mm). The desired peptide was eluted at 21.3 min and isolated as a white solid after lyophilization (14 mg, 17%). Monoisotopic mass calculated for $C_{100}H_{163}BrN_{34}O_{20}$ 747.4076, found (FTICR-ESI-MS) 747.4062 $[M + 3H]^{3+}$.

#### 5.3.1.8 Synthesis of hArg*N*MeCha17A2 (26)

Fmoc-Phe(4-Br)-OH was loaded onto 2-chlorotrityl chloride resin using the general resin loading procedure at a 0.8 mmol/g loading scale. Resin-bound Fmoc-Phe(4-Br)-OH was then subjected to manual SPPS (general method) introducing L-amino acids in the following order: Fmoc-Aib-OH, Fmoc-Nle-OH, Fmoc-Pro-OH, Fmoc-Gly-OH, Fmoc-Lys(Boc)-OH, Fmoc-His(Trt)-OH, and Fmoc-Ser(tBu)-OH. The synthesized Fmoc-hArg(Boc)$_2$-*N*Me-Cha-OH (**33**) was attached manually as described previously.[258] The peptide was then extended with manual SPPS with additional amino acids in the following order: Fmoc-Pro-OH, Fmoc-Arg(Pmc)-OH, Fmoc-Gln(Trt)-OH, Fmoc-Arg(Pmc)-OH, Fmoc-Arg(Pmc)-OH, Fmoc-Phe-OH, and Fmoc-Lys(Boc)-OH. The resin-bound peptide was subsequently cleaved from the resin. The peptide was purified with a Phenomenex Luna $C_{18}$ RP-HPLC column (100 Å, 5 µm, 250 mm × 4.6 mm). The desired peptide was eluted at 21.5 min and isolated as a white solid after lyophilization (14 mg, 17%). Monoisotopic mass calculated for $C_{100}H_{165}BrN_{34}O_{20}$ 564.3025, found (FTICR-ESI-MS) 564.3103 $[M + 4H]^{4+}$.

#### 5.3.1.9 Synthesis of hArg*N*MeLeu17A2 (27)

Fmoc-Phe(4-Br)-OH was loaded onto 2-chlorotrityl chloride resin using the general resin loading procedure at a 0.8 mmol/g loading scale. Resin-bound Fmoc-Phe(4-Br)-OH was then subjected to manual SPPS (general method) introducing L-amino acids in the following order: Fmoc-Aib-OH, Fmoc-Nle-OH, Fmoc-Pro-OH, Fmoc-Gly-OH, Fmoc-Lys(Boc)-OH, Fmoc-His(Trt)-OH, and Fmoc-Ser(tBu)-OH. The synthesized Fmoc-hArg(Boc)$_2$-*N*MeLeu-OH (**36**) was attached manually as described previously.[258] The peptide was then extended with manual SPPS with additional amino acids in the following order: Fmoc-Pro-OH, Fmoc-Arg(Pmc)-OH, Fmoc-

Gln(Trt)-OH, Fmoc-Arg(Pmc)-OH, Fmoc-Arg(Pmc)-OH, Fmoc-Phe-OH, and Fmoc-Lys(Boc)-OH. The resin-bound peptide was subsequently cleaved from the resin. The peptide was purified with a Phenomenex Luna $C_{18}$ RP-HPLC column (100 Å, 5 μm, 250 mm × 4.6 mm). The desired peptide was eluted at 21.3 min and isolated as a white solid after lyophilization (16 mg, 19%). Monoisotopic mass calculated for $C_{98}H_{161}BrN_{34}O_{20}$ 554.3025, found (FTICR-ESI-MS) 554.2950 $[M + 4H]^{4+}$.

### 5.3.2 Synthesis of hArg-(NMe)Cha dipeptides

#### 5.3.2.1 Synthesis of (4*S*)-3-(9-Fluorenylmethyloxycarbonyl)-4-cyclohexylalanine-5-oxo-oxazolidinone (28)

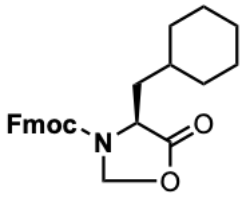


This reaction was adapted from a literature procedure.[259] Fmoc-L-Cha-OH (2.00 g, 5.08 mmol) was suspended in toluene (100 mL), and paraformaldehyde (1.06 g, 33.8 mmol) and *p*-toluenesulfonic acid (0.12 g, 0.55 mmol) were subsequently added. The mixture was refluxed at 120 ℃ for 2 h with azeotropic water removal, resulting in a pale-white suspension. The solution was cooled to room temperature and subsequently washed with 1 M $NaHCO_3$ (3 × 50 mL) and brine (3 × 50 mL). The organic layer was dried over $Na_2SO_4$ and concentrated *in vacuo*. The product was purified by flash chromatography (silica gel, 25% EtOAc in hexanes), yielding **28** (1.90 g, 95%) as a white solid. ($R_f$ =0.29 on $SiO_2$, 25% EtOAc in hexanes); $[\alpha]_D^{26}$ 63.36 (c 0.65 $CH_2Cl_2$); IR ($CH_2Cl_2$ cast) 3067, 3041, 3019, 2924, 2851, 1801, 1716, 1478, 1450, 1417, 1056 $cm^{-}$

[1]; $^1$H ($CDCl_3$, 400 MHz) δ 7.78 (dd, J = 3.3 Hz, 2H, Fmoc Ar-H), 7.54 (d, J = 7.3 Hz, 2H, Fmoc Ar-H), 7.42 (dt, J = 7.5 Hz, 2H, Fmoc Ar-H), 7.33 (dt, 7.39 Hz, 2H, Fmoc Ar-H), 5.34 (app. s, 1H, Fmoc-CH), 5.07 (d, J = 4.61 Hz, 2H, Fmoc-$CH_2$), 4.68 (app. s, 2H, oxazolidinone $CH_2$), 4.23, (t, J = 4.74, 1H, Cha-CH$\alpha$), 1.80 – 1.60 (app. s, 6H, Cha-$CH_2$), 1.45 – 1.35 (app. s, 2H, Cha-$CH_2\beta$), 1.25 – 1.15 (app. s, 4H, Cha-$CH_2$), 1.00 – 0.60 (app. s, 1H, Cha-CH$\gamma$); $^{13}$C ($CDCl_3$, 100 MHz) $\delta$ 188.9, 172.5, 141.5, 128.0, 127.3, 127.2, 124.6, 120.2, 65.9, 52.9, 47.3, 37.8, 33.2, 26.3, 26.1, 26.0, 15.3; HRMS (ESI) Calculated for $C_{25}H_{27}NO_4$ 405.1940, found 428.1831 $[M+Na]^+$.

### 5.3.2.2 Synthesis of Fmoc-*N*MeCha-OH (29)

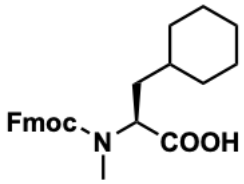


This reaction was adapted from a literature procedure.[259] The oxazolidinone intermediate **28** (1.90 g, 4.67 mmol) was dissolved in $CHCl_3$, and trifluoroacetic acid (30 mL) and triethylsilane (2.35 mL, 14.67 mmol) were added. The solution was stirred at room temperature for 22 h followed by concentration *in vacuo*, affording a sticky yellow solid. The product was purified by flash chromatography (silica gel, 5% MeOH in $CH_2Cl_2$), yielding **29** (1.50 g, 80%) as an off-white solid. ($R_f$ =0.54 on $SiO_2$, 5% MeOH in $CH_2Cl_2$); $[\alpha]_D^{26}$ -22.05 (c 1.16 $CH_2Cl_2$); IR ($CH_2Cl_2$ cast) 3067, 3043, 3019, 2924, 2851, 1742, 1706, 1478, 1451 cm$^{-1}$; $^1$H ($CDCl_3$, 400 MHz) δ 8.68 (bs, 1H, COOH), 7.75 (d, J = 7.6 Hz, 2H, Fmoc Ar-H), 7.65 – 7.52 (t, J = 6.6 Hz, 2H, Fmoc Ar-H), 7.39 (dt, J = 7.4 Hz, 2H, Fmoc Ar-H), 7.37 – 7.27 (dt, 6.89 Hz, 2H, Fmoc Ar-H), 5.01 – 4.50 (d, 4.8 Hz, 2H, Fmoc-$CH_2$), 4.46 (t, J = 7.6 Hz, Cha-CH$\alpha$), 4.34 – 4.19 (t, J = 7.0 Hz, 1H, Fmoc-CH), 2.88 (s, 3H, N-$CH_3$), 1.92-1.48 (m, 6H, Cha-$CH_2$), 1.34 – 1.08 (m, 4H, Cha-$CH_2$), 1.05 – 0.91 (m,

2H, Cha-$CH_2\beta$), 0.83 – 0.71 (m, 1H, Cha-$CH\gamma$); $^{13}C$ ($CDCl_3$, 100 MHz) δ 177.7, 157.2, 144.0, 141.4, 127.7, 127.1, 125.1, 124.8, 120.0, 67.9, 56.1, 47.3, 36.0, 33.9, 31.9, 31.8, 30.5, 26.4, 26.3, 26.0; HRMS (ESI) Calculated for $C_{25}H_{29}NO_4$ 407.2097, found 408.2165 $[M+H]^+$.

#### 5.3.2.3 Synthesis of Fmoc-*N*MeCha-OBn (30)

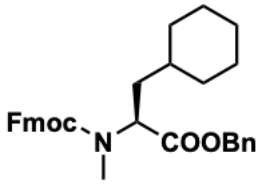


This reaction was adapted from a literature procedure.[260] A solution of **29** (1.50 g, 3.68 mmol) in DMF (100 mL) was cooled to 0 ℃. $K_2CO_3$ (0.67 g, 4.86 mmol) was added, and the reaction mixture was stirred at 0 ℃ for 1 h. Subsequently, benzyl bromide (0.58 mL, 4.86 mmol) was added, and the reaction was stirred at 0 ℃ for 30 min and then reacted at room temperature overnight to afford an off-white solution. The solution was poured into $H_2O$ (200 mL) and extracted with hexane (4 × 200 mL). The organic layers were combined and washed with cold $H_2O$ (2 × 200 mL) and brine (2 × 200 mL), then dried over $Na_2SO_4$ and concentrated *in vacuo* to afford a yellow oil. The product was purified by flash chromatography (silica gel, 6:1 hexane:EtOAc), yielding **30** (1.33 g, 89%) as white crystals. ($R_f$ = 0.41 on $SiO_2$, 6:1 hexane:EtOAc); $[\alpha]_D^{26}$ -13.47 (c 1.24 $CH_2Cl_2$); IR ($CH_2Cl_2$ cast) 3089, 3066, 3037, 2924, 2851, 1740, 1703, 1149 $cm^{-1}$; $^1H$ ($CDCl_3$, 400 MHz) δ 7.80 – 7.58 (d, J = 7.5 Hz, 2H, Fmoc Ar-H), 7.76 – 7.49 (t, J = 6.8 Hz, 2H, Fmoc Ar-H), 7.43 – 7.34 (dt, J = 7.4 Hz, 2H, Fmoc Ar-H), 7.33 – 7.27 (m, 2H, Fmoc Ar-H), 7.33 – 7.27 (m, 5H, Ar-H), 5.15 (s, 2H, Ar-$CH_2$), 5.03 – 4.57 (d, J = 4.9 Hz, 2H, Fmoc- $CH_2$), 4.41 (t, J = 7.3 Hz, Cha-$CH\alpha$), 4.28 (t, J = 7.1 Hz, 1H, Fmoc-CH), 2.86 (s, 3H, $NCH_3$), 1.74 – 1.60 (m, 6H, Cha- $CH_2$), 1.29 – 1.17 (m, 4H, Cha- $CH_2$), 1.17 – 1.08 (m, 2H, Cha-

$CH_2\beta$), 0.98 – 0.89 (m, 1H, Cha-$CH\gamma$); $^{13}C$ ($CDCl_3$, 100 MHz) δ 172.1, 171.2 156.5, 143.6, 140.9, 135.3, 128.2, 127.9, 127.8, 127.7, 127.3, 126.6, 124.6, 123.4, 119.6, 67.2, 66.4, 55.6, 46.9, 35.9, 35.7, 33.5, 31.6, 29.8, 26.0, 25.9, 25.6; HRMS (ESI) Calculated for $C_{32}H_{35}NO_4$ 497.2566, found 498.2646 $[M+H]^+$.

#### 5.3.2.4 Synthesis of Fmoc-Lys(Boc)-*N*MeCha-OBn (31)

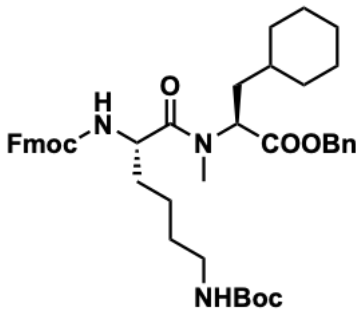


This reaction was adapted from a literature procedure.[57] **30** (0.67 g, 1.35 mmol) was dissolved in a 1:1 solution of DEA:DCM (2 mL) and stirred at room temperature for 1 h. The reaction mixture was concentrated under reduced pressure affording a sticky yellow oil. The free amine was used as the crude for the next step. Fmoc-L-Lys(Boc)-OH (1.71 g, 3.65 mmol), PYBOP (1.39 g, 2.67 mmol), HOBt (0.36 g, 2.67 mmol) and DIPEA (3.5 mL, 16 mmol) were dissolved in DMF (20 mL) and allowed to pre-activate for 10 min. The free amine was dissolved in dry $CH_2Cl_2$ (30 mL) and DIPEA (0.47 mL, 2.7 mmol) was added to it, where the solution was then added to the previous step. The reaction was stirred at room temperature for 22 h. Subsequently, the reaction was washed with saturated $NaHCO_3$ (50 mL) and EtOAc (50 mL) was added to dissolve the resulting precipitate. The organic layer was washed with 10% citric acid (50 mL), cold $H_2O$ (50 mL) and brine (50 mL), then dried over $Na_2SO_4$ and concentrated under reduced pressure to give a sticky yellow oil. The product was purified by flash chromatography (silica gel, 33% EtOAc in hexane), yielding **31** (0.43 g, 64%) as a white powder. ($R_f$ =0.43 on $SiO_2$, 33% EtOAc in hexane);

$[\alpha]_D^{26}$ -15.59 (c 0.88 $CH_2Cl_2$); IR ($CH_2Cl_2$ cast) 3333, 3289, 3066, 3043 2854, 2979, 2928, 1721, 1640, 1619, 1499 $cm^{-1}$; $^1H$ ($CDCl_3$, 400 MHz) δ 7.76 (d, J = 7.4 Hz, 2H, Fmoc Ar-H), 7.59 (dd, J = 7.2, 4.0 Hz, 2H, Fmoc Ar-H), 7.40 – 7.37 (m, 2H, Fmoc Ar-H), 7.36 – 7.28 (m, 2H, Fmoc Ar-H), 7.36 – 7.28 (m, 5H, Ar-H), 5.68 – 4.59 (d, J = 8.4 Hz, 2H, Ar-$CH_2$), 5.39 (dd, J = 10.8, 5.0 Hz, 1H, Lys- CH$\alpha$), 5.13 (dd, J = 12.2, 10.8 Hz, 1H, Cha-CH$\alpha$), 4.36 (d, J = 7.0 Hz, 2H, Fmoc-$CH_2$), 4.22 (t, J = 7.1 Hz, 1H, Fmoc-CH), 3.07 (m, 2H, Lys-$CH_2\varepsilon$), 2.94 (s, 3H, N-$CH_3$), 1.88-1.74 (m, 2H, Lys-$CH_2\beta$), 1.73 – 1.56 (m, 2H, Lys-$CH_2\delta$),1.73 – 1.56 (m, 6H, Cha-$CH_2$), 1.43 (s, 9H, Boc-$(CH_3)_3$), 1.37 (m, 2H, Lys-$CH_2\gamma$), 1.18 – 1.07 (m, 1H, Cha-CH$\gamma$), 1.18 – 1.07 (m, 4H, Cha-$CH_2$), 1.04 – 0.78 (q, J = 10.4 Hz, 1H, Cha-$CH_2\beta$), 1.04 – 0.78 (q, J = 11.4 Hz, 1H, Cha-$CH_2\beta$); $^{13}C$ ($CDCl_3$, 100 MHz) δ 172.3, 171.2, 158.4, 155.6, 143.4, 140.9, 135.4, 128.2, 128.1, 127.9, 127.3, 126.7, 124.7, 119.6, 109.6, 66.7, 53.7, 50.5, 46.8, 43.0, 35.1, 33.8, 33.7, 32.0, 31.7, 30.7, 28.8, 28.1, 26.0, 25.8, 25.6, 21.8; HRMS (ESI) Calculated for $C_{42}H_{55}N_3O_7$ 725.4055, found 726.4129 $[M+H]^+$.

#### 5.3.2.5 Synthesis of Fmoc-hArg(Boc)$_2$-*N*MeCha-OBn (32)

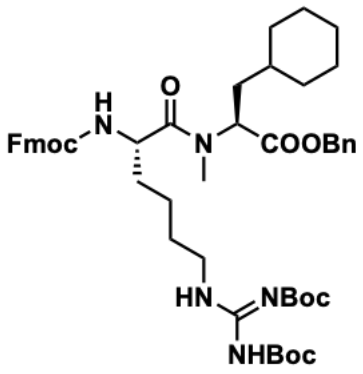


This reaction was adapted from a literature procedure.[57] Dipeptide **31** (0.43 g, 0.59 mmol) was dissolved in dry $CH_2Cl_2$ (20 mL) and TFA (10 mL) was added to the solution. The reaction was stirred at room temperature for 1.5 h and concentrated *in vacuo* giving a sticky yellow foam.

The foam was resuspended in dry $CH_2Cl_2$ (20 mL) with the addition of *N*,*N*'-di-Boc-*N*"-guanidine triflate (0.254 g, 0.65 mmol) and $Et_3N$ (0.18 mL, 1.3 mmol) and stirred at room temperature for 1.5 h. The reaction was washed with 2 M $NaHSO_4$ (20 mL), 10% $NaHCO_3$ (20 mL) and brine (20 mL), then dried over $Na_2SO_4$ and concentrated *in vacuo* to give an off-white foam. The product was purified by flash chromatography (silica gel, 33% EtOAc in hexane), yielding **32** (0.28 g, 65%) as a white powder. ($R_f$ =0.57 on $SiO_2$, 33% EtOAc in hexane); $[\alpha]_D^{26}$ -12.70 (c 0.63 $CH_2Cl_2$); IR ($CH_2Cl_2$ cast) 3333, 3066, 2978, 2929, 2854, 1721, 1640, 1134 $cm^{-1}$; $^1H$ ($CDCl_3$, 400 MHz) δ 7.76 (d, J = 7.4 Hz, 2H, Fmoc Ar-H), 7.59 (dd, J = 7.2, 4.0 Hz, 2H, Fmoc Ar-H), 7.43 – 7.35 (m, 2H, Fmoc Ar-H), 7.35 – 7.25 (m, 2H, Fmoc Ar-H), 7.35 – 7.25 (m, 5H, Ar-H), 5.60 (dd, J = 8.2 Hz, 1H, Cha-CH$\alpha$), 5.38 (dd, J = 10.6, 5.0 Hz, 1H, Lys-CH$\alpha$), 5.10 (dd, J = 12.7, 12.0 Hz, Ar-$CH_2$), 4.64 (app. s, 1H, Lys-NH$\alpha$), 4.35 (m, 2H, Fmoc-$CH_2$), 4.19 (t, J = 7.0 Hz, 1H, Fmoc-CH), 3.37 (m, 2H, Lys-$CH_2\varepsilon$), 2.92 (s, 3H, N-$CH_3$), 1.90 – 1.74 (m, 2H, Lys $CH_2\beta$), 1.74 – 1.55 (m, 6H, Cha- $CH_2$), 1.74 – 1.55 (m, 2H, Lys-$CH_2\delta$), 1.50 (s, 9H, Boc-$(CH_3)_3$), 1.47 (s, 9H, Boc-$(CH_3)_3$), 1.37 (m, 2H, Lys-$CH_2\gamma$), 1.26 – 1.07 (m, 4H, Cha-$CH_2$), 1.26 – 1.07 (m, 1H, Cha-CH), 0.97 – 0.85 (dd, J = 10.4 Hz, 2H, Cha-$CH_2\beta$); $^{13}C$ ($CDCl_3$, 100 MHz) δ 172.8, 171.4, 168.3, 156.1, 153.4, 143.9, 143.8, 141.3, 135.4, 128.6, 128.5, 128.4, 127.7, 127.1, 125.2, 120.0, 67.1, 54.1, 50.1, 47.2, 35.5, 34.1, 33.8, 32.4, 32.1, 28.3, 28.1, 26.4, 26.2, 25.4, 22.4; HRMS (ESI) Calculated for $C_{49}H_{65}N_5O_9$ 867.4776, found 868.4849 $[M+H]^+$.

### 5.3.2.6 Synthesis of Fmoc-hArg(Boc)$_2$-*N*MeCha-OH (33)

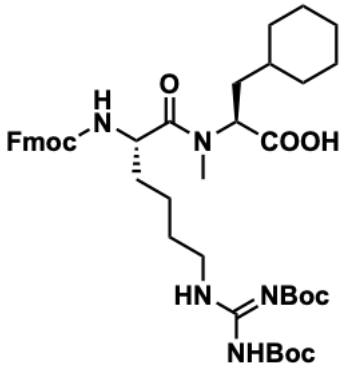


This reaction was adapted from a literature procedure.[57] A solution of **32** (0.28 g, 0.32 mmol) was dissolved in MeOH (25 mL) and 10% Pd/C (20 mg) was added to it. The suspension was stirred under $H_2$ gas (1 atm) overnight, filtered through a pad of celite and concentrated *in vacuo* to give a white powder. The product was purified by flash chromatography (silica gel, 2% MeOH in EtOAc), yielding **33** (0.20 g, 71%) as a white powder. ($R_f$ =0.31 on $SiO_2$, 2% MeOH in EtOAc); $[\alpha]_D^{26}$ -5.20 (c 0.75 $CH_2Cl_2$); IR ($CH_2Cl_2$ cast) 3332, 3283, 3138, 3057, 2979, 2928, 2853, 1721, 1640, 1577, 1158 $cm^{-1}$; $^1H$ ($CDCl_3$, 400 MHz) δ 7.75 (d, J = 7.6 Hz, 2H, Fmoc Ar-H), 7.62 (t, J = 8.1 Hz, 2H, Fmoc Ar-H), 7.38 (dt, J = 7.3, 4.8 Hz, 2H, Fmoc Ar-H), 7.29 (m, 2H, Fmoc Ar-H), 5.39 (dd, J = 10.6, 4.7 Hz, 1H, Lys-CH$\alpha$), 4.74 (d, J = 5.4 Hz, 1H, Cha-CH$\alpha$), 4.32 (d, J = 7.1 Hz, 2H, Fmoc-$CH_2$), 4.20 (t, J = 7.4 Hz, 1H, Fmoc-CH), 3.90 (t, J = 6.0 Hz, Lys-$CH_2\varepsilon$), 2.92 (s, 3H, $NCH_3$), 2.06 – 1.94 (m, 2H, Lys-$CH_2\beta$), 1.74 – 1.66 (m, 6H, Cha-$CH_2$), 1.74 – 1.66 (m, 2H, Lys-$CH_2\delta$), 1.50 (s, 9H, Boc-$(CH_3)_3$), 1.49 (s, 9H, Boc-$(CH_3)_3$), 1.37 (m, 2H, Lys-$CH_2\gamma$), 1.33 – 1.06 (m, 4H, Cha-$CH_2$), 1.33 – 1.06 (m, 1H, Cha-CH), 1.04 – 0.81 (m, 2H, Cha-$CH_2\beta$); $^{13}C$ ($CDCl_3$, 100 MHz) δ 172.8, 171.4, 168.0, 165.9, 152.9, 126.6, 124.9, 119.5, 59.5, 55.4, 46.8, 41.0, 35.2, 33.7, 33.5, 32.6, 28.2, 27.9, 27.7, 25.9, 25.7, 25.5, 22.7; HRMS (ESI) Calculated for $C_{42}H_{60}N_5O_9$ 777.4313, found 778.4376 $[M+H]^+$.

### 5.3.2.7 Synthesis of Fmoc-Lys(Boc)-*N*MeLeu-OBn (34)

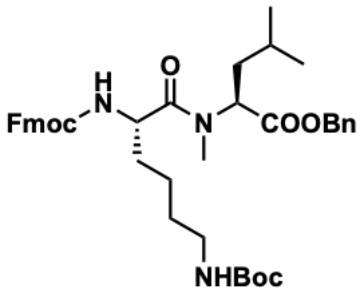


This reaction was adapted from a literature procedure.[57] Fmoc-*N*-Me-Leu-Bn (0.60 g, 1.63 mmol) was dissolved in a 1:1 solution of DEA:DCM (2 mL) and stirred at room temperature for 1 h. The reaction mixture was concentrated under reduced pressure affording a white powder. The free amine was used directly in the next step. Fmoc-L-Lys(Boc)-OH (1.71 g, 3.65 mmol), PyBOP (1.39 g, 2.67 mmol), HOBt (0.36 g, 2.67 mmol) and DIPEA (3.5 mL, 16 mmol) were dissolved in DMF (20 mL) and allowed to pre-activate for 10 min. The free amine was dissolved in dry $CH_2Cl_2$ (30 mL) and DIPEA (0.47 mL, 2.7 mmol) was added to it, where the solution was then added to the previous step. The reaction was stirred at room temperature for 22 h. Subsequently, the reaction was washed with saturated $NaHCO_3$ (50 mL) and EtOAc was added to dissolve the resulting precipitate (50 mL). The organic layer was washed with 10% citric acid (50 mL), cold $H_2O$ (50 mL) and brine (50 mL), then dried over $Na_2SO_4$ and concentrated under reduced pressure to give a pale yellow oil. The product was purified by flash chromatography (silica gel, 10% EtOAc in $CH_2Cl_2$), yielding **34** (0.39 g, 65%) as a white powder. ($R_f$ = 0.23 on $SiO_2$, 10% EtOAc in $CH_2Cl_2$); $[\alpha]_D^{26}$ -17.03 (c 0.91 $CH_2Cl_2$); IR ($CH_2Cl_2$ cast) 3321, 3065, 3038, 2956, 2869, 1713, 1645, 1511, 1248, 1172 $cm^{-1}$; $^1H$ ($CDCl_3$, 400 MHz) δ 7.76 (d, J = 7.5 Hz, 2H, Fmoc Ar-H), 7.59 (d, J = 7.4 Hz, 2H, Fmoc Ar-H), 7.45 – 7.35 (m, 2H, Fmoc Ar-H), 7,.45 – 7.35 (m, 5H, Ar-H), 5.36 (dd, J = 10.7, 5.0 Hz, 1H, Lys-CH$\alpha$), 5.14 (t, J = 10.0 Hz, 2H, Lys-$CH_2\varepsilon$), 4.65 (m, 1H, Leu-CH$\alpha$), 4.36 (d, J = 7.2 Hz, 2H, Fmoc-$CH_2$), 4.21 (t, J = 6.9 Hz, 1H, Fmoc-CH), 3.07 (m, 2H, Ar-$CH_2$), 2.93 (s,

3H, N-$CH_3$), 1.89 – 1.63 (m, 2H, Leu-$CH_2\beta$), 1.60 – 1.49 (m, 2H, Lys-$CH_2\beta$), 1.49 – 1.46 (m, 1H, Leu-$CH\gamma$), 1.43 (s, 9H, Boc-$(CH_3)_3$), 1.41 – 1.36 (m, 2H, Lys-$CH_2\delta$), 1.30 – 1.26 (m, 2H, Lys-$CH_2\gamma$), 0.94 (d, J = 6.7 Hz, 3H, Leu-$CH_3$), 0.90 (d, J = 6.5 Hz, 3H, Leu-$CH_3$); $^{13}C$ ($CDCl_3$, 100 MHz) δ 172.4, 171.0, 162.7, 155.7, 155.4, 143.4, 140.9, 135.0, 128.3, 128.1, 127.9, 127.3, 126.7, 124.8, 119.6, 66.7, 54.4, 50.5, 46.8, 36.4, 32.0, 28.1, 24.5, 22.8, 21.7, 21.0; HRMS (ESI) Calculated for $C_{40}H_{51}N_3O_7$ 685.3727, found 683.3791$[M+H]^+$.

### 5.3.2.8 Synthesis of Fmoc-hArg(Boc)$_2$-*N*MeLeu-OBn (35)

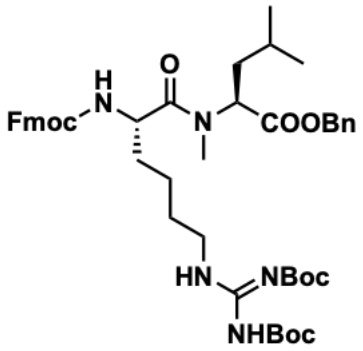


This reaction was adapted from a literature procedure.[57] Dipeptide **34** (0.39 g, 0.57 mmol) was dissolved in dry $CH_2Cl_2$ (20 mL) and TFA (10 mL) was added to the solution. The reaction was stirred at room temperature for 1.5 h and concentrated *in vacuo* giving a sticky yellow foam. The foam was resuspended in dry $CH_2Cl_2$ (20 mL) with the addition of *N*,*N*'-di-Boc-*N*"-guanidine triflate (0.254 g, 0.65 mmol) and $Et_3N$ (0.18 mL, 1.3 mmol) and stirred at room temperature for 1.5 h. The reaction was washed with 2 M $NaHSO_4$ (20 mL), 10% $NaHCO_3$ (20 mL) and brine (20 mL), then dried over $Na_2SO_4$ and concentrated *in vacuo* to give an off-white foam. The product was purified by flash chromatography (silica gel, 25% EtOAc in hexane), yielding **35** (0.29 g, 74%) as a white powder. ($R_f$ =0.26 on $SiO_2$, 25% EtOAc in hexane); $[\alpha]_D^{26}$ -12.00 (c 0.84 $CH_2Cl_2$); IR ($CH_2Cl_2$ cast) 3333, 3065, 3038, 2957, 2869, 1720, 1640, 1575, 1156, 1134 $cm^{-1}$; $^1H$ ($CDCl_3$,

400 MHz) δ 7.76 (d, J = 7.5 Hz, 2H, Fmoc Ar-H), 7.59 (d, J = 7.4 Hz, 2H, Fmoc Ar-H), 7.43 – 7.37 (m, 2H, Fmoc Ar-H), 7,.44 – 7.37 (m, 5H, Ar-H), 5.36 (dd, J = 10.7, 4.8 Hz, 1H, Leu-CH$\alpha$), 5.13 (t, J = 12.2 Hz, 2H, Lys-$CH_2\varepsilon$), 4.64 (m, 1H, Lys-CH$\alpha$), 4.36 (d, J = 7.2 Hz, 2H, Fmoc-$CH_2$), 4.21 (t, J = 6.9 Hz, 1H, Fmoc-CH), 3.35 (m, 2H, Ar-$CH_2$), 2.93 (s, 3H, N-$CH_3$), 1.85 – 1.74 (m, 2H, Leu- $CH_2\beta$), 1.72– 1.58 (m, 2H, Lys-$CH_2\beta$), 1.57 – 1.52 (m, 1H, Leu-CH$\gamma$), 1.50 (s, 9H, Boc-$(CH_3)_3$), 1.48 (s, 9H, Boc-$(CH_3)_3$), 1.43 – 1.33 (m, 2H, Lys-$CH_2\delta$), 1.31 – 1.16 (m, 2H, Lys-$CH_2\gamma$), 0.93 (d, J = 6.7 Hz, 3H, Leu-$CH_3$), 0.90 (d, J = 6.5 Hz, 3H, Leu-$CH_3$); $^{13}C$ ($CDCl_3$, 100 MHz) δ 171.0, 170.9, 163.5, 155.7, 155.4, 143.5, 140.1, 135.0, 128.3, 128.1, 128.0, 127.3, 126.7, 124.8, 119.5, 66.7, 54.4, 50.5, 46.8, 36.4, 32.1, 28.0, 27.7, 24.5, 22.8, 22.0, 21.0; HRMS (ESI) Calculated for $C_{46}H_{61}N_5O_9$ 827.4469, found 828.4535 $[M+H]^+$.

**5.3.2.9 Synthesis of Fmoc-hArg(Boc)$_2$-*N*MeLeu-OH (36)**

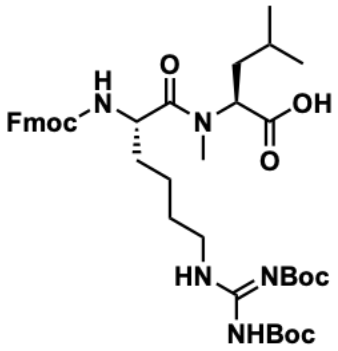


This reaction was adapted from a literature procedure.[57] A solution of **35** (0.29 g, 0.35 mmol) was dissolved in MeOH (25 mL) and 10% Pd/C (20 mg) was added to it. The suspension was stirred under $H_2$ gas (1 atm) overnight, filtered through a pad of celite and concentrated *in vacuo* to give a clear oil. The product was purified by flash chromatography (silica gel, 25% EtOAc in hexane), yielding **36** (0.18 g, 62%) as a white powder. ($R_f$ =0.72 on $SiO_2$, 25% EtOAc in hexane); $[\alpha]_D^{26}$ -6.00 (c 0.26 $CH_2Cl_2$); IR ($CH_2Cl_2$ cast) 3325, 3287, 3065, 2957, 2924, 2870, 1721,

1641, 1415, 1368, 1137 $cm^{-1}$; $^{1}H$ ($CDCl_3$, 400 MHz) δ 8.36 (bs, 1H, COOH), 7.76 (d, J = 7.7 Hz, 2H, Fmoc Ar-H), 7.60 (dd, J = 13.8, 7.6 Hz, 2H, Fmoc Ar-H), 7.41 – 7.34 (m, 2H, Fmoc Ar-H), 7.34 – 7.28 (m, 2H, Fmoc Ar-H), 5.35 (dd, J = 10.8, 4.8 Hz, 1H, Leu-CH$\alpha$), 4.75 (dd, J = 13.9, 6.1 Hz, 2H, Lys-$CH_2\alpha$), 4.32 (d, J = 7.6 Hz, 2H, Fmoc-$CH_2$), 4.19 (t, J = 7.5 Hz, 1H, Fmoc-CH), 3.40 (m, 2H, Leu-$CH_2\varepsilon$), 3.00 (s, 3H, N-$CH_3$), 1.89 – 1.74 (m, 2H, Leu-$CH_2\beta$), 1.73 – 1.58 (m, 2H, Lys-$CH_2\beta$), 1.54 – 1.52 (m, 1H, Leu-CH$\gamma$), 1.50 (s, 9H, Boc-$(CH_3)_3$), 1.49 (s, 9H, Boc-$(CH_3)_3$), 1.46 – 1.35 (m, 2H, Lys-$CH_2\delta$), 1.31 – 1.24 (m, 2H, Lys-$CH_2\gamma$), 0.97 (d, J = 6.7 Hz, 3H, Leu-$CH_3$), 0.89 (d, J = 6.5 Hz, 3H, Leu-$CH_3$); $^{13}C$ ($CDCl_3$, 100 MHz) δ 171.0, 170.9, 165.9, 155.7, 155.4, 128.3, 128.2, 127.9, 127.3, 126.7, 124.8, 119.5, 54.4, 50.5, 46.8, 36.4, 32.2, 28.1, 27.7, 24.5, 22.8, 21.9, 21.0; HRMS (ESI) Calculated for $C_{39}H_{55}N_5O_9$ 737.4000, found 738.4062 $[M+H]^+$.

### 5.3.3 *In Vitro* Human and Mice Plasma Stability Assays

Procedures for the quantification of peptides in plasma were adapted from a published protocol.[261] Briefly, 20 $\mu$L of plasma (human or mice) was pre-portioned into microcentrifuge tubes and incubated at 37 °C for 15 min. Next, 5 $\mu$L of apelin peptide (1 mM) was added to each 20 $\mu$L plasma sample, and then subsequently incubated at 37 °C at varying time points (t (human) = 0, 1, 2, 4, 6, 24 h, and t (mice) = 0, 5, 10, 15, 30, 60, 180 min). The reaction solution was then quenched with 25 $\mu$L 6 M GuHCl and 300 $\mu$L 80% ACN/$H_2O$, 5 $\mu$L of internal standard (1 mM Dans-YVG) was added. The plasma sample was vortexed prior to centrifugation at 13,200 × *g* for 5 min. The supernatant was transferred to a 1 mL microcentrifuge tube and evaporated. The dried samples were then reconstituted with 150 $\mu$L 0.1% aqueous acetic acid (v/v) and loaded onto a pre-equilibrated $C_{18}$ spin column, which had been previously wetted with 2 × 150 $\mu$L 30 % acetonitrile in 0.1% aqueous TFA and 2 × 150 $\mu$L 0.1% aqueous acetic acid (v/v), centrifuging at

280 × *g* for 2 min between each 150 $\mu$L aliquot. The resultant filtrate was reloaded onto the column along with 150 $\mu$L 0.1% aqueous acetic acid (v/v) and centrifuged at 280 × *g* for another 2 min; the filtrate was then discarded. The loaded peptide was washed with 2 × 150 $\mu$L 5% MeOH in 1 % aqueous acetic acid (v/v) and eluted from the column using 100 $\mu$L 60% MeOH in 10% aqueous acetic acid (v/v). The eluate was injected and analyzed using LCMS quantification, where the ratio of apelin peptide to the internal standard was calculated based on the area under the curve. The 0 h incubation ratio was used to compare the apelin peptide/internal standard ratios for the time experiments.

## 5.4 Procedures for the Investigation of the KFRR Motif

### 5.4.1 Synthesis of peptide alanine-scan analogues (37-44)

#### 5.4.1.1 Synthesis of AFRRQRPRLSHKGPMPF (37)

Fmoc-Phe-OH was loaded onto 2-chlorotrityl chloride resin using the general resin loading procedure at 0.8 mmol/g loading scale. Resin-bound Fmoc-Phe-OH was then subject to manual SPPS (general method) introducing L-amino acids in the following order: Fmoc-Pro-OH, Fmoc-Met-OH, Fmoc-Pro-OH, Fmoc-Gly-OH, Fmoc-Lys(Boc)-OH, Fmoc-His(Trt)-OH, and Fmoc-Ser(t-Bu)-OH, Fmoc-Leu-OH, Fmoc- Arg(Pmc)-OH, Fmoc-Pro-OH, Fmoc-Arg(Pmc)-OH, Fmoc-Gln(Trt)-OH, Fmoc-Arg(Pmc)-OH, Fmoc- Arg(Pmc)-OH, Fmoc-Phe-OH, and Fmoc-Ala-OH, with end-capping after each step. After the final *N*-terminal deprotection, the peptide was then cleaved from the resin and purified using the HPLC general method and a Phenomenex Luna $C_{18}$ RP-HPLC column (100 Å, 5 $\mu$m, 250 mm × 4.6 mm). The desired peptide was isolated as a white solid after lyophilization (15 mg, 9.6%). Monoisotopic mass calculated for $C_{93}H_{152}N_{33}O_{20}S^{3+}$ 694.7210, found (FTICR-ESI-MS) 695.0449 $[M + 3H]^{3+}$.

#### 5.4.1.2 Synthesis of KARRQRPRLSHKGPMPF (38)

Fmoc-Phe-OH was loaded onto 2-chlorotrityl chloride resin using the general resin loading procedure at 0.8 mmol/g loading scale. Resin-bound Fmoc-Phe-OH was then subjected to the general manual SPPS method introducing L-amino acids in the following order: Fmoc-Pro-OH, Fmoc-Met-OH, Fmoc-Pro-OH, Fmoc-Gly-OH, Fmoc-Lys(Boc)-OH, Fmoc-His(Trt)-OH, and Fmoc-Ser(t-Bu)-OH, Fmoc-Leu-OH, Fmoc-Arg(Pmc)-OH, Fmoc-Pro-OH, Fmoc-Arg(Pmc)-OH,

Fmoc-Gln(Trt)-OH, Fmoc-Arg(Pmc)-OH, Fmoc-Arg(Pmc)-OH, Fmoc-Ala-OH, and Fmoc-Lys(Boc)-OH, with end-capping after each step. After the final *N*-terminal deprotection, the peptide was then cleaved from the resin and purified using the HPLC general method and a Phenomenex Luna $C_{18}$ RP-HPLC column (100 Å, 5 $\mu$m, 250 mm × 4.6 mm). The desired peptide was isolated as a white solid after lyophilization (11 mg, 7.1%). Monoisotopic mass calculated for $C_{90}H_{155}N_{34}O_{20}S^{3+}$ 688.3965, found (FTICR-ESI-MS) 688.3969 $[M+3H]^{3+}$.

#### 5.4.1.3 Synthesis of KFARQRPRLSHKGPMPF (39)

Fmoc-Phe-OH was loaded onto 2-chlorotrityl chloride resin using the general resin loading procedure at 0.8 mmol/g loading scale. Resin-bound Fmoc-Phe-OH was then subjected to the general manual SPPS method introducing L-amino acids in the following order: Fmoc-Pro-OH, Fmoc-Met-OH, Fmoc-Pro-OH, Fmoc-Gly-OH, Fmoc-Lys(Boc)-OH, Fmoc-His(Trt)-OH, and Fmoc-Ser(t-Bu)-OH, Fmoc-Leu-OH, Fmoc-Arg(Pmc)-OH, Fmoc-Pro-OH, Fmoc-Arg(Pmc)-OH, Fmoc-Gln(Trt)-OH, Fmoc-Arg(Pmc)-OH, Fmoc-Ala-OH, Fmoc-Phe-OH, and Fmoc-Lys(Boc)-OH, with end-capping after each step. After the final *N*-terminal deprotection, the peptide was then cleaved from the resin and purified using the HPLC general method and a Phenomenex Luna $C_{18}$ RP-HPLC column (100 Å, 5 $\mu$m, 250 mm × 4.6 mm). The desired peptide was isolated as a white solid after lyophilization (14 mg, 9.0%). Monoisotopic mass calculated for $C_{93}H_{152}N_{31}O_{20}S^{3+}$ 685.3856, found (FTICR-ESI-MS) 685.3857 $[M + 3H]^{3+}$.

#### 5.4.1.4 Synthesis of KFRAQRPRLSHKGPMPF (40)

Fmoc-Phe-OH was loaded onto 2-chlorotrityl chloride resin using the general resin loading procedure at 0.8 mmol/g loading scale. Resin-bound Fmoc-Phe-OH was then subjected to the

general manual SPPS method introducing L-amino acids in the following order: Fmoc-Pro-OH, Fmoc-Met-OH, Fmoc-Pro-OH, Fmoc-Gly-OH, Fmoc-Lys(Boc)-OH, Fmoc-His(Trt)-OH, and Fmoc-Ser(t-Bu)-OH, Fmoc-Leu-OH, Fmoc-Arg(Pmc)-OH, Fmoc-Pro-OH, Fmoc-Arg(Pmc)-OH, Fmoc-Gln(Trt)-OH, Fmoc-Ala-OH, Fmoc-Arg(Pmc)-OH, Fmoc-Phe-OH, and Fmoc-Lys(Boc)-OH, with end-capping after each step. After the final *N*-terminal deprotection, the peptide was then cleaved from the resin and purified using the HPLC general method and a Phenomenex Luna $C_{18}$ RP-HPLC column (100 Å, 5 $\mu$m, 250 mm × 4.6 mm). The desired peptide was isolated as a white solid after lyophilization (12 mg, 7.8%). Monoisotopic mass calculated for $C_{93}H_{150}N_{31}O_{20}S^{3+}$ 685.3856, found (FTICR-ESI-MS) 685.3861 $[M+3H]^{3+}$.

#### 5.4.1.5 Synthesis of AFRRQRPRLSHKGPNleAibBrF (41)

Fmoc-Phe-OH was loaded onto 2-chlorotrityl chloride resin using the general resin loading procedure at 0.8 mmol/g loading scale. Resin-bound Fmoc-Phe-OH was then subjected to the general manual SPPS method introducing L-amino acids in the following order: Fmoc-Aib-OH, Fmoc-Nle-OH, Fmoc-Pro-OH, Fmoc-Gly-OH, Fmoc-Lys(Boc)-OH, Fmoc-His(Trt)-OH, and Fmoc-Ser(t-Bu)-OH, Fmoc- Leu-OH, Fmoc-Arg(Pmc)-OH, Fmoc-Pro-OH, Fmoc-Arg(Pmc)-OH, Fmoc-Gln(Trt)-OH, Fmoc-Arg(Pmc)-OH, Fmoc-Arg(Pmc)-OH, Fmoc-Phe-OH, and Fmoc-Ala-OH, with end-capping after each step. After the final *N*-terminal deprotection, the peptide was then cleaved from the resin and purified using the HPLC general method and a Phenomenex Luna $C_{18}$ RP-HPLC column (100 Å, 5 $\mu$m, 250 mm × 4.6 mm). The desired peptide was isolated as a white solid after lyophilization (16 mg, 10%). Monoisotopic mass calculated for $C_{93}H_{150}BrN_{33}O_{20}^{3+}$ 710.3712, found (FTICR-ESI-MS) 710.3700 $[M+3H]^{3+}$.

#### 5.4.1.6 Synthesis of K<u>A</u>RRQRPRLSHKGPNleAibBrF (42)

Fmoc-Phe-OH was loaded onto 2-chlorotrityl chloride resin using the general resin loading procedure at 0.8 mmol/g loading scale. Resin-bound Fmoc-Phe-OH was then subjected to the general manual SPPS method introducing L-amino acids in the following order: Fmoc-Aib-OH, Fmoc-Nle-OH, Fmoc-Pro-OH, Fmoc-Gly-OH, Fmoc-Lys(Boc)-OH, Fmoc-His(Trt)-OH, and Fmoc-Ser(t-Bu)-OH, Fmoc- Leu-OH, Fmoc-Arg(Pmc)-OH, Fmoc-Pro-OH, Fmoc-Arg(Pmc)-OH, Fmoc-Gln(Trt)-OH, Fmoc- Arg(Pmc)-OH, Fmoc-Arg(Pmc)-OH, Fmoc-Ala-OH, and Fmoc-Lys(Boc)-OH, with end-capping after each step. After the final *N*-terminal deprotection, the peptide was then cleaved from the resin and purified using the HPLC general method and a Phenomenex Luna $C_{18}$ RP-HPLC column (100 Å, 5 $\mu$m, 250 mm × 4.6 mm). The desired peptide was isolated as a white solid after lyophilization (9 mg, 5.7%). Monoisotopic mass calculated for $C_{90}H_{153}BrN_{34}O_{20}^{3+}$ 704.0467, found (FTICR-ESI-MS)704.0458 $[M+3H]^{3+}$.

#### 5.4.1.7 Synthesis of KF<u>A</u>RQRPRLSHKGPNleAibBrF (43)

Fmoc-Phe-OH was loaded onto 2-chlorotrityl chloride resin using the general resin loading procedure at 0.8 mmol/g loading scale. Resin-bound Fmoc-Phe-OH was then subjected to the general manual SPPS method introducing L-amino acids in the following order: Fmoc-Aib-OH, Fmoc-Nle-OH, Fmoc-Pro-OH, Fmoc-Gly-OH, Fmoc-Lys(Boc)-OH, Fmoc-His(Trt)-OH, and Fmoc-Ser(t-Bu)-OH, Fmoc- Leu-OH, Fmoc-Arg(Pmc)-OH, Fmoc-Pro-OH, Fmoc-Arg(Pmc)-OH, Fmoc-Gln(Trt)-OH, Fmoc- Arg(Pmc)-OH, Fmoc-Ala-OH, Fmoc-Phe-OH, and Fmoc-Lys(Boc)-OH, with end-capping after each step. After the final *N*-terminal deprotection, the peptide was then cleaved from the resin and purified using the HPLC general method and a Phenomenex Luna $C_{18}$ RP-HPLC column (100 Å, 5 $\mu$m, 250 mm × 4.6 mm). The desired peptide was isolated as a white

solid after lyophilization (15 mg, 9.5%). Monoisotopic mass calculated for $C_{93}H_{150}BrN_{31}O_{20}^{3+}$ 701.0358, found (FTICR-ESI-MS) 701.0351 $[M+3H]^{3+}$.

#### 5.4.1.8 Synthesis of KFRAQRPRLSHKGPNleAibBrF (44)

Fmoc-Phe-OH was loaded onto 2-chlorotrityl chloride resin using the general resin loading procedure at 0.8 mmol/g loading scale. Resin-bound Fmoc-Phe-OH was then subjected to the general manual SPPS method introducing L-amino acids in the following order: Fmoc-Aib-OH, Fmoc-Nle-OH, Fmoc-Pro-OH, Fmoc-Gly-OH, Fmoc-Lys(Boc)-OH, Fmoc-His(Trt)-OH, and Fmoc-Ser(t-Bu)-OH, Fmoc- Leu-OH, Fmoc-Arg(Pmc)-OH, Fmoc-Pro-OH, Fmoc-Arg(Pmc)-OH, Fmoc-Gln(Trt)-OH, Fmoc-Ala-OH, Fmoc-Arg(Pmc)-OH, Fmoc-Phe-OH, and Fmoc-Lys(Boc)-OH, with end-capping after each step. After the final *N*-terminal deprotection, the peptide was then cleaved from the resin and purified using the HPLC general method and a Phenomenex Luna $C_{18}$ RP-HPLC column (100 Å, 5 $\mu$m, 250 mm × 4.6 mm). The desired peptide was isolated as a white solid after lyophilization (14 mg, 8.9%). Monoisotopic mass calculated for $C_{93}H_{150}BrN_{31}O_{20}^{3+}$ 701.0358, found (FTICR-ESI-MS) 701.0348 $[M+3H]^{3+}$.

### 5.4.2 Synthesis of Methylated Arg14 Apelin Analogues (45, 46)

#### 5.4.2.1 Synthesis of *N*MeArg14-*N*Me17A2 (45)

Fmoc-Phe(4-Br)-OH was loaded onto 2-chlorotrityl chloride resin using the general resin loading procedure at a 1.5 mmol/g loading scale. Resin-bound Fmoc-Phe(4-Br)-OH was then subject to manual SPPS (general method), introducing L-amino acids in the following order. Fmoc-Aib-OH, Fmoc-Nle-OH, Fmoc-Pro-OH, Fmoc-Gly-OH, Fmoc-Lys(Boc)-OH, Fmoc-His(Trt)-

OH, and Fmoc-Ser(t-Bu)-OH, with end-capping after each step. The *N*MeLeu subunit was added as a Fmoc-Arg(Boc)-*N*MeLeu-OH dipeptide, synthesized following a previously described protocol but extended for 4 hours, followed by end-capping.[57] Manual SPPS was then continued with the L-amino acids in the following order: Fmoc-Pro-OH, Fmoc-Arg(Pmc)-OH, Fmoc-Gln(Trt)-OH with end-capping after each step. The *N*MeArg amino acid was added as Fmoc-*N*MeArg(Mtr)-OH, following the general method, but for an extended time of 4 hours, followed by end-capping. The next amino acid Fmoc-Arg(Pmc)-OH was coupled using the general method, but allowed to couple for an extended time of 4 hours. The final two amino acids Fmoc-Phe-OH, and Fmoc-Lys(Boc)-OH were coupled according to the general method, then end-capped and *N*-terminally deprotected. The peptide was then cleaved from the resin and purified using the HPLC general method and a Phenomenex Luna $C_{18}$ RP-HPLC column (100 Å, 5 $\mu$m, 250 mm × 10.00 mm). The desired peptide was isolated as a white solid after lyophilization (12 mg, 8%). Monoisotopic mass calculated for $C_{98}H_{161}BrN_{34}O_{20}$ 2213.1810, found (FTICR-ESI-MS) 2213.1749 $[M+H]^+$.

#### 5.4.2.2 Synthesis of *α*MeArg14-*N*Me17A2 (46)

Fmoc-Phe(4-Br)-OH was loaded onto 2-chlorotrityl chloride resin using the general resin loading procedure at 0.8 mmol/g loading scale. Resin bound Fmoc-Phe(4-Br)-OH was then subject to manual SPPS (general method), introducing L-amino acids in the following order. Fmoc-Aib-OH, Fmoc-Nle-OH, Fmoc-Pro-OH, Fmoc-Gly-OH, Fmoc-Lys(Boc)-OH, Fmoc-His(Trt)-OH, and Fmoc-Ser(t-Bu)-OH, with end-capping after each step. The *N*MeLeu subunit was added as a Fmoc-Arg(Boc)-*N*MeLeu-OH dipeptide, synthesized following a previously described protocol but extended for 4 hours, followed by end-capping.[57] Manual SPPS was then continued with the L-

amino acids in the following order: Fmoc-Pro-OH, Fmoc-Arg(Pmc)-OH, Fmoc-Gln(Trt)-OH with end-capping after each step. The $\alpha$MeArg subunit was added as Fmoc-$\alpha$MeArg(Boc)-OH, synthesized as described below. The $\alpha$MeArg was coupled following the general method, but for an extended time of 4 hours, followed by end-capping. The final three amino acids Fmoc-Arg(Pmc)-OH, Fmoc-Phe-OH, and Fmoc-Lys(Boc)-OH were coupled according to the general method, then end-capped and *N*-terminally deprotected. The peptide was then cleaved from the resin and purified using the HPLC general method and a Phenomenex Luna $C_{18}$ RP-HPLC column (100 Å, 5 $\mu$m, 250 mm × 10.00 mm). The desired peptide was isolated as a white solid after lyophilization (1 0mg, 6%). Monoisotopic mass calculated for $C_{98}H_{161}BrN_{34}O_{20}$ 2213.1810, found (FTICRESI- MS) 2213.1734 $[M+H]^+$.

### 5.4.3 Synthesis of precursors for $\alpha$MeArg14-*N*Me17A2 (46)

#### 5.4.3.1 Synthesis of (2*S*)-2-(3'-azidopropyl)-2-methyl-glycine-Ni(II)-(S)-BPB (47)

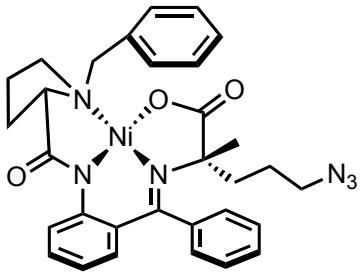


The nickel complex **47** was prepared according to a literature procedure and the data was identical to that which was reported in the literature.[57,262,263]

**5.4.3.2 Synthesis of ((*S*)-2-amino-5-azido-2-methylpentanoic acid (48)**

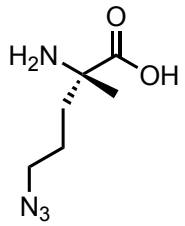


Amino acid **48** was prepared with an adapted literature procedure.[263] Nickel complex **47** (1.49 g, 2.51 mmol) was dissolved in 15 mL of 2:1 MeOH:DCM and added dropwise to 20 mL of 3 M 1:1 HCl:MeOH over 5 min. The reaction mixture was stirred for 30 min at 60 °C, turning the reaction mixture from bright red to green. The reaction mixture was cooled to room temperature and concentrated *in vacuo* to produce a green-brown solid. The solid was resuspended in 50 mL of 1:1 DCM: $H_2O$ and filtered to remove the insoluble BPB ligand. The aqueous layer was washed with DCM (3 × 25 mL). The aqueous layer was concentrated *in vacuo* and the product was purified by an ion exchange column (Dowex 50WX2 50-100 mesh). The amino acid was eluted using $H_2O$:$NH_4OH$ (10-80% gradient), yielding **48** (0.36 g, 84%) as a fluffy white solid. $[\alpha]_D^{26}$ 1.81 (c 0.56 $H_2O$); IR ($H_2O$ cast) 3117, 2973, 2940, 2099, 1607, 1522, 1460, 1407, 1269 $cm^{-1}$; $^1H$ ($D_2O$, 400 MHz): δ 3.40 (t, J = 6.8, Hz, 2H, $CH_2$-$N_3$), 2.01 – 1.93 (m, 1H, Orn- $CH_2\beta$), 1.89 – 1.81 (m, 1H, Orn-$CH_2\beta$), 1.77 – 1.66 (m, 1H, Orn-$CH_2\gamma$), 1.62 – 1.54 (m, 1H, Orn-$CH_2\gamma$), 1.52 (s, 3H, -$CH_3$); $^{13}C$ ($D_2O$, 175 MHz): $\delta$ 177.3, 62.1, 51.5, 35.2, 23.9, 23.2; HRMS (ESI) Calculated for $C_6H_{12}N_4O_2$ 172.0960, found 172.0960 $[M-H]^-$.

### 5.4.3.3 Synthesis of (*S*)-2-((((9H-fluoren-9-yl)methoxy)carbonyl)amino)-5-azido-2-methylpentanoic acid (49)

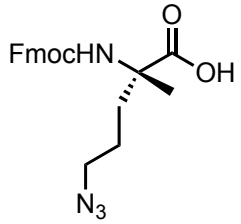


This reaction was adapted from a literature procedure.[263] Amino acid **48** (0.22 g, 1.30 mmol) was suspended in 20 mL dry DCM and TMSCl (0.50 mL, 3.90 mmol) was added to it and heated at reflux for 3 h. The reaction mixture was cooled down to room temperature, then to 0 °C. Fmoc-Cl (0.37 g, 1.43 mmol) was dissolved in 5 mL dry DCM and added dropwise to the reaction mixture over 5 min. Finally, DIPEA (0.68 mL, 3.9 mmol) was added, and the mixture was allowed to warm up to room temperature and stir for 3 h. The reaction was quenched with 20 mL of 1 M HCl, and the aqueous layer was extracted with EtOAc (2 × 20 mL). The organic layer was dried over $Na_2SO_4$, filtered, and concentrated *in vacuo*. The product was purified by flash chromatography (silica gel, 40% EtOAc in hexanes 0.1% AcOH), yielding **49** (0.45 g, 87%) as a white solid. ($R_f$ =0.53 on $SiO_2$, 9:1 EtOAc:MeOH 0.1% AcOH); $[\alpha]_D^{26}$ 2.34 (c 0.36 $CH_2Cl_2$); IR ($CH_2Cl_2$ cast) 3398, 3334, 3066, 3050, 3019, 2941, 2878, 2098, 1715, 1510, 1478, 1451, 1262, 1088 $cm^{-1}$; $^1H$ ($CDCl_3$, 600 MHz): $\delta$ 7.77 (d, J = 7.8 Hz, 2H, Ar-H), 7.59 (d, J = 6.6 Hz, 2H, Ar-H), 7.41 (dt, J = 7.2, 3.0 Hz, 2H, Ar-H), 7.32 (dt, J = 7.8, 1.2 Hz, 2H, Ar-H), 5.54 (br s, 1H, Fmoc-NH), 4.42 (d, J = 7.2 Hz, 2H, Fmoc-$CH_2$), 4.21 (t, J = 7.2 Hz, 1H, Fmoc-CH), 3.34 – 3.20 (m, 2H, -$CH_2N_3$), 2.28 – 2.18 (m, 1H Orn-$CH_2\beta$), 2.02 – 1.92 (m, 1H, Orn-$CH_2\beta$), 1.61 (s , 3H, -$CH_3$), 1.50 – 1.40 (m, 1H, Orn-$CH_2\gamma$), 1.38 – 1.26 (m, 1H Orn-$CH_2\gamma$); $^{13}C$ ($CDCl_3$, 175 MHz): $\delta$ 177.1, 155.4, 143.9, 127.9, 127.2, 125.1, 120.2, 66.6, 59.6, 51.2, 47.4, 47.2, 33.6, 23.8, 23.7; HRMS (ESI) Calculated for $C_{21}H_{21}N_4O_4$ 393.1568, found 383.1558 $[M-H]^-$.

### 5.4.3.4 Synthesis of (*S*)-2-((((9H-fluoren-9-yl)methoxy)carbonyl)amino)-5-(2,3-bis(tertbutoxycarbonyl)guanidino)-2-methylpentanoic acid (50)

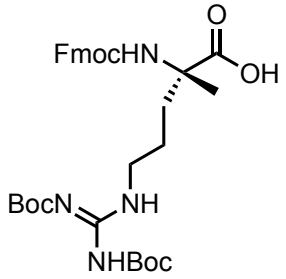


This reaction was adapted from a literature procedure.[263] Amino acid **49** (0.31 g, 0.77 mmol) was dissolved in 15 mL of dry DCM and 10% Pd/C (0.03 g) was added. The suspension was stirred under $H_2$ gas for 18 h, filtered through a pad of celite and concentrated *in vacuo*. The crude mixture was dissolved in 20 mL of dry DCM and TMSCl (0.29 mL, 2.31 mmol) was added and heated at reflux for 3 h. The reaction mixture was cooled down to room temperature, then to 0 °C, then $Et_3N$ (0.32 mL, 2.31 mmol) and *N*,*N*'-di-Boc-*N*''-guanidine triflate (0.33 g, 0.85 mmol) were added. The reaction was left to warm up to room temperature and stir overnight. The mixture was diluted with 20 mL of DCM and then washed with 1 M HCl (3 × 20 mL). The organic layer was dried over $Na_2SO_4$, filtered, concentrated *in vacuo,* and purified using flash chromatography (silica gel, 10-50% acetone in $CH_2Cl_2$ gradient), yielding **50** (0.26 g, 55%) as a white solid. ($R_f$ =0.41 on $SiO_2$, 1:1 $CH_2Cl_2$:acetone); $[\alpha]_D^{26}$ 10.2 (c 0.44 $CH_2Cl_2$); IR ($CH_2Cl_2$ cast) 3408, 3325, 3161, 3067, 3050, 3008, 2981, 2937, 1721, 1641, 1617, 1503, 1478, 1451, 1368, 1331, 1138 $cm^{-1}$; $^1H$ ($CDCl_3$, 600 MHz): $\delta$ 8.41 (br s, 1H, Arg-NH), 7.76 (d, J = 7.2 Hz, 2H, Ar-H), 7.60 (d, J = 7.2 Hz, 2H, Ar-H), 7.39 (t, J = 7.2 Hz, 2H, Ar-H), 7.31 (dt, J = 7.2, 1.2 Hz, 2H, Ar-H), 5.87 (br s, 1H, Fmoc-NH), 4.48 – 4.32 (m, 2H, Fmoc-$CH_2$), 4.23 (t, J = 6.6 Hz, 1H, Fmoc- CH), 3.42 – 3.26 (m, 2H, Arg-$CH_2\delta$), 2.48 – 2.28 (m, 1H, Arg-$CH_2\beta$), 1.92 – 1.80 (m, 1H, Arg-$CH_2$), 1.62 (s, 3H, Arg-$CH_3$), 1.58 – 1.44 (m, 20H, 2 x –$C(CH_3)_3$, Arg-$CH_2\delta$); $^{13}C$ ($CDCl_3$, 175 MHz): 177.5, 166.2,

156.1, 155.9, 153.3, 144.1, 144.0, 141.5, 127.8, 127.2, 120.1, 83.6, 79.3, 66.5, 53.9, 47.4, 40.9, 29.4, 28.4, 28.2, 24.2, 23.7; HRMS (ESI) Calculated for $C_{32}H_{41}N_4O_8$ 610.3003, found 610.3004 $[M-H]^-$.

## 5.5 Procedures for the Pharmacokinetics Studies and Development of Oral Apelin

### 5.5.1 *In Vivo* Canine Plasma Stability Assays

All experiments were performed by Dr. Oudit's lab, with experimental discussions and advice with our lab. Three dogs were given 0.5 $\mu$mol/kg of apelin analogue **13** intravenously. The canine blood was extracted at 0, 15, 30, and 60 min and then analyzed using LCMS quantification, where the ratio of apelin peptide to the internal standard was calculated based on the area under the curve. The 0 h incubation ratio was used to compare the apelin peptide/internal standard ratios for the time experiments.

### 5.5.2 *In vitro* Metabolic Enzyme Plasma Stability Assays

Quantification of peptides in plasma were adapted from a published protocol.[258] Briefly, 20 $\mu$L of 1 mM of enzyme (elastase, carboxypeptidase A, trypsin, or chymotrypsin) was pre-portioned into microcentrifuge tubes and incubated at 37 °C for 20 min. Next, 5 $\mu$L of apelin peptide (1 mM) was added to each 20 $\mu$L enzyme aliquot, and then subsequently incubated at 37 °C at varying time points (t = 0, 1, 2, 4, 6, 24 h). The reaction solution was then quenched with 25 $\mu$L 6 M GuHCl and 300 $\mu$L 80% ACN/$H_2O$, 5 $\mu$L of internal standard (1 mM Dans-G) was added. The plasma sample was vortexed prior to centrifugation at 13.2 rpm for 5 min. The supernatant was transferred to a microcentrifuge tube and evaporated. The dried samples were then reconstituted with 150 $\mu$L 0.1% aqueous acetic acid (v/v) and loaded onto a pre-equilibrated $C_{18}$ spin column, which had been previously wetted with 2 × 150 $\mu$L 30% acetonitrile in 0.1 % aqueous TFA and 2 × 150 $\mu$L 0.1% aqueous acetic acid (v/v), centrifuging at 2.8 rpm for 2 min between each 150 $\mu$L aliquot. The resultant filtrate was reloaded onto the column along with 150 $\mu$L 0.1%

aqueous acetic acid (v/v) and centrifuged at 2.8 rpm for another 2 min; the filtrate was then discarded. The loaded peptide was washed with 2 × 150 $\mu$L 5 % MeOH in 1% aqueous acetic acid (v/v) and eluted from the column using 100 $\mu$L 60% MeOH in 10% aqueous acetic acid (v/v). The eluate was injected and analyzed using LCMS quantification, where the ratio of apelin peptide to the internal standard was calculated based on the area under the curve. The 0 h incubation ratio was used to compare the apelin peptide/internal standard ratios for the time experiments.

### 5.5.3 Synthesis of Chitosan-Cyclodextrin-Derived Hydrogel (53)

#### 5.5.3.1 Synthesis of CMC (51)

Compound **51** was synthesized as previously described.[16,111] Chitosan (10.40 g, 57 mmol for the monomer unit) was added to 100 mL of 4:1 isopropyl alcohol and 40% aqueous NaOH (v/v) solution and stirred using a Teflon impeller at 300 rpm at 25 ℃ for 1 h. Monochloroacetic acid (15.00 g, 170 mmol), dissolved in 20 mL of isopropyl alcohol, was added to the suspension in five equal portions over a period of 20 min. The mixture was heated at 50 ℃ and stirred for another 5 h. The reaction mixture was subsequently neutralized with 4 M HCl and filtered to remove any undissolved residue. The resulting CMC was precipitated with methanol. The precipitate was washed with 3 × 100 mL of 1:1 MeOH:$H_2O$ and dried under vacuum at 40 ℃ overnight affording **51** (9.13 g) as an off-white powder.

#### 5.5.3.1 Synthesis of CMCD (52)

Compound **52** was synthesized as previously described.[16,111] Monochloroacetic acid (3.80 g, 40 mM final concentration) was dissolved in 80 mL of 40% aqueous NaOH, and $\beta$-cyclodextrin

(22.80 g, 20 mmol) was then added. The reaction mixture was then heated to 50 °C and stirred for 5 h. Subsequently, the reaction mixture was neutralized with 4 M aqueous HCl and the obtained product was precipitated by the addition of an excess amount of methanol. The precipitate was washed with 3 × 100 mL of 1:1 MeOH:$H_2O$ and dried under reduced pressure at 40 °C overnight, affording **52** (8.32 g) as a white solid.

#### 5.5.3.3 Synthesis of CMCD-*g*-CMC (53)

Compound **53** was synthesized as previously described.[16,111] CMC **51** (4.00 g, 17 mmol for the anhydroglucose unit) and CMCD **52** (4.00 g, 3.3 mmol) were dissolved in 100 mL of distilled water containing 1-ethyl-3-[3-(dimethylamino)propyl]carbodiimide hydrochloride (3.68 g, 19.2 mmol) and *N*-hydroxysuccinimide (2.21 g, 19.2 mmol). The reaction was carried out at 25 °C for 24 h under continuous stirring with a Teflon impeller at 300 rpm. The highly viscous solution obtained was precipitated with methanol and the resulting precipitate was filtered. The obtained precipitate was swollen with distilled water and the resulting hydrogel was dialyzed against deionized water using dialysis tubing (2 kDa cut-off) for 3 d. The dialyzed hydrogel was precipitated with excess methanol and then dried under reduced pressure at 40 °C overnight, affording **53** (2.41 g) as a white granular hydrogel.

## 5.6 Procedures for the Investigation of Retro-Enantio Peptides

### 5.6.1 *In vitro* Human and Mice Plasma Stability Assays

Quantification of peptides in plasma was adapted from a published protocol.[261] Briefly, 20 $\mu$L of plasma (human or mice) was pre-portioned into microcentrifuge tubes and incubated at 37 °C for 20 min. Next, 5 $\mu$L of apelin peptide (1 mM) was added to each 20 $\mu$L plasma sample, and then subsequently incubated at 37 °C at varying time points (t = 0, 1, 2, 4, 6, 24 h). The reaction solution was then quenched with 25 $\mu$L 6 M GuHCl and 300 $\mu$L 80% ACN/$H_2O$, 5 $\mu$L of internal standard (1 mM Dans-G) was added. The plasma sample was vortexed prior to centrifugation at 13.2 rpm for 10 min. The supernatant was transferred to a 1 mL microcentrifuge tube and evaporated. The dried samples were then reconstituted with 100 $\mu$L 0.1% aqueous acetic acid (v/v) and loaded onto a pre-equilibrated $C_{18}$ spin column, which had been previously wetted with 2 × 100 $\mu$L 30% acetonitrile in 0.1 % aqueous TFA and 2 × 100 $\mu$L 0.1% aqueous acetic acid (v/v), centrifuging at 2.8 rpm for 2 min between every 100 $\mu$L aliquots. The resultant filtrate was reloaded onto the column along with 100 $\mu$L 0.1% aqueous acetic acid (v/v) and centrifuged at 2.8 rpm for another 2 min and the filtrate was discarded. The loaded peptide was washed with 2 × 100 $\mu$L 5% MeOH in 1 % aqueous acetic acid (v/v) and eluted from the column using 100 $\mu$L 60% MeOH in 10% aqueous acetic acid (v/v). The eluate was injected and analyzed using LCMS quantification, where the ratio of apelin peptide to the internal standard was calculated based on the area under the curve. The 0 h incubation ratio was used to compare the apelin peptide/internal standard ratios for the time experiments.

### 5.6.2 Synthesis of Retro-Enantio Apelin Analogues (54-57)

#### 5.6.2.1 Synthesis of REA13 (54)

Fmoc-D-Gln(Trt)-OH was loaded onto 2-chlorotrityl chloride resin using the general resin loading procedure at 0.8 mmol/g loading scale. Resin-bound Fmoc-D-Gln(Trt)-OH was then subject to manual SPPS (general method) introducing amino acids in the following order: Fmoc-D-Arg(Pbf)-OH, Fmoc-D-Pro-OH, Fmoc-d-Arg(Pbf)-OH, Fmoc-D-Leu-OH, Fmoc-D-Ser(*t*Bu)-OH, Fmoc-D-His(Trt)-OH, Fmoc-D-Lys(Boc)-OH, Fmoc-Gly-OH, Fmoc-D-Pro-OH, Fmoc-D-Met-OH, Fmoc-D-Pro-OH, and Fmoc-D-Phe-OH, with end-capping after each step. After the final *N*-terminal deprotection, the peptide was then cleaved from the resin and purified using the HPLC general method and an Agilent $C_{18}$ RP-HPLC column (100 Å, 5 $\mu$m, 250 mm, 4.6 mm). The desired peptide was isolated as a white solid after lyophilization (6 mg, 12%). Monoisotopic mass calculated for $C_{69}H_{111}N_{23}O_{16}S$ 775.9223, found (FTICR-ESI-MS) 775.9216 $[M + 2H]^{2+}$.

#### 5.6.2.2 Synthesis of RE13A2 (55)

Fmoc-D-Gln(Trt)-OH was loaded onto 2-chlorotrityl chloride resin using the general resin loading procedure at 0.8 mmol/g loading scale. Resin-bound Fmoc-D-Gln(Trt)-OH was then subject to manual SPPS (general method) introducing amino acids in the following order: Fmoc-D-Arg(Pbf)-OH, Fmoc-D-Pro-OH, Fmoc-D-Arg(Pbf)-OH, Fmoc-D-Leu-OH, Fmoc-D-Ser(*t*Bu)-OH, Fmoc-D-His(Trt)-OH, Fmoc-D-Lys(Boc)-OH, Fmoc-Gly-OH, Fmoc-D-Pro-OH, Fmoc-D-Met-OH, Fmoc-Aib-OH, and Fmoc-D-BrF-OH, with end-capping after each step. After the final *N*-terminal deprotection, the peptide was then cleaved from the resin and purified using the HPLC general method and an Agilent $C_{18}$ RP-HPLC column (100 Å, 5 $\mu$m, 250 mm, 4.6 mm). The desired

peptide was isolated as a white solid after lyophilization (8 mg, 16%). Monoisotopic mass calculated for $C_{69}H_{112}BrN_{23}O_{16}$ 799.8993, found (FTICR-ESI-MS) 799.8981 $[M + 2H]^{2+}$.

#### 5.6.2.3 Synthesis of REA17 (56)

Fmoc-D-Lys(Boc)-OH was loaded onto 2-chlorotrityl chloride resin using the general resin loading procedure at 0.8 mmol/g loading scale. Resin-bound Fmoc-D-Lys(Boc)-OH was then subject to manual SPPS (general method) introducing amino acids in the following order: Fmoc-D-Phe-OH, Fmoc-D-Arg(Pbf)-OH, Fmoc-D-Arg(Pbf)-OH, Fmoc-D-Gln(Trt)-OH, Fmoc-D-Arg(Pbf)-OH, Fmoc-D-Pro-OH, Fmoc-D-Arg(Pbf)-OH, Fmoc-D-Leu-OH, Fmoc-D-Ser(*t*Bu)-OH, Fmoc-D-His(Trt)-OH, Fmoc-D-Lys(Boc)-OH, Fmoc-Gly-OH, Fmoc-D-Pro-OH, Fmoc-D-Met-OH, Fmoc-D-Pro-OH, and Fmoc-D-Phe-OH, with end-capping after each step. After the final *N*-terminal deprotection, the peptide was then cleaved from the resin and purified using the HPLC general method and an Agilent $C_{18}$ RP-HPLC column (100 Å, 5 $\mu$m, 250 mm, 4.6 mm). The desired peptide was isolated as a white solid after lyophilization (15 mg, 30%). Monoisotopic mass calculated for $C_{96}H_{156}N_{34}O_{20}S$ 1069.6051, found (FTICR-ESI-MS) 1069.605 $[M + 2H]^{2+}$.

#### 5.6.2.4 Synthesis of RE17A2 (57)

Fmoc-D-Lys(Boc)-OH was loaded onto 2-chlorotrityl chloride resin using the general resin loading procedure at 0.8 mmol/g loading scale. Resin-bound Fmoc-D-Lys(Boc)-OH was then subject to manual SPPS (general method) introducing amino acids in the following order: Fmoc-D-Phe-OH, Fmoc-D-Arg(Pbf)-OH, Fmoc-D-Arg(Pbf)-OH, Fmoc-D-Gln(Trt)-OH, Fmoc-D-Arg(Pbf)-OH, Fmoc-D-Pro-OH, Fmoc-D-Arg(Pbf)-OH, Fmoc-D-Leu-OH, Fmoc-D-Ser(*t*Bu)-OH, Fmoc-D-His(Trt)-OH, Fmoc-D-Lys(Boc)-OH, Fmoc-Gly-OH, Fmoc-D-Pro-OH, Fmoc-D-Nle-OH,

Fmoc-Aib-OH, and Fmoc-D-BrF-OH, with end-capping after each step. After the final *N*-terminal deprotection, the peptide was then cleaved from the resin and purified using the HPLC general method and an Agilent $C_{18}$ RP-HPLC column (100 Å, 5 $\mu$m, 250 mm, 4.6 mm). The desired peptide was isolated as a white solid after lyophilization (12 mg, 24%). Monoisotopic mass calculated for $C_{96}H_{157}BrN_{34}O_{20}$ 1093.5821, found (FTICR-ESI-MS) 1093.5839 $[M + 2H]^{2+}$.

## 5.7 Experimental Procedures for the Role of *Bacillus* Strains in *Daqu* Fermentation

### 5.7.1 Strains Used and Preparation of Inocula

All experiments were performed by Dr. Gänzle's lab, with experimental discussions and advice from our lab. The strains used, their origin, and growth conditions, are listed in Table 10. Lysogeny broth (LB) (SigmaAldrich, ON, Canada) was inoculated with a single colony of *Bacillus amyloliquefaciens* Fad We, *Bacillus amyloliquefaciens* Fad 82, *Bacillus velezensis* FUA2155, or *Kosakonia cowanii* FUA10121 and incubated at 37 °C at 200 rpm agitation. *Weissella cibaria* FUA3456 cultures were prepared in a similar manner but grown in modified MRS (mMRS) broth[264] at 30 °C for 2 d without agitation. Spore suspensions of the following fungal strains, *Aspergillus niger* FUA5001, *Aspergillus clavatus* FUA5004, *Aspergillus clavatus* FUA5005, *Mucor racemosus* FUA5009, and *Penicillium roqueforti* FUA5012, were prepared with malt extract agar (MEA, SigmaAldrich, ON, Canada) plates at 25 °C for 7 d.[265] The conidia were harvested from the MEA plates by adding 10 mL of sterile distilled water and collecting the fungal biomass with an L-shaped cell spreader (Fisher Scientific, ON, Canada). The spore suspensions were filtered to separate mycelial cells, and the spores were harvested *via* centrifugation. The spores were quantified using a haemocytometer (Fein-Optik, Jena, Germany). Inocula of *Saccharomyces cerevisiae* FUA4002, *Saccharomycopsis fibuligera* FUA4036, and *Pichia kudriavzevii* FUA4039, were prepared using malt extract broth (MEB, SigmaAldrich, ON, Canada), using single colonies, and incubated at 30 °C for 2 d, where the cell counts were determined with a haemocytometer.

**Table 10** Bacterial, fungal, and yeast strains used in this study. FUA = Food microbiology culture collection at the University of Alberta. LB = liquid broth. mMRS = modified MRS broth. MEA = malt extract agar. MIC = minimum inhibitory concentration.

| | **Strains and origin** | **Incubation conditions** | **Purpose in this study** |
|---|---|---|---|
| *Bacillus amyloliquefaciens* | Fad We, ropy bread | 37 ℃, LB | Simplified and complex *daqu* fermentation |
| *B. amyloliquefaciens* | Fad 82, ropy bread | 37 ℃, LB | Simplified and complex *daqu* fermentation |
| *B. velezensis* | FUA2155[a], *daqu* | 37 ℃, LB | Simplified and complex *daqu* fermentation |
| *Kosakonia cowanii* | FUA10121, *daqu* | 37 ℃, LB | Complex *daqu* fermentation |
| *Weissella cibaria* | FUA3456, sourdough | 30 ℃, mMRS | Complex *daqu* fermentation |
| *Saccharomyces cerevisiae* | FUA4002, sourdough | 30 ℃, MEA | Complex *daqu* fermentation and MIC test |
| *Saccharomycopsis fibuligera* | FUA4036, *daqu* starter | 30 ℃, MEA | Complex *daqu* fermentation and MIC test |
| *Pichia kudriavzevii* | FUA4039, *daqu* starter | 30 ℃, MEA | Complex *daqu* fermentation and MIC test |
| *Aspergillus niger* | FUA5001 | 25 ℃, MEA | Complex *daqu* fermentation and MIC test |
| *Mucor racemosus* | FUA5009 | 25 ℃, MEA | Complex *daqu* fermentation and MIC test |
| *Penicillium roqueforti* | FUA5012 | 25 ℃, MEA | Complex *daqu* fermentation and MIC test |
| *A. clavatus* | FUA5004 | 25 ℃, MEA | MIC test |
| *A. clavatus* | FUA5005 | 25 ℃, MEA | MIC test |

### 5.7.2 *In silico* Prediction of Lipopeptides Produced by *Bacillus* Spp.

All experiments were performed by Dr. Gänzle's lab. Biosynthetic gene clusters responsible for antimicrobial secondary metabolites were identified using the genome sequences of *Bacillus* strains[266] using the bacterial version of antiSMASH.[267] Gene clusters encoding different lipopeptides in the genomes of *B. amyloliquefaciens* Fad We, *B. amyloliquefaciens* Fad 82, and *B. velezensis* FUA2155, were identified and verified by BLAST in NCBI. All gene clusters identified by antiSMASH were used as query sequences for BLASTn against the NCBI nucleotide database.

### 5.7.3 Extraction and Purification of Antifungal Lipopeptides from LB Cultures

All experiments were performed by Dr. Gänzle's lab, with experimental discussions and advice from our lab. The antifungal lipopeptides produced by *B. amyloliquefaciens* Fad We, *B. amyloliquefaciens* Fad 82, and *B. velezensis* FUA2155 were extracted from 150 mL of the stationary phase cultures in LB broth.[268] The cultures were incubated at 37 °C and shaken at 200 rpm for 3 d, and the cells were removed *via* centrifugation at 12,000 × *g* for 20 min. The pH of the supernatants was adjusted to 2 with 6 M HCl, then incubated again at 4 °C overnight. The solid crude lipopeptides were collected *via* centrifugation at 12,000 × *g* for 20 min, and the precipitate was extracted with methanol. The organic solvent was evaporated *in vacuo* at 50 °C. The extracted peptides were dissolved in 1 mL methanol and filtered through 0.45 $\mu$m filters to remove the solids.

### 5.7.4 Minimum Inhibitory Concentration Assay

All experiments were performed by Dr. Gänzle's lab. Critical dilution assays were performed to determine the minimum inhibitory concentration (MIC) of fengycin and iturin A

(Sigma-Aldrich, Oakville, Canada), and surfactin (MedChemExpress, Monmout Junction, USA). The indicator strains are listed here: the mycelial fungi *A. niger* FUA5001, *A. clavatus* FUA5004, *A. clavatus* FUA5005, *M. racemosus* FUA5009, *P. roqueforti* FUA5012, and the yeasts, *S. cerevisiae* FUA4002, *S. fibuligera* FUA4036 and *P. kudriavzevii* FUA4039. Inocula were prepared as described above, and the growth was visually observed, and MIC values recorded one day after visible growth. MIC values were determined in three independent experiments of replication preparations of the conidiospores. Fengycin, iturin A, and surfactin were dissolved in DMSO to 5 g/L stock solutions. Each individual experiment mixed MEB (for fungi) or mMRS broth (for yeasts) with 90 $\mu$L of fengycin, iturin, and surfactin in 96-well microtiter plates, then serially-diluted 2-fold to cover the concentration range of 2.5 g/L to 2.5 mg/L. Each well was inoculated with 10 $\mu$L of $10^6$ CFU/mL. Control cells contained the inocula grown on distilled water in the absence of the lipopeptide solutions.

### 5.7.5 Preparation of Simplified *Daqu* Model

All experiments were performed by Dr. Gänzle's lab. Production of antifungal peptides by three *Bacillus* strains (*B. amyloliquefaciens* Fad We, *B. amyloliquefaciens* Fad 82, and *B. velezensis* FUA2155) was initially assessed in simplified *daqu* inoculated with only one *Bacillus* strain. 100 mL LB broth was inoculated with single colonies of the three *Bacillus* strains and shaken at 200 rpm and incubated at 37 °C for 24 h. Cells were harvested by centrifugation and resuspended in sterile water to obtain a $10^9$ to $10^{10}$ CFU/mL cell count, and 1 mL of this inoculum was mixed with 60 g wheat flour and 30 mL sterile tap water in a sterile plastic bag to give a final cell count of $10^7$ to $10^8$ CFU/g and a 35 % water content. Control inocula were prepared without inoculation of the *Bacillus* strains. The *daqu* samples were manually pressed and shaped in Petri

dishes and incubated at the following stages and conditions for medium-temperature *daqu*[134]: shaping stage, 30 ℃, relative humidity (Rh) 95 %, 1 d; ripening stage, 37 ℃, Rh 95 %, 2 d; high-temperature stage, 55 ℃, Rh 90 %, 7 d; and maturation stage, 37 ℃, Rh 75 % for 6 d. Samples were incubated in sealed containers and the Rh was controlled with the following salt solutions: $K_2SO_4$, Rh 95%; $KNO_3$, Rh 90%; NaCl, Rh 75%. The microbial population remained stable and the *daqu* samples were dry after the high-temperature stage, therefore, incubation was completed on day 16.

### 5.7.6 Determination of pH and Total Bacterial Cell Counts of Simplified *Daqu* Model, and Observation of Mould Growth

All experiments were performed by Dr. Gänzle's lab. 0.5 g *daqu* samples were collected and diluted 10-fold with sterile 18 MΩ water, and further diluted with peptone water, then plated on LB agar. The pH of the first dilution was measured with a glass electrode. The LB agar plates were incubated at 37 ℃ for 24 h and counted for the total number of colonies per plate; differential cell counts of *Bacillus* species were done based on the colony morphology. Fungal growth was indicated as follows: —, no visible mycelial growth; +, small spots of mycelial growth; + +, spots of mycelial growth and conidia, + + +, 25-50% of the surface covered by mycelia; and + + + +, >50% of the surface covered by mycelia.

### 5.7.7 Quantification of Expression of Genes Encoding for the Biosynthesis of Target Antifungal Lipopeptides in the Simplified *Daqu* Model, Through Reverse Transcription Quantitative PCR (RT-qPCR)

All experiments were performed by Dr. Gänzle's lab. 0.5 g *daqu* samples were mixed with 3 mL RNAprotect Bacteria Reagent (Qiagen, Germantown, USA) and incubated for 10 min. The mixture was centrifuged at 500 × *g* for 10 min, and the cells were harvested. The RNA was isolated from the cell pellets using TRIzol LS reagent based on the manufacturer's instructions (ThermoFisher Scientific, Waltham, USA). DNase treatment with RQ1 RNase-Free DNase (Fisher Scientific) was used to digest contaminant genomic DNA, and cDNA libraries were generated by reverse transcription using the QuantiTect Reverse Transcription Kit (Qiagen). The *fenA, ituA,* and *sefAA* genes, encoding the NRPS subunits of fengycin, iturin A, and surfactin, were used to quantify the expression of genes that encode the lipopeptides. The single-copy gene *gyB*, which encodes for the DNA gyrase subunit B, was used as the housekeeping gene for the relative quantification. Gene expression was measured by QuantiFast SYBR Green PCR Kit Qiagen) and reverse-transcriptase qPCR (7500 Fast, Applied Biosystems, Foster City, CA). Reference conditions included cells exponentially growing in LB broth ($OD_{600nm}$ 0.8). Negative controls include a no-template control and DNase-treated RNA. Gene expression was calculated and $\log_2$ transformed. Significant differences were assessed with a *t*-test and an error probability of 5% ($P < 0.05$). Data are represented as mean ± standard deviation of three independent fermentations.

### 5.7.8 Preparation of Complex Model of *Daqu* Fermentation

All experiments were performed by Dr. Gänzle's lab. A complex *daqu* model was prepared to further study the role of antifungal peptides produced by *Bacillus* spp. in *daqu*. This consisted of the inclusion of one representative of major groups of fermentation organisms. In addition to the *Bacillus* strains, *A. niger* FUA5001, *M. racemosus* FUA5009, *P. roqueforti* FUA5012, *S. cerevisiae* FUA4002, *S. fibuligera* FUA4036, and *P. kudriavzevii* FUA4039 were added to give a

final concentration of $10^5$ CFU/g, each. Furthermore, cell suspensions of *K. cowani*i FUA10121 and W. c*ibaria* FUA3456 were added to give a final cell count of $10^6$ CFU/g, each. The complex *daqu* samples were incubated at the same conditions described above for the simplified *daqu* model.

### 5.7.9 Extraction and Purification of Lipopeptides from the Complex *Daqu* Model

All experiments were performed by Dr. Gänzle's lab, with experimental discussions and advice from our lab. *Daqu* samples were obtained on incubation days 1, 3, 6, 10, and 16, to monitor the production of antifungal lipopeptides in the complex *daqu* model. The extraction procedure for the lipopeptides was similar, as described previously for extraction from LB cultures, but with an additional homogenization step. Approximately 8.5 g of the *daqu* samples were homogenized in 50 mL distilled water by stomaching for 5 min, and the samples were centrifuged at 12,000 × *g* for 20 min to remove the solids. The complex *daqu* samples were processed using the same procedure as the LB cultures.

### 5.7.10 Measurement of Antifungal Activity of Lipopeptides Produced by *Bacillus* Spp. in the Complex *Daqu* Model

All experiments were performed by Dr. Gänzle's lab, with experimental discussions and advice from our lab. Using *A. niger* FUA5001 as the indicator strain, methanol *daqu* extracts were used to determine the production of antifungal lipopeptides in the complex *daqu* model. Serial 2-fold dilutions of the peptide extracts and MEB were prepared in 96-well microtiter plates and inoculated with 10 $\mu$L of *A. niger* FUA5001 conidial suspension to give a final cell concentration

of $10^6$ CFU/mL. The plates were incubated at 25 ℃ for 5 d and fungal growth was observed visually.

### 5.7.11 Mass Spectral Analysis of LB and Complex *Daqu* Model Extracts

To qualitatively identify the antifungal lipopeptides produced by *B. amyloliquefaciens* Fad We, *B. amyloliquefaciens* Fad 82, and *B. velezensis* FUA2155, each sample was analysed by reverse phase-high performance liquid chromatography coupled to mass spectrometry (RP-HPLC-MS). Analysis was performed using an Agilent 1200 SL HPLC System with a Phenomenex Aeris XB-C8 column (Phenomenex, Torrance, USA). 3.6 $\mu$m, 100 Å, 50 × 2.1 mm with a guard thermostated at 35 ℃. An eluent gradient composed of 0.1% formic acid in water (mobile phase A) and 0.1% formic acid in acetonitrile (mobile phase B) was used. A 2 $\mu$L aliquot was loaded onto the column, at a flow rate of 0.45 mL/min and an initial buffer composition of 95% mobile phase A and 5% mobile phase B for 0.5 min, to effectively remove the salts. The elution of the lipopeptides was performed using a linear gradient from 5% to 65% mobile phase B for 4.8 min, 65%–95% mobile phase B for 1.0 min, 9 5% mobile phase B for 0.8 min, then back to the initial eluent conditions in 0.5 min. Mass signatures were acquired in a positive mode of ionization using an Agilent 6220 Accurate-Mass TOF HPLC/MS system (Santa Clara, CA, USA), equipped with a dual sprayer electrospray ionization source; the second sprayer providing a reference mass solution. Each individual spectrum was mass-corrected using peaks at *m/z* 121.0509 and 922.0098 from the reference solution. The conditions for mass spectrometry are as stated: drying gas 10 L/min at 350 ℃, nebulizer at 30 psi, a mass range of 100–3200 Da, an acquisition rate of ~1.03 spectra/sec, a fragmentor voltage at 175 V, a skimmer voltage at 65 V, a capillary voltage at 4000

V, and an instrument state 2 GHz High Dynamic Range. Mass spectral analysis was performed using the Agilent MassHunter Qualitative Analysis software package version B.07.00 SP2.

## 5.8 Experimental Procedures for the Greenhouse and Field Studies of *Beauveria bassiana* against MPB populations.

### 5.8.1 *Beauveria bassiana* Strains and Cultivation

Five *Beauveria bassiana* strains were obtained from various culture collections: UAMH 299, UAMH 4510, and UAMH 1076 from the UAMH Centre for Global Microfungal Biodiversity (University of Toronto, Toronto, ON, Canada), ANT-03 from Anatis Bioprotection (Laval, QC, Canada), and 110.25 from the CBS Culture Collection (Delft, Netherlands). All strains were grown on Czapex Dox agar yeast extract (CDAYE) and incubated at 28 °C for 14-21 days. The conidial biomass was harvested with a Drigalski spatula and resuspended in 0.1% Tween 80 for further biological assays and culture propagation, or for long-term storage at -20 °C.

### 5.8.2 Production of *B. bassiana* Conidia *via* Biphasic Liquid-Solid State Fermentation

In order to perform large-scale greenhouse and field infection bioassays, a conidial powder with long-term viability and a high conidial effective dose was developed (**Fig. 50**). This prompted us to use a biphasic liquid-solid fermentation approach using fungal broth and parboiled rice substrate.[225] *B. bassiana* strains UAMH 299 and 1076, the red-pigmented isolates, were selected because they showed robust UV resistance, provided the fastest lethal time against MPB, yielded high conidial spores, and are easily harvested from solid fermentation substrates.[210]

Conidia were harvested from 21 day-old CDAYE-grown conidial inoculums using a Drigalski spatula. The harvested conidia were titered to $1.0 \times 10^{-8}$ conidia/mL using a haemocytometer. Subsequently, the titered conidia were used to inoculate a 100 mL of liquid

Czapex Dox Yeast Extract Broth medium (CDBYE) to give a final concentration of $1.0 \times 10^{-7}$ and incubated at 28 ℃ for 72-96 h at 175 rpm. Commercially available parboiled rice (Grace Kennedy Inc., Walmart, Canada) was dry sterilized at 121 ℃ for 20 min, and the cooled sterile rice was aseptically cooked with equal volume (1 g/mL) of sterile 10% yeast water in a microwave for 8 min until all the liquid had evaporated. Next, 100 mL of the 72 h-grown dense mycelial liquid inoculum was mixed with 1,000 g of room-temperature cooked parboiled rice. 150 µg/mL or µg/g of chloramphenicol was added to each liquid-solid substrate to limit bacterial growth throughout the fermentation. The homogenized mixture (one-inch depth) was grown in sterile aluminum pans and incubated at 28 ℃, 70% relative humidity under a 12/12 h (L/D, light/dark) cycle for 10 d.

The parboiled rice-mycelial cake was visually inspected every three days for pigmentation and non-white conidiation. Subsamples were obtained and assessed for axenic status by spread-plating randomized collected samples. The subsamples were cored using a sterile metal spatula and then serially diluted, ten-fold, using a 0.05% Tween 80 diluent. A 100 µL aliquot was spread-plated, done in triplicates, on CDAYE media amended with or without 150 µg/mL chloramphenicol. After incubation at 28 ℃ for 72 h, pre-counting of fungal microcolonies was performed, and after 10 d of incubation, the red pigment-producing *B. bassiana* colony was verified.

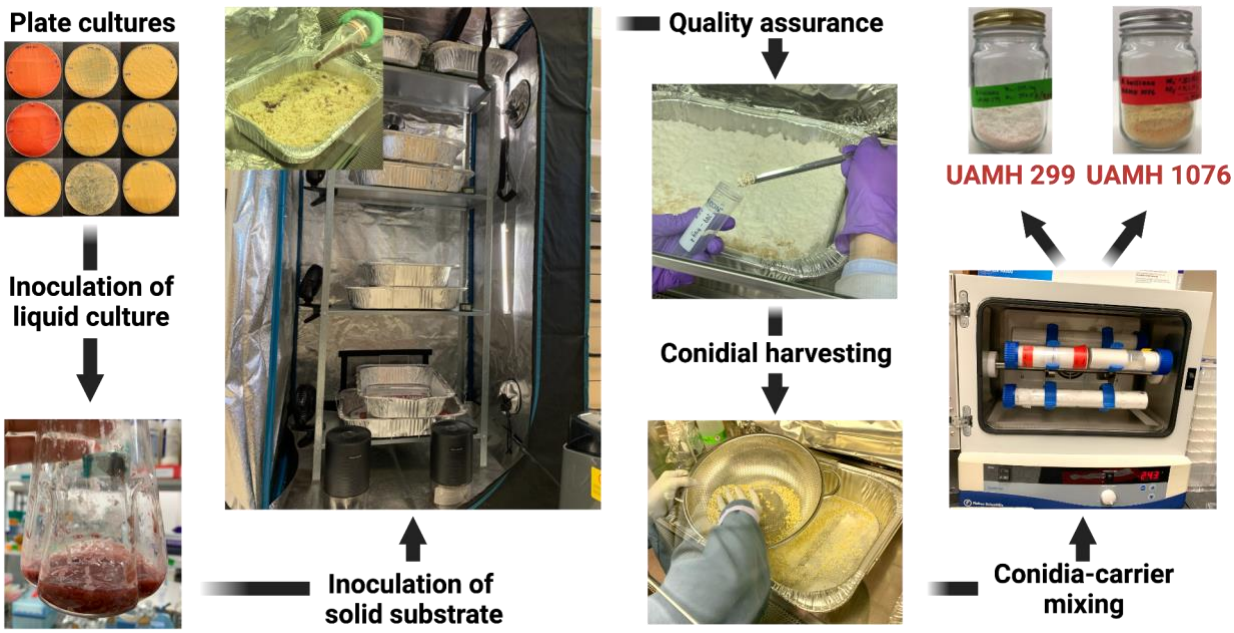


**Fig. 50** Workflow of the liquid-solid fermentation approach for the large-scale production of *Beauveria bassiana* conidial biomass.

### 5.8.3 *B. bassiana* Conidia Drying and Harvesting

A two-stage drying process was used to thoroughly dry the conidia for harvest. After 10 d of growth of the mycelial-rice biomass, the relative humidity in the holding fermentation incubator was brought down from 70% to 50% throughout a 5 d span, using a dehumidifier to induce conidiation. The relative humidity was brought down further from 50% to 20% throughout another 5 d span, using a dehumidifier and continuous airflow. The drying of the fungal mycelia was necessary to allow for ease of manual separation of the conidia, as a powder, from the parboiled rice substrate.[225]

Subsequently, the dried *B. bassiana*-parboiled rice cake was processed inside a sterile BioSafety Cabinet model BM4-2A-49 (Caltec Scientific, Calgary, AB, Canada). The rice cakes were manually separated aseptically into individual rice grains. The loosened rice grains were repeatedly pressed against a sterile metal mesh (0.25 $mm^2$), to allow for the conidial powder to be

sieved through. The conidial viability was titered as previously described, and the resulting conidial powder was used for the development of the powder carrier formulation, to be used for long-term storage viability assays, and *in planta* and *in natura* infection experiments.

### 5.8.4 Preparation of *B. bassiana* Powder Formulation

Based on the proprietary powder formulation from Anatis Bioprotection, a dry formulation of kaolin clay-soluble starch-xantham gum-calcium carbonate was made. The harvested UAMH 299 and 1076 conidial powder were diluted to final concentrations of $1.0 \times 10^6$ and $1.0 \times 10^8$ conidia/g. The commercially available BioTitan WP product from Anatis Bioprotection, consisting of the *B. bassiana* strain ANT-03 (www.hc-sc.gc.ca, PMRA Reg. No 31230 and 33923, Agricultural Research Services Patent Collection NNRL 50797), was diluted to give a final concentration of $1.0 \times 10^7$ and $1.0 \times 10^9$ conidia/g.

### 5.8.5 Stability of *B. bassiana* Powder Formulation Under 4 °C Storage Conditions

Five conidial treatments were assessed for *B. bassiana* conidial stability using our carrier powder formulations. Two packages of commercial mycoinsecticide BioTitan WP, with at least $1.0 \times 10^{10}$ conidia/g of the *B. bassiana* ANT-03 strain, were obtained from Anatis Bioprotection. The first package was given in January 2020 (labelled as BioTitan WP (year-old)), and the second package was obtained in January 2021 (labelled as BioTitan WP); both packages were kept at 4 °C storage until processing. In addition, three in-house *B. bassiana* strains (UAMH 299, UAMH 4510, and 110.25), a representative from each of the three morphotypes,[210] were harvested from CDAYE agar media and mixed with the carrier powder formulation using a hybridization oven system model 642 (Thermo Scientific, Dubuque, Iowa, USA), to attain a minimum conidial density

of $1.0 \times 10^7$ conidia/g. All the powder mixtures were stored at 4 °C and aseptically subsampled weekly for four weeks and then after eight weeks. Subsamples (1 g) were collected and serially diluted, tenfold, using 0.05% Tween 80. A 100 µL aliquot of the dilutions was spread-plated in triplicate on CDAYE medium amended with 150 µg/mL chloramphenicol. After incubation at 25 °C for 72 h, pre-counting of fungal microcolonies was performed, and the sporulated *B. bassiana* count was verified after 10 d.

### 5.8.6 Greenhouse *In Planta* Conidial Viability at 25 °C

Four conidial powder formulation treatments were assessed for conidial viability in planta, under greenhouse conditions. The formulations were applied on the surface of 0.4 m lodgepole pine bolts harvested near Whitecourt, AB, Canada, in September 2020. The bolts were incubated in a greenhouse with the following conditions: 26-30% relative humidity, 25 °C temperature, and continuous illumination (30 µmol photons $m^{-2}$ $s^{-1}$). The BioTitan WP high dose ($1.0 \times 10^9$ conidia/$cm^2$) treatments were aseptically sampled weekly for eight weeks and then after three months. The BioTitan WP low dose ($1.0 \times 10^7$ conidia/$cm^2$), UAMH 299 high dose ($1.0 \times 10^8$ conidia/$cm^2$), and UAMH 299 low dose ($1.0 \times 10^6$ conidia/$cm^2$) treatments were subsampled only at the beginning of the incubation period and after eight weeks. Three 1 $cm^2$ areas on the bark were swabbed with a Letheen broth quick swab kit (3M Inc., London, ON, Canada). Both of the high and low doses of UAMH 299 were not considered for further viability tests because the viable and culturable conidial density was below $1.0 \times 10^3$ conidia/$cm^2$ after the eight-week incubation. We opted not to test further into the third month because we saw that on three of our treatments described above, we observed advanced stages of bolt decay (e.g., drying and cracking of the sapwood).

### 5.8.7 Assessment of *B. bassiana*-Associated Mycosis From Emerged MPB

Pine trees, naturally-infested by MPBs, were felled near Whitecourt, AB, Canada, in September 2020, and were cut into 0.4 m subsections, and used to establish the in planta efficacy of the *B. bassiana* powder formulations. Both ends to the bolts were sealed with wax to reduce desiccation and then stored at 4 ℃ for two months to stimulate winter. The bolts were then placed in emergence bins at 25 ℃ for the *in planta* experiments, described below. Emerged mountain pine beetles from these bolts were used to infest healthy bolts in order to provide an F1 generation of MPB.[210] *B. bassiana* strains, UAMH 299 and ANT-03 (BioTitan WP), were tested under greenhouse conditions because of their long-term greenhouse stability and high *in vitro* MPB virulence.[210]

Five bolt treatments (T), performed in three replicates, were prepared and sprayed with different titers (CFU/g = colony forming unit per gram) of the conidial powder formulations: T1 – ANT-03 (BioTitan WP) at $1.0 \times 10^9$ CFU/g, T2 – ANT-03 (BioTitan WP) at $1.0 \times 10^7$ CFU/g, T3 – UAMH 299 at $1.0 \times 10^8$ CFU/g, T4 – UAMH 299 at $1.0 \times 10^6$ CFU/g, and T5 – carrier powder negative control. Each *B. bassiana* powder formulation was sprayed directly on the surface of the respective pine bolts, in a sterile BioSafety Cabinet model MB4-2A-49, using a powder duster application pump (Amazon, Toronto, Canada). The bolts were stored in sealed rearing plastic bins fitted with meshed glass traps for collection of the emerged MPBs. The bins were incubated in the BioTron Facility greenhouse at the University of Alberta, under the following conditions: 25 ℃, 26-30% relative humidity, and continuous illumination (30 μmol photons $m^{-2}$ $s^{-1}$).

The emerged MPBs that reached the glass collection jars through phototropism, dead or alive, were collected and counted daily.[228] All collected MPB from each respective bin were

transferred to a Petri dish lined with a moist Kimwipe and incubated at 25 ℃ until each beetle was dead (lethal time). Once the MPB were dead, the carcasses were transferred to individual cells in a 96-well titer plate, lined with a moist Kimwipe to maintain a constant relative humidity (70%), then incubated at 25 ℃ for 14 d. Collection of emerged MPBs from the greenhouse bins continued for 55 d, and the mean lethal time and corresponding *B. bassiana*-associated mycosis was assessed and reported. In addition, the pine tree bolts were debarked and assessed for *B. bassiana*-associated mycosis.

Three parameters were used to assess the individual wells for *B. bassiana*-associated mycosis. First, the individual MPB was assessed for distinct white and granular conidiation. Second, the mycosed MPB was viewed under a dissecting microscope and analyzed for the characteristic staphylococcal-like arrangement at the conidiophore ends of the *B. bassiana* conidial clusters.[229] Third, we assessed the *B. bassiana* mycelial morphology by swabbing the mycelial biomass with a nichrome wire, and the mycelia were stained with lactophenol blue and viewed under an inverted phase contrast microscope. Lastly, to support the classical Koch's postulate of infection, we used an inoculating needle to touch-point *B. bassiana*-infected MPBs from the debarked pine bolts. The needle was used to spot inoculate CDAYE media amended with 150 μg/mL chloramphenicol. The non-*B. bassiana*-mycosed MPBs were evaluated in the same method.

### 5.8.8 Conidial Viability *In Natura* Semi-Field (Acreage) Conditions

Four conidial treatments were assessed for conidial viability *in natura* semi-field conditions at a private acreage in Strathcona County, AB, Canada. Since the conidial viability of both titers of the UAMH 299 formulation decreased under the viable and effective conidial titre, $1.0 \times 10^3$ conidia/cm$^2$, we opted to substitute this strain with *B. bassiana* UAMH 1076, another strain representative of the red morphotypes. This strain has shown comparable UV light resistance and improved conidial fermentation yield, corroborated by our liquid-solid biphasic fermentation results.[210] The four treatments: BioTitan WP high ($1.0 \times 10^9$ conidia/cm$^2$), BioTitan WP low ($1.0 \times 10^7$ conidia/cm$^2$), UAMH 1076 high ($1.0 \times 10^8$ conidia/cm$^2$) and UAMH 1076 low ($1.0 \times 10^6$ conidia/cm$^2$) doses were subsampled weekly for three weeks. Three 5 cm$^2$ areas on the bark surface were swabbed using a Letheen broth quick swab kit (3M Inc., London, ON, Canada), and the fungal suspension was serially diluted ten-fold using 0.05% Tween 80. A 100 µL aliquot was spread-plated on CDAYE media amended with 150 µg/mL chloramphenicol. These experiments were performed in triplicates. After the three-week incubation, the viable and culturable *B. bassiana* conidial density was below the effective lethal dose, $1.0 \times 10^6$ conidia/cm$^2$. Due to the low conidial density potentially resulting in low infection success,[223] no further testing was performed.

### 5.8.9 BioTitan WP Formulation Efficacy *In Natura*

*In vitro* and *in planta* results showed the robust stability of the BioTitan WP powder formulation, therefore, we wanted to test our hypothesis that the active ingredient, *B. bassiana* ANT-03, is (1) pathogenic and virulence against field populations of MPB in a dynamic forest ecosystem, and (2) can cause sufficient reproductive success to control a local MPB infestation.

Field trials were performed in a lodgepole-dominated forest stand near Hinton, AB, Canada (53°47’03.5”N, 117°03’53.9”W) (Fig. 51). The stand consisted of 60% of lodgepole pines, averaging 138 years old and 34.5 cm DBH (diameter at breast height; 1.3 m), with a mixture of black spruce (*Picea mariana*), white spruce (*Picea glauca*), and trembling aspen (*Populus tremuloides*).

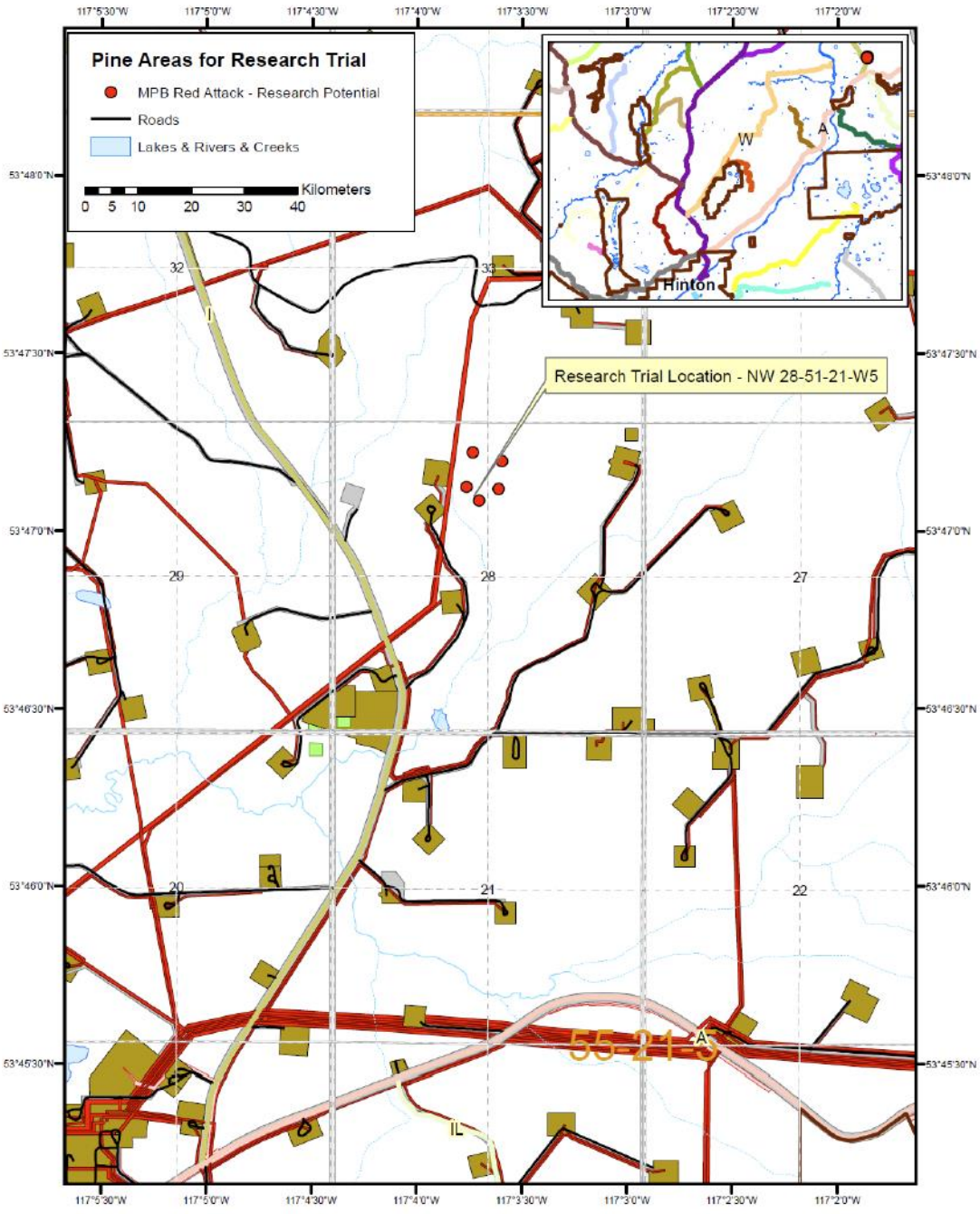


**Fig. 51** Map of research trial site located ~ 55 km NW of Hinton, AB, Canada. BioTitan WP (*Beauveria bassiana* strain ANT-03) powder formulations were manually applied on pine forest stands owned by West Fraser. The present lodgepole pine population represents a 100-year-old pine forest stand. Map provided by West Fraser.

Lodgepole pines that were successfully colonized by MPB (n = 6) and non-infested lodgepole pines (n = 4) were felled and cut into 1.8 m bolts. The bolts were arranged vertically in pairs (one non-infested and one infested) and enclosed in fine-mesh cages (Fig. 52). This enclosure promotes attacks on the non-infested logs by emerging MPBs from the infested logs. A translucent plastic sheet was added on top of the enclosures to mimic the forest canopy and the resulting light penetration. Each pair was considered a replicate. Two potential modes of infection, beetle exit and beetle entry, were developed to assess the capacity for BioTitan WP to kill MPB populations under forest stand conditions. The beetle exit infection mode (designated as "I" for infested) was designed to use MPB-infested bolts that were incubated with an adjacent non-infested bolt. The infested bolts were sprayed with two concentrations of BioTitan WP based on the *in vitro* experiments[210] which resulted in an effective mean lethal time of 3-5 d: high (H; $1.0 \times 10^9$ CFU/cm$^2$) and low (L; $1.0 \times 10^7$ CFU/cm$^2$). This infection mode mimics a scenario where newly emerging MPBs from an infested tree will passively pick up *B. bassiana* conidia as they exit the bolts prior to colonizing a healthy, non-infested tree. The entry infection mode (designated as "N" for non-infested) was designed to use non-infested bolts, sprayed with the two titers of BioTitan WP, incubated with an adjacent MPB-infested bolt. This infection mode mimics a scenario where emerging MPB pick up *B. bassiana* conidia as they colonize a healthy, non-infested tree, testing the potential protective effects of the BioTitan WP formulation.

**Fig. 52** *In natura* field set-up consisting of paired infested (I) and non-infested (N) *Pinus contorta* bolts. The white bolt (front) represents a 1.8-m lodgepole pine section sprayed with the BioTitan WP (*Beauveria bassiana* ANT-03) powder formulation.

## 5.9 Experimental Procedures for the Genomics, Transcriptomics and Exometabolomics Analyses

### 5.9.1 *Beauveria bassiana* Strains and Cultivation

Eight strains of *B. bassiana* were obtained from several culture collections: UAMH 298, UAMH 298-UVR, UAMH 299, UAMH 299-UVR, UAMH 1076, and UAMH 4510 from the UAMH Centre for Global Microfungal Biodiversity (University of Toronto, Toronto, ON, Canada), ANT-03 from Anatis Bioprotection (Laval, WC, Canada), and 110.25 from the CBS Culture Collection (Delft, Netherlands). All strains were grown on Czapek Dox agar yeast extract (CDAYE) and incubated at 28 °C for 14-21 days. The conidial biomass was harvested with a Drigalski spatula and resuspended in 0.01% Tween 80 for culturing for genomic and transcriptomic bioassays.

### 5.9.2 Extraction and Detection of Oosporein From *Beauveria bassiana*

Eight *Beauveria bassiana* strains, with varying pigmentation, were selected and grown to determine the detection limits for oosporein production. The starting fungal inoculum was obtained from frozen mycelial stocks and reactivated using Czapex Dox agar yeast extract (CDAYE) and incubated at 25 °C for 4-6 weeks, or until the conidial lawn is at its maximum. The conidia was harvested, titered, and then used to inoculate a 25 mL Czapex Dox broth yeast extract (CDBYE) to give a final concentration of 1.0 $\times$g $10^7$ conidia/mL and then incubated at 28 °C for 72-96 h and shaken at 175 rpm. After incubation, a 1 mL aliquot was used to inoculate 250 mL of CDBYE and incubated at 28 °C and shaken at 175 rpm. After 5 days of incubation, mycelial mixtures (2 x 30 mL) were harvested via centrifugation at 10,000 $\times$ g for 15 min at 4 °C. The supernatant was

transferred to a sterile conical tube and the resulting mycelial pellet was washed twice with ice-cold TE buffer (10 mM Tris/1 mM EDTA, pH 8.0), and the resulting supernatant was combined with the previous. The mycelial cultures were further incubated and extracted again after days 10 and 15. The supernatant was further extracted with ethyl acetate (4 × 20 mL), concentrated *in vacuo*, and purified through the general high-performance liquid chromatography (HPLC) method. Liquid chromatography mass spectrometry (LCMS) was used to detect the oosporein concentration through comparison to a previously synthesized oosporein standard.[214,269] LCMS was further used to determine the limit of detection of oosporein using 10-fold serial dilutions.

### 5.9.3 DNA Sample Preparation for Genomic Analysis

*B. bassiana* strains were grown to obtain DNA samples to establish high quality draft genome reference sequences. The starting fungal inoculum, obtained from frozen mycelial stocks, were reactivated using Czapex Dox agar yeast extract (CDAYE), and incubated at 25 °C for 4-6 weeks, or until conidial growth is at its maximum. The conidia were harvested, titered, and used to inoculate a 100 mL of CDBYE to give a final concentration of $1.0 \times 10^7$ conidia/mL and incubated at 28 °C for 72-96 h and shaken at 175 rpm. The mycelia were harvested via centrifugation at 5000 × g for 20 min at 4 °C. The resulting mycelia pellet was washed twice with ice-cold TE buffer, and flash-frozen in liquid nitrogen and stored at -80 °C until processing. The frozen mycelial pellets were sent to the Michael Smith Laboratories, University of British Columbia, for extraction of DNA. Quality control analyses were performed for all samples to establish the absence of bacterial contamination. A mycelial aliquot was serially diluted ten-fold up to $1.0 \times 10^6$, and all dilutions were spread-plated (in four replicates) on Standard Methods Agar

(SMA; BD Difco Laboratories, Sparks, MD, USA) with 100 U/mL nystatin. Duplicate plates were incubated to assess bacterial load at either 28 ℃ or 35 ℃ for 28-72 h.

### 5.9.4 DNA Extraction

A modified protocol was used to isolate fungal DNA from the lyophilized mycelium (~ 5 g).[270] These modifications include the washing of the initial pellet with 75% ethanol with 10 mM ammonium acetate, the addition of 3% of mercaptoethanol to the lysis extraction buffer, and incubation at 60 ℃ for 45 minutes. After incubation with RNAse and proteinase K at 37 ℃, an additional solvent cleaning with 25:24:1 phenol:chloroform:isoamyl solution was included. The quality and concentration of DNA were verified using a Quantiflor (Promega Corporation, Madison, WI, USA), a Nanodrop 2000c (ThermoFisher Scientific, Waltham, MA, USA), and 0.8 % agarose gel. The total DNA for each strain (~3-4 μg) was sent to Canada's Michael Smith Genome Sciences Centre for sequencing.

### 5.9.5 Whole Genome Sequencing

These experiments were performed by Canada's Michael Smith Genome Sciences Centre. A microfluidic partitioned library was created using the Chromium system (10x Genomics, Pleasanton, CA, USA). The 10x Genomics Chromium Controller instrument was used to prepare Gel beads-in-Emulsion (GEMs) by combining DNA, Master Mix, partitioning oil, and the microfluidic Genome Chip [PN-120216] (10x Genomics). The DNA underwent isothermal amplification and a barcode was added to each fragment. The barcoded fragments underwent Illumina library construction based on the Chromium Genome Reagent Kits Version 2 User Guide [PN-120229].

The quality was assessed for the resulting library using a DNA 1000 assay and the Agilent 2100 Bioanalyzer (Agilent Technologies, Santa Clara, CA, USA). The median insert size was 550 base pairs. The library was quantified with a Quant-iT dsDNA High Sensitivity Kit on a Qubit fluorometer (Invitrogen, Waltham, MA, USA) before pooling the library and size-correcting the final molar concentration calculations for Illumina HiSeqX sequencing with paired-end 150 base reads. Read trimming, barcode error correction, whitelisting, and barcode assignment were performed using the Long Ranger BASIC pipeline (v2.1.3).[270]

### 5.9.6 *De novo* Genome Assembly

These experiments were performed by Dr. Birol's lab. The genomes were assembled using Supernova v2.1.1,[248] which regulates the long-range information provided by linked reads. The read coverages were higher than the recommended range of 38-56X for assembly, so 15 million reads were selected (approximately 56X coverage) using --maxreads=15000000. The output FASTA files were created using the --style=pseudohap option to generate a single record per scaffold; scaffolds shorter than 1 kb were excluded from the final assembly. BWA-MEM v0.7.17r1188 was used to polish the draft genomes by aligning 80X downsampled reads to their respective genomes.[271,272] These alignments were supplied to Pilon v1.23. The genic completeness of the assemblies was assessed with BUSCO v5.1.2[273] using theHypocreales_odb10 database in genome mode. Other assembly metrics were calculated with QUAST v5.0.2.[274] Repetive sequences within the polished assemblies were identified and annotated using EDTA v1.9.4[275] and RepeatModeler v2.0.1[276]. The coding sequences of *B. bassiana* strain ARSEF 8028[277] were supplied to EDTA to ensure that the gene sequences were excluded from the resulting libraries. All identified repeats were merged with the Repbase v23,12, a database of eukaryotic repeat

sequences,[278] and redundant sequences were removed using the cleanup_nested.pl script from EDTA.[275] This repeat library was used as input for RepeatMasker v4.1.1[279] to annotate and soft-mask repetitive sequences in the resulting polished genome assemblies.

### 5.9.7 Phylogenetic Inference

These experiments were performed by Dr. Birol's lab, with experimental discussion and advice from our lab. The evolutionary relationships between the *B. bassiana* strains were assessed using RAxML v8.2.12.[280] The reference strain, *B. bassiana* ARSEF 2860[281], and *B. pseudobassiana* strain KACC 47484 (unpublished; GenBank accession: GCA_003267905.1) were also included in the analysis. C. militaris strain CM01[282] was also included and set as the outgroup with the -o option. The phylogeny was generated using single-copy BUSCO sequences because the annotations were not available for the *B. pseudobassiana* genome assembly. The shared BUSCO sequences were used to generate multiple sequence alignments with MAFFT v7.475[283], selecting the appropriate strategy automatically (--auto), and the resulting amino acid alignments were joined into a single matrix. A rapid Bootstrap analysis and search for the best-scoring Maximum Likelihood tree was performed to generate the phylogeny, using the PROTGAMMAAUTO model of amino acid substitution and 100 bootstrap replicates.

### 5.9.8 Genome Annotation and Orthogroup Inference

These experiments were performed by Dr. Birol's lab, with experimental discussion and advice from our lab. Genome annotation was performed using the MAKER (v2.31.10) pipeline,[284] which combines ab initio gene predictions and homology evidence. Ab initio gene predictions were performed using SNAP v2006-07-28,[285,286] GeneMark.hmm-E v3.47 and AUGUSTUS v3.3.3.[287]

SNAP and GeneMark were both trained on the UAMH 299 assembly, and *Fusarium graminearum* was used as the gene prediction species model for AUGUSTUS. Coding sequences of *B. bassiana* strain ARSEF 8028[277] were supplied as expressed sequence tag (EST) evidence. The UniProtKB/Swiss-Prot database of protein sequences[288] was used as evidence for protein homology. The gene predictions were processed using Genome Annotation Generator v2.0.1,[289] which added start and stop codons as well as removed transcripts with introns shorter than 10 bp or coding sequences shorter than 90 bp. Annotations missing a start and/or stop codon were manually removed. The filtered annotations were assessed with GeneValidator v2.1.10 (73) using the TrEMBL database[288] to determine their quality. These scores were considered when selecting genes of interest in further analyses. Functional annotations were assigned to protein sequences by running stages 4 and 5 of the EnTAP[290] pipeline (v0.10.7-beta). These stages included a similarity search to the Uniref90[288] database, then GO term and Pfam domain assignments were performed using InterProScan v5.30-69.0.[291] Gene predictions that were not annotated by similarity search or gene family assignment were filtered out. BUSCO[273] was ran in protein mode to assess the completeness of the final gene annotations.

Orthogroups (OGs) were inferred from the protein sequences, with default parameters, using OrthoFinder v2.5.1,[249] and the longest isoform of each gene was supplied for this analysis. OGs were annotated functionally using Gene Ontology terms and Pfam domains by selecting the most prevalent terms and domains assigned to the genes included in each OG. Core orthogroups were identified by OGs that included one or more gene in every stain, and core, single-copy OGs were present in only one copy in each OG. Singleton OGs were identified as those present only in one strain, and accessory OGs were those present in two or more, but not all strains. Group-specific OGs were extracted manually by identifying those that included one or more genes from each

strain of a given group, while not containing other genes from the strains in other groups. GO enrichment analyses were performed with clusterProfiler v3.18.1,[292] to assess the functional relevance of the orthogroup sets. The false discovery rate (FDR)[293] was used to correct p-values for multiple comparisons, leading to significant enrichment of GO terms identified at $\alpha = 0.05$.

### 5.9.9 Biosynthetic Gene Cluster Mining

These experiments were performed by Dr. Birol's lab, with experimental discussion and advice from our lab. Biosynthetic gene clusters within the genome were identified using antiSMASH v5.1.2[269] using the --taxon fungi option. The MAKER annotations were supplied using the --genefinding-gff3 option. Active site finder analysis (--asf) was used, and clusters were compared against a database of antiSMASH-predicted clusters (--cb-general), known gene clusters from the MIBiG database (--cb-knownclusters), and known subclusters (--cb-subclusters). The fungal-specific Cluster Assignment by Islands of Sites (CASSIS) algorithm[294] was used to aid in the prediction of cluster regions by searching for conserved binding motifs in promoter regions using the --cassis option. Extra clusters were found using the --cf-create-clusters option, and the Pfam and GO terms were mapped with --pfam2go.

### 5.9.10 RNA Sample Preparation for Transcriptomic Analysis

*B. bassiana* strains were grown to obtain RNA samples for transcriptomic analysis. The starting fungal inoculum, obtained from frozen mycelial stocks, was reactivated through spot inoculation of PDA media, and incubated for 3-5 d at 25 °C. One (1) $cm^2$ agar blocks were cored from the mycelial culture and transferred to four different pigment-inducing media: CDAYE (induces red pigmentation), MEA (yellow pigmentation), PDA (yellow pigmentation), and 0.25x

SDA (induction of conidiation). After analysis of the cultures (i.e., morphology, pigment-production, and conidial density), the conidia from the 0.25x SDA media were harvested and titered, and then used to inoculate 20 mL of CDBYE to give a final concentration of 1.0 $\times g$ $10^7$ conidia/mL and incubated for 72 h at 28 °C at 175 rpm. An aliquot of the active mycelial culture was used to aliquot 100 mL of CDBYE (10 % v/v/ inoculum) and incubated for 72-96 h at 28 °C at 175 rpm. The mycelial slurries were separated using a Stericup Quick Release-GP vacuum filtration system (0.22 μm, polyethersulfone membrane; Millipore-Sigma, USA). The mycelial mat was transferred aseptically to a pre-weighed, sterile, 50 mL conical tube. The mycelial samples were then flash frozen with liquid nitrogen and stored at -80 °C until processing. Quality control analysis, as previously described, was carried out to determine bacterial contamination for all samples. The frozen mycelial mats were sent to the Michael Smith Laboratories, University of British Columbia, for RNA extraction.

### 5.9.11 RNA Extraction

These experiments were performed by Dr. Bohlmann's lab, with experimental discussion and advice from our lab. Each of the 8 isolates, with three biological replicates, was extracted for total RNA. Frozen samples (2-5 g each, except for ANT-03 which required 7-9 g) were ground with liquid nitrogen using a mortar and pestle to get a fine powder. Kolosova *et al.*'s RNA extraction protocol was used to process 100-200 mg of ground tissue.[295] The RNA pellet was spun for an addition 30 seconds, and the remaining liquid was removed with a micropipette tip, and the samples were further air-dried for 1 min. The final dried pellet was resuspended in 30 $\mu$L of Nuclease-Free water. Total RNA concentration was assessed using a NanoDrop 1000 (ThermoFisher Scientific). The RNA quality was assessed on an Agilent 2100 Bioanalyzer and

Agilent RNA 6000 Nano Kit LabChips. The total RNA (37.5 ng/$\mu$L) was sent to Canada's Michael Smith Genome Sciences Centre for sequencing.

### 5.9.12 Transcriptome Sequencing

These experiments were performed by Canada's Michael Smith Genome Sciences Centre. Total RNA sample qualities were assessed using an Agilent Bioanalyzer RNA Nanochip and arrayed into a 96-well plate (ThermoFisher Scientific). Polyadenylated RNA was purified using the NEBNext Poly(A) mRNA Magnetic Isolation Module [E7490L] (New England Biolabs, Ipswich, MA, USA) from 1000 ng of total RNA. Messenger RNA (mRNA) selection was performed using NEBNext Oligo d(T)25 beads (New England Biolabs) incubated at 65°C for 5 min, followed by snap-chilling at 4 °C to denature RNA and facilitate binding of poly(A) mRNA to the beads. NEBNext Tris Buffer from the NEBNext Poly(A) Magnetic Isolation Kit (New England Biolabs) was used to elute the mRNA from the beads, which were then incubated at 80 °C for 2 min, then held at 25 °C for 2 min. The mRNA was allowed to re-bind to the beads using the RNA binding buffer, and then mixed 10 times and incubated at room temperature for 5 min. The supernatant was discarded, and the mRNA bound beads were washed twice before being placed on the magnet. The mRNA was eluted from the beads using 20 $\mu$L Tris buffer incubated at 80 °C for 2 min. The eluted mRNA was transferred to a new sterile 96-well plate. First-strand cDNA was synthesized from heat-denatured, purified mRNA using a Maxima H Minus First Strand cDNA Synthesis kit (ThermoFisher Scientific) and various hexamer primers at a concentration of 200 ng/µL amended with a final concentration of 40 ng/µL Actinomycin D, followed by PCR Clean DX (Aline Biosciences, Woburn, MA, USA) bead purification on a Microlab NIMBUS robot (Hamilton Company, Reno, NV, USA). The second strand cDNA was

synthesized following the NEBNext Ultra Directional Second Strand cDNA Synthesis protocol (New England Biolabs). This protocol incorporates dUTP in the dNTP mix, allowing the second strand to be digested using USER™ enzyme (New England Biolabs) in the post-adapter ligation reaction, therefore, achieving strand specificity.

cDNA was fragmented using a Covaris LE220 sonicator to achieve 250-300 bp average fragment lengths. The paired-end sequencing library was prepared following Canada's Michael Smith Genome Sciences Centre strand-specific, plate-based library construction protocol on a Microlab NIMBUS robot (Hamilton Company). End-repair and phosphorylation were performed on the sheared cDNA in a single reaction using an enzyme mix containing T4 DNA polymerase, Klenow DNA Polymerase and T4 polynucleotide kinase (New England Biolabs). The reaction mixture was incubated at 20 ℃ for 30 min. Repaired cDNA was purified in a 96-well format using PCR Clean dX beads (Aline Biosciences) and 3' A-tailed (adenylation) using Klenow fragment (3' to 5' exo minus) and incubated at 37 ℃ for 30 min. Enzyme heat activation was performed, and Illumina TruSeq adapters were ligated at 20 ℃ for 15 min. PCR Clean DX beads were used to purify the adapter-ligated products, which were then digested using USER™ enzyme (1U/μL) (New England Biolabs) at 37 ℃ for 15 min. 10 cycles of indexed PCR, using NEBNext Ultra II Q5 Master Mix (New England Biolabs) and Illumina's primer set, were performed. The PCR products were purified and size-selected twice using a 1:1 PCR Clean DX beads-to-sample ratio. The eluted DNA quality was assessed with Caliper LabChip GX for DNA samples using the High Sensitivity Assay (PerkinElmer, Waltham, MA, USA) and quantified using a Quant-iT dsDNA High Sensitivity Assay Kit on a Qubit fluorimeter (Invitrogen) prior to library pooling and size-corrected final molar concentration calculation for Illumina HiSeq sequencing with paired-end 150

base reads. The samples were submitted to the NCBI SRA under BioProject accession PRJNA877233. The corresponding BioSample accessions are presented in **Table 11**.

**Table 11** BioSample accession information for *Beauveria bassiana* strains used in this study.

| Strain | Sample Title | Accession Number | Sample Name |
|---|---|---|---|
| UAMH 298 | *Beauveria bassiana* strain UAMH 298 | SAMN30686974 | Bb_UAMH_298 |
| UAMH 298-UVR | *Beauveria bassiana* strain UAMH 298 (UV-resistant derivative) | SAMN30686975 | Bb_UAMH_298-YVR |
| UAMH 299 | *Beauveria bassiana* strain UAMH 299 | SAMN30686972 | Bb_UAMH_299 |
| UAMH 299-UVR | *Beauveria bassiana* strain UAMH 299 (UV-resistant derivative) | SAMN30686973 | Bb_UAMH_299-UVR |
| UAMH 1076 | *Beauveria bassiana* strain UAMH 1076 | SAMN30686976 | Bb_UAMH_1076 |
| ANT-03 | *Beauveria bassiana* strain ANT-03 | SAMN30686977 | Bb_UAX-29 |
| UAMH 4510 | *Beauveria bassiana* strain UAMH 4510 | SAMN30686978 | Bb_UAMH_4510 |
| 110.25 | *Beauveria bassiana* strain 110.25 | SAMN30686979 | Bb_110.25 |

### 5.9.13 Differential Expression and Co-Expression Analysis

These experiments were performed by Dr. Birol's lab, with experimental discussion and advice from our lab. Coding sequences from the reference *B. bassiana* strain, ARSEF 2860[281] were used to quantify gene-level expression of the eight strains, using Salmon v1.5.2.[296] Salmon was run in quasi-mapping mode, and corrected for sequence-specific and fragment-level GC biases using the --seqBias and --gcBias options. Differential expression analysis was carried out using DESeq2.[297] Gene expression was compared between the red and non-red strains, with the non-red strains used as the reference level. Differential expression (DE) was tested using a $\log_2$ fold change (LFC) threshold of 1 and altHypothesis="greaterAbs", to identify upregulation and downregulation. Significant DE genes were selected at FDR < 0.05. GO enrichment analysis was

performed using clusterProfiler.[292] The ARSEF 2860 annotations were obtained from AnnotationHubv2.22.1[298] under the record AH86840, and significantly enriched terms were selected at FDR < 0.05. Genes with mean normalized count values of 0 were excluded from the background gene set for the GO enrichment analysis.

Differential co-expression was assessed using the DGCA R package (v1.0.2).[299] Variance stabilizing transformation from DESeq2 was applied to the raw count data with blind=F. The genes in the lowest 25$^{th}$ percentile of variants were filtered out. Co-expression was calculated between gene pairs consisting of all filtered genes and OpS1 (BBA_08179) and OpS3 (BBA_08181). The differential correlation was identified between red and non-red strains. P-values were adjusted using FDR and significantly co-expressed gene pairs were identified between red and non-red strains at FDR < 0.05.

# Works Cited


(1) Lau, J. L.; Dunn, M. K. Therapeutic Peptides: Historical Perspectives, Current Development Trends, and Future Directions. *Bioorg Med Chem* **2018**, *26* (10), 2700–2707.

(2) Apostolopoulos, V.; Bojarska, J.; Chai, T. T.; Elnagdy, S.; Kaczmarek, K.; Matsoukas, J.; New, R.; Parang, K.; Lopez, O. P.; Parhiz, H.; Perera, C. O.; Pickholz, M.; Remko, M.; Saviano, M.; Skwarczynski, M.; Tang, Y.; Wolf, W. M.; Yoshiya, T.; Zabrocki, J.; Zielenkiewicz, P.; Alkhazindar, M.; Barriga, V.; Kelaidonis, K.; Sarasia, E. M.; Toth, I. A Global Review on Short Peptides: Frontiers and Perspectives. *Molecules* **2021**, *26* (2), 430.

(3) Wang, L.; Wang, N.; Zhang, W.; Cheng, X.; Yan, Z.; Shao, G.; Wang, X.; Wang, R.; Fu, C. Therapeutic Peptides: Current Applications and Future Directions. *Signal Transduct Target Ther* **2022**, *7* (1).

(4) Lohans, C. T.; Vederas, J. C. Development of Class IIa Bacteriocins as Therapeutic Agents. *Int J Microbiol* **2012**.

(5) Kraut, J. How Do Enzymes Work? *Nature* **1988**, *242*, 533–540.

(6) Drag, M.; Salvesen, G. S. Emerging Principles in Protease-Based Drug Discovery. *Nat Rev Drug Discov* **2010**, *9* (9), 690–701.

(7) Fosgerau, K.; Hoffmann, T. Peptide Therapeutics: Current Status and Future Directions. *Drug Discov Today* **2015**, *20* (1).

(8) Drucker, D. J. Advances in Oral Peptide Therapeutics. *Nat Rev Drug Discov* **2020**, *19* (4), 277–289.

(9) Mirabeau, O.; Perlas, E.; Severini, C.; Audero, E.; Gascuel, O.; Possenti, R.; Birney, E.; Rosenthal, N.; Gross, C. Identification of Novel Peptide Hormones in the Human Proteome by Hidden Markov Model Screening. *Genome Res* **2007**, *17* (3), 320–327.

(10) Shoulders, M. D.; Raines, R. T. Collagen Structure and Stability. *Annu Rev Biochem* **2009**, *78*, 929–958.

(11) Banting, F. G.; Best, C. H.; Collip, J. B.; Campbell, W. R.; Fletcher, A. A. Pancreatic Extracts in the Treatment of Diabetes Mellitus. *The Canadian Medical Association Journal* **1922**, *12*, 141–146.

(12) Diao, L.; Meibohm, B. Pharmacokinetics and Pharmacokinetic-Pharmacodynamic Correlations of Therapeutic Peptides. *Clin Pharmacokinet* **2013**, *52* (10), 855–868.

(13) Pan, X.; Xu, J.; Jia, X. Research Progress Evaluating the Function and Mechanism of Anti-Tumor Peptides. *Cancer Manag Res* **2020**, *12*, 397–409.

(14) Henninot, A.; Collins, J. C.; Nuss, J. M. The Current State of Peptide Drug Discovery: Back to the Future? *J Med Chem* **2018**, *61* (4), 1382–1414.

(15) Fischer, E.; Fourneau, E. Ueber Einige Derivate Des Glykocolls. *Berichte der deutschen chemischen Gesellschaft* **1901**, *34* (2), 2868–2877.

(16) Yang, Y.; Liu, Y.; Chen, S.; Cheong, K. L.; Teng, B. Carboxymethyl β-Cyclodextrin Grafted Carboxymethyl Chitosan Hydrogel-Based Microparticles for Oral Insulin Delivery. *Carbohydr Polym* **2020**, *246*.

(17) Vigneaud, V. du; Ressler, C.; Swan, C. J. M.; Roberts, C. W.; Katsoyannis, P. G.; Gordon, S. The Synthesis of an Octapeptide Amide with the Hormonal Activity of Oxytocin. *J Am Chem Soc* **1953**, *75*, 4879–4880.

(18) Merrifield, R. B. Solid Phase Peptide Synthesis. I. Synthesis of a Tetrapeptide. *J Am Chem Soc* **1963**, *85*, 2149–2154.

(19) Stawikowski, M.; Fields, G. B. Introduction to Peptide Synthesis. *Curr Protoc Protein Sci* **2001**, *26* (1).

(20) Carpino, L. A.; Han, G. Y. 9-Fluorenylmethoxycarbonyl Function, a New Base-Sensitive Amino-Protecting Group. *J Am Chem Soc* **1970**, *92*, 5748–5749.

(21) Atherton, E.; Sheppard, R. C. Solid Phase Peptide Synthesis Using N,-Fluorenylmethoxycarbonylamino Acid Pentafluorophenyl Esters. *J Chem Soc Chem Commun* **1985**, *3*, 165–166.

(22) Valeur, E.; Bradley, M. Amide Bond Formation: Beyond the Myth of Coupling Reagents. *Chem Soc Rev* **2009**, *38* (2), 606–631.

(23) El-Faham, A.; Albericio, F. Peptide Coupling Reagents, More than a Letter Soup. *Chem Rev* **2011**, *111* (11), 6557–6602.

(24) Dawson, P. E.; Muir, T. W.; Clark-Lewis, I.; Kent, S. B. H. Synthesis of Proteins by Native Chemical Ligation. *Science (1979)* **1994**, *266*, 776–779.

(25) Kent, S. B. H. Total Chemical Synthesis of Proteins. *Chem Soc Rev* **2009**, *38* (2), 338–351.

(26) Hartrampf, N.; Saebi, A.; Poskus, M.; Gates, Z. P.; Callahan, A. J.; Cowfer, A. E.; Hanna, S.; Antilla, S.; Schissel, C. K.; Quartararo, A. J.; Ye, X.; Mijalis, A. J.; Simon, M. D.; Loas, A.; Liu, S.; Jessen, C.; Nielsen, T. E.; Pentelute, B. L. Synthesis of Proteins by Automated Flow Chemistry. *Science (1979)* **2020**, *368*, 980–987.

(27) López-Otín, C.; Bond, J. S. Proteases: Multifunctional Enzymes in Life and Disease. *Journal of Biological Chemistry* **2008**, *283* (45), 30433–30437.

(28) Werner, H. M.; Cabalteja, C. C.; Horne, W. S. Peptide Backbone Composition and Protease Susceptibility: Impact of Modification Type, Position, and Tandem Substitution. *ChemBioChem* **2016**, *17* (8), 712–718.

(29) Chatterjee, J.; Rechenmacher, F.; Kessler, H. N-Methylation of Peptides and Proteins: An Important Element for Modulating Biological Functions. *Angewandte Chemie - International Edition* **2013**, *52* (1), 254–269.

(30) Traoré, M.; Doan, N. D.; Lubell, W. D. Diversity-Oriented Synthesis of Azapeptides with Basic Amino Acid Residues: Aza-Lysine, Aza-Ornithine, and Aza-Arginine. *Org Lett* **2014**, *16* (13), 3588–3591.

(31) Cheloha, R. W.; Watanabe, T.; Dean, T.; Gellman, S. H.; Gardella, T. J. Backbone Modification of a Parathyroid Hormone Receptor-1 Antagonist/Inverse Agonist. *ACS Chem Biol* **2016**, *11* (10), 2752–2762

(32) Chingle, R.; Proulx, C.; Lubell, W. D. Azapeptide Synthesis Methods for Expanding Side-Chain Diversity for Biomedical Applications. *Acc Chem Res* **2017**, *50* (7), 1541–1556.

(33) Pelay-Gimeno, M.; Glas, A.; Koch, O.; Grossmann, T. N. Structure-Based design of Inhibitors of Protein–Protein Interactions: Mimicking Peptide Binding Epitopes. *Angewandte Chemie* **2015**, *127* (31), 9022–9054.

(34) Yang, P. Y.; Zou, H.; Lee, C.; Muppidi, A.; Chao, E.; Fu, Q.; Luo, X.; Wang, D.; Schultz, P. G.; Shen, W. Stapled, Long-Acting Glucagon-like Peptide 2 Analog with Efficacy in Dextran Sodium Sulfate Induced Mouse Colitis Models. *J Med Chem* **2018**, *61* (7), 3218–3223.

(35) Finegold, J. A.; Asaria, P.; Francis, D. P. Mortality from Ischaemic Heart Disease by Country, Region, and Age: Statistics from World Health Organisation and United Nations. *Int J Cardiol* **2013**, *168* (2), 934–945.

(36) Guo, R.; Rogers, O.; Nair, S. Targeting Apelinergic System in Cardiometabolic Disease. *Curr Drug Targets* **2016**, *18* (15).

(37) Smolderen, K. G.; Md, A. B.; Lei, Y.; Cohen, E. A.; Steg, G.; Bhatt, D. L.; Mahoney Scd, E. M. One-Year Costs Associated with Cardiovascular Disease in Canada: Insights from the REduction of Atherothrombosis for Continued Health (REACH) Registry. *Can J Cardiol* **2010**, *26*, e297–e305.

(38) Benjamin, E. J.; Blaha, M. J.; Chiuve, S. E.; Cushman, M.; Das, S. R.; Deo, R.; De Ferranti, S. D.; Floyd, J.; Fornage, M.; Gillespie, C.; Isasi, C. R.; Jiménez, M. C.; Jordan, L. C.; Judd, S. E.; Lackland, D.; Lichtman, J. H.; Lisabeth, L.; Liu, S.; Longenecker, C. T.; MacKey, R. H.; Matsushita, K.; Mozaffarian, D.; Mussolino, M. E.; Nasir, K.; Neumar, R. W.; Palaniappan, L.; Pandey, D. K.; Thiagarajan, R. R.; Reeves, M. J.; Ritchey, M.; Rodriguez, C. J.; Roth, G. A.; Rosamond, W. D.; Sasson, C.; Towfghi, A.; Tsao, C. W.; Turner, M. B.;

Virani, S. S.; Voeks, J. H.; Willey, J. Z.; Wilkins, J. T.; Wu, J. H. Y.; Alger, H. M.; Wong, S. S.; Muntner, P. Heart Disease and Stroke Statistics-2017 Update: A Report from the American Heart Association. *Circulation* **2017**, *135* (10), e146–e603.

(39) González-Montero, J.; Brito, R.; Gajardo, A. I. J.; Rodrigo, R. Myocardial Reperfusion Injury and Oxidative Stress: Therapeutic. *World J Cardiol* **2018**, *10*, 74–86.

(40) Krzywonos-Zawadzka, A.; Franczak, A.; Sawicki, G.; Woźniak, M.; Bil-Lula, I. Multidrug Prevention or Therapy of Ischemia-Reperfusion Injury of the Heart—Mini-Review. *Environ Toxicol Pharmacol* **2017**, *55*, 55–59.

(41) O'Dowd, B. F.; Heiber, M.; Chan, A.; Heng, H. H. Q.; Tsui, L.-C.; Kennedy, J. L.; Shi, X.; Petronis, A.; George, S. R.; Nguyen, T. A Human Gene That Shows Identity with the Gene Encoding the Angiotensin Is Located on Chromosome 11. *Gene* **1993**, *136*, 355–360.

(42) Pauli, A.; Norris, M. L.; Valen, E.; Chew, G. L.; Gagnon, J. A.; Zimmerman, S.; Mitchell, A.; Ma, J.; Dubrulle, J.; Reyon, D.; Tsai, S. Q.; Joung, J. K.; Saghatelian, A.; Schier, A. F. Toddler: An Embryonic Signal That Promotes Cell Movement via Apelin Receptors. *Science (1979)* **2014**, *343* (6172).

(43) Yang, P.; Maguire, J. J.; Davenport, A. P. Apelin, Elabela/Toddler, and Biased Agonists as Novel Therapeutic Agents in the Cardiovascular System. *Trends Pharmacol Sci* **2015**, *36* (9), 560–567.

(44) Zhong, J. C.; Zhang, Z. Z.; Wang, W.; McKinnie, S. M. K.; Vederas, J. C.; Oudit, G. Y. Targeting the Apelin Pathway as a Novel Therapeutic Approach for Cardiovascular Diseases. *Biochim Biophys Acta Mol Basis Dis* **2017**, *1863* (8), 1942–1950.

(45) Galanth, C.; Hus-Citharel, A.; Li, B.; Llorens-Cortès, C. Apelin in the Control of Body Fluid Homeostasis and Cardiovascular Functions. *Curr Pharm Des* **2012**, *18*, 789–798.

(46) Tatemoto, K.; Takayama, K.; Zou, M.-X.; Kumaki, I.; Zhang, W.; Kumano, K.; Fujimiya, M. The Novel Peptide Apelin Lowers Blood Pressure via a Nitric Oxide-Dependent Mechanism. *Regul Pept* **2001**, *99*, 87–92.

(47) Japp, A. G.; Cruden, N. L.; Barnes, G.; Van Gemeren, N.; Mathews, J.; Adamson, J.; Johnston, N. R.; Denvir, M. A.; Megson, I. L.; Flapan, A. D.; Newby, D. E. Acute Cardiovascular Effects of Apelin in Humans: Potential Role in Patients with Chronic Heart Failure. *Circulation* **2010**, *121* (16), 1818–1827.

(48) Barnes, G. D.; Alam, S.; Carter, G.; Pedersen, C. M.; Lee, K. M.; Hubbard, T. J.; Veitch, S.; Jeong, H.; White, A.; Cruden, N. L.; Huson, L.; Japp, A. G.; Newby, D. E. Sustained Cardiovascular Actions of Apj Agonism during Renin-Angiotensin System Activation and in Patients with Heart Failure. *Circ Heart Fail* **2013**, *6* (3), 482–491.

(49) Bertrand, C.; Valet, P.; Castan-Laurell, I. Apelin and Energy Metabolism. *Front Physiol* **2015**, *6*, 1–5.

(50) Folino, A.; Montarolo, P. G.; Samaja, M.; Rastaldo, R. Effects of Apelin on the Cardiovascular System. *Heart Fail Rev* **2015**, *20* (4), 505–518.

(51) Yang, Y.; Lv, S. Y.; Ye, W.; Zhang, L. Apelin/APJ System and Cancer. *Clinica Chimica Acta* **2016**, *457*, 112–116.

(52) Masoud, A. G.; Lin, J.; Azad, A. K.; Farhan, M. A.; Fischer, C.; Zhu, L. F.; Zhang, H.; Sis, B.; Kassiri, Z.; Moore, R. B.; Kim, D.; Anderson, C. C.; Vederas, J. C.; Adam, B. A.; Oudit,

G. Y.; Murray, A. G. Apelin Directs Endothelial Cell Differentiation and Vascular Repair Following Immune-Mediated Injury. *Journal of Clinical Investigation* **2020**, *130* (1), 94–107.

(53) Vinel, C.; Lukjanenko, L.; Batut, A.; Deleruyelle, S.; Pradère, J. P.; Le Gonidec, S.; Dortignac, A.; Geoffre, N.; Pereira, O.; Karaz, S.; Lee, U.; Camus, M.; Chaoui, K.; Mouisel, E.; Bigot, A.; Mouly, V.; Vigneau, M.; Pagano, A. F.; Chopard, A.; Pillard, F.; Guyonnet, S.; Cesari, M.; Burlet-Schiltz, O.; Pahor, M.; Feige, J. N.; Vellas, B.; Valet, P.; Dray, C. The Exerkine Apelin Reverses Age-Associated Sarcopenia. *Nat Med* **2018**, *24* (9), 1360–1371.

(54) Tatemoto, K.; Hosoya, M.; Habata, Y.; Fujii, R.; Kakegawa, T.; Zou, M.-X.; Kawamata, Y.; Fukusumi, S.; Hinuma, S.; Kitada, C.; Kurokawa, T.; Onda, H.; Fujino, M. Isolation and Characterization of a Novel Endogenous Peptide Ligand for the Human APJ Receptor. *Biochem Biophys Res Commun* **1998**, *251*, 471–476.

(55) Lee, D. L.; Cheng, R.; Nguyen, T.; Fan, T.; Kariyawasam, A. P.; Liu, Y.; Osmond, D. H.; George, S. R.; O'Dowd, B. F. Characterization of Apelin, the Ligand for the APJ Receptor. *J Neurochem* **2000**, *74* (1), 34–41.

(56) Pitkin, S. L.; Maguire, J. J.; Bonner, T. I.; Davenport, A. P. International Union of Basic and Clinical Pharmacology. LXXIV. Apelin Receptor Nomenclature, Distribution, Pharmacology, and Function. *Pharmacol Rev* **2010**, *62* (3), 331–342.

(57) McKinnie, S. M. K.; Wang, W.; Fischer, C.; McDonald, T.; Kalin, K. R.; Iturrioz, X.; Llorens-Cortes, C.; Oudit, G. Y.; Vederas, J. C. Synthetic Modification within the "RPRL"

Region of Apelin Peptides: Impact on Cardiovascular Activity and Stability to Neprilysin and Plasma Degradation. *J Med Chem* **2017**, *60* (14), 6408–6427.

(58) Shin, K.; Kenward, C.; Rainey, J. K. Apelinergic System Structure and Function. *Compr Physiol* **2018**, *8* (1), 407–450.

(59) Shin, K.; Pandey, A.; Liu, X. Q.; Anini, Y.; Rainey, J. K. Preferential Apelin-13 Production by the Proprotein Convertase PCSK3 Is Implicated in Obesity. *FEBS Open Bio* **2013**, *3*, 328–333.

(60) Adam, F.; Khatib, A.-M.; Lopez, J. J.; Vatier, C.; Turpin, S.; Muscat, A.; Soulet, F.; Aries, A.; Jardin, I.; Bobe, R.; Stepanian, A.; De Prost, D.; Dray, C.; Rosado, J. A.; Valet, P.; Feve, B.; Siegfried, G. Apelin: An Antithrombotic Factor That Inhibits Platelet Function. *Blood, The Journal of the American Society of Hematology* **2016**, *127*, 908–920.

(61) Lee, D. K.; Ferguson, S. S. G.; George, S. R.; O'Dowd, B. F. The Fate of the Internalized Apelin Receptor Is Determined by Different Isoforms of Apelin Mediating Differential Interaction with β-Arrestin. *Biochem Biophys Res Commun* **2010**, *395* (2), 185–189.

(62) Zhen, E. Y.; Higgs, R. E.; Gutierrez, J. A. Pyroglutamyl Apelin-13 Identified as the Major Apelin Isoform in Human Plasma. *Anal Biochem* **2013**, *442* (1), 1–9.

(63) Maguire, J. J.; Kleinz, M. J.; Pitkin, S. L.; Davenport, A. P. [Pyr1]Apelin-13 Identified as the Predominant Apelin Isoform in the Human Heart: Vasoactive Mechanisms and Inotropic Action in Disease. *Hypertension* **2009**, *54* (3), 598–604.

(64) Chatterjee, P.; Gheblawi, M.; Wang, K.; Vu, J.; Kondaiah, P.; Oudit, G. Y. Interaction between the Apelinergic System and ACE2 in the Cardiovascular System: Therapeutic Implications. *Clin Sci* **2020**, *134* (17), 2319–2336.

(65) de Oliveira, A. A.; Vergara, A.; Wang, X.; Vederas, J. C.; Oudit, G. Y. Apelin Pathway in Cardiovascular, Kidney, and Metabolic Diseases: Therapeutic Role of Apelin Analogs and Apelin Receptor Agonists. *Peptides*. Elsevier Inc. January 1, 2022.

(66) Japp, A. G.; Cruden, N. L.; Amer, D. A. B.; Li, V. K. Y.; Goudie, E. B.; Johnston, N. R.; Sharma, S.; Neilson, I.; Webb, D. J.; Megson, I. L.; Flapan, A. D.; Newby, D. E. Vascular Effects of Apelin in Vivo in Man. *J Am Coll Cardiol* **2008**, *52* (11), 908–913.

(67) Wang, W.; McKinnie, S. M. K.; Farhan, M.; Paul, M.; McDonald, T.; McLean, B.; Llorens-Cortes, C.; Hazra, S.; Murray, A. G.; Vederas, J. C.; Oudit, G. Y. Angiotensin-Converting Enzyme 2 Metabolizes and Partially Inactivates Pyr-Apelin-13 and Apelin-17: Physiological Effects in the Cardiovascular System. *Hypertension* **2016**, *68* (2), 365–377.

(68) Fischer, C.; Lamer, T.; Wang, W.; McKinnie, S. M. K.; Iturrioz, X.; Llorens-Cortes, C.; Oudit, G. Y.; Vederas, J. C. Plasma Kallikrein Cleaves and Inactivates Apelin-17: Palmitoyl- and PEG-Extended Apelin-17 Analogs as Metabolically Stable Blood Pressure-Lowering Agents. *Eur J Med Chem* **2019**, *166*, 119–124.

(69) Berry, M. F.; Pirolli, T. J.; Jayasankar, V.; Burdick, J.; Morine, K. J.; Gardner, T. J.; Woo, Y. J. Apelin Has in Vivo Inotropic Effects on Normal and Failing Hearts. *Circulation* **2004**, *110* (11), 187–193.

(70) Perjés, Á.; Skoumal, R.; Tenhunen, O.; Kónyi, A.; Simon, M.; Horváth, I. G.; Kerkelä, R.; Ruskoaho, H.; Szokodi, I. Apelin Increases Cardiac Contractility via Protein Kinase Cε-And Extracellular Signal-Regulated Kinase-Dependent Mechanisms. *PLoS One* **2014**, *9* (4), e93473.

(71) Salcedo, A.; Garijo, J.; Monge, L.; Fernández, N.; Luis García-Villalón, A.; Sánchez Turrión, V.; Cuervas-Mons, V.; Diéguez, G. Apelin Effects in Human Splanchnic Arteries. Role of Nitric Oxide and Prostanoids. *Regul Pept* **2007**, *144* (1–3), 50–55.

(72) Murza, A.; Parent, A.; Besserer-Offroy, E.; Tremblay, H.; Karadereye, F.; Beaudet, N.; Leduc, R.; Sarret, P.; Marsault, É. Elucidation of the Structure-Activity Relationships of Apelin: Influence of Unnatural Amino Acids on Binding, Signaling, and Plasma Stability. *ChemMedChem* **2012**, *7* (2), 318–325.

(73) Gerbier, R.; Alvear-Perez, R.; Margathe, J. F.; Flahault, A.; Couvineau, P.; Gao, J.; De Mota, N.; Dabire, H.; Li, B.; Ceraudo, E.; Hus-Citharel, A.; Esteoulle, L.; Bisoo, C.; Hibert, M.; Berdeaux, A.; Iturrioz, X.; Bonnet, D.; Llorens-Cortes, C. Development of Original Metabolically Stable Apelin-17 Analogs with Diuretic and Cardiovascular Effects. *FASEB Journal* **2017**, *31* (2), 687–700.

(74) Hamada, J.; Kimura, J.; Ishida, J.; Kohda, T.; Morishita, S.; Ichihara, S.; Fukamizu, A. Evaluation of Novel Cyclic Analogues of Apelin. *Int J Mol Med* **2008**, *22* (4), 547–552.

(75) Trân, K.; Murza, A.; Sainsily, X.; Coquerel, D.; Côté, J.; Belleville, K.; Haroune, L.; Longpré, J. M.; Dumaine, R.; Salvail, D.; Lesur, O.; Auger-Messier, M.; Sarret, P.; Marsault, É. A Systematic Exploration of Macrocyclization in Apelin-13: Impact on

Binding, Signaling, Stability, and Cardiovascular Effects. *J Med Chem* **2018**, *61* (6), 2266–2277.

(76) Juhl, C.; Els-Heindl, S.; Schönauer, R.; Redlich, G.; Haaf, E.; Wunder, F.; Riedl, B.; Burkhardt, N.; Beck-Sickinger, A. G.; Bierer, D. Development of Potent and Metabolically Stable APJ Ligands with High Therapeutic Potential. *ChemMedChem* **2016**, *11* (21), 2378–2384.

(77) O'Harte, F. P. M.; Parthsarathy, V.; Hogg, C.; Flatt, P. R. Long-Term Treatment with Acylated Analogues of Apelin-13 Amide Ameliorates Diabetes and Improves Lipid Profile of High-Fat Fed Mice. *PLoS One* **2018**, *13* (8).

(78) Turecek, P. L.; Bossard, M. J.; Schoetens, F.; Ivens, I. A. PEGylation of Biopharmaceuticals: A Review of Chemistry and Nonclinical Safety Information of Approved Drugs. *J Pharm Sci* **2016**, *105* (2), 460–475.

(79) Fischer, C.; Lamer, T.; Fernandez, K.; Gheblawi, M.; Wang, W.; Pascoe, C.; Lambkin, G.; Iturrioz, X.; Llorens-Cortes, C.; Oudit, G. Y.; Vederas, J. C. Optimizing PEG-Extended Apelin Analogues as Cardioprotective Drug Leads: Importance of the KFRR Motif and Aromatic Head Group for Improved Physiological Activity. *J Med Chem* **2020**, *63* (20), 12073–12082.

(80) McKinnie, S. M. K.; Fischer, C.; Tran, K. M. H.; Wang, W.; Mosquera, F.; Oudit, G. Y.; Vederas, J. C. The Metalloprotease Neprilysin Degrades and Inactivates Apelin Peptides. *ChemBioChem* **2016**, 1495–1498.

(81) Bell, R. M.; Mocanu, M. M.; Yellon, D. M. Retrograde Heart Perfusion: The Langendorff Technique of Isolated Heart Perfusion. *J Mol Cell Cardiol* **2011**, *50* (6), 940–950.

(82) Fishburn, C. S. The Pharmacology of PEGylation: Balancing PD with PK to Generate Novel Therapeutics. *J. Pharm. Sci.* **2008**, *97*, 4167.

(83) Ghosh, A. K.; Brindisi, M. Organic Carbamates in Drug Design and Medicinal Chemistry. *J Med Chem* **2015**, *58* (7), 2895–2940.

(84) Varshavsky, A. The N-End Rule Pathway and Regulation by Proteolysis. *Protein Science* **2011**, *20* (8), 1298–1345.

(85) Wang, W.; McKinnie, S. M. K.; Patel, V. B.; Haddad, G.; Wang, Z.; Zhabyeyev, P.; Das, S. K.; Basu, R.; McLean, B.; Kandalam, V.; Penninger, J. M.; Kassiri, Z.; Vederas, J. C.; Murray, A. G.; Oudit, G. Y. Loss of Apelin Exacerbates Myocardial Infarction Adverse Remodeling and Ischemia-Reperfusion Injury: Therapeutic Potential of Synthetic Apelin Analogues. *J Am Heart Assoc* **2013**, *2* (4).

(86) Zhang, Z. Z.; Wang, W.; Jin, H. Y.; Chen, X.; Cheng, Y. W.; Xu, Y. Le; Song, B.; Penninger, J. M.; Oudit, G. Y.; Zhong, J. C. Apelin Is a Negative Regulator of Angiotensin II-Mediated Adverse Myocardial Remodeling and Dysfunction. *Hypertension* **2017**, *70* (6), 1165–1175.

(87) Brash, L.; Barnes, G. D.; Brewis, M. J.; Church, A. C.; Gibbs, S. J.; Howard, L. S. G. E.; Jayasekera, G.; Johnson, M. K.; McGlinchey, N.; Onorato, J.; Simpson, J.; Stirrat, C.; Thomson, S.; Watson, G.; Wilkins, M. R.; Xu, C.; Welsh, D. J.; Newby, D. E.; Peacock, A.

J. Short-Term Hemodynamic Effects of Apelin in Patients with Pulmonary Arterial Hypertension. *JACC Basic Transl Sci* **2018**, *3* (2), 176–186.

(88) Wang, W.; Shen, M.; Fischer, C.; Basu, R.; Hazra, S.; Couvineau, P.; Paul, M.; Wang, F.; Toth, S.; Mix, D. S.; Poglitsch, M.; Gerard, N. P.; Bouvier, M.; Vederas, J. C.; Penninger, J. M.; Kassiri, Z.; Oudit, G. Y. Apelin Protects against Abdominal Aortic Aneurysm and the Therapeutic Role of Neutral Endopeptidase Resistant Apelin Analogs. *Proc Natl Acad Sci U S A* **2019**, *116* (26), 13006–13015.

(89) Ma, Y.; Yue, Y.; Ma, Y.; Zhang, Q.; Zhou, Q.; Song, Y.; Shen, Y.; Li, X.; Ma, X.; Li, C.; Hanson, M. A.; Han, G. W.; Sickmier, E. A.; Swaminath, G.; Zhao, S.; Stevens, R. C.; Hu, L. A.; Zhong, W.; Zhang, M.; Xu, F. Structural Basis for Apelin Control of the Human Apelin Receptor. *Structure* **2017**, *25* (6), 858–866.

(90) Bovy, P. R.; O'Neal, J. M.; Olins, G. M.; Patton, D. R.; Mehta, P. P.; McMahon, E. G.; Palomo, M.; Schuh, J.; Blehm, D. A Synthetic Linear Decapeptide Binds to the Atrial Natriuretic Peptide Receptors and Demonstrates Cyclase Activation and Vasorelaxant Activity. *Journal of Biological Chemistry* **1983**, *264* (34), 20309–20313.

(91) Chatenet, D.; Dubessy, C.; Boularan, C.; Scalbert, E.; Pfeiffer, B.; Renard, P.; Lihrmann, I.; Pacaud, P.; Tonon, M. C.; Vaudry, H.; Leprince, J. Structure-Activity Relationships of a Novel Series of Urotensin II Analogues: Identification of a Urotensin II Antagonist. *J Med Chem* **2006**, *49* (24), 7234–7238.

(92) Pilz, S.; Meinitzer, A.; Gaksch, M.; Grübler, M.; Verheyen, N.; Drechsler, C.; Hartaigh, B.; Lang, F.; Alesutan, I.; Voelkl, J.; März, W.; Tomaschitz, A. Homoarginine in the Renal and Cardiovascular Systems. *Amino Acids* **2015**, *47* (9), 1703–1713.

(93) Chafai, A.; Fromm, M. F.; König, J.; Maas, R. The Prognostic Biomarker L-Homoarginine Is a Substrate of the Cationic Amino Acid Transporters CAT1, CAT2A and CAT2B. *Sci Rep* **2017**, *7* (1).

(94) Ravani, P.; Maas, R.; Malberti, F.; Pecchini, P.; Mieth, M.; Quinn, R.; Tripepi, G.; Mallamaci, F.; Zoccali, C. Homoarginine and Mortality in Pre-Dialysis Chronic Kidney Disease (CKD) Patients. *PLoS One* **2013**, *8* (9).

(95) Ryan, W. L.; Wells, I. C. Homocitrulline and Homoarginine Synthesis from Lysine. *Science (1979)* **1964**, *144* (3622), 1122–1127.

(96) Ryan, W. L.; Barak, A. J.; Johnson, R. J. Lysine, Homocitruliine, and Homoarginine Metabolism by the Isolated Perfused Rat Liver'. *Arch Biochem Biophys* **1968**, *123*, 294–297.

(97) Jaźwińska-Kozuba, A.; Martens-Lobenhoffer, J.; Kruszelnicka, O.; Rycaj, J.; Chyrchel, B.; Surdacki, A.; Bode-Böger, S. M. Opposite Associations of Plasma Homoarginine and Ornithine with Arginine in Healthy Children and Adolescents. *Int J Mol Sci* **2013**, *14* (11), 21819–21832.

(98) Atzler, D.; Cracowski, J. L.; Cordts, K.; Böger, R. H.; Humbert, M.; Schwedhelm, E. Homoarginine Predicts Mortality in Treatment-Naive Patients with Pulmonary Arterial Hypertension. *Int J Cardiol* **2016**, *217*, 12–15.

(99) Demetrius, L. Of Mice and Men: When It Comes to Studying Ageing and the Means to Slow It down, Mice Are Not Just Small Humans. *EMBO Rep* **2005**, *6*, S39–S44.

(100) Tucker, T. J.; Lumma, W. C.; Lewis, S. D.; Gardell, S. J.; Lucas, B. J.; Baskin, E. P.; Woltmann, R.; Lynch, J. J.; Lyle, E. A.; Appleby, S. D.; Chen, I.-W.; Dancheck, K. B.; Vacca, J. P. Expedited Articles Potent Noncovalent Thrombin Inhibitors That Utilize the Unique Amino Acid D-Dicyclohexylalanine in the P3 Position. Implications on Oral Bioavailability and Antithrombotic Efficacy. *J Med Chem* **1997**, *40*, 1565–1569.

(101) Fan, X.; Zhou, N.; Zhang, X.; Mukhtar, M.; Lu, Z.; Fang, J.; DuBois, G. C.; Pomerantz, R. J. Structural and Functional Study of the Apelin-13 Peptide, an Endogenous Ligand of the HIV-1 Coreceptor, APJ. *Biochemistry* **2003**, *42* (34), 10163–10168.

(102) Medhurst, A. D.; Jennings, C. A.; Robbins, M. J.; Davis, R. P.; Ellis, C.; Winborn, K. Y.; Lawrie, K. W. M.; Hervieu, G.; Riley, G.; Bolaky, J. E.; Herrity, N. C.; Murdock, P.; Darker, J. G. Pharmacological and Immunohistochemical Characterization of the APJ Receptor and Its Endogenous Ligand Apelin. *J Neurochem* **2003**, *84* (5), 1162–1172.

(103) Allolio, C.; Magarkar, A.; Jurkiewicz, P.; Baxová, K.; Javanainen, M.; Mason, P. E.; Šachl, R.; Cebecauer, M.; Hof, M.; Horinek, D.; Heinz, V.; Rachel, R.; Ziegler, C. M.; Schröfel, A.; Jungwirth, P. Arginine-Rich Cell-Penetrating Peptides Induce Membrane Multilamellarity and Subsequently Enter via Formation of a Fusion Pore. *Proc Natl Acad Sci U S A* **2018**, *115* (47), 11923–11928.

(104) Freidinger, R. M.; Perlow, D. S.; Veber, D. F. Protected Lactam-Bridged Dipeptides for Use as Conformational Constraints in Peptides. *Journal of Organic Chemistry* **1982**, *47* (1), 104–109.

(105) Van Ameijde, J.; Poot, A. J.; Van Wandelen, L. T. M.; Wammes, A. E. M.; Ruijtenbeek, R.; Rijkers, D. T. S.; Liskamp, R. M. J. Preparation of Novel Alkylated Arginine Derivatives

Suitable for Click-Cycloaddition Chemistry and Their Incorporation into Pseudosubstrate- and Bisubstrate-Based Kinase Inhibitors. *Org Biomol Chem* **2010**, *8* (7), 1629–1639.

(106) Yue, Y.; Liu, L.; Wu, L. J.; Wu, Y.; Wang, L.; Li, F.; Liu, J.; Han, G. W.; Chen, B.; Lin, X.; Brouillette, R. L.; Breault, É.; Longpré, J. M.; Shi, S.; Lei, H.; Sarret, P.; Stevens, R. C.; Hanson, M. A.; Xu, F. Structural Insight into Apelin Receptor-G Protein Stoichiometry. *Nat Struct Mol Biol* **2022**, *29* (7), 688–697.

(107) Karas, J. A.; Wade, J. D.; Hossain, M. A. The Chemical Synthesis of Insulin: An Enduring Challenge. *Chem Rev* **2021**, *121* (8), 4531–4560.

(108) Fei Liu, X.; Lin Guan, Y.; Zhi Yang, D.; Yao, K. DE. Antibacterial Action of Chitosan and Carboxymethylated Chitosan. *J Appl Polym Sci* **2000**, *79*, 1324–1335.

(109) Fernández, M.; Villalonga, M. L.; Fragoso, A.; Cao, R.; Baños, M.; Villalonga, R. α-Chymotrypsin Stabilization by Chemical Conjugation with O-Carboxymethyl-Poly-β-Cyclodextrin. *Process Biochemistry* **2004**, *39* (5), 535–539.

(110) Wang, J.; Chen, J. S.; Zong, J. Y.; Zhao, D.; Li, F.; Zhuo, R. X.; Cheng, S. X. Calcium Carbonate/Carboxymethyl Chitosan Hybrid Microspheres and Nanospheres for Drug Delivery. *Journal of Physical Chemistry C* **2010**, *114* (44), 18940–18945.

(111) Kono, H.; Teshirogi, T. Cyclodextrin-Grafted Chitosan Hydrogels for Controlled Drug Delivery. *Int J Biol Macromol* **2015**, *72*, 299–308.

(112) Brakel, A.; Volke, D.; Kraus, C. N.; Otvos, L.; Hoffmann, R. Quantitation of a Novel Engineered Anti-Infective Host Defense Peptide, ARV-1502: Pharmacokinetic Study of Different Doses in Rats and Dogs. *Front Chem* **2019**, *7*.

(113) Alleyne, C.; Amin, R. P.; Bhatt, B.; Bianchi, E.; Blain, J. C.; Boyer, N.; Branca, D.; Embrey, M. W.; Ha, S. N.; Jette, K.; Johns, D. G.; Kerekes, A. D.; Koeplinger, K. A.; Laplaca, D.; Li, N.; Murphy, B.; Orth, P.; Ricardo, A.; Salowe, S.; Seyb, K.; Shahripour, A.; Stringer, J. R.; Sun, Y.; Tracy, R.; Wu, C.; Xiong, Y.; Youm, H.; Zokian, H. J.; Tucker, T. J. Series of Novel and Highly Potent Cyclic Peptide PCSK9 Inhibitors Derived from an MRNA Display Screen and Optimized via Structure-Based Design. *J Med Chem* **2020**, *63* (22), 13796–13824.

(114) Rietschel, B.; Arrey, T. N.; Meyer, B.; Bornemann, S.; Schuerken, M.; Karas, M.; Poetsch, A. Elastase Digests: New Ammunition for Shotgun Membrane Proteomics. *Molecular and Cellular Proteomics* **2009**, *8* (5), 1029–1043.

(115) Morrison, H. Carboxypeptidase A. In *Enzyme Active Sites and their Reaction Mechanisms*; Elsevier, 2021; pp 37–40.

(116) Manea, M.; Mezo, G.; Hudecz, F.; Przybylski, M. Mass Spectrometric Identification of the Trypsin Cleavage Pathway in Lysyl-Proline Containing Oligotuftsin Peptides. *Journal of Peptide Science* **2007**, *13* (4), 227–236.

(117) Morrison, H. Chymotrypsin. In *Enzyme Active Sites and their Reaction Mechanisms*; Elsevier, 2021; pp 41–44.

(118) Mardirossian, M.; Rubini, M.; Adamo, M. F. A.; Scocchi, M.; Saviano, M.; Tossi, A.; Gennaro, R.; Caporale, A. Natural and Synthetic Halogenated Amino Acids—Structural and Bioactive Features in Antimicrobial Peptides and Peptidomimetics. *Molecules* **2021**, *26* (23).

(119) Das, S. S.; Bharadwaj, P.; Bilal, M.; Barani, M.; Rahdar, A.; Taboada, P.; Bungau, S.; Kyzas, G. Z. Stimuli-Responsive Polymeric Nanocarriers for Drug Delivery, Imaging, and Theragnosis. *Polymers (Basel)* **2020**, *12* (6).

(120) Lee, A. C. L.; Harris, J. L.; Khanna, K. K.; Hong, J. H. A Comprehensive Review on Current Advances in Peptide Drug Development and Design. *Int J Mol Sci* **2019**, *20* (10), 2383.

(121) Bruno, B. J.; Miller, G. D.; Lim, C. S. Basics and Recent Advances in Peptide and Protein Drug Delivery. *Therapeutic Delivery*. November 2013, pp 1443–1467.

(122) Corbi-Verge, C.; Garton, M.; Nim, S.; Kim, P. M. Strategies to Develop Inhibitors of Motif-Mediated Protein-Protein Interactions as Drug Leads. *Annual Review of Pharmacology and Toxicology*. Annual Reviews Inc. January 6, 2017, pp 39–60.

(123) Jilek, A.; Kreil, G. D-Amino Acids in Animal Peptides. *Monatsh Chem* **2008**, *139* (1), 1–5.

(124) Grishin, D. V.; Zhdanov, D. D.; Pokrovskaya, M. V.; Sokolov, N. N. D-Amino Acids in Nature, Agriculture and Biomedicine. *Front Life Sci* **2020**, *13* (1), 11–22.

(125) Fletcher, M. D.; Campbell, M. M. Partially Modified Retro-Inverso Peptides: Development, Synthesis, and Conformational Behavior. *Chem Rev* **1998**, *98*, 763–795.

(126) Di, L. Strategic Approaches to Optimizing Peptide ADME Properties. *AAPS Journal* **2015**, *17* (1), 134–143.

(127) Xi, W.; Hansmann, U. H. E. The Effect of Retro-Inverse D-Amino Acid Aβ-Peptides on Aβ-Fibril Formation. *Journal of Chemical Physics* **2019**, *150* (9).

(128) Doti, N.; Mardirossian, M.; Sandomenico, A.; Ruvo, M.; Caporale, A. Recent Applications of Retro-Inverso Peptides. *International Journal of Molecular Sciences*. MDPI AG August 2, 2021.

(129) Harrison, K.; Mackay, A. S.; Kambanis, L.; Maxwell, J. W. C.; Payne, R. J. Synthesis and Applications of Mirror-Image Proteins. *Nature Reviews Chemistry*. Nature Research 2023.

(130) Li, C.; Zhan, C.; Zhao, L.; Chen, X.; Lu, W. Y.; Lu, W. Functional Consequences of Retro-Inverso Isomerization of a Miniature Protein Inhibitor of the P53-MDM2 Interaction. *Bioorg Med Chem* **2013**, *21* (14), 4045–4050.

(131) Taylor, E. M.; Otero, D. A.; Banks, W. A.; O'brien, J. S. Retro-Inverso Prosaptide Peptides Retain Bioactivity, Are Stable In Vivo, and Are Blood-Brain Barrier Permeable. *Journal of Pharmacology and Experimental Therapeutics* **2000**, *295*, 190–194.

(132) Gallo, M.; Moreno, E.; Defaus, S.; Ortega-Alvaro, A.; Gonzalez, A.; Robledo, P.; Cavaco, M.; Neves, V.; Castanho, M. A. R. B.; Casadó, V.; Pardo, L.; Maldonado, R.; Andreu, D. Orally Active Peptide Vector Allows Using Cannabis to Fight Pain While Avoiding Side Effects. *J Med Chem* **2021**, *64* (10), 6937–6948.

(133) Lander, A. J.; Jin, Y.; Luk, L. Y. P. D-Peptide and D-Protein Technology: Recent Advances, Challenges, and Opportunities**. *ChemBioChem*. John Wiley and Sons Inc February 14, 2023.

(134) Zheng, X. W.; Han, B. Z. *Baijiu* (白酒), Chinese Liquor: History, Classification and Manufacture. *Journal of Ethnic Foods* **2016**, *3* (1), 19–25.

(135) Zheng, X. W.; Tabrizi, M. R.; Robert Nout, M. J.; Han, B. Z. *Daqu*-a Traditional Chinese Liquor Fermentation Starter. *Journal of the Institute of Brewing* **2011**, *117* (1), 82–90.

(136) Gibbons, J. G.; Salichos, L.; Slot, J. C.; Rinker, D. C.; McGary, K. L.; King, J. G.; Klich, M. A.; Tabb, D. L.; McDonald, W. H.; Rokas, A. The Evolutionary Imprint of Domestication on Genome Variation and Function of the Filamentous Fungus *Aspergillus Oryzae*. *Current Biology* **2012**, *22* (15), 1403–1409.

(137) Jin, G.; Zhu, Y.; Xu, Y. Mystery behind Chinese Liquor Fermentation. *Trends Food Sci Technol* **2017**, *63*, 18–28.

(138) Marco, M. L.; Sanders, M. E.; Gänzle, M.; Arrieta, M. C.; Cotter, P. D.; De Vuyst, L.; Hill, C.; Holzapfel, W.; Lebeer, S.; Merenstein, D.; Reid, G.; Wolfe, B. E.; Hutkins, R. The International Scientific Association for Probiotics and Prebiotics (ISAPP) Consensus Statement on Fermented Foods. *Nat Rev Gastroenterol Hepatol* **2021**, *18* (3), 196–208.

(139) Gänzle, M. The Periodic Table of Fermented Foods: Limitations and Opportunities. *Appl Microbiol Biotechnol* **2022**, *106* (8), 2815–2826.

(140) Huang, Y.; Yi, Z.; Jin, Y.; Huang, M.; He, K.; Liu, D.; Luo, H.; Zhao, D.; He, H.; Fang, Y.; Zhao, H. Metatranscriptomics Reveals the Functions and Enzyme Profiles of the Microbial Community in Chinese Nong-Flavor Liquor Starter. *Front Microbiol* **2017**, *8* (SEP).

(141) He, G.; Huang, J.; Zhou, R.; Wu, C.; Jin, Y. Effect of Fortified *Daqu* on the Microbial Community and Flavor in Chinese Strong-Flavor Liquor Brewing Process. *Front Microbiol* **2019**, *10*, 56.

(142) Sakandar, H. A.; Hussain, R.; Farid Khan, Q.; Zhang, H. Functional Microbiota in Chinese Traditional *Baijiu* and *Mijiu Qu* (Starters): A Review. *Food Research International* **2020**, *138*, 109830.

(143) Xiao, C.; Lu, Z. M.; Zhang, X. J.; Wang, S. T.; Ao, L.; Shen, C. H.; Shi, J. S.; Xu, Z. H. Bio-Heat Is a Key Environmental Driver Shaping the Microbial Community of Medium-Temperature *Daqu*. *Appl Environ Microbiol* **2017**, *83* (23).

(144) Chen, Y.; Li, K.; Liu, T.; Li, R.; Fu, G.; Wan, Y.; Zheng, F. Analysis of Difference in Microbial Community and Physicochemical Indices between Surface and Central Parts of Chinese Special-Flavor *Baijiu Daqu*. *Front Microbiol* **2021**, *11*.

(145) Wang, C. L.; Shi, D. J.; Gong, G. L. Microorganisms in *Daqu*: A Starter Culture of Chinese Maotai-Flavor Liquor. *World J Microbiol Biotechnol* **2008**, *24* (10), 2183–2190.

(146) Zheng, Y.; Zheng, X. W.; Han, B. Z.; Han, J. S.; Robert Nout, M. J.; Chen, J. Y. Monitoring the Ecology of *Bacillus* during *Daqu* Incubation, a Fermentation Starter, Using Culture-Dependent and Culture-Independent Methods. *J Microbiol Biotechnol* **2013**, *23* (5), 614–622.

(147) Deng, Y.; Huang, D.; Han, B.; Ning, X.; Yu, D.; Guo, H.; Zou, Y.; Jing, W.; Luo, H. Correlation: Between Autochthonous Microbial Diversity and Volatile Metabolites during the Fermentation of Nongxiang *Daqu*. *Front Microbiol* **2021**, *12*.

(148) Li, Z.; Siepmann, F. B.; Rojas Tovar, L. E.; Chen, X.; Gänzle, M. G. Effect of Copy Number of the SpoVA2mob Operon, Sourdough and Reutericyclin on Ropy Bread Spoilage Caused by *Bacillus* Spp. *Food Microbiol* **2020**, *91*, 103507.

(149) Robinson, R. J.; Fraaije, B. A.; Clark, I. M.; Jackson, R. W.; Hirsch, P. R.; Mauchline, T. H. Endophytic Bacterial Community Composition in Wheat (*Triticum Aestivum*) Is Determined by Plant Tissue Type, Developmental Stage and Soil Nutrient Availability. *Plant Soil* **2016**, *405* (1–2), 381–396.

(150) Shahzad, R.; Waqas, M.; Khan, A. L.; Asaf, S.; Khan, M. A.; Kang, S. M.; Yun, B. W.; Lee, I. J. Seed-Borne Endophytic *Bacillus Amyloliquefaciens* RWL-1 Produces Gibberellins and Regulates Endogenous Phytohormones of *Oryza Sativa*. *Plant Physiology and Biochemistry* **2016**, *106*, 236–243.

(151) Setlow, P. Spores of *Bacillus Subtilis*: Their Resistance to and Killing by Radiation, Heat and Chemicals. *J Appl Microbiol* **2006**, *101* (3), 514–525.

(152) Li, Z.; Bai, Z.; Wang, D.; Zhang, W.; Zhang, M.; Lin, F.; Gao, L.; Hui, B.; Zhang, H. Cultivable Bacterial Diversity and Amylase Production in Three Typical *Daqus* of Chinese Spirits. *Int J Food Sci Technol* **2014**, *49* (3), 776–786.

(153) Liu, J.; Chen, J.; Fan, Y.; Huang, X.; Han, B. Biochemical Characterisation and Dominance of Different Hydrolases in Different Types of *Daqu* – a Chinese Industrial Fermentation Starter. *J Sci Food Agric* **2018**, *98* (1), 113–121.

(154) Li, P.; Aflakpui, F. W. K.; Yu, H.; Luo, L.; Lin, W. T. Characterization of Activity and Microbial Diversity of Typical Types of *Daqu* for Traditional Chinese Vinegar. *Ann Microbiol* **2015**, *65* (4), 2019–2027.

(155) Cochrane, S. A.; Vederas, J. C. Lipopeptides from *Bacillus* and *Paenibacillus* Spp.: A Gold Mine of Antibiotic Candidates. *Med Res Rev* **2016**, *36* (1), 4–31.

(156) Zhang, B.; Xu, L.; Ding, J.; Wang, M.; Ge, R.; Zhao, H.; Zhang, B.; Fan, J. Natural Antimicrobial Lipopeptides Secreted by *Bacillus* Spp. and Their Application in Food Preservation, a Critical Review. *Trends Food Sci Technol* **2022**, *127*, 26–37.

(157) Roongsawang, N.; Washio, K.; Morikawa, M. Diversity of Nonribosomal Peptide Synthetases Involved in the Biosynthesis of Lipopeptide Biosurfactants. *Int J Mol Sci* **2011**, *12* (1), 141–172.

(158) Li, T.; Li, L.; Du, F.; Sun, L.; Shi, J.; Long, M.; Chen, Z. Activity and Mechanism of Action of Antifungal Peptides from Microorganisms: A Review. *Molecules* **2021**, *26* (11), 3438.

(159) Wu, X.; Jiang, Q.; Wang, Z.; Xu, Y.; Chen, W.; Sun, J.; Liu, Y. Diversity, Enzyme Production and Antibacterial Activity of *Bacillus* Strains Isolated from Sesame-Flavored Liquor *Daqu*. *Arch Microbiol* **2021**, *203* (9), 5831–5839.

(160) Chen, Z.; Wu, Q.; Wang, L.; Chen, S.; Lin, L.; Wang, H.; Xu, Y. Identification and Quantification of Surfactin, a Nonvolatile Lipopeptide in *Moutai* Liquor. *Int J Food Prop* **2020**, *23* (1), 189–198.

(161) Zhang, R.; Wu, Q.; Xu, Y.; Qian, M. C. Isolation, Identification, and Quantification of Lichenysin, a Novel Nonvolatile Compound in Chinese Distilled Spirits. *J Food Sci* **2014**, *79* (10), C1907–C1915.

(162) Im, S. M.; Yu, N. H.; Joen, H. W.; Kim, S. O.; Park, H. W.; Park, A. R.; Kim, J. C. Biological Control of Tomato Bacterial Wilt by Oxydifficidin and Difficidin-Producing *Bacillus Methylotrophicus* DR-08. *Pestic Biochem Physiol* **2020**, *163*, 130–137.

(163) Nagao, T.; Adachi, K.; Sakai, M.; Nishijima, M.; Sanoll, H. Novel Macrolactins as Antibiotic Lactones from a Marine Bacterium. *J Antibiot (Tokyo)* **2001**, *54* (4), 333–339.

(164) Wang, Z.; Li, P.; Luo, L.; Simpson, D. J.; Gänzle, M. G. *Daqu* Fermentation Selects for Heat-Resistant *Enterobacteriaceae* and Bacilli. *Appl Environ Microbiol* **2018**, *84* (21).

(165) Röcken, W.; Spicher, G. Fadenziehende Bakterien-Vorkommen, Bedeutung, Gegenmaßnahmen. *Getreide Mehl Brot* **1993**, *47*, 30–35.

(166) Lee, J. Y.; Shim, J. M.; Yao, Z.; Liu, X.; Lee, K. W.; Kim, H. J.; Ham, K. S.; Kim, J. H. Antimicrobial Activity of *Bacillus Amyloliquefaciens* EMD17 Isolated from *Cheonggukjang* and Potential Use as a Starter for Fermented Soy Foods. *Food Sci Biotechnol* **2016**, *25* (2), 525–532.

(167) Owusu-Kwarteng, J.; Parkouda, C.; Adewumi, G. A.; Ouoba, L. I. I.; Jespersen, L. Technologically Relevant *Bacillus* Species and Microbial Safety of West African Traditional Alkaline Fermented Seed Condiments. *Crit Rev Food Sci Nutr* **2022**, *62* (4), 871–888.

(168) Deleu, M.; Paquot, M.; Nylander, T. Fengycin Interaction with Lipid Monolayers at the Air-Aqueous Interface - Implications for the Effect of Fengycin on Biological Membranes. *J Colloid Interface Sci* **2005**, *283* (2), 358–365.

(169) Gordillo, A.; Maldonado, M. C. Purification of Peptides from *Bacillus* Strains with Biological Activity. *Chromatography and its Applications* **2012**, 201–225.

(170) Ongena, M.; Jacques, P. *Bacillus* Lipopeptides: Versatile Weapons for Plant Disease Biocontrol. *Trends Microbiol* **2008**, *16* (3), 115–125.

(171) Hubrich, F.; B€ Osch, N. M.; Chepkirui, C.; Morinaka, B. I.; Rust, M.; Gugger, M.; Robinson, S. L.; Vagstad, A. L.; Orn Piel, J.; Khosla, C. Ribosomally Derived Lipopeptides Containing Distinct Fatty Acyl Moieties. *Proceedings of the National Academy of Sciences* **2022**, *119*, e2113120119.

(172) Carrillo, C.; Teruel, J. A.; Aranda, F. J.; Ortiz, A. Molecular Mechanism of Membrane Permeabilization by the Peptide Antibiotic Surfactin. *Biochim Biophys Acta Biomembr* **2003**, *1611* (1–2), 91–97.

(173) Cho, K. M.; Math, R. K.; Hong, S. Y.; Asraful Islam, S. M.; Mandanna, D. K.; Cho, J. J.; Yun, M. G.; Kim, J. M.; Yun, H. D. Iturin Produced by *Bacillus Pumilus* HY1 from Korean Soybean Sauce (*Kanjang*) Inhibits Growth of Aflatoxin Producing Fungi. *Food Control* **2009**, *20* (4), 402–406.

(174) Dunlap, C. A.; Schisler, D. A.; Price, N. P.; Vaughn, S. F. Cyclic Lipopeptide Profile of Three *Bacillus Subtilis* Strains; Antagonists of *Fusarium* Head Blight. *Journal of Microbiology* **2011**, *49* (4), 603–609.

(175) Fifani, B.; Steels, S.; Helmus, C.; Delacuvellerie, A.; Deracinois, B.; Phalip, V.; Delvigne, F.; Jacques, P. Coculture of <i>Trichoderma Harzianum/<i> and *Bacillus Velezensis* Based on Metabolic Cross-Feeding Modulates Lipopeptide Production. *Microorganisms* **2022**, *10* (5).

(176) Wang, Q.-Y.; Lin, Q.-L.; Peng, K.; Cao, J.-Z.; Yang, C.; Xu, D. Surfactin Variants from *Bacillus Subtilis Natto* CSUF5 and Their Antifungal Properities against *Aspergillus Niger*. *J Biobased Mater Bioenergy* **2017**, *11*, 210–215.

(177) Kang, B. R.; Park, J. S.; Jung, W. J. Antifungal Evaluation of Fengycin Isoforms Isolated from *Bacillus Amyloliquefaciens* PPL against *Fusarium Oxysporum* f. Sp. *Lycopersici*. *Microb Pathog* **2020**, *149*, 104509.

(178) Kourmentza, K.; Gromada, X.; Michael, N.; Degraeve, C.; Vanier, G.; Ravallec, R.; Coutte, F.; Karatzas, K. A.; Jauregi, P. Antimicrobial Activity of Lipopeptide Biosurfactants against Foodborne Pathogen and Food Spoilage Microorganisms and Their Cytotoxicity. *Front Microbiol* **2021**, *11*.

(179) Corbett, L. J.; Withey, P.; Lantz, V. A.; Ochuodho, T. O. The Economic Impact of the Mountain Pine Beetle Infestation in British Columbia: Provincial Estimates from a CGE Analysis. *Forestry* **2016**, *89* (1), 100–105.

(180) Fettig, C. J.; Asaro, C.; Nowak, J. T.; Dodds, K. J.; Gandhi, K. J. K.; Moan, J. E.; Robert, J. Trends in Bark Beetle Impacts in North America during a Period (2000–2020) of Rapid Environmental Change. *J For* **2022**, *120* (6), 693–713.

(181) Raffa, K. F.; Aukema, B. H.; Bentz, B. J.; Carroll, A. L.; Hicke, J. A.; Turner, M. G.; Romme, W. H. Cross-Scale Drivers of Natural Disturbances Prone to Anthropogenic Amplification: The Dynamics of Bark Beetle Eruptions. *Bioscience* **2008**, *58* (6), 501–517.

(182) Lusebrink, I.; Erbilgin, N.; Evenden, M. L. The Lodgepole × Jack Pine Hybrid Zone in Alberta, Canada: A Stepping Stone for the Mountain Pine Beetle on Its Journey East across the Boreal Forest? *J Chem Ecol* **2013**, *39* (9), 1209–1220.

(183) Janes, J. K.; Li, Y.; Keeling, C. I.; Yuen, M. M. S.; Boone, C. K.; Cooke, J. E. K.; Bohlmann, J.; Huber, D. P. W.; Murray, B. W.; Coltman, D. W.; Sperling, F. A. H. How the Mountain

Pine Beetle (*Dendroctonus Ponderosae*) Breached the Canadian Rocky Mountains. *Mol. Biol. Evol.* **2014**, *31* (7), 1803–1815.

(184) Erbilgin, N.; Ma, C.; Whitehouse, C.; Shan, B.; Najar, A.; Evenden, M. Chemical Similarity between Historical and Novel Host Plants Promotes Range and Host Expansion of the Mountain Pine Beetle in a Naïve Host Ecosystem. *New Phytologist* **2014**, *201* (3), 940–950.

(185) Burke, J. L.; Bohlmann, J.; Carroll, A. L. Consequences of Distributional Asymmetry in a Warming Environment: Invasion of Novel Forests by the Mountain Pine Beetle. *Ecosphere* **2017**, *8* (4).

(186) Cudmore, T. J.; Björklund, N.; Carroll, A. L.; Staffan Lindgren, B. Climate Change and Range Expansion of an Aggressive Bark Beetle: Evidence of Higher Beetle Reproduction in Naïve Host Tree Populations. *Journal of Applied Ecology* **2010**, *47* (5), 1036–1043.

(187) Clark, E. L.; Pitt, C.; Carroll, A. L.; Staffan Lindgren, B.; Huber, D. P. W. Comparison of Lodgepole and Jack Pine Resin Chemistry: Implications for Range Expansion by the Mountain Pine Beetle, Dendroctonus Ponderosae (Coleoptera: Curculionidae). *PeerJ* **2014**, *2014* (1), e240.

(188) Erbilgin, N. Phytochemicals as Mediators for Host Range Expansion of a Native Invasive Forest Insect Herbivore. *New Phytologist* **2019**, *221* (3), 1268–1278.

(189) Cullingham, C. I.; Cooke, J. E. K.; Dang, S.; Davis, C. S.; Cooke, B. J.; Coltman, D. W. Mountain Pine Beetle Host-Range Expansion Threatens the Boreal Forest. *Mol Ecol* **2011**, *20* (10), 2157–2171.

(190) Cooke, B. J.; Carroll, A. L. Predicting the Risk of Mountain Pine Beetle Spread to Eastern Pine Forests: Considering Uncertainty in Uncertain Times. *For Ecol Manage* **2017**, *396*, 11–25.

(191) James, P. M. A.; Huber, D. P. W. TRIA-Net: 10 Years of Collaborative Research on Turning Risk into Action for the Mountain Pine Beetle Epidemic. *Canadian Journal of Forest Research* **2019**, *49* (12), 3–5.

(192) Carroll, A. L.; Shore, T. L.; Safranyik, L. Direct Control: Theory and Practice. In *The mountain pine beetle: a synthesis of biology, management, and impacts on lodgepole pine.*; 2006; pp 155–172.

(193) Safranyik, L.; Carroll, A. L. *The Biology and Epidemiology of the Mountain Pine Beetle in Lodgepole Pine Forests*; Victoria, 2006.

(194) Paine, T. D.; Raffa, K. F.; Harrington, T. C. Interactions among Scolytid Bark Beetles, Their Associated Fungi, and Live Host Conifers. *Annu. Rev. Entomol* **1997**, *42*, 179–206.

(195) Fettig, C. J.; Munson, A. S.; Grosman, D. M.; Bush, P. B. Evaluations of Emamectin Benzoate and Propiconazole for Protecting Individual *Pinus Contorta* from Mortality Attributed to Colonization by *Dendroctonus Ponderosae* and Associated Fungi. *Pest Manag Sci* **2014**, *70* (5), 771–778.

(196) Holmes, S. B.; MacQuarrie, C. J. K. Chemical Control in Forest Pest Management. *Canadian Entomologist* **2016**, *148* (S1), S270–S295.

(197) Hastings, F. L.; Holsten, E. H.; Shea, P. J.; Werner, R. A. Carbaryl: A Review of Its Use against Bark Beetles in Coniferous Forests of North America. *Environ Entomol* **2001**, *30* (5), 803–810.

(198) Özkara, A.; Akyil, D.; Konuk, M. Pesticides, Environmental Pollution, and Health. In *Environmental Health Risk - Hazardous Factors to Living Species*; InTech, 2016.

(199) Islam, W.; Adnan, M.; Shabbir, A.; Naveed, H.; Abubakar, Y. S.; Qasim, M.; Tayyab, M.; Noman, A.; Nisar, M. S.; Khan, K. A.; Ali, H. Insect-Fungal-Interactions: A Detailed Review on Entomopathogenic Fungi Pathogenicity to Combat Insect Pests. *Microb Pathog* **2021**, *159*.

(200) Grabowski, P.; Musumba, M.; Palm, C.; Snapp, S. Sustainable Agricultural intensification and Measuring the Immeasurable: Do We Have a Choice? In *Routledge Handbook of Sustainability Indicators*; 2018; pp 453–476.

(201) Ji, C.; Song, Q.; Chen, Y.; Zhou, Z.; Wang, P.; Liu, J.; Sun, Z.; Zhao, M. The Potential Endocrine Disruption of Pesticide Transformation Products (TPs): The Blind Spot of Pesticide Risk Assessment. *Environ Int* **2020**, *137*.

(202) Nechols, J. R. The Potential Impact of Climate Change on Non-Target Risks from Imported Generalist Natural Enemies and on Biological Control. *BioControl* **2021**, *66* (1), 37–44.

(203) Um, M.; Zakaria, D.; Galadima, I. B.; Gambo, F. M. A Review on the Use of Entomopathogenic Fungi in the Management of Insect Pests of Field Crops. *J Entomol Zool Stud* **2018**, *6* (1), 27–32.

(204) Ainsworth, G. C. Agostino Bassi, 1773 – 1856. *Nature* **1956**, *177*, 255–257.

(205) Lutczyk, P.; Swiezynska, H. Trials of control of the larger pine-shoot beetle (*Tomicus piniperda* L.) with the use of the fungus *Beauveria bassiana* (Bals.) Vuill. on piled wood. *Sylwan (Poland)* **1984**, *128*, 41–45.

(206) Hallet, S.; Gregoire, J. C.; J, C. P. Prospects in the Use of the Entomopathogenous Fungus *Beauveria Bassiana* (Bals.) Vuill. (Deuteromycetes: Hyphomycetes) to Control the Spruce Bark Beetle *Ips Typographus* L. (Coleoptera: Scolytidae). *Mededelingen Faculteit Landbouwkundige en Toegepaste Biologische Wetenschappen Universiteit Gent* **1994**, *59*, 379–383.

(207) Davis, T. S.; Mann, A. J.; Malesky, D.; Jankowski, E.; Bradley, C. Laboratory and Field Evaluation of the Entomopathogenic Fungus *Beauveria Bassiana* (Deuteromycotina: Hyphomycetes) for Population Management of Spruce Beetle, *Dendroctonus Rufipennis* (Coleoptera: Scolytinae), in Felled Trees and Factors Limiting Pathogen Success. *Environ Entomol* **2018**, *47* (3), 594–602.

(208) Dembilio, Ó.; Moya, P.; Vacas, S.; Ortega-García, L.; Quesada-Moraga, E.; Jaques, J. A.; Navarro-Llopis, V. Development of an Attract-and-Infect System to Control *Rhynchophorus Ferrugineus* with the Entomopathogenic Fungus *Beauveria Bassiana*. *Pest Manag Sci* **2018**, *74* (8), 1861–1869.

(209) Hunt, D. W. A.; Borden, J. H.; Rahe, J. E.; Whitney, H. S. Nutrient-Mediated Germination of *Beauveria Bassiana* Conidia on the Integument of the Bark Beetle *Dendroctonus Ponderosae* (Coleoptera:Scolytidae). *J Invertebr Pathol* **1984**, *44*, 304–314.

(210) Rosana, A. R. R.; Pokorny, S.; Klutsch, J. G.; Ibarra-Romero, C.; Sanichar, R.; Engelhardt, D.; Van Belkum, M. J.; Erbilgin, N.; Bohlmann, J.; Carroll, A. L.; Vederas, J. C. Selection

of Entomopathogenic Fungus *Beauveria Bassiana* (Deuteromycotina: Hyphomycetes) for the Biocontrol of *Dendroctonus Ponderosae* (Coleoptera: Curculionidae, Scolytinae) in Western Canada. *Appl Microbiol Biotechnol* **2021**, *105*, 2541–2557.

(211) Zhang, L. W.; Liu, Y. J.; Yao, J.; Wang, B.; Huang, B.; Li, Z. Z.; Fan, M. Z.; Sun, J. H. Evaluation of *Beauveria Bassiana* (Hyphomycetes) Isolates as Potential Agents for Control of *Dendroctonus Valens*. *Insect Sci* **2011**, *18* (2), 209–216.

(212) Shipp, J. L.; Zhang, Y.; Hunt, D. W. A.; Ferguson, A. G. Influence of Humidity and Greenhouse Microclimate on the Efficacy of *Beauveria Bassiana* (Balsamo) for Control of Greenhouse Arthropod Pests. *Environ. Entomol* **2003**, *32* (5), 1154–1163.

(213) Huang, B. F.; Feng, M. G. Comparative Tolerances of Various *Beauveria Bassiana* Isolates to UV-B Irradiation with a Description of a Modeling Method to Assess Lethal Dose. *Mycopathologia* **2009**, *168* (3), 145–152.

(214) Love, B. E.; Bonner-Stewart, J.; Forrest, L. A. An Efficient Synthesis of Oosporein. *Tetrahedron Lett* **2009**, *50* (35), 5050–5052.

(215) Fan, Y.; Liu, X.; Keyhani, N. O.; Tang, G.; Pei, Y.; Zhang, W.; Tong, S. Regulatory Cascade and Biological Activity of *Beauveria Bassiana* Oosporein That Limits Bacterial Growth after Host Death. *Proc Natl Acad Sci U S A* **2017**, *114* (9), E1578–E1586.

(216) Wei, G.; Lai, Y.; Wang, G.; Chen, H.; Li, F.; Wang, S. Insect Pathogenic Fungus Interacts with the Gut Microbiota to Accelerate Mosquito Mortality. *Proc Natl Acad Sci U S A* **2017**, *114* (23), 5994–5999.

(217) Mc Namara, L.; Dolan, S. K.; Walsh, J. M. D.; Stephens, J. C.; Glare, T. R.; Kavanagh, K.; Griffin, C. T. Oosporein, an Abundant Metabolite in *Beauveria Caledonica*, with a Feedback Induction Mechanism and a Role in Insect Virulence. *Fungal Biol* **2019**, *123* (8), 601–610.

(218) Kocacevik, S.; Sevim, A.; Eroglu, M.; Demirbag, Z.; Demir, I. Molecular Characterization, Virulence and Horizontal Transmission of *Beauveria Pseudobassiana* from *Dendroctonus Micans* (Kug.) (Coleoptera: Curculionidae). *Journal of Applied Entomology* **2015**, *139* (5), 381–389.

(219) Wang, H.; Peng, H.; Li, W.; Cheng, P.; Gong, M. The Toxins of *Beauveria Bassiana* and the Strategies to Improve Their Virulence to Insects. *Front Microbiol* **2021**, *12*.

(220) Santurio, J. M.; Zanette, R. A.; Da Silva, A. S.; De La Rue, M. L.; Monteiro, S. G.; Alves, S. H. Improved Method for *Duddingtonia Flagrans* Chlamydospores Production for Livestock Use. *Vet Parasitol* **2009**, *164* (2–4), 344–346.

(221) Jakuš, R.; Blaženec, M. Treatment of Bark Beetle Attacked Trees with Entomopathogenic Fungus *Beauveria Bassiana* (Balsamo) Vuillemin. *Folia Forestalia Polonica* **2011**, *53* (2), 150–155.

(222) Grodzki, W.; Kosibowicz, M. An Attempt to Use the Fungus *Beauveria Bassiana* (Bals.) Vuill. in Forest Protection against the Bark Beetle *Ips Typographus* (L.) in the Field. *Forest Research Papers* **2015**, *76* (1), 5–17.

(223) Barta, M.; Kautmanová, I.; Čičková, H.; Ferenčík, J.; Florián, Š.; Novotný, J.; Kozánek, M. The Potential of *Beauveria Bassiana* Inoculum Formulated into a Polymeric Matrix for a Microbial Control of Spruce Bark Beetle. *Biocontrol Sci Technol* **2018**, *28* (7), 718–735.

(224) Mann, A. J.; Davis, T. S. Plant Secondary Metabolites and Low Temperature Are the Major Limiting Factors for *Beauveria Bassiana* (Bals.-Criv.) Vuill. (Ascomycota: Hypocreales) Growth and Virulence in a Bark Beetle System. *Biological Control* **2020**, *141*.

(225) Posada-Flórez, F. J. Production of *Beauveria Bassiana* Fungal Spores on Rice to Control the Coffee Berry Borer, *Hypothenemus Hampei*, in Colombia. *Journal of Insect Science* **2008**, *8*, 1–13.

(226) Das, P.; Hazarika, L. K.; Bora, D. Study on Mass Production of *Beauveria Bassiana* (Bals.) Vuill. for the Management of Rice Hispa, *Dicladispa Armigera* (Olivier). In *Cutting-edge Research in Agricultural Sciences Vol. 11*; Book Publisher International (a part of SCIENCEDOMAIN International), 2021; pp 100–107.

(227) Bleiker, K. P.; Van Hezewijk, B. H. Flight Period of Mountain Pine Beetle (Coleoptera: Curculionidae) in Its Recently Expanded Range. *Environ Entomol* **2016**, *45* (6), 1561–1567.

(228) Meurisse, N.; Pawson, S. Quantifying Dispersal of a Non-Aggressive Saprophytic Bark Beetle. *PLoS One* **2017**, *12* (4).

(229) Campos, R. A.; Arruda, W.; Boldo, J. T.; Da Silva, M. V.; De Barros, N. M.; De Azevedo, J. L.; Schrank, A.; Vainstein, M. H. *Boophilus Microplus* Infection by *Beauveria Amorpha* and *Beauveria Bassiana*: SEM Analysis and Regulation of Subtilisin-like Proteases and Chitinases. *Curr Microbiol* **2005**, *50* (5), 257–261.

(230) Segre, J. A. What Does It Take to Satisfy Koch's Postulates Two Centuries Later?: Microbial Genomics and Propionibacteria Acnes. *Journal of Investigative Dermatology* **2013**, *133* (9), 2141–2142.

(231) Hunt, D. W. A. Absence of Fatty Acid Germination Inhibitors for Conidia of *Beauveria Bassiana* on the Integument of the Bark Beetle *Dendroctonus Ponderosae* (Coleoptera: Scolytidae). *Can Entomol* **1986**, *118* (8), 837–838.

(232) Mann, A. J.; Davis, T. S. Entomopathogenic Fungi to Control Bark Beetles: A Review of Ecological Recommendations. *Pest Manag Sci* **2021**, *77* (9), 3841–3846.

(233) Rohrlich, C.; Merle, I.; Hassani, I. M.; Verger, M.; Zuin, M.; Besse, S.; Robène, I.; Nibouche, S.; Costet, L. Variation in Physiological Host Range in Three Strains of Two Species of the Entomopathogenic Fungus *Beauveria*. *PLoS One* **2018**, *13* (7).

(234) Amin, G. A.; Youssef, N. A.; Bazaid, S.; Saleh, W. D. Assessment of Insecticidal Activity of Red Pigment Produced by the Fungus *Beauveria Bassiana*. *World J Microbiol Biotechnol* **2010**, *26* (12), 2263–2268.

(235) Feng, P.; Shang, Y.; Cen, K.; Wang, C. Fungal Biosynthesis of the Bibenzoquinone Oosporein to Evade Insect Immunity. *Proc Natl Acad Sci U S A* **2015**, *112* (36), 11365–11370.

(236) Lee, S.; Kim, J.-J.; Breuil, C. Diversity of Fungi Associated with Mountain Pine Beetle, *Dendroctonus Ponderosae*, and Infested Lodgepole Pines in British Columbia. *Fungal Divers* **2006**, *22*, 91–105.

(237) Tsui, C. K.-M.; Beauseigle, S.; Ojeda Alayon, D. I.; Rice, A. V.; Cooke, J. E. K.; Sperling, F. A. H.; Roe, A. D.; Hamelin, R. C. Fine-Scale Genetic Diversity and Relatedness in Fungi Associated with the Mountain Pine Beetle. *Canadian Journal of Forest Research* **2019**, *49* (8), 933–941.

(238) Rumbold, C. T. A Blue Stain Fungus, *Ceratostomella Montium* n. Sp., and Some Yeasts Associated with Two Species of *Dendroctonus*. *J Agric Res* **1941**, *62*, 589–601.

(239) Lee, S.; Kim, J. J.; Breuil, C. *Leptographium Longiclavatum* Sp. Nov., a New Species Associated with the Mountain Pine Beetle, *Dendroctonus Ponderosae*. *Mycol Res* **2005**, *109* (10), 1162–1170.

(240) Zipfel, R. D.; De Beer, Z. W.; Jacobs, K.; Wingfield, B. D.; Wingfield, M. J. Multi-Gene Phylogenies Define *Ceratocystiopsis* and <i>Grosmannia<.I> Distinct from *Ophiostoma*. *Stud Mycol* **2006**, *55*, 75–97.

(241) Plattner, A.; Kim, J. J.; DiGuistini, S.; Breuil, C. Variation in Pathogenicity of a Mountain Pine Beetle-Associated Blue-Stain Fungus, *Grosmannia Clavigera*, on Young Lodgepole Pine in British Columbia. *Canadian Journal of Plant Pathology* **2008**, *30* (3), 457–466.

(242) Khadempour, L.; LeMay, V.; Jack, D.; Bohlmann, J.; Breuil, C. The Relative Abundance of Mountain Pine Beetle Fungal Associates through the Beetle Life Cycle in Pine Trees. *Microb Ecol* **2012**, *64* (4), 909–917.

(243) Cale, J. A.; Klutsch, J. G.; Dykstra, C. B.; Peters, B.; Erbilgin, N. Pathophysiological Responses of Pine Defensive Metabolites Largely Lack Differences between Pine Species

but Vary with Eliciting Ophiostomatoid Fungal Species. *Tree Physiol* **2019**, *39* (7), 1121–1135.

(244) Eley, K. L.; Halo, L. M.; Song, Z.; Powles, H.; Cox, R. J.; Bailey, A. M.; Lazarus, C. M.; Simpson, T. J. Biosynthesis of the 2-Pyridone Tenellin in the Insect Pathogenic Fungus *Beauveria Bassiana*. *ChemBioChem* **2007**, *8* (3), 289–297.

(245) Rehner, S. A.; Buckley, E. A *Beauveria* Phylogeny Inferred from Nuclear ITS and EF1-α Sequences: Evidence for Cryptic Diversification and Links to Cordyceps Teleomorphs. *Mycologia* **2017**, *97* (1), 84–98.

(246) Álvarez-Baz, G.; Fernández-Bravo, M.; Pajares, J.; Quesada-Moraga, E. Potential of Native *Beauveria Pseudobassiana* Strain for Biological Control of Pine Wood Nematode Vector *Monochamus Galloprovincialis*. *J. Invertebr. Pathol.* **2015**, *132*, 48–56.

(247) Altimira, F.; De La Barra, N.; Rebufel, P.; Soto, S.; Soto, R.; Estay, P.; Vitta, N.; Tapia, E. Potential Biological Control of the Pupal Stage of the European Grapevine Moth *Lobesia Botrana* by the Entomopathogenic Fungus *Beauveria Pseudobassiana* in the Winter Season in Chile. *BMC Res. Notes* **2019**, *12* (1), 1–6.

(248) Weisenfeld, N. I.; Kumar, V.; Shah, P.; Church, D. M.; Jaffe, D. B. Direct Determination of Diploid Genome Sequences. *Genome Res.* **2017**, *27* (5), 757–767.

(249) Emms, D. M.; Kelly, S. OrthoFinder: Phylogenetic Orthology Inference for Comparative Genomics. *Genome Biol.* **2019**, *20* (1), 1–14.

(250) Cornforth, J. W.; Ryback, G.; Robinson, P. M.; Park, D. Isolation and Characterization of a Fungal Vacuolation Factor (Bikaverin). *J. Chem. Soc. C.* **1971**, No. 0, 2786–2788.

(251) Limón, M. C.; Rodríguez-Ortiz, R.; Avalos, J. Bikaverin Production and Applications. *Appl. Microbiol. Biotechnol.* **2010**, *87* (1), 21–29.

(252) Luo, Z.; Li, Y.; Mousa, J.; Bruner, S.; Zhang, Y.; Pei, Y.; Keyhani, N. O. Bbmsn2 Acts as a PH-Dependent Negative Regulator of Secondary Metabolite Production in the Entomopathogenic Fungus *Beauveria Bassiana*. *Environ. Microbiol.* **2015**, *17* (4), 1189–1202.

(253) Wang, D. Y.; Tong, S. M.; Guan, Y.; Ying, S. H.; Feng, M. G. The Velvet Protein VeA Functions in Asexual Cycle, Stress Tolerance and Transcriptional Regulation of *Beauveria Bassiana*. *Fungal Genet. Biol.* **2019**, *127*, 1–11.

(254) Banker, M. J.; Clark, T. H.; Williams, J. A. Development and Validation of a 96-Well Equilibrium Dialysis Apparatus for Measuring Plasma Protein Binding. *J Pharm Sci* **2003**, *92*, 967–974.

(255) OECD Test No. 107: Partition Coefficient (n-Octanol/Water): Shake Flask Method. In *OECD Guidelines for the Testing of Chemicals*; 1995.

(256) Iturrioz, X.; Gerbier, R.; Leroux, V.; Alvear-Perez, R.; Maigret, B.; Llorens-Cortes, C. By Interacting with the C-Terminal Phe of Apelin, Phe255 and Trp259in Helix VI of the Apelin Receptor Are Critical for Internalization. *Journal of Biological Chemistry* **2010**, *285* (42), 32627–32637.

(257) Gerbier, R.; Leroux, V.; Couvineau, P.; Alvear-Perez, R.; Maigret, B.; Llorens-Cortes, C.; Iturrioz, X. New Structural Insights into the Apelin Receptor: Identification of Key Residues for Apelin Binding. *FASEB Journal* **2015**, *29* (1), 314–322.

(258) Fernandez, K. X.; Fischer, C.; Vu, J.; Gheblawi, M.; Wang, W.; Gottschalk, S.; Iturrioz, X.; Llorens-Cortés, C.; Oudit, G. Y.; Vederas, J. C. Metabolically Stable Apelin-Analogues, Incorporating Cyclohexylalanine and Homoarginine, as Potent Apelin Receptor Activators. *RSC Med Chem* **2021**, *12* (8), 1402–1413.

(259) Freidinger, R. M.; Hinkle, J. S.; Perlow, D. S.; Arison, B. H. Synthesis of 9-Fluorenylmethyloxycarbonyl-Protected IV-Alkyl Amino Acids by Reduction of Oxazolidinones. *J. Org. Chem* **1983**, *48*, 77–81.

(260) Dutton, F. E.; Lee, B. H.; Johnson, S. S.; Coscarelli, E. M.; Lee, P. H. Restricted Conformation Analogues of an Anthelmintic Cyclodepsipeptide. *J Med Chem* **2003**, *46* (11), 2057–2073.

(261) Nyimanu, D.; Kay, R. G.; Sulentic, P.; Kuc, R. E.; Ambery, P.; Jermutus, L.; Reimann, F.; Gribble, F. M.; Cheriyan, J.; Maguire, J. J.; Davenport, A. P. Development and Validation of an LC-MS/MS Method for Detection and Quantification of in Vivo Derived Metabolites of [Pyr1]Apelin-13 in Humans. *Sci Rep* **2019**, *9* (1).

(262) Belokon', Y. N.; Tararov, V. I.; Maleev, V. I.; Savel'eva, T. F.; Ryzhov, M. G. Improved Procedures for the Synthesis of (S)-2-[N-(N-Benzyl-Prolyl)Amino]Benzophenone (BPB) and Ni(II) Complexes of Schiff's Bases Derived from BPB and Amino Acids. *Tetrahedron Asymmetry* **1998**, *9*, 4249–4252.

(263) Nash, H. M.; Annis, D. A.; Guerlavais, V.; Licklider, L. Improved Peptidomimetic Macrocycles. WO 2011047215, April 21, 2011.

(264) Gänzle, M. G.; Ehmann, M.; Hammes, W. P. Modeling of Growth of *Lactobacillus Sanfranciscensis* and *Candida Milleri* in Response to Process Parameters of Sourdough Fermentation. *Appl Environ Microbiol* **1998**, *64* (7), 2616–2623.

(265) Zhang, C.; Brandt, M. J.; Schwab, C.; Gänzle, M. G. Propionic Acid Production by Cofermentation of *Lactobacillus Buchneri* and *Lactobacillus Diolivorans* in Sourdough. *Food Microbiol* **2010**, *27* (3), 390–395.

(266) Li, Z.; Schottroff, F.; Simpson, D. J.; Gänzle, M. G. The Copy Number of the SpoVA 2mob Operon Fetermines Pressure Resistance of *Bacillus* Endospores. *Appl Environ Microbiol* **2019**, *85*, e01596-19.

(267) Blin, K.; Shaw, S.; Kloosterman, A. M.; Charlop-Powers, Z.; Van Wezel, G. P.; Medema, M. H.; Weber, T. AntiSMASH 6.0: Improving Cluster Detection and Comparison Capabilities. *Nucleic Acids Res* **2021**, *49* (W1), W29–W35.

(268) Yang, H.; Li, X.; Li, X.; Yu, H.; Shen, Z. Identification of Lipopeptide Isoforms by MALDI-TOF-MS/MS Based on the Simultaneous Purification of Iturin, Fengycin, and Surfactin by RP-HPLC. *Anal Bioanal Chem* **2015**, *407* (9), 2529–2542.

(269) Blin, K.; Shaw, S.; Steinke, K.; Villebro, R.; Ziemert, N.; Lee, S. Y.; Medema, M. H.; Weber, T. AntiSMASH 5.0: Updates to the Secondary Metabolite Genome Mining Pipeline. *Nucleic Acids Res.* **2019**, *47* (W1), W81–W87.

(270) Marks, P.; Garcia, S.; Barrio, A. M.; Belhocine, K.; Bernate, J.; Bharadwaj, R.; Bjornson, K.; Catalanotti, C.; Delaney, J.; Fehr, A.; Fiddes, I. T.; Galvin, B.; Heaton, H.; Herschleb, J.; Hindson, C.; Holt, E.; Jabara, C. B.; Jett, S.; Keivanfar, N.; Kyriazopoulou-

Panagiotopoulou, S.; Lek, M.; Lin, B.; Lowe, A.; Mahamdallie, S.; Maheshwari, S.; Makarewicz, T.; Marshall, J.; Meschi, F.; O'Keefe, C. J.; Ordonez, H.; Patel, P.; Price, A.; Royall, A.; Ruark, E.; Seal, S.; Schnall-Levin, M.; Shah, P.; Stafford, D.; Williams, S.; Wu, I.; Xu, A. W.; Rahman, N.; MacArthur, D.; Church, D. M. Resolving the Full Spectrum of Human Genome Variation Using Linked-Reads. *Genome Res.* **2019**, *29* (4), 635–645.

(271) Li, H.; Durbin, R. Fast and Accurate Short Read Alignment with Burrows–Wheeler Transform. *Bioinformatics* **2009**, *25* (14), 1754–1760.

(272) Li, H. Aligning Sequence Reads, Clone Sequences and Assembly Contigs with BWA-MEM. **2013**.

(273) Manni, M.; Berkeley, M. R.; Seppey, M.; Simão, F. A.; Zdobnov, E. M. BUSCO Update: Novel and Streamlined Workflows along with Broader and Deeper Phylogenetic Coverage for Scoring of Eukaryotic, Prokaryotic, and Viral Genomes. *Mol. Biol. Evol.* **2021**, *38* (10), 4647–4654.

(274) Gurevich, A.; Saveliev, V.; Vyahhi, N.; Tesler, G. QUAST: Quality Assessment Tool for Genome Assemblies. *Bioinformatics* **2013**, *29* (8), 1072–1075.

(275) Ou, S.; Su, W.; Liao, Y.; Chougule, K.; Agda, J. R. A.; Hellinga, A. J.; Lugo, C. S. B.; Elliott, T. A.; Ware, D.; Peterson, T.; Jiang, N.; Hirsch, C. N.; Hufford, M. B. Benchmarking Transposable Element Annotation Methods for Creation of a Streamlined, Comprehensive Pipeline. *Genome Biol.* **2019**, *20* (1), 1–18.

(276) Flynn, J. M.; Hubley, R.; Goubert, C.; Rosen, J.; Clark, A. G.; Feschotte, C.; Smit, A. F. RepeatModeler2 for Automated Genomic Discovery of Transposable Element Families. *Proc. Natl. Acad. Sci. U.S.A.* **2020**, *117* (17), 9451–9457.

(277) Valero-Jiménez, C. A.; Faino, L.; Spring in't Veld, D.; Smit, S.; Zwaan, B. J.; van Kan, J. A. L. Comparative Genomics of *Beauveria Bassiana*: Uncovering Signatures of Virulence against Mosquitoes. *BMC Genom.* **2016**, *17* (1), 1–11.

(278) Bao, W.; Kojima, K. K.; Kohany, O. Repbase Update, a Database of Repetitive Elements in Eukaryotic Genomes. *Mob. DNA* **2015**, *6* (1), 1–6.

(279) Smit, A. F. A.; Hubley, R.; Green, P. RepeatMasker Open-4.0.

(280) Stamatakis, A. RAxML Version 8: A Tool for Phylogenetic Analysis and Post-Analysis of Large Phylogenies. *Bioinformatics* **2014**, *30* (9), 1312–1313.

(281) Xiao, G.; Ying, S. H.; Zheng, P.; Wang, Z. L.; Zhang, S.; Xie, X. Q.; Shang, Y.; St. Leger, R. J.; Zhao, G. P.; Wang, C.; Feng, M. G. Genomic Perspectives on the Evolution of Fungal Entomopathogenicity in *Beauveria Bassiana*. *Sci. Rep.* **2012**, *2* (1), 1–10.

(282) Zheng, P.; Xia, Y.; Xiao, G.; Xiong, C.; Hu, X.; Zhang, S.; Zheng, H.; Huang, Y.; Zhou, Y.; Wang, S.; Zhao, G. P.; Liu, X.; St Leger, R. J.; Wang, C. Genome Sequence of the Insect Pathogenic Fungus *Cordyceps Militaris*, a Valued Traditional Chinese Medicine. *Genome Biol.* **2011**, *12* (11), 1–22..

(283) Katoh, K.; Standley, D. M. MAFFT Multiple Sequence Alignment Software Version 7: Improvements in Performance and Usability. *Mol. Biol. Evol.* **2013**, *30* (4), 772–780.

(284) Holt, C.; Yandell, M. MAKER2: An Annotation Pipeline and Genome-Database Management Tool for Second-Generation Genome Projects. *BMC Bioinform.* **2011**, *12* (1), 1–14.

(285) Korf, I. Gene Finding in Novel Genomes. *BMC Bioinform.* **2004**, *5* (1), 1–9.

(286) Borodovsky, M.; Lomsadze, A. Eukaryotic Gene Prediction Using GeneMark.Hmm-E and GeneMark-ES. *Curr. Protoc. Bioinform.* **2011**, *35*, 4.6.1-4.6.10.

(287) Stanke, M.; Keller, O.; Gunduz, I.; Hayes, A.; Waack, S.; Morgenstern, B. AUGUSTUS: Ab Initio Prediction of Alternative Transcripts. *Nucleic Acids Res.* **2006**, *34* (suppl_2), W435–W439.

(288) Bateman, A.; Martin, M. J.; Orchard, S.; Magrane, M.; Agivetova, R.; Ahmad, S.; Alpi, E.; Bowler-Barnett, E. H.; Britto, R.; Bursteinas, B.; Bye-A-Jee, H.; Coetzee, R.; Cukura, A.; da Silva, A.; Denny, P.; Dogan, T.; Ebenezer, T. G.; Fan, J.; Castro, L. G.; Garmiri, P.; Georghiou, G.; Gonzales, L.; Hatton-Ellis, E.; Hussein, A.; Ignatchenko, A.; Insana, G.; Ishtiaq, R.; Jokinen, P.; Joshi, V.; Jyothi, D.; Lock, A.; Lopez, R.; Luciani, A.; Luo, J.; Lussi, Y.; MacDougall, A.; Madeira, F.; Mahmoudy, M.; Menchi, M.; Mishra, A.; Moulang, K.; Nightingale, A.; Oliveira, C. S.; Pundir, S.; Qi, G.; Raj, S.; Rice, D.; Lopez, M. R.; Saidi, R.; Sampson, J.; Sawford, T.; Speretta, E.; Turner, E.; Tyagi, N.; Vasudev, P.; Volynkin, V.; Warner, K.; Watkins, X.; Zaru, R.; Zellner, H.; Bridge, A.; Poux, S.; Redaschi, N.; Aimo, L.; Argoud-Puy, G.; Auchincloss, A.; Axelsen, K.; Bansal, P.; Baratin, D.; Blatter, M. C.; Bolleman, J.; Boutet, E.; Breuza, L.; Casals-Casas, C.; de Castro, E.; Echioukh, K. C.; Coudert, E.; Cuche, B.; Doche, M.; Dornevil, D.; Estreicher, A.; Famiglietti, M. L.; Feuermann, M.; Gasteiger, E.; Gehant, S.; Gerritsen, V.; Gos, A.; Gruaz-Gumowski, N.;

Hinz, U.; Hulo, C.; Hyka-Nouspikel, N.; Jungo, F.; Keller, G.; Kerhornou, A.; Lara, V.; Le Mercier, P.; Lieberherr, D.; Lombardot, T.; Martin, X.; Masson, P.; Morgat, A.; Neto, T. B.; Paesano, S.; Pedruzzi, I.; Pilbout, S.; Pourcel, L.; Pozzato, M.; Pruess, M.; Rivoire, C.; Sigrist, C.; Sonesson, K.; Stutz, A.; Sundaram, S.; Tognolli, M.; Verbregue, L.; Wu, C. H.; Arighi, C. N.; Arminski, L.; Chen, C.; Chen, Y.; Garavelli, J. S.; Huang, H.; Laiho, K.; McGarvey, P.; Natale, D. A.; Ross, K.; Vinayaka, C. R.; Wang, Q.; Wang, Y.; Yeh, L. S.; Zhang, J. UniProt: The Universal Protein Knowledgebase in 2021. *Nucleic Acids Res.* **2021**, *49* (D1), D480–D489.

(289) Geib, S. M.; Hall, B.; Derego, T.; Bremer, F. T.; Cannoles, K.; Sim, S. B. Genome Annotation Generator: A Simple Tool for Generating and Correcting WGS Annotation Tables for NCBI Submission. *Gigascience* **2018**, *7* (4), 1–5.

(290) Hart, A. J.; Ginzburg, S.; Xu, M.; Fisher, C. R.; Rahmatpour, N.; Mitton, J. B.; Paul, R.; Wegrzyn, J. L. EnTAP: Bringing Faster and Smarter Functional Annotation to Non-Model Eukaryotic Transcriptomes. *Mol. Ecol. Resour.* **2020**, *20* (2), 591–604.

(291) Jones, P.; Binns, D.; Chang, H. Y.; Fraser, M.; Li, W.; McAnulla, C.; McWilliam, H.; Maslen, J.; Mitchell, A.; Nuka, G.; Pesseat, S.; Quinn, A. F.; Sangrador-Vegas, A.; Scheremetjew, M.; Yong, S. Y.; Lopez, R.; Hunter, S. InterProScan 5: Genome-Scale Protein Function Classification. *Bioinformatics* **2014**, *30* (9), 1236–1240.

(292) Yu, G.; Wang, L. G.; Han, Y.; He, Q. Y. ClusterProfiler: An R Package for Comparing Biological Themes among Gene Clusters. *OMICS J. Integr. Biol.* **2012**, *16* (5), 284–287.

(293) Benjamini, Y.; Hochberg, Y. Controlling the False Discovery Rate: A Practical and Powerful Approach to Multiple Testing. *J. R. Stat. Soc.* **1995**, *57* (1), 289–300.

(294) Wolf, T.; Shelest, V.; Nath, N.; Shelest, E. CASSIS and SMIPS: Promoter-Based Prediction of Secondary Metabolite Gene Clusters in Eukaryotic Genomes. *Bioinformatics* **2016**, *32* (8), 1138.

(295) Kolosova, N.; Miller, B.; Ralph, S.; Ellis, B. E.; Douglas, C.; Ritland, K.; Bohlmann, J. Isolation of High-Quality RNA from Gymnosperm and Angiosperm Trees. *Biotechniques* **2004**, *36* (5), 821–824.

(296) Patro, R.; Duggal, G.; Love, M. I.; Irizarry, R. A.; Kingsford, C. Salmon Provides Fast and Bias-Aware Quantification of Transcript Expression. *Nat. Methods* **2017**, *14* (4), 417–419.

(297) Love, M. I.; Huber, W.; Anders, S. Moderated Estimation of Fold Change and Dispersion for RNA-Seq Data with DESeq2. *Genome Biol.* **2014**, *15* (12), 1–21.

(298) Morgan, M.; Shepherd, L. AnnotationHub: Client to Access AnnotationHub Resources. 2022.

(299) McKenzie, A. T.; Katsyv, I.; Song, W. M.; Wang, M.; Zhang, B. DGCA: A Comprehensive R Package for Differential Gene Correlation Analysis. *BMC Syst. Biol.* **2016**, *10* (1), 1–25.